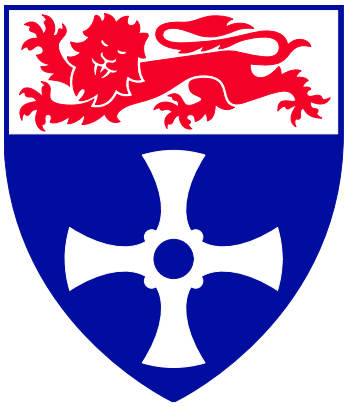

Newcastle University

Faculty of Science, Agriculture and Engineering
School of Electrical and Electronic Engineering

PhD
March 2016

Shipboard Electrification

Emission Reduction and Energy Control

Edward Arthur Sciberras

Supervised by
Dr B Zahawi
Dr D J Atkinson

A dissertation submitted for the degree of
Doctor of Philosophy in Electrical and Electronic Engineering
at Newcastle University

All I know is that electricity and water should not mix.*

A project officer who shall remain unnamed

*Except perhaps in Lead-acid batteries.

Abstract

The application of green technology to marine transport is high on the sector's agenda, both for environmental reasons, as well as the potential to positively impact on ship operator running costs. In this thesis, electrical technologies and systems as enablers of green vessels were examined for reducing emissions and fuel consumption in a number of case studies, using computer based models and simulations, coupled with real operational data.

Bidirectional auxiliary drives were analysed while providing propulsion during low speed manoeuvring, coupling an electrical machine with power electronic converter and feeding power to the propulsion system from the auxiliary generators. Models were built to enable quantification of losses in various topologies and machine setups, showing how permanent magnet machines compared to induction machines, as well as examining different losses in different topologies.

Another examination of topologies was performed for onshore power supply systems, where a number of different network configurations were modelled and examined based on the visiting profile for a particular port. A Particle Swarm Optimisation algorithm was developed to identify optimal configurations considering both capital costs as well as operational efficiency. This was additionally coupled with the consideration of shore-based LNG generation giving a hybrid onshore power supply configuration.

Hybrid systems on vessels are more complex in terms of energy management, particularly with on-board energy storage. Particle Swarm Optimisation was applied to a model of a hybrid shipboard power system, optimising continuously for the greenest configuration during the ship's voyage. This was developed into a generic and scalable Energy Management System, with the objective of minimising fuel consumption, and applied to a case study.

Acknowledgements

Like an iceberg, this thesis only shows a small portion of the journey of the last four years which finally led to this tome. This work builds upon results obtained as part of the TEFLES and INOMANS^{2}HIP projects, which received funding from the European Union Seventh Framework Programme FP7/2007-2013 (grant agreement nos. 266126 and 266082). All real operational profiles and background information in this thesis come from these projects. This would not have happened without the contributions of all the project partners, who must be collectively thanked.

For all their work on TEFLES, special mention must be given to Aitor, Adrian, Juan and Alberto. In INOMANS^{2}HIP, the guys at IMTECH must be mentioned for their motivation and for being the industrial rudder. Alexander, Walter, Peter and Despoina must be swarming about PSO and EMS by now. Hans must be thanked as the father of GES. In Newcastle, Jon must be thanked for keeping the wheels oiled on both projects, neither of which would have been possible to start with without Tony. And of course this thesis wouldn't have got here without the support from my supervisors Dave and Bashar. Thanks for your trust and belief all the way.

My four years in Newcastle seem to have flown by. To blame for this are the people who have been part of this adventure. Guys from the lab - Chris, Kris, Dave (x2), Steve, Andrew, Maede, Ding, Ben, Jamie and everyone who ever contributed to buttery sessions and endured my excuses for 'jokes'. Climbers and friends of the North - Eva, Richard, Adrian, Nick, Sarah, Myriam, Vicky, Davva, Neil, Leslie. You have all made Newcastle feel like home. And of course Kerrie, whose 'mean dishes' and companionship have made the last year so much fuller.

Last but not least, my parents - for always being there.

ed

September 2015

Contents

Nomenclature

AFE	Active Front End
AFM	Axial Flux Machine
AMCS	Alarm Monitoring and Control System
CFD	Computational Fluid Dynamics
CPP	Controllable Pitch Propeller
EMS	Energy Management System
eSFC	equivalent Specific Fuel Consumption
ESR	Equivalent Series Resistance
FOC	Field Oriented Control
FPP	Fixed Pitch Propeller
GA	Genetic Algorithm
HFO	Heavy Fuel Oil
HIL	Hardware In the Loop
HRG	High Resistance Grounding
HV	High Voltage
IEA	International Energy Agency
IGBT	Insulated Gate Bipolar Transistor
IGCT	Insulated Gate-Commutated Thyristor

IM	Induction Machine
LNG	Liquefied Natural Gas
LPF	Low Pass Filter
LUT	Look Up Table
LUT	Look Up Table
MDO	Marine Diesel Oil
MGO	Marine Gas Oil
MOPSO	Multi-Objective Particle Swarm Optimisation
MRG	Main Reduction Gearbox
MTPA	Maximum Torque Per Amp
MV	Medium Voltage
NGR	Neutral Grounding Resistance
PCC	Point of Common Coupling
PM	Permanent Magnet
PMS	Power Management System
PMSM	Permanent Magnet Synchronous Machines
PSO	Particle Swarm Optimisation
PTI	Power Take-Off/Power Take-In
RO	Residual Oil
SFC	Specific Fuel Consumption
T&D	Transmission and Distribution
THD	Total Harmonic Distortion
UKGHGI	United Kingdom GreenHouse Gas Inventory
VSI	Voltage Source Inverter

List of Figures

List of Algorithms

List of Tables

Preface

Ships are all small when out there in the ocean.

Perhaps this is one of the reasons why the marine market has traditionally been seen as relatively conservative, sticking to tried and tested machinery and systems. Ships are currently responsible for moving about 80% of the world's trade (by volume) and contribute about 2.7% of the total man-made CO_2 emissions worldwide. With current and predicted growth rates, this implies a corresponding increase in airborne emissions by shipping if no measures are taken to reduce the environmental impact of vessels [1]. Airborne emissions have a direct impact both on human health as well as the environment, which arise from the combustion of fossil fuels onboard vessels, typically in diesel engines used both for propulsion as well as onboard power generation [2].

In the vast majority of cases, a propeller is used to convert the mechanical rotational power from the engine to a thrust able to propel a ship's hull through the water. This rotational power is transferred from the engine to the propeller by a combination of shafts and gearboxes and associated couplings. This raises one of the inherent limitations of this mechanical arrangement, in that the possible layouts of engine and propulsion systems are constrained by shafting complexities.

Electric propulsion gives a broader degree of freedom to the designer, in that the provision of mechanical rotating power does not need to be in the same location as the chemical energy (stored in the fuel) conversion stage. This means that diesel engines and generators can be located remotely from the propulsion system, with electric cables being much easier to route than mechanical shafts. This concept of flexibility in installation is extended to further flexibility in operation, facilitated by the use of electric propulsion decoupling prime mover operation and propulsion demands. With a number of diesel generators installed onboard, superior fuel consumption can

be obtained by better matching of the number of generators to the demanded power.

Electrification's major advantage can be summed up as *flexibility*. This does not however imply that electrification results in fuel savings, or improved performance. Rather it can be better put that electrification gives a *potential* for improved performance. This potential can be realised (or not!) based on the usage profile of the vessel.

Electrifying the propulsion system after all will introduce additional components compared to a mechanical system, such as frequency converters, transformer, switchgear and filters in addition to the actual propulsion motor. Each of these components introduces inefficiencies to the system, and additional components in series imply the potential for lower reliability. Hence the operational benefits of an onboard electrified system must be elucidated based on the usage profile of the vessel and correct energy management approach. Existing vessels can help give a better picture of the uptake of electric propulsion on onboard machinery systems.

Figure 1 shows the fraction of total installed power which is available for propulsion, plotted against the deadweight-speed product for a selection of 190 ships of various types built between 2007 and 2012 [3–7][1]. Grouped according to propulsion type, some interesting trends can be observed. The y-axis is a ratio of the total propulsion power to the total installed power onboard. A low value indicates a high level of auxiliary power (needed for other purposes than strictly propulsion of the vessel), while a value of 1 indicates that the vessel has no auxiliary generators. The vessel deadweight was multiplied with the vessel (rated) speed in knots as it was observed to give a more distinct resultant plot by accounting for additional power required due to a higher ship speed.

Direct mechanical propulsion (diesel engines) can be seen to occupy the whole range of deadweight-speed values, with installed power ratios above 60%. Vessels with high-speed engines (and reduction gearing) are restricted to lower deadweight-speed ranges, but similarly are found with ratios over 60%. Steam turbine vessels are restricted to a very distinct cluster in a very narrow range, all six of which are liquefied gas carriers.

Of most relevance to this work are the vessels installed with electric propulsion. Clearly, the ratio of installed power is spread over a much larger range, with total

[1]Ships in the database do not include smaller workboats and vessels.

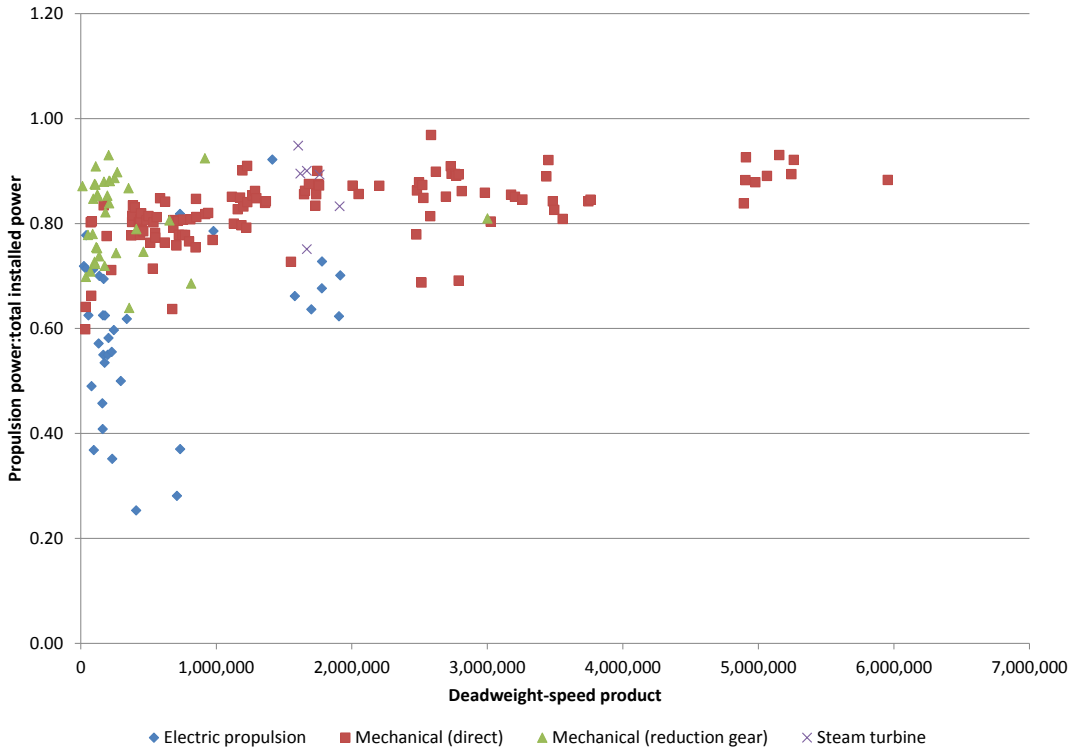

Figure 1 – Onboard power ratio vs deadweight-speed product, grouped by propulsion type.

dominance in ratios below 60%. Six diesel-electric vessels also fall in the same range as the steam turbine powered vessels. On closer examination it is seen that these vessels are also liquefied gas carriers.

Figure 2 focuses solely on the vessels equipped with electric propulsion. The distinct set of liquefied gas carriers can again be clearly discerned. The motivation for electric propulsion in these large deadweight carriers stems from the natural availability of boil-off gas, which is an unavoidable consequence of heat ingress into insulated cargo tanks. This boil-off gas was typically fired in steam turbine installations for propulsion purposes, which are however, bulky and complex [8]. The advent of modern dual-fuel engines permits this boil-off gas to be used in reciprocating engines. Because of the additional electrical loads associated with the liquefied gas fuel system, a diesel-electric installation is utilised.

The impact of significant electric loads is also apparent in the specialised ships category of figure 2. These include offshore support vessels, drillships and dredgers, where once again, the significant electrical load is seen with the (relatively) low number of propulsion:total-installed-power ratio. These types of vessels also typically exhibit a number of operating modes, with different power levels in each. Finally,

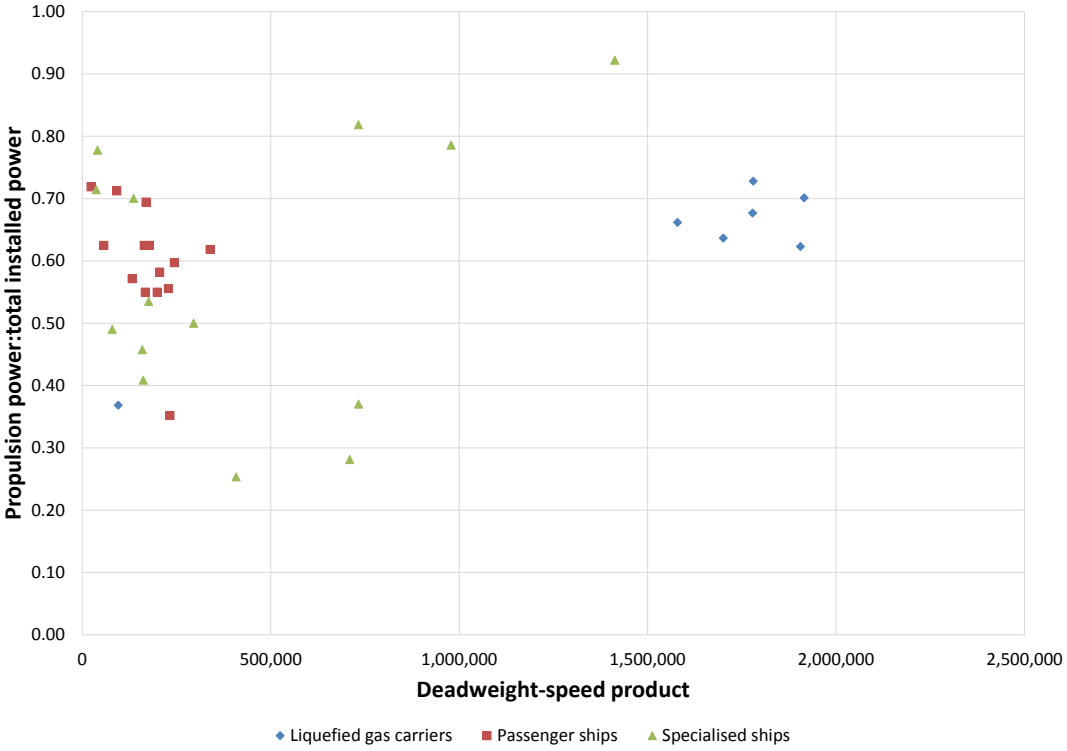

Figure 2 – Onboard power ratio vs deadweight-speed product for electric propulsion vessels, grouped by vessel type.

passenger ships (including ferries and cruise vessels) make up the rest of the electric propulsion category. A large onboard hotelling load is also seen on these vessels, together with the additional requirement for onboard comfort.

In all these vessels, electric propulsion shows advantages over conventional systems, summed as *flexibility*. Passenger ships can benefit from electric thrusters for reduced vibration and noise. Ships with large electric loads can have one common electric bus for both the propulsion and the auxiliary system. And various operating modes can be better accommodated with electric systems. Final operational economy is therefore the junction of both operational demands and the installed machinery systems.

The importance of system design and operation based on matching with operational data is highlighted in this thesis which focuses on environmental benefits in terms of fuel consumption and airborne emissions by the use of electrified systems. This work has been motivated by participation in two European FP7 research projects which provided the scope of work, as well as real operational data. TEFLES was concerned with Technologies and Scenarios for Low Emissions Shipping and ran from 2011 till 2013. INOMANS^{2}HIP considered the development of an INOvative energy

MANagement System for cargo SHIP and ran in parallel with TEFLES, finishing in 2015.

This thesis is a story of three parts, each focusing on a different aspect of electrification. Chapters 1 and 2 look at the use of hybridisation of the propulsion system through the use of bidirectional auxiliary drives. Their use is considered on a car carrier vessel and a tug boat, considering the effect on fuel consumption and emissions based on their operating profiles. An overview of the proposed setups is given, followed by the modelling methodology used for assessing the impact of the use of auxiliary drives.

Onshore power supply (also known as cold ironing) is then discussed in chapters 3 and 3.3, looking at the resultant impact on airborne emissions due to the plugging of berthed ships to the shoreside grid. The components required are discussed, in light of recent legislation on the matter and the developed models explained in chapter 4. A search algorithm using Particle Swarm Optimisation is then considered in chapters 5 and 6 to identify optimal shore network configurations for a case harbour based on the usage profile over a working week. This is then extended to consider a hybrid approach combining cold ironing with shoreside generation using LNG-fuelled generators and examining the cost influence on the resulting system configuration.

Finally in chapters 7 and 7.3, the focus is on the actual management of the onboard energy considering a combination of novel sources as well as storage. A generic Energy Management System using Particle Swarm Optimisation is developed in chapter 7.6, which searches for the optimal configuration for a particular system setpoint, and demonstrated for a RoRo vessel using its actual operating profile.

The appendices contain the salient elements of the code and models developed in this work, together with additional results placed in the appendix for continuity of the main text.

Aims of the work

This thesis sets out to identify the potential savings in airborne emissions and fuel consumption to be had by the application of electric technologies and systems to marine applications. Hybrid drives, cold ironing and advanced energy management are considered, and aim to:

- Develop a fast simulation framework to permit assessment and quantification of any emissions/consumption reductions.
- Develop an optimisation framework to permit identification of optimal systems.
- Assess the reductions possible with hybridisation of the propulsion system.
- Assess the reductions possible through the use of cold ironing.
- Assess the reductions possible through the development and application of an energy management system on complex systems.

The research for the auxiliary drives and shore supply studies was carried out under the scope of the TEFLES project, while the Energy Management System work was part of the INOMANS^{2}HIP project. The outcomes of the research have already been documented as parts of deliverables associated with the projects, together with additional contributions from the other project partners. In addition to this, a number of peer-reviewed publications and conference proceedings have been published over the course of the research work, and are further expanded upon in this thesis.

The work on auxiliary drives has been presented in two conferences as well as a journal publication:

- E. Sciberras, B. Zahawi, D. J. Atkinson, A. Juandó, M. Solla, and A. Sarasquete, "Auxiliary drives for emissions reduction," in *Low Carbon Shipping Conference, Newcastle upon Tyne 2012*. Newcastle University, 2012.
- E. A. Sciberras, B. Zahawi, and D. J. Atkinson, "Simulation-based efficiency evaluation of auxiliary drives for marine vessels," in *13th International Conference on Computer and IT Applications in the Maritime Industries*, V. Bertram, Ed. Hamburg: Technische Universität Hamburg Harburg, 2014, pp. 427–436.
- E. A. Sciberras, B. Zahawi, D. J. Atkinson, and A. Juandó, "Electric auxiliary propulsion for improved fuel efficiency and reduced emissions," *Proceedings of the Institution of Mechanical Engineers, Part M: Journal of Engineering for the Maritime Environment*, vol. 229, no. 1, pp. 36–44, 2015.

A further two journal publications have been published based on the outcomes from the research on onshore power supply, together with presentations at two conferences.

- E. A. Sciberras, B. Zahawi, D. J. Atkinson, and A. Juandó, "Cold ironing for greener port stays," in *Low Carbon Shipping Conference, London 2013*. UCL, 2013.
- E. A. Sciberras and B. Zahawi, "Emissions reduction while at port," in *Green Ports Energy Conference*, Vigo, June 2013.
- E. A. Sciberras, B. Zahawi, D. J. Atkinson, A. Juandó, and A. Sarasquete, "Cold ironing and onshore generation for airborne emission reductions in ports," *Proceedings of the Institution of Mechanical Engineers, Part M: Journal of Engineering for the Maritime Environment*, vol. 230, no. I, pp. 67–82, 2016.
- E. A. Sciberras, B. Zahawi, and D. J. Atkinson, "Electrical characteristics of cold ironing energy supply for berthed ships," *Transportation Research Part D: Transport and Environment*, vol. 39, pp. 31–43, 2015.

Two further journal publications have been prepared and are currently undergoing peer review process. One analyses the impact of auxiliary drives together with onshore power supply and the combined emissions and fuel consumption reductions achievable with the inclusion of onboard battery storage. The second paper presents the development and results of the energy management system and how fuel savings can be realised when combined with an advanced onboard machinery installation.

- E. Sciberras, B. Zahawi, and D. J. Atkinson, "Reducing shipboard emissions – assessment of the role of electrical technologies," *Transportation Research Part D: Transport and Environment*, 2016, submitted for peer review.
- E. A. Sciberras, B. Zahawi, and D. J. Atkinson, "Managing shipboard energy – a stochastic approach," *IEEE Transactions on Transportation Electrification*, 2016, submitted for peer review.

A note on fuels and emissions

This work addresses airborne emissions and fuel consumption onboard vessels. A number of fuels are used onboard, which in turn are responsible for a larger variety of emissions which are generated by the fuels' combustion. Table 1 lists and defines the

Fuel name	Abbreviation	ISO identifier
Heavy Fuel Oil	HFO	RMH35
Marine Diesel Oil	MDO	DMB
Marine Gasoil	MGO	DMX

Table 1 – Definition of fuel types.

marine fuels as considered in this text, together with the ISO identifier. Marine fuels are obtained from the refining of crude oil, where following processes of distillation, the more volatile distillate products are successively extracted. These include gaseous fuels such as methane and propane, light fuels as used in road transportation and aviation and diesel fuels. The product left at the end of the distillation process are the residual fuels. Heavy Fuel Oil (HFO) is the common name used for the residual fuel used onboard ships, which can be blended with diesel fuel to form Intermediate Fuel Oil (IFO). The various fuels can be characterised by their viscosity, and this is used in the definitions of the individual products as per ISO 8217. The common names for the fuel as used in industry are used in this text.

The combustion of the above fuels results in a number of emissions. Of concern in this work are the three major airborne emissions namely CO_2, NO_x and SO_x. Carbon Dioxide (CO_2) is formed by the combustion of Carbon which is burnt to its dioxide. This gas is non-toxic, however it is a greenhouse gas attribute to global warming. The amount of CO_2 released is dictated by the Carbon content of the fuel and is therefore directly related to the amount of fuel burnt. Similarly, the Sulphur Oxides (SO_x) which are composed mostly of Sulphur Dioxide (SO_2) are defined by the Sulphur content of the fuel. On the other hand, the Nitrogen Oxides (NO_x) are produced during the combustion process and are dependent on temperature as well as reaction time. SO_x and NO_x are both pollutants, leading to acidification as well as being damaging to human health.

Chapter 1

Hybridisation

Diesel engines account for the vast majority of prime movers found on ships, with Heavy Fuel Oil (HFO) being the fuel of choice due to its lower cost [18, 19]; its combustion however, generates significant emissions. Furthermore, main engines are typically sized for the continuous at sea power rating, hence when they operate in harbour at reduced speed, they are operating at low load factors, with associated increases in emissions, Specific Fuel Consumption (SFC) and sooting [20].

A hybrid propulsion system consisting of at least two energy sources addresses this mismatch between peak and actual power demands by exploiting the advantages of two separate systems, whose operating points are optimised for different power requirements [21]. Though typically associated with automotive vehicles, marine hybrids in the form of mechanical parallel hybrids such as COmbined Diesel And Gas turbine (CODAG) and serial electric hybrids such as diesel-electric submarines have been used in naval applications for a large number of years [22]. Diesel-electric submarines from a hundred years ago are after all series-hybrids.

Most seagoing (commercial) vessels which employ mechanical main propulsion with diesel engines already have a link to the onboard electric system in the form of a mechanically-driven shaft generator. In almost all cases, this is a conventional wound-rotor synchronous alternator mounted along the propeller shaft line to generate electricity at the cheapest possible cost from the main engine [20, 23]. This arrangement can be further taken advantage of by reversing power flow through the electric machine to provide an electric motoring capability at the cost of additional complexity, namely the need for a bidirectional power converter in order to permit

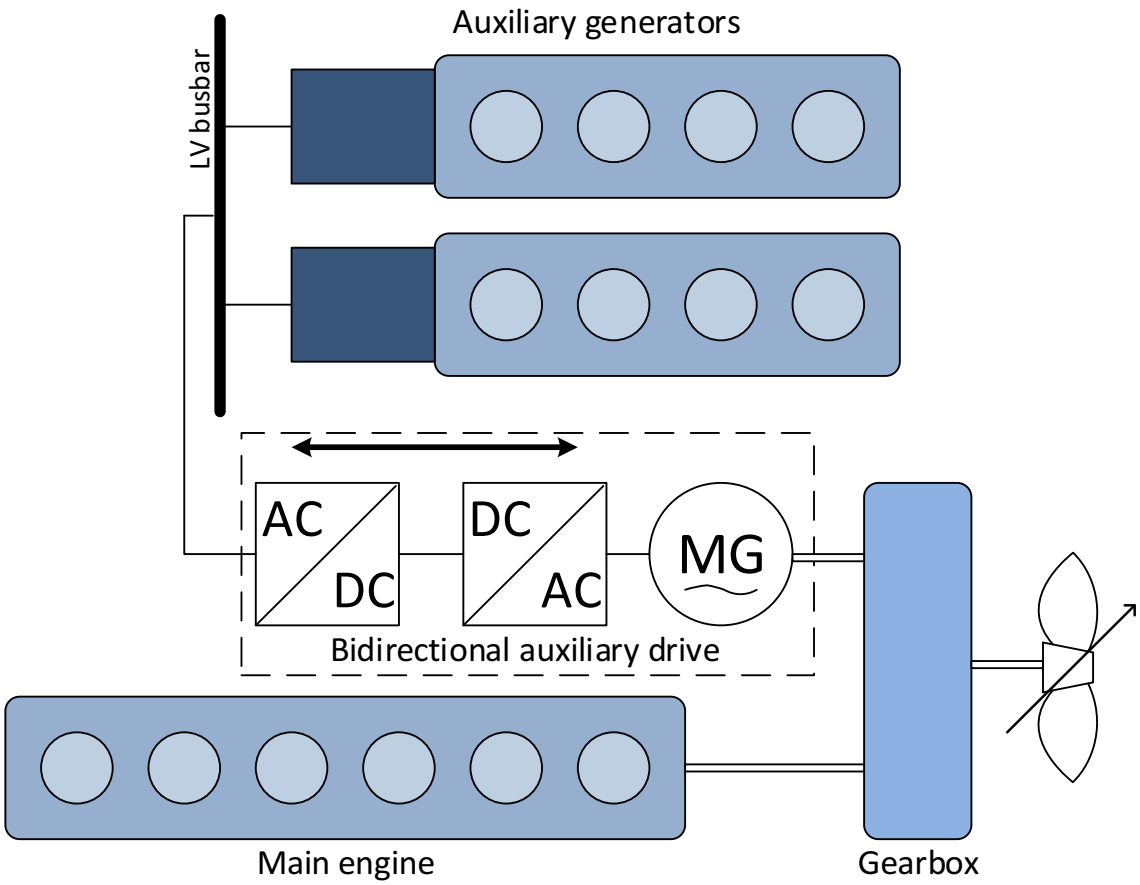

Figure 1.1 – Generic overview diagram of an auxiliary drive.

controlled four-quadrant operation of the machine. The shaft generator in this configuration can operate as an auxiliary propulsion drive [24–26]. This can help meet the stringent emission limits by exploiting the flexibility of the electric system to provide power from compliant sources while in sensitive areas.

In this work, auxiliary drives are understood to be a bidirectional electric drive (consisting of an electric machine, power electronic converter and control algorithms), mounted in parallel to the prime source of propulsion power, as illustrated schematically in figure 1.1. Since the auxiliary drive is found on vessels which do not employ electric (main) propulsion, the onboard electrical system is typically a low voltage one. Improving efficiency in this case refers specifically to improvements in the mechanical and electrical systems such that losses in the propulsive chain are minimised.

The prime difference from a conventional shaft generator system is the bidirectional power control equipment which permits a propulsive (motoring mode) capability. This consists of a Voltage Source Inverter (VSI) which uses Insulated Gate Bipolar

Transistor (IGBT) power electronic switches to convert the onboard AC fixed voltage and fixed frequency supply into a variable output via an intermediate DC link. The use of an IGBT front-end also permits reactive power flow from and into the drive to be controlled (up to the kVA rating of the drive). Such variable frequency drives are now commonplace in industry due to their much greater operational flexibility and improved harmonic performance compared to conventional thyristor controlled drives [27].

The electric machine is therefore fully controlled by the converter in all its operational modes, permitting motoring or generating action at the required power factor (unity power factor when operating as a motor and providing reactive power to the load when operating as a generator). Permanent magnet machines offer higher power density and efficiency compared to conventional wound-rotor machines [28] allowing for more compact installations, especially important in the cramped spaces of an engine room.

The placement of the drive along the propulsion chain determines the speed rating of the machine, in turn affecting the size, weight and cost of the system. For the same power rating, low speed machines require higher torque, which translates to a higher current requirement and hence bigger conductors. Higher-speed machines are generally smaller and lighter due to the reduced torque/current requirements but need mechanical reduction gears in order to be matched to the speed required by the propeller.

In case of a slow-speed diesel engine installation, a direct-drive is typically provided between the engine flywheel and propeller, avoiding the need for any gearing [22]. This reduces transmission losses to a minimum – hence any auxiliary drive installed with a gearbox would introduce additional losses and encroach on existing physical space. In a medium or high-speed engine installation, a step-down gearbox is a necessary part of the propulsion package in the form of the Main Reduction Gearbox (MRG). In this case, the presence of the MRG can be exploited since this does not introduce any (additional) losses or components, and an even higher-speed machine can be utilised by providing the MRG with a Power Take-Off/Power Take-In (PTO/PTI) facility. This consists of a secondary gear on the MRG, permitting two-way mechanical power flow to and from any connected auxiliary machinery [24–26, 29, 30].

In this work, different setups of auxiliary drives are examined for two case studies, a

RoRo vessel and tug boat, with the aim to reduce fuel consumption and airborne emissions. Permanent magnet and induction machines were selected from commercially available ranges to examine the influences of setup on overall efficiency using real operational data for the two vessels. A first order model system was set up which permitted detailed drive models to be used to generate efficiency Look Up Tables for the required operating points, which then facilitate fast steady-state energy studies. The detailed models were then used to consider the differences between permanent magnet machines and induction machines based on the operational profiles of the RoRo and the resultant operating points.

1.1 The machines

The machines in the auxiliary drives convert electrical energy to rotational mechanical energy and vice-versa, hence they represent the point where two otherwise separate systems meet (mechanical propulsion and onboard electric system). Auxiliary drives are sized to cater for a portion of the propulsive demand and are hence inherently smaller than machines employed for main propulsion. The mode of operation of the electric machine is determined by the direction of power flow through its armature windings. Thus if power is flowing from the electrical supply to produce mechanical torque at the output shaft, the machine operates in motoring mode, while if power is fed back to the electric supply, the same machine operates in generating mode. Two types of machines have been considered for application in shipboard auxiliary drives, namely permanent magnet synchronous machines (PMSM) and induction machines (IM). These are both commercially available in marine certifications, and are already found in shipboard applications as off the shelf components. For completeness, wound rotor synchronous machines are also described.

1.1.1 Permanent Magnet machines

The fundamental principle of operation of any electric machine is the interaction between a current carrying conductor and a magnetic field. In conventional wound-rotor machines, this magnetic field is established by the injection of a field current, with an associated power loss. In Permanent Magnet (PM) machines, the magnetic field is established by hard magnetic materials, permitting increased torque densities

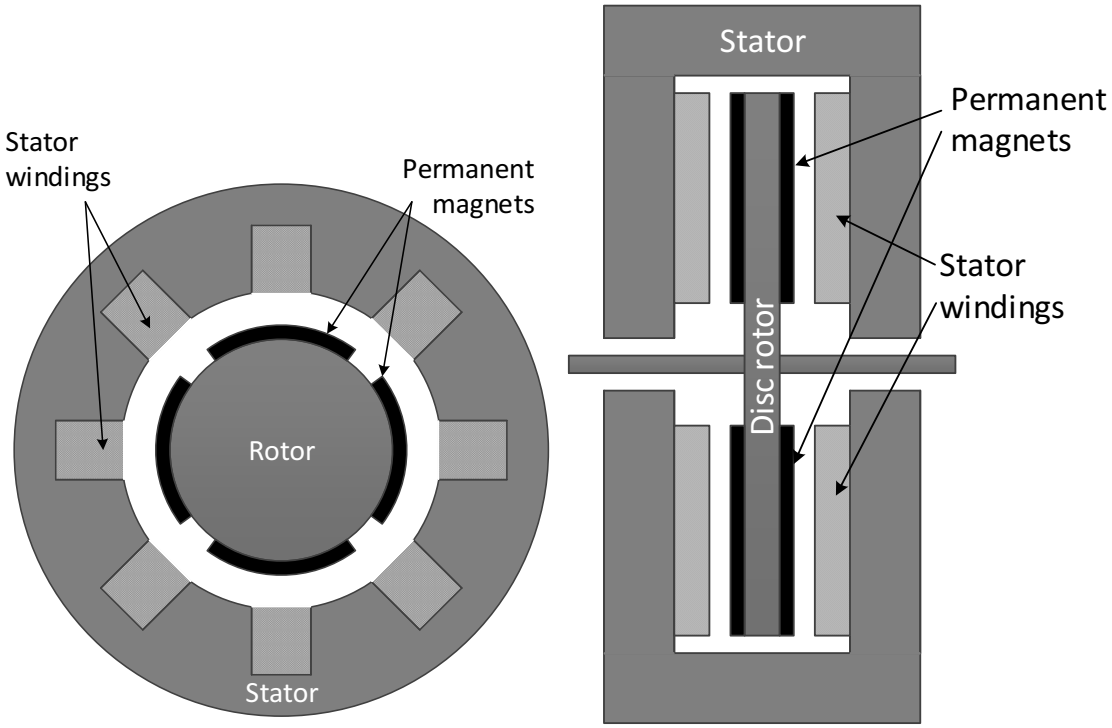

(a) PMSM cross-section. **(b)** AFM transverse view.

Figure 1.2 – PM machines comparison.

and higher efficiencies [31]. The magnets are generally mounted on the rotor, avoiding the need to conduct power to the moving component via brushes, reducing maintenance needs and easing cooling requirements. Radial flux PM machines have their magnets establishing radially directed flux, linking with the conventionally wound stator. In such a setup, the machine operates as a Permanent Magnet Synchronous Machine (PMSM) where the rotor rotates in synchronism with the rotating magnetic field established through the stator.

In contrast, Axial Flux Machines (AFM), as their name suggests, reorient the magnet placements such that flux is established in an axial direction along the shaft. Such a construction leads to very axially compact machines, permitting stacking of rotor discs in order to achieve the required power rating [32]. They are however not as widely commercially available as PMSMs. Figure 1.2 shows a cross-sectional diagram of both machine topologies.

1.1.2 Induction machines

Induction machines transfer energy to the rotor by means of magnetic induction. The fundamental principle of operation is based on a speed difference between the speed

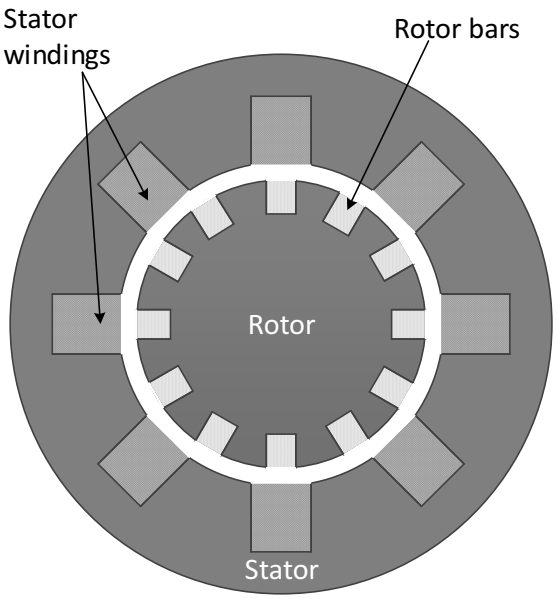

Figure 1.3 – Cross-section of a squirrel cage induction machine.

of the stator-produced rotating magnetic field and the speed of the rotor, inducing a rotor voltage and causing rotor currents to flow. Hence induction motors operate at a speed slightly slower than the synchronous speed (slip speed). Induction motors are the most popular type of motor in industrial applications, due to their inherent simplicity and robustness. Modern power electronic drives now permit variable speed operation to be achieved by these machines further increasing their attractiveness.

The more popular type of induction machine consists of solid metal bars (generally aluminium, though copper is also used in some higher efficiency grades [33]) cast into the laminated rotor periphery. Solid metal rings short these bars at each end forming a cage, permitting current to flow, thus making for a very rugged rotor. This type of motor is the workhorse of industrial power conversion. A cross section of such a machine is shown in figure 1.3.

PM machines are inherently more efficient than their equivalent induction machines since no additional current is needed to set up the magnetic field. They can therefore be more compact and power dense, especially at lower speed ratings. However this comes at a significant price penalty compared to the much simpler IM due to the cost of the permanent magnets.

1.1.3 Wound rotor synchronous machines

Synchronous machines are a type of AC machine that operate with a DC field on the rotor such as that set up by the permanent magnets in the PMSM. This is the reverse construction of a traditional DC machine, where the field is placed on the stator. By having a stationary armature however, less current needs to be conducted through slip rings to the rotor since the load current is now carried by the stator windings. Cooling of the machine is also facilitated by easier heat removal from a stationary component. The DC field can be established by injecting a DC current into the rotor via slip rings. However, a more common method for obtaining the DC field current is to mount a smaller synchronous generator (exciter) on the same shaft with a stationary field, with a rotating solid state rectifier producing the required field current for the main machine. These two topologies are illustrated in figure 1.4 where a direct exciter is shown, which is able to generate an adjustable DC field through a controlled rectifier, as well as a brushless exciter which includes a rectifier mounted on the rotor shaft together with the exciter generator. The advantage of the direct exciter is quick response since the DC voltage input to the rotor is directly controlled. On the other hand adjustments to the field in the brushless exciter's case will take longer to settle since the exciter machine must first react. However the omission of the slip rings is a major advantage as this eliminates the need for periodic maintenance and renewal as well as reducing the incidence of arcing.

Synchronous machines operate at a fixed speed determined by the supply frequency and the number of machine poles as $n_s = {}^{60f}/_{P}$ where $\mathrm{n_s}$ is the synchronous speed in rpm, f is the supply frequency in Hz and P is the number of poles of the machine. This clearly shows how a large number of poles are required for low speed ratings, leading to larger diameter machines. This inherent speed holding capability makes synchronous machines very suitable for fixed speed applications. However the most popular application of a synchronous machine is as a generator, where it is directly coupled to a diesel engine or a turbine to generate electric power.

In marine applications, synchronous generators coupled to diesel engines are almost invariably used for on-board generation in auxiliary generator sets. Set to run at a fixed speed (depending on the desired output frequency), control of the field current (or the excitation) determines the flow of reactive power and hence the terminal voltage, while the prime mover input power determines the flow of real

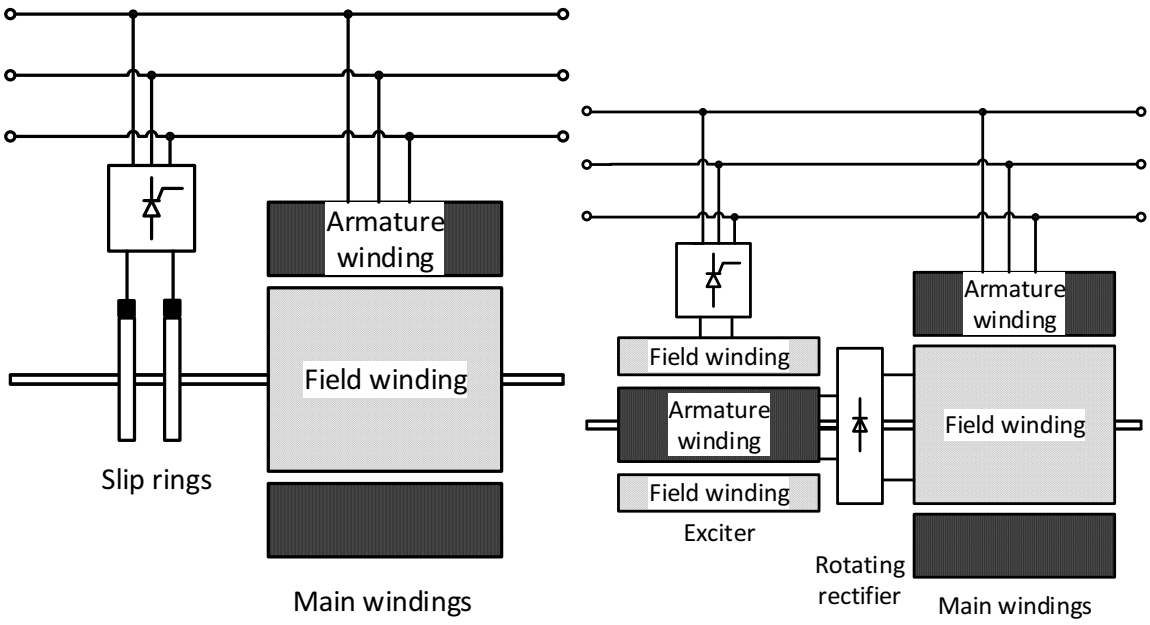

(a) Direct excitation. **(b)** Brushless excitation.

Figure 1.4 – Synchronous machine excitation setups.

power. In motoring applications, synchronous machines are generally employed in larger power ratings, where the possibility of controlling excitation and hence the operating power factor can be a significant detail. Furthermore, when used as a part of a line commutated converter (LCI) drive, a leading power factor is required in order to provide the necessary voltages needed to naturally commutate the thyristor switches used in the machine side converter, thus precluding the use of an induction machine.

For the application of auxiliary drives, the rating of the electrical machine will be much smaller than one used for main propulsion, an application where large synchronous machines are typically used. PMSMs and IMs are therefore considered in the rest of this work for application as auxiliary drives.

1.2 Drives

Modern power electronics and low-cost and powerful digital processing have permitted electrical machines to be precisely and efficiently controlled. A Voltage Source Inverter with an Active Front End (AFE) is shown in figure 1.5, showing the detailed setup including the control algorithm. The Clarke and Park transformations are mathematical tools which convert three-phase AC quantities into equivalent constant values by aligning with a synchronous rotating frame, using the rotor shaft angle

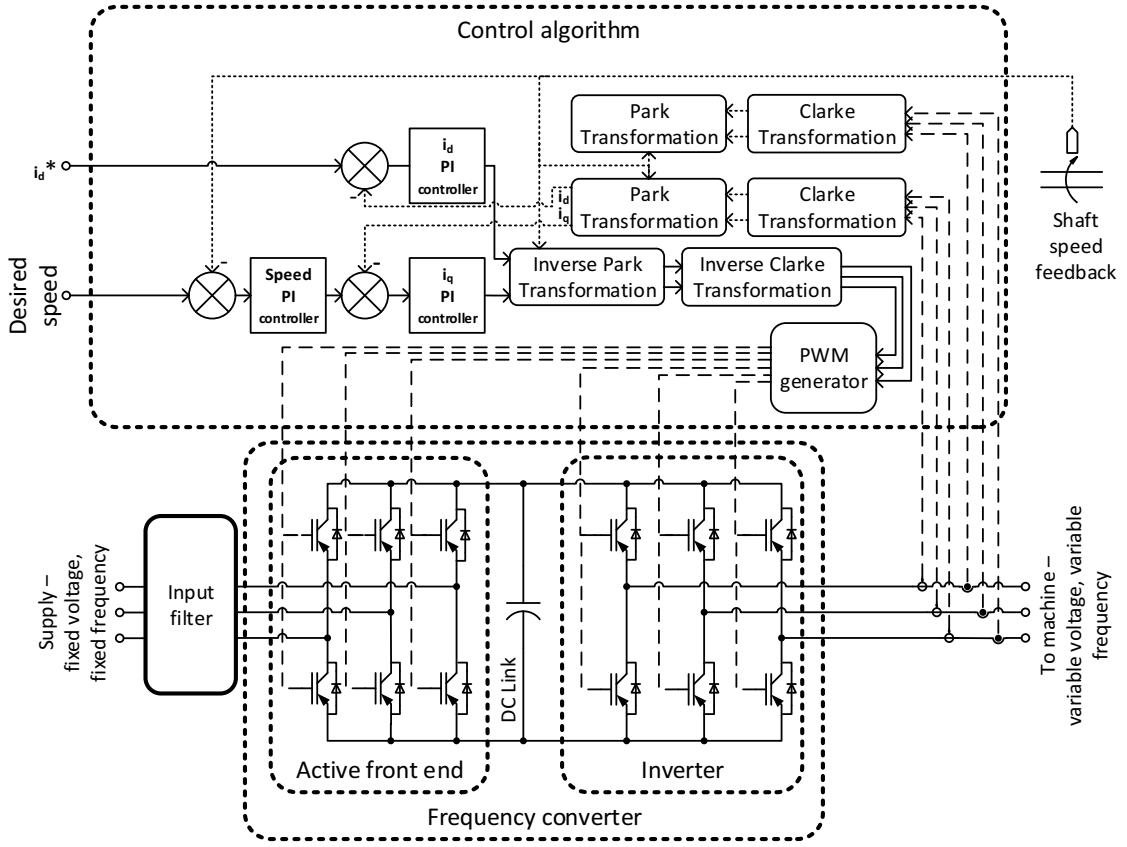

Figure 1.5 – Voltage Source Inverter with Active Front End.

as a reference. The transformed currents are known as the direct axis current (i_d) and the quadrature axis current (i_q) which are oriented using the rotor flux vector as reference (in the case of PM machines). Under proper field orientation conditions, i_d is termed the field-forcing current, while i_q is the torque-producing current. These transformations can be considered to be the digital equivalent of the mechanical commutator found on DC machines.

With an AFE, the flow of power into the drive can be controlled, such that current waveforms can be modulated to control aspects such as power factor. Most importantly for the purposes of auxiliary drives, it permits the flow of power back to the supply. This is not possible with a simple diode bridge rectifier, albeit cost is significantly increased.

Proportional-Integral (PI) Control is used to control motor speed and currents using a cascaded multi-loop system. A fast, inner current control loop controls i_d and i_q according to the current setpoints defined by the slower outer control loop. The outer control loop includes a further PI controller which sets the desired i_q setpoint, based on the error between the desired and actual shaft speeds. The field-forcing current setpoint can be set to a predetermined value or controlled by means of Look

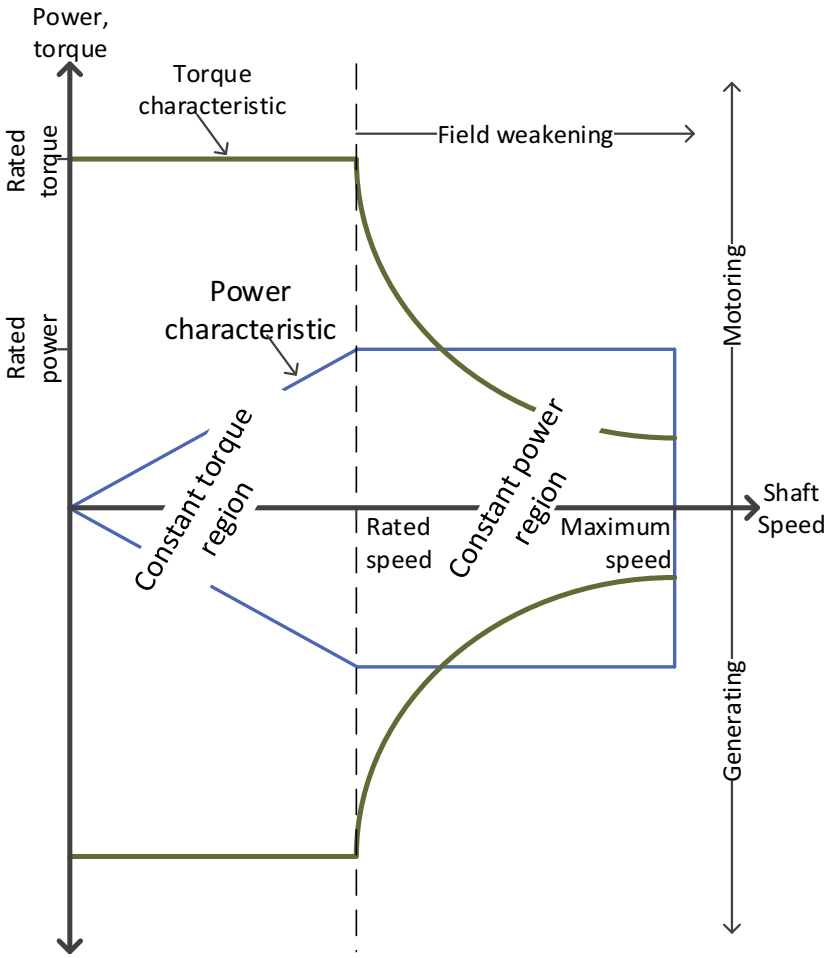

Figure 1.6 – Electric drive operating envelope.

Up Tables (LUTs) based on the machine's operating point. This control technique is known as Field Oriented Control (FOC).

The region of operation of an AC drive under FOC is shown in figure 1.6 (shown only for forward operation - reverse operation would imply a reflection about the y-axis). Here a drive is able to develop rated torque up to its rated speed, at which point rated power is reached. Operation above this base speed is possible using a technique known as field-weakening. In this region of operation, the machine can develop up to its rated power. Since $P = T\omega$, for a constant power (P) and an increasing shaft speed (ω), the torque produced must drop. Operation in this region is possible until the maximum current limit through the drive is reached, or until other mechanical or magnetic constraints are reached.

The fundamental model for an electric machine is given using the standard d-q (direct and quadrature axes) equations below for a non-salient PM machine

$$v_d = R_s i_d + L_d \frac{di_d}{dt} - \omega_r L_q i_q \quad (1.1)$$

$$v_q = R_s i_q + L_q \frac{di_q}{dt} + \omega_r \left(L_d i_d + \Psi_{rd}\right) \quad (1.2)$$

$$T_e(t) = K_t i_q(t) \quad (1.3)$$

$$P_{in}(t) = \frac{3}{2}\left(V_d(t) i_d(t) + V_q(t) i_q(t)\right) \quad (1.4)$$

$$P_{out}(t) = T_m(t)\omega_m(t) \quad (1.5)$$

where the subscripts d and q refer to the direct and quadrature axes, respectively. R_s is the stator resistance, L_q and L_d are the quadrature and direct axis inductances respectively, and K_t is the torque constant. The $^3/_2$ factor comes in to play to provide equivalence of power to preserve the transformation from three-phases to the two quadrature phases. Ψ_{rd} refers to the flux established by the permanent magnets on the rotor.

1.2.1 Field-weakening operation

In a PMSM, the magnetic field is set up inherently by the rotor. Once the magnets have been assembled, no direct control of the magnetic field is possible. Under normal operation therefore, the field-forcing current (i_d) is maintained at 0A for minimum copper losses with the torque produced being directly proportional to i_q. This is known as Maximum Torque Per Amp (MTPA) operation, as all available current is used for torque generation. This is the case for machines which do not exhibit any saliency, such that $L_d = L_q = L_s$.

For operation beyond base speed, the magnetic field set up by the magnets must be decreased. This is achieved by injecting a negative value of i_d such that a stator field opposing that set up by the magnets is created, [34]. Care must be taken since irreversible demagnetisation can occur on the magnets if these are exposed to high levels of opposing flux. Machine designs such as those using interior mounting of the permanent magnets helps to avoid the risk of damage to the magnets, [28]. Furthermore, additional current (since i_d was previously zero) needs to be injected into the machine, increasing Ohmic losses.

At steady state, from equations 1.1 and 1.2, equations 1.6 and 1.7 can be derived for

the stator direct and quadrature voltages as

$$v_{sd} = R_s i_d - \omega_r L_s i_q \tag{1.6}$$

$$v_{sq} = R_s i_q + \omega_r \left(L_s i_d + \Psi_{rd}\right) \tag{1.7}$$

At high-speed, the terms with ω_r dominate the expressions such that $\omega_r L_s i \gg R_s i$ such that

$$v_{sd} \approx -\omega_r L_s i_q$$

$$v_{sq} \approx \omega_r \left(L_s i_d + \Psi_{rd}\right)$$

The stator voltage is limited by the maximum voltage supplied by the converter such that

$$v_{max}^2 \geq \left(\omega_r L_s i_q\right)^2 + \left(\omega_r \left(L_s i_d + \Psi_{rd}\right)\right)^2$$

leading to

$$\left(\frac{v_{max}}{\omega_r}\right)^2 \geq L_d^2 \left(\frac{\Psi_{rd}}{L_d} + i_d\right)^2 + \left(L_q i_q\right)^2 \tag{1.8}$$

This describes an ellipse centred at $i = (^{-\Psi_{rd}}/_{L_d}, 0)$ with radius $^{v_{max}}/_{\omega_r}$. This implies a voltage and speed-dependent limit, leading to a series of circular limits [35], as illustrated in figure 1.7.

For a PM machine, from equation 1.3 it can be observed that the maximum torque is produced when $i_q = I_{max}$ (and $i_d = 0$) where $\mathrm{I_{max}}$ is the maximum current supplied by the converter, leading to the the base speed being defined as

$$\omega_b = \frac{V_{max}}{\sqrt{\Psi_{rd}^2 + \left(L_q I_{max}\right)^2}}$$

This speed is the the maximum speed at which the nominal torque can be produced before the voltage limit is reached. Operation above ω_b can be maintained by operating at the maximum voltage limit, such that from equation 1.8, the desired value of $\mathrm{i_d}$ can be determined as equation 1.9 which results in a current trajectory within the shaded area of figure 1.7.

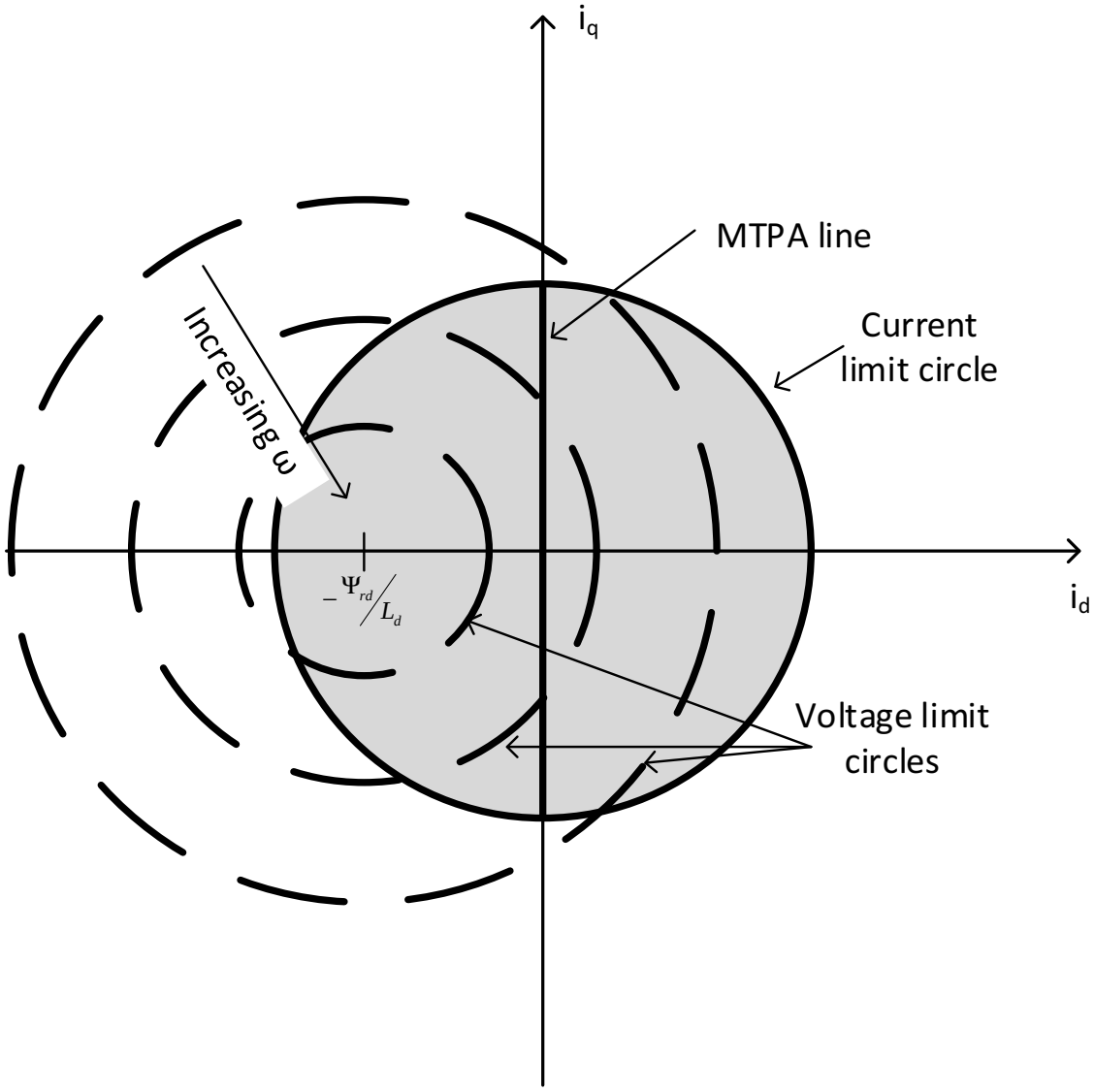

Figure 1.7 – Current and voltage limit loci for non-salient PM machine.

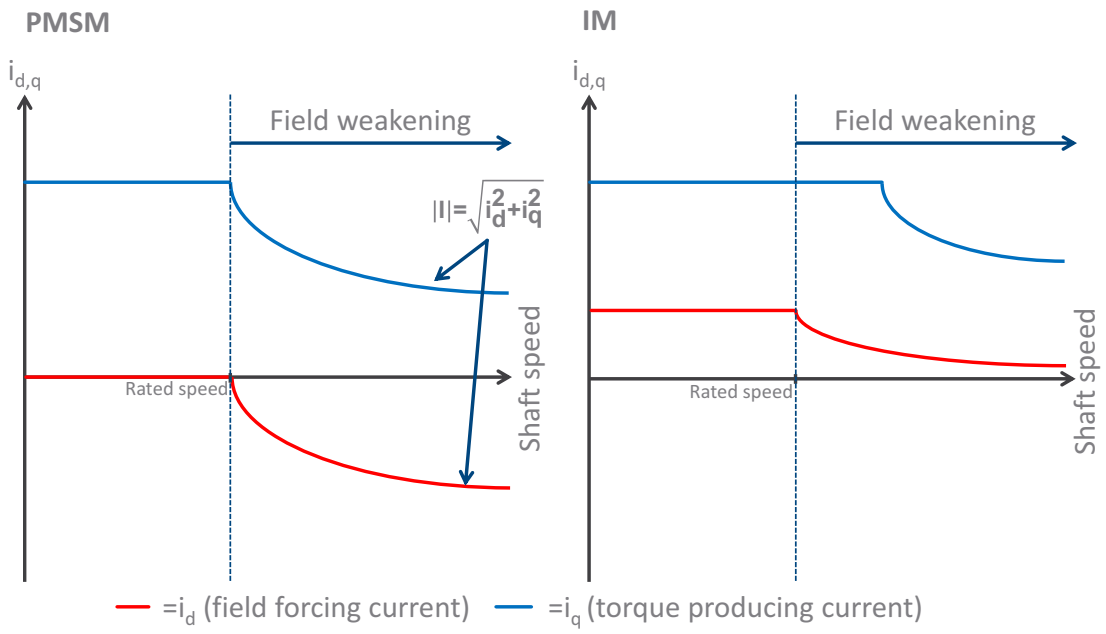

Figure 1.8 – Comparison of field-weakening operation and stator currents for permanent magnet and induction machines.

$$i_d = \frac{-\Psi_{rd} + \sqrt{\left(\frac{v_{max}}{\omega_r}\right)^2 - (L_d i_q)^2}}{L_d} \tag{1.9}$$

In an induction machine on the other hand, the magnetic field must (always) be set up using an external power source, leading to a non-zero value of i_d. Up to base speed, the field-forcing current is set to maintain rated flux levels in the machine such that such that $\Psi_{rd}^{rat} = L_m i_d^{rat}$. Beyond base speed, in order to reduce the flux in the machine (in a simple implementation of field-weakening), i_d is simply reduced proportionally while maintaining i_q such that [36]:

$$i_d = \frac{\Psi_{rd}^{rat}}{L_m}\frac{\omega_b}{\omega}$$

Hence at higher speeds, less current is potentially required by an IM than a PMSM. Figure 1.8 shows this conceptually by comparing the stator currents in field-weakening operation for a permanent magnet machine with an induction machine. A comparison of the two machines' operation must therefore be performed in order to analyse the balance of overall efficiency due to the different operating modes.

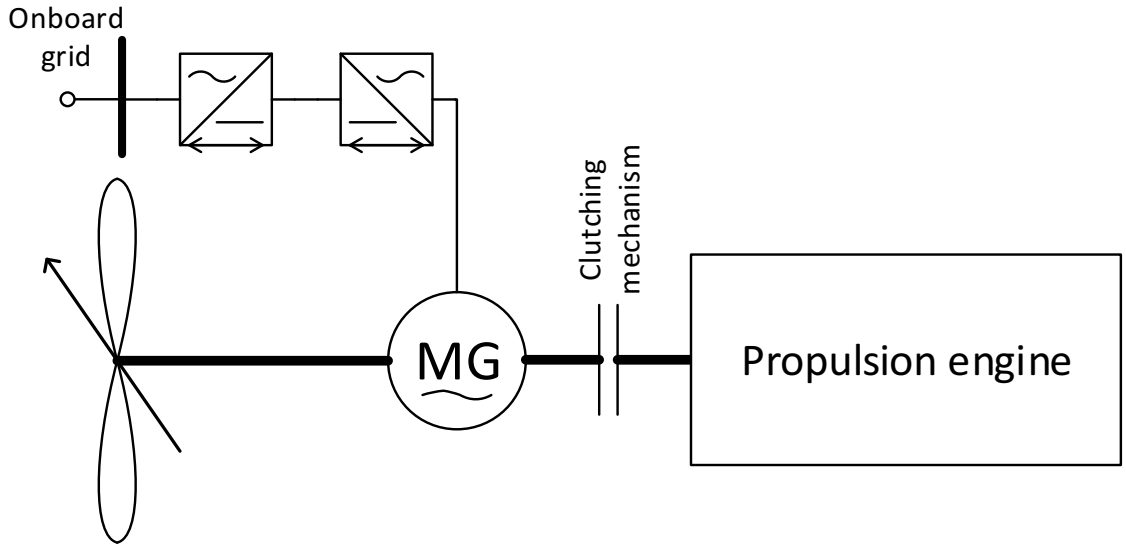

(a) Direct-drive installation with low speed machine.

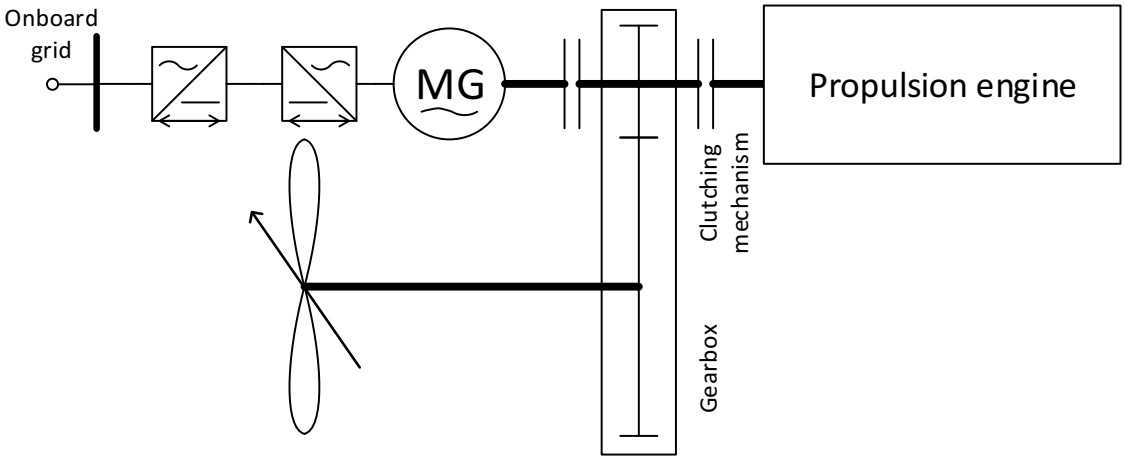

(b) Geared installation with high-speed machine.

Figure 1.9 – Topologies of different auxiliary drive installations..

1.3 Setups

Two different setups are investigated, namely a direct-drive low-speed setup and a high-speed setup with a PTO/PTI on the gearbox. The two fundamental arrangements are illustrated in figure 1.9, showing a direct-drive machine mounted directly on the propeller shaft, as well as a high-speed machine mounted on the gearbox.

The use of a gearbox permits higher-speed machines to be utilised. These have the advantage of lower cost and weight when compared with equivalent lower speed devices of the same power rating. For the geared installation, the total step-down ratio includes the Main Reduction Gear (MRG) in addition to the PTO ratio (if any). Keeping the number of gearing stages low decreases the efficiency drops along the chain, with approximately 98% efficiency at each stage [22, 37].

Geared installation	Direct drive
Higher speed electric machine	Low speed electric machine
Cheaper machine	More expensive machine
Low current/torque ratings	Higher current/torque ratings
Mechanical declutching possible	Mechanical decoupling is complex
Two stage transmission inefficiency	Least transmission losses

Table 1.1 – Comparison of auxiliary drive installations.

A further important consideration is the possibility of mechanical decoupling of the shaftline components. Ideally for auxiliary propulsion, the main engine is de-clutched, reducing the mechanical load on the drive and permitting independent propulsion in case of mechanical failure in the engine. For the geared installation, a single declutching device would be necessary at the main engine side to isolate the engine when not required. Similarly, a clutching device on the PTO/PTI would permit the auxiliary drive to be engaged/disengaged only when required. This would also permit maintenance to be carried out while at sea.

In the direct-drive topology, isolation of the main engine is only possible with a clutching mechanism on the main shaft between the engine and the direct-drive motor. In this case, however, there is no possibility of isolation of the auxiliary drive since this is directly mounted on the propeller shaft. Compared with the first two topologies, clutching possibilities are less straightforward, although commercially available systems can utilise tunnel gearing to decouple the main engine [38]. A point which emerges with respect to the difficulty of de-clutching the electric machine (if a permanent magnet rotor is used) is the voltage induced in the stator whenever the shaft is turning. This can be undesirable in situations such as maintenance and will need to be considered in further detail to ensure safe working conditions. Furthermore, even at no load this represents a power loss due to the no-load losses in the electric machine such as cogging torque. The comparison between the direct drive and geared installation topologies is summarised in table 1.1.

Conventional shaft generator systems implement variants of these same topologies, without bidirectional power converters or the need for decoupling of the main engine. The purpose of using a shaft generator is to generate electricity at the lowest possible cost, which comes about by raising the main engine's operating point and the use of low grade fuel on the main engine [23].

1.4 Propulsion modes

The propulsion setup is an inherent part of the vessel design, and it directly influences the auxiliary drive's operating envelope. This is mainly a design philosophy that is decided on in the initial design stages, when operational requirements such as speed and manoeuvrability are defined. This influences the naval architecture decision on what propulsion strategy to implement on the vessel.

1.4.1 Fixed speed operation

With a fixed (shaft) speed setup, the propeller rate of revolutions is kept constant, and vessel speed is controlled by means of a Controllable Pitch Propeller (CPP). Ship speed is adjusted by control of the propeller blade angle, permitting smooth speed control as well as astern propulsion without changing the engine speed. This is beneficial for manoeuvrability since ship speed can be very quickly adjusted due to the relatively short time constants associated with the pitch control. A Look Up Table (LUT) maps ship speed to propeller pitch.

By maintaining a constant shaft speed, electrical generation using a conventional shaft alternator is simpler, as a fixed frequency output will be generated which can be used to supply the onboard auxiliary system directly. This can be sustained over a wide ship speed range as the shaft generator speed is kept close to its nominal design value. However propulsive efficiency is somewhat reduced as the larger propeller hub necessary for the CPP mechanism increases the drag, as well as complexity and expense [39].

1.4.2 Variable speed operation

Ship speed is in this case controlled by adjustment of the propeller rotational speed which involves a Fixed Pitch Propeller (FPP). This makes for a much simpler installation as no hydraulic pitch adjustment mechanism is required. Ship speed is (roughly) directly proportional to the propeller speed such that $v \propto n$ (where v is the ship speed and n the propeller rate of revolutions). Limits on ship speed are therefore dependent on engine speed ranges, with a minimum engine speed dictating the minimum possible ship speed . A minimum engine speed is in place because

of mechanical limits imposed by lubrication needs as well as a consequent loss of compression and ignition failure. Similarly, at low torque loadings, combustion in the engine takes place at lower temperatures than the design temperature, leading to cylinder fouling [40].

A conventional shaft generator would only be operational when the ship is at nominal speed, since at off-design conditions the generated frequency will not match that required by the onboard grid. Either a complex variable speed gearbox would be required, or a power electronic converter used to ensure correct electrical frequency across a wider speed range.

Variable speed operation raises an operational issue with the auxiliary drive itself. Figure 1.10 shows the operating envelope of an auxiliary drive superimposed on a theoretical propeller curve and engine operating curve. Two regions are of interest, namely the vicinity of point A where the vessel is to operate under auxiliary propulsion (slow speed), and point B where the vessel is at rated speed, powered by the main engine. At point A, all power (auxiliary drive as well as electric power) is provided by the onboard generators, while at point B, the main engines supply propulsive as well as the electric power via the auxiliary drive. Two distinct operating modes can therefore be identified, namely low-speed motoring, and high-speed generating mode.

These two operating points will therefore determine the rating of the machine, chiefly the speed and power ratings. Comparing the operating envelopes of figures 1.6 and 1.10, the most realistic sizing is one where the machine is rated for the propulsion at low speed (point A), and then provides power in generating mode at point B under field-weakening operation above rated speed [25].

1.4.3 Combinator mode

Since a propeller is designed for a particular nominal speed, operating at off-design conditions with an FPP will imply that the propeller is not operating at its optimal pitch. If a CPP is available, adjusting both propeller pitch and speed implies that the propeller's operating point can be optimised over two dimensions. This is known as combinator mode, but is not commonly implemented (on commercial vessels) since this would necessitate two adjustable systems (both speed and pitch), increasing cost and complexity.

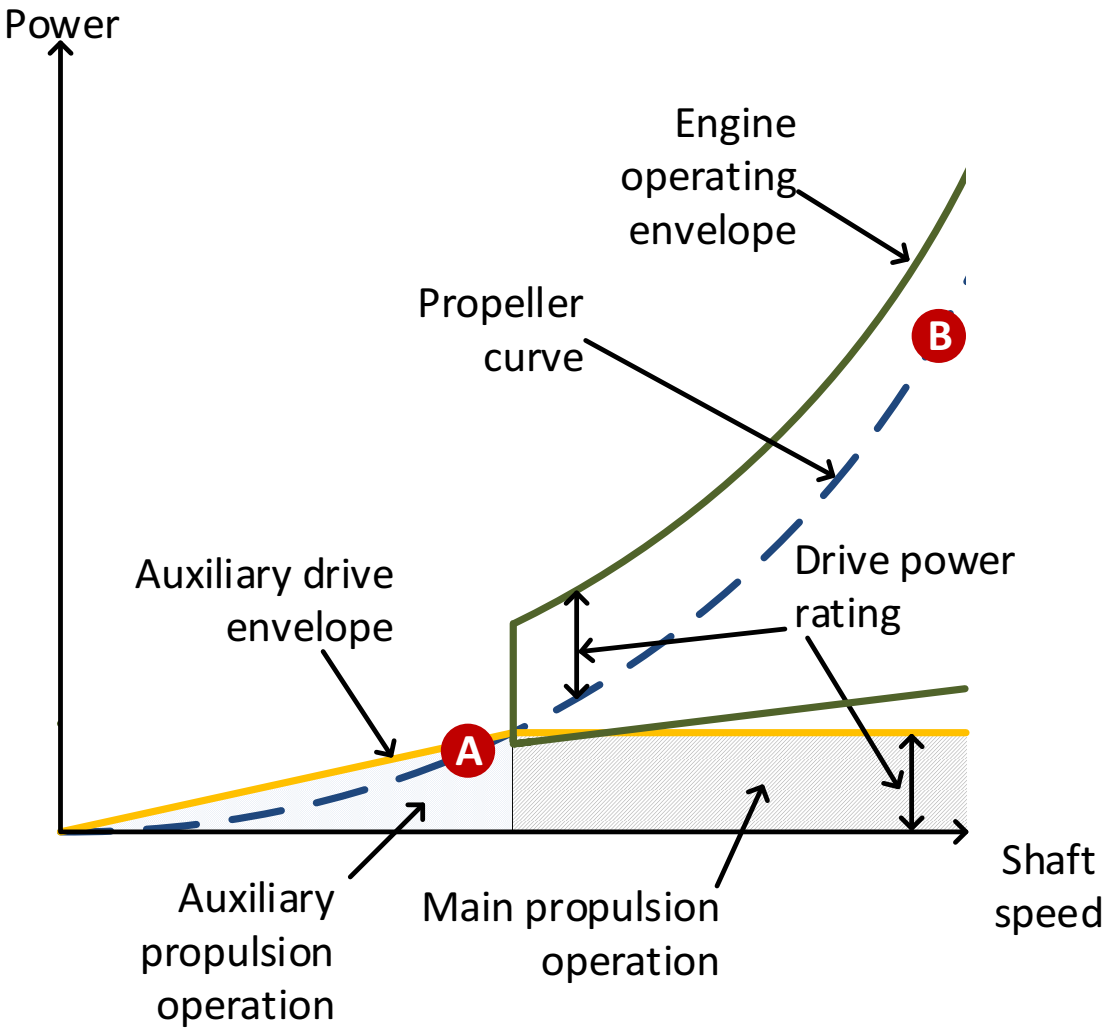

Figure 1.10 – Operating envelopes of auxiliary drive, main engine and propeller curve. Operating point A corresponds to low speed propulsion, while operating point B is sailing at rated speed.

In order to fully exploit the benefits of the (necessary) power electronic converter in the auxiliary drive, the adjustable speed capability of the drive should be utilised in order to operate in combinator mode, i.e. adjustable pitch and variable speed. By reducing shaft speed and adjusting propeller pitch for optimised efficiency the required shaft power can be optimised [41]. The rest of this work considers a system with a CPP operating in combinator mode.

Chapter 2

Vessel case studies

Data from two separate vessels, namely a RoRo vessel and a harbour tug was used as the basis for the analysis presented in this work. In close collaboration with the vessel operators, operational data was logged by the project partners from which the propulsion characteristics and operating profiles were documented [42]. These two vessels were selected because of the availability of data and relevance to the TEFLES project. They represent two different categories of vessel with their own individual machinery arrangements and operating profiles.

2.1 RoRo vessel

Within the TEFLES project, RoRo ferries were the main focus of work. In collaboration with a particular operator, a vessel was made available for case study, providing operational data to serve as the basis for investigation. The main particulars of the MV Auto Baltic (figure 2.1) are given in table 2.1. This vessel sails between the port of Vigo in North-West Spain and St-Nazaire on the French Atlantic coast transporting new vehicles for the European market. Its propulsion system consists of a single shaft installation with a CPP and a medium speed diesel engine with reduction gearbox.

Most importantly for the analysis, vessel operational data was also logged in order to design and assess the performance of the auxiliary drive system. An example of the measured speed and power profiles for the RoRo vessel is given in figure 2.2, from which a typical manoeuvring average was obtained across a number of similar

Parameter	Quantity
Vessel name	M/V Auto Baltic
Vessel length	138.5m
Gross Tonnage	18,979t
Main Engine rating	Wärtsilä 16V46A - 14,480kW at 500rpm
Service speed	20.2kt (10.4m/s)
Propulsion system	CPP at a nominal speed of 150rpm
Auxiliary system	
Average electrical power (at sea)	385kW
Average power factor	0.76
Average apparent power	503kVA

Table 2.1 – RoRo vessel particulars. [42]

Figure 2.1 – Case vessel MV Auto Baltic [42].

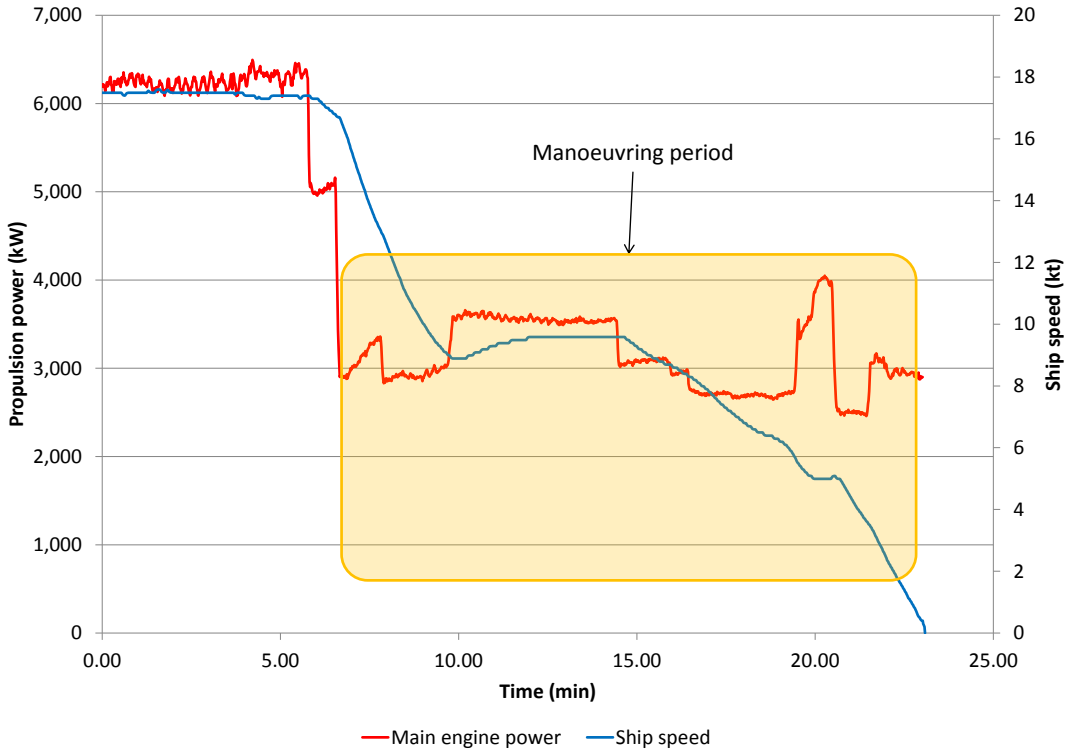

Figure 2.2 – Measured RoRo manoeuvring speed and power profile.

voyages. The RoRo's profile focuses on the in-harbour manoeuvring time between the point of port entry and berthing. This involves a manoeuvring period of around six minutes sailing at 6kt (3.09m/s). The use of the auxiliary drive to provide propulsion will be examined during this period of operation. Operational data was collected every second and averaged over the length of each individual operating condition (such as manoeuvring), giving piecewise linear approximations of the profiles. In the absence of standardised operating profile for marine vessels, this averaging process gives a representative profile of the vessel's operation, which is more indicative of typical operation and energy consumption patterns.

With the auxiliary drive directly replacing the main engine in this setup, a significant power demand over 1MW would be required even at just 6kt. In order to fully exploit the benefits of the (necessary) power electronic converter, the adjustable speed capability of the auxiliary drive should be utilised in order to operate in combinator mode, i.e. adjustable pitch and variable speed.

Based on Computational Fluid Dynamics (CFD) simulations the adjusted power demands were determined [42], tabulated in table 2.2. This demonstrates the significant power savings obtained by taking advantage of the controllability introduced

Ship speed (m/s)	Ship speed (kt)	Propeller power at 500rpm (kW)	Adjusted propeller power at 350rpm (kW)
0	0	2,190	751
3.6	7	2,700	1,085
5.1	10	2,980	1,676

Table 2.2 – RoRo propeller power demands at different speeds with adjusted pitch (combinator mode) [42].

by the bidirectional drive when compared with constant speed operation. These figures are then used for the adjusted propeller demand to obtain the averaged operating profile. The speeds indicated reflect engine shaft speed, with 350rpm being the manufacturer's minimum recommended speed for this engine. Hence low speed auxiliary propulsion is considered at the engine's minimum speed, permitting a smooth changeover from main engine to auxiliary propulsion.

For the RoRo vessel, three different permanent magnet machines were selected from commercially available devices as listed in table 2.3. Machines A and B are radial flux PMSMs while machine C is an axial flux PM machine. Machine A is mounted directly onto the propeller shaft while B and C are mounted on the high-speed side of the reduction gearbox. All three drives were sized for propulsion at manoeuvring, taking into consideration the use of combinator mode as outlined previously. The speed rating of the machine is determined by the installation topology, and hence whether mechanical reduction gears are used. All machines have similar (high) efficiencies, making savings highly dependent on the operating profile and propulsion setup. The direct-drive setup (Machine A) will have lower losses due to the absence of a gearbox. The other two drives are modelled with a constant 2% power loss at each gearing stage [22].

The different installations are illustrated in the structural drawings of figure 2.3 showing three different machines selected from commercially available devices. It must be noted that the AFM is of a significantly higher speed rating, but this serves to illustrate the size/space advantage. The figure also includes an illustration of the existing shaft generator arrangement, which consists of a conventional synchronous alternator. Comparing the setups it is clear how there is a significant size decrease in going to higher-speed machines (on the PTO/PTI), especially with an AFM.

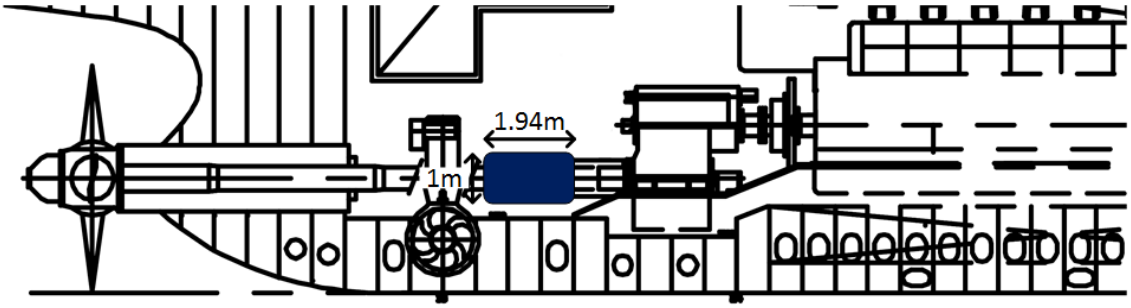

(a) direct-drive setup (machine A).

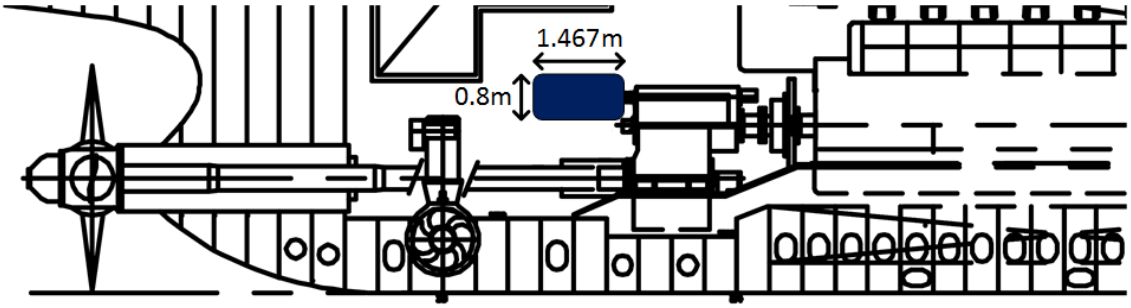

(b) High-speed setup on PTO/PTI (machine B).

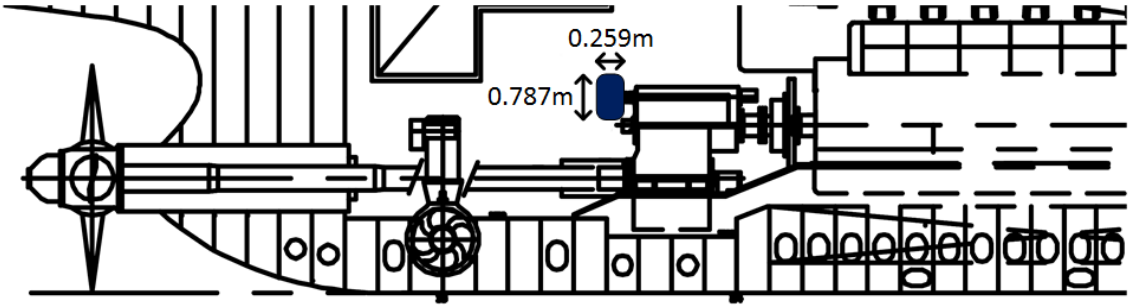

(c) AFM high-speed setup on PTO/PTI (machine C).

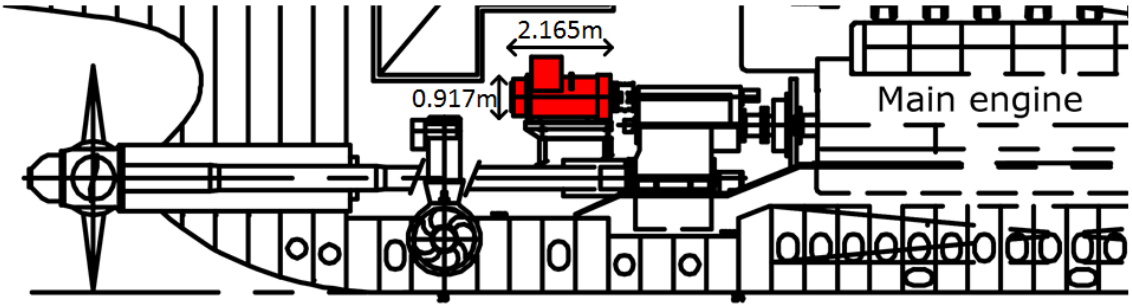

(d) Setup of existing shaft generator.

Figure 2.3 – Auxiliary drive machine setups.

	Machine A	Machine B	Machine C
Rated power (kW)	893	875	746
Rated speed (rpm)	173	400	3600
Rated torque (Nm)	49,296	20,900	1,980
Mass (kg)	12,470	4,680	340
Installation location	Direct	Geared	Geared
Machine type	Radial flux	Radial flux	Axial flux
Torque p.u. mass (Nm/kg)	3.95	4.47	5.82
Torque p.u. volume (kNm/m^3)	32.4	24.3	15.7
Efficiency at rated (%)	96.4	96.5	96

Table 2.3 – Selection of electric machines for auxiliary drive application on RoRo.

Parameter	Quantity
Tug name	Roque S
Type	Harbour tug
Vessel length	25.36m
Bollard pull	53t
Main Engine	2×1,469kW at 1,600rpm
Propulsion system	FPP

Table 2.4 – Tug particulars. [42]

2.2 Tug boat

The vessel details for the tug boat (figure 2.4) are listed in table 2.4, with the operating profile shown in figure 2.5, including actual port and starboard engine measurements together with the boat speed profile [42]. This reflects a typical working day of the tug in Vigo harbour which is the vessel's operating base. The power spikes seen during the standby period are associated with the tug maintaining station (hence the zero speed). The tug's propulsion arrangement consists of two high-speed diesel engines on two separate shaftlines powering two azimuthing thrusters.

The selection of machines for the tug case is listed in table 2.5, showing two machines (both PMSM) sized for two different operating cases. In the first case, Machine A is sized to provide auxiliary propulsion in the standby mode of operation. In the second case, Machine B is sized to provide power during the transit periods. In either case, the only possible installation is on the high-speed shaft at the main engine side,

Figure 2.4 – Case tug Roque S [42].

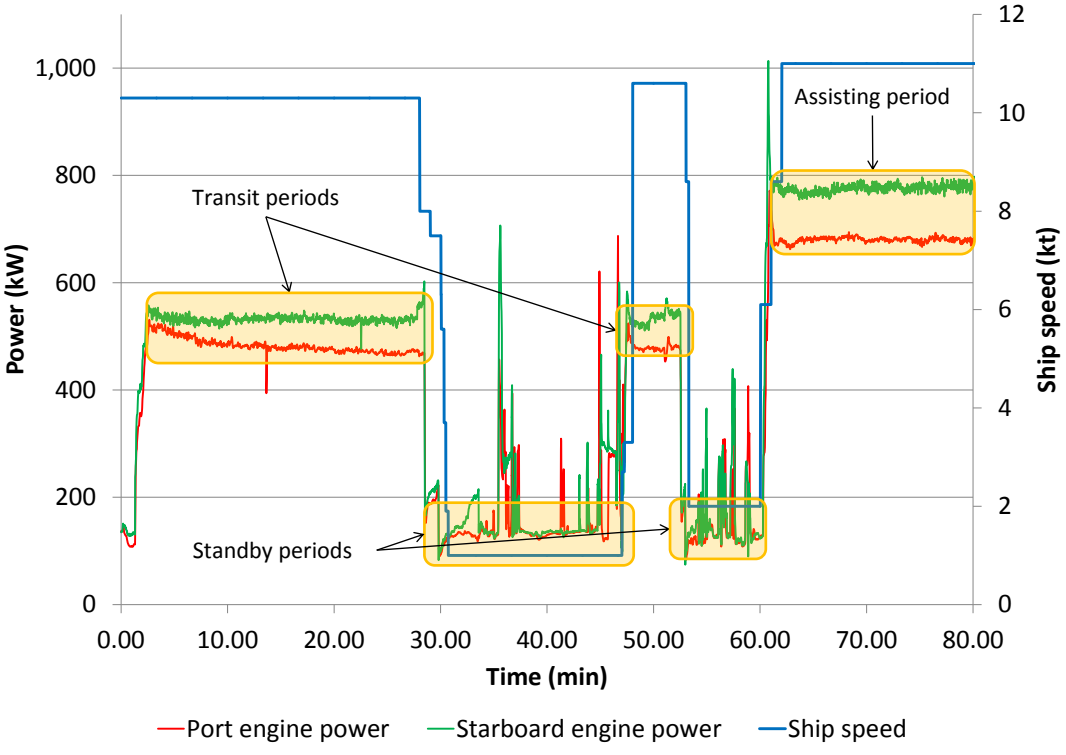

Figure 2.5 – Measured tug operating profile; in-harbour operation.

	Machine A	Machine B
Tug operation (under auxiliary propulsion)	Idling	Transit
Rated power (kW)	160	628
Rated speed (rpm)	600	800
Rated torque (Nm)	2,546	7,500
Mass (kg)	1,125	3,040
Machine type	Radial flux	Radial flux
Torque p.u. mass (Nm/kg)	2.26	2.47
Torque p.u. volume (kNm/m^3)	21.4	12.44
Efficiency at rated (%)	95.5	97.2

Table 2.5 – Selection of auxiliary drives for auxiliary drive application on tug.

since the reduction gearbox is integrated to the azimuthing thrusters.

2.3 Modelling

In order to make use of the available operational data and obtain estimates of the emissions produced by the various machinery setups, a complete propulsion system model was built. The averaged operational profiles of the two vessels (obtained from the data of figures 2.2 and 2.5) are used as inputs to the model. This determines the instantaneous power demands on the propulsion system and defines the total energy required by the vessel over the snapshots of the operational scenarios considered in this study. The emissions produced are a function of the energy consumption and the various sources of the energy itself, i.e. main engine or auxiliary engines.

2.3.1 Electric drive model

The drive equations allow accurate simulations of drive behaviour but present a computational penalty in terms of long simulation times. The solution adopted in this investigation was to create an efficiency chart of the machine according to the operating points demanded by the particular propulsion system topology, generating a look up table of overall efficiencies, obtained from the ratio P_{out}:P_{in} calculated using the detailed simulation model. The detailed d-q simulation is therefore performed across all operating points of interest as defined *a priori* by the drive topology and operating points, by varying the load torque (T_l) and the desired speed setting ω^*,

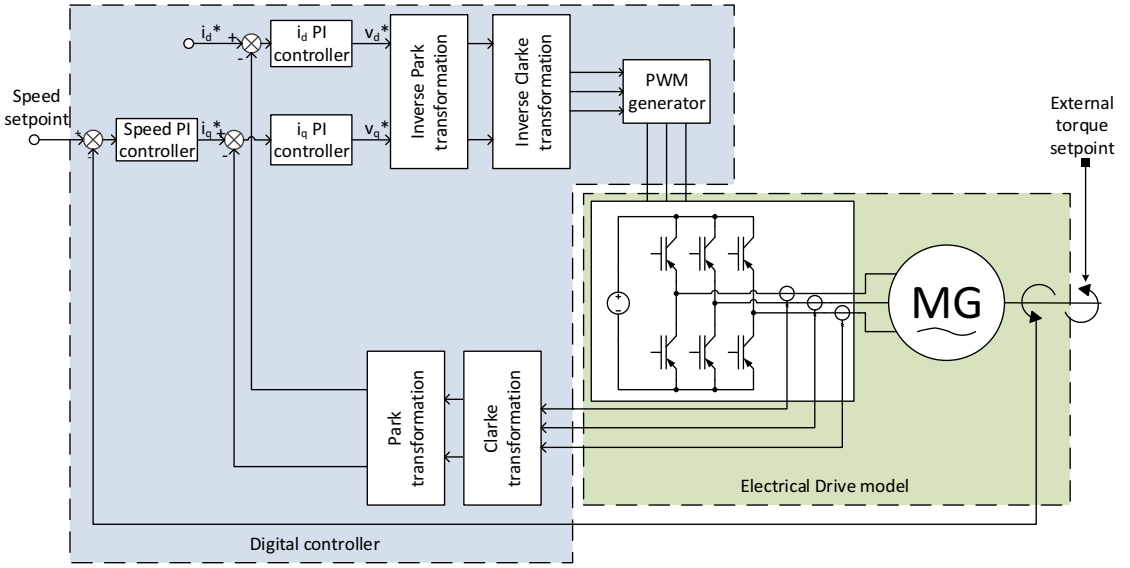

Figure 2.6 – Drive simulation overview.

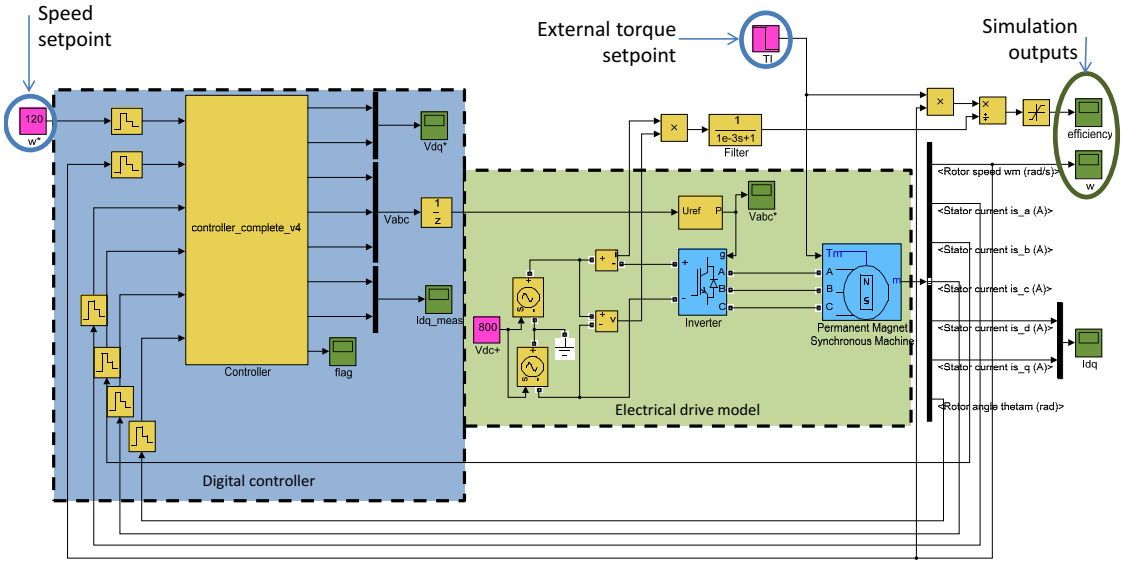

Figure 2.7 – Drive model setup in Simulink.

schematically illustrated as figure 2.6 and implemented in Simulink as figure 2.7. The parameters associated with the machine model are obtained from manufacturer data available in product catalogues. This methodology therefore permits commercially available machines and converters to be easily represented. The algorithm developed for the drive controller in figure 2.7 is listed as Appendix E.

Losses across the power electronic converter are treated similarly by utilising an efficiency plot as a function of percentage loading, obtained from manufacturer catalogues, allowing quick simulation without a detailed representation of device switching action. The combination of calculated machine efficiencies and converter losses permit the total drive loss at each identified operating point to be determined

Auxiliary engine type	Fuel type	Emission factor (g/kWh)					sfc (g/kWh)
		NO_x	SO_2	CO_2	HC	PM	
Medium-speed diesel	MGO	13.9	1.1	690	0.4	0.3	217
	MGO (0.1% S)	13.9	0.44	690	0.4	0.3	217
	MDO	13.9	4.3	690	0.4	0.3	217
	RO	14.7	12.3	722	0.4	0.8	227
High-speed diesel	MGO	10.9	1.1	690	0.4	0.3	217
	MGO (0.1% S)	10.9	0.44	690	0.4	0.3	217
	MDO	10.9	4.3	690	0.4	0.3	217
	RO	11.6	12.3	722	0.4	0.8	227

Table 2.6 – Emission factors for auxiliary engines [19].

by means of interpolation for intermediate points.

2.3.2 Combustion engine model

The purpose of this model is to determine the fuel consumption and emissions produced by engine operation. The approach adopted was to consider the cumulative energy demanded from each prime mover as the integral of instantaneous power loadings. The emissions produced by the engines to generate this energy (kWh) are obtained by means of emission factors [19]. These averaged emission factors are particular to individual engine types, and also vary according to the fuel used. Since no journey will be identical to another even when under similar conditions, this averaging (combined with the averaged power profiles) gives a basis for comparison and evaluation of improvements brought about by auxiliary drives or hybridised sources. A further variable is the different percentage loadings on the engine, which is addressed by using different emission factors for different operating modes [19]. Tables 2.6 and 2.7 list the emission factors for auxiliary engines (powering generator sets) and main engines for different types of fuel. MGO represents Marine Gasoil (with a Sulphur percentage content of 0.25%), while MDO represents Marine Diesel Oil, and RO describes Residual Oil (which is used interchangeably with HFO).

2.3.3 Power loading

The allocation of power demands to the different subsystems is at the heart of this or any hybridised drive system. This directly determines the energy generated by each prime mover and hence the resultant emission figures.

Auxiliary engine type	Fuel type	Emission factor (g/kWh)					sfc (g/kWh)
		NO_x	SO_2	CO_2	HC	PM	
Medium-speed diesel	MGO	10.6	1.1	710	1.5	0.9	223
	MGO (0.1% S)	10.6	0.44	710	1.5	0.9	223
	MDO	10.6	4.5	710	1.5	0.9	223
	RO	11.2	12.7	745	1.5	2.4	234
High-speed diesel	MGO	9.6	1.1	710	0.6	0.9	223
	MGO (0.1% S)	9.6	0.44	710	0.6	0.9	223
	MDO	9.6	4.5	710	0.6	0.9	223
	RO	10.2	12.7	745	0.6	2.4	234

Table 2.7 – Emission factors for main engines [19].

The vessel speed demand in the form of a speed time-series is used as an input to the model. This speed demand is converted to a propulsive power demand by means of a speed-power look up table obtained from vessels' sea trials data. As a result, the power demand profile is a direct representation of the real propulsive power without any additional model uncertainties. This speed-power look up table takes into account the combinator mode power demand.

The load is allocated to the electric drive by a control logic decision block which assumes a changeover threshold figure corresponding to the drive's rating. This maximises the time spent in auxiliary propulsion such that the main engine load is reduced to zero once the power demand drops below the drive's rating. Throughout the operational scenario, the vessel's auxiliary electrical demand is imposed as an additional load on the auxiliary generators. This rule-based system was adopted to examine the effect of the auxiliary drive itself without detailed consideration of the energy management system, which is addressed separately in chapter 7.

Such a simulation setup is energy-centric by design where the consideration of interest is the power loss across the various propulsion chain components. This permits the comparison of different auxiliary drive topologies and strategies without requiring detailed simulations capturing transient behaviour. The overall schematic of the developed model is illustrated in figure 2.8, showing the topology of the various sub-models described in the previous sections.

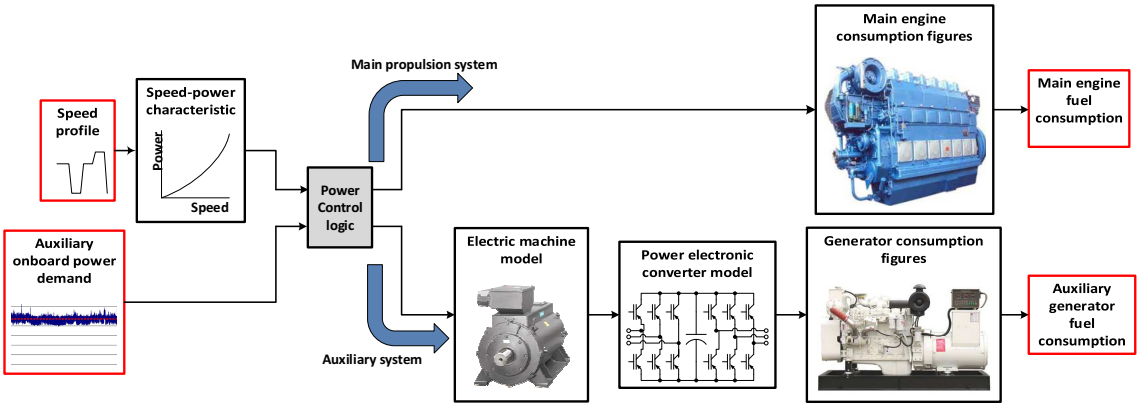

Figure 2.8 – Propulsion system simulation setup.

2.4 Results

2.4.1 Topology comparison

The results for the RoRo case are summarised in table 2.8 for the six minute averaged manoeuvring period. The savings between the three drives are very similar, with Machine A showing marginally higher savings due to the reduced mechanical losses compared to the other setups as expected. The savings in fuel consumption, CO_2 and NO_x emissions are around 45% of the original conventional case. On the other hand SO_x emissions are significantly reduced, due to the use of marine gasoil (MGO) with a much lower Sulphur content (0.1%) as opposed to the heavy fuel oil used in the main engines. Conversely this cleaner fuel is more expensive than the HFO and hence fuel savings (monetary) are not commensurate with the actual consumption savings due to the higher cost of the MGO [11, 16].

Table 2.9 shows the results of the tug case simulation for the standby and transit auxiliary propulsion cases. In these cases, the use of auxiliary drives has not resulted in any reductions in consumption and emissions; instead these have increased. This was an unexpected result since it was initially assumed that due to the greater variability in the operating profile (see figure 2.5), an overall improvement in fuel consumption and emissions would be observed. This outcome can be explained by the fact that the use of the auxiliary drive in the tug case adds additional losses to the propulsion chain. The main (mechanical) propulsion system returns better consumption figures than the electrical auxiliary system at higher loadings, such that over the complete scenario study, the net overall performance in terms of emissions was inferior to the original case with no auxiliary propulsion. This is in agreement

	Current estimate	Machine A		Machine B		Machine C	
Setup type		Direct		Geared		Geared	
Fuel consumption (kg)	28.15	15.12	-46.29%	15.15	-46.18%	15.33	-45.54%
Fuel cost (€)	14.41	10.90	-24.37%	10.92	-24.23%	11.05	-23.33%
CO_2 emission (kg)	89.63	48.07	-46.37%	48.18	-46.25%	48.73	-45.63%
NO_x emission (g)	1.35	0.76	-43.62%	0.76	-43.50%	0.77	-42.85%
SO_x emission (kg)	1.53	0.08	-94.98%	0.08	-94.97%	0.08	-94.92%

Table 2.8 – Results comparison for RoRo case.

with the observation made in [43]. Contrary to the RoRo ship, the main engine on the tug runs on the same fuel as the auxiliary engines, hence no emission savings are realised by the possibility of running on different, cleaner fuels.

2.4.2 Machine comparison

A separate comparison was performed to compare induction and permanent magnet machines over the vessel's complete operating profile, i.e. over both manoeuvring and at sea conditions. It has been established in the previous section how savings are realisable using auxiliary drives on the RoRo during the manoeuvring condition. Using data available for the RoRo vessel which typically operates with the operating profile of table 2.10 the relative merits of different machines can be examined. Within these conditions, propulsion is to be provided by the auxiliary drive for the manoeuvring periods, while the drive is to provide power to the onboard grid by operating as a shaft generator when at sea. The whole propulsion system is considered to be shut down while the vessel is berthed.

For a direct comparison, two similarly rated machines were selected from manufacturer catalogues, fitted to a PTO/PTI on the MRG (as in figure 1.9b), with an additional PTO gear ratio of 2.3. This gives electrical machine speeds of 800rpm and 1142rpm

	Standby operation			Transit operation		
	Machine A	Current estimate	Difference	Machine B	Current estimate	Difference
Fuel consumption (kg)	37.34	36.66	1.85%	177.04	175.24	1.03%
Fuel cost (€)	26.92	26.43	1.85%	127.65	126.35	1.03%
CO_2 emissions (kg)	118.76	116.70	1.77%	563.00	558.00	0.90%
NO_x emissions (kg)	1.88	1.58	18.88%	8.89	7.54	17.90%
SO_x emissions (kg)	0.19	0.18	4.71%	0.90	0.86	3.82%

Table 2.9 – Results comparison for tug case.

Operating condition	Percentage of time
At sea	75%
Berthed	20%
Manoeuvring	5%

Table 2.10 – Time spent in each operating condition [42].

for the motoring and generation periods respectively, for the operating specifications as defined in table 2.11. These two operating conditions correspond to points A and B in the operating envelope of figure 1.10. The parameters for the PMSM and IM are given in table 2.12. Since the influence of the additional current for field-weakening was to be examined on the overall losses, a detailed model of the power electronic converter was used to generate a LUT at the operating points of interest similar to the method employed in the electric machine models described previously. A simple field-weakening strategy was implemented as described in section 1.2.1. The simulation was run until steady state was reached and the resultant efficiency determined at each operating point of interest.

An example of the simulation of field-weakening operation is shown as figure 2.9 which shows the step response of the auxiliary drive with a PMSM accelerating to the motoring setpoint as defined in table 2.11. The direct axis current is maintained at 0A for minimum copper losses, while the quadrature current is clamped to rated value for maximum torque during acceleration. Once the desired speed has been

Motoring condition	
Drive speed	800 rpm
Power demand (mechanical)	580 kW
Generating condition	
Drive speed	1,143 rpm
Auxiliary power demand (electrical)	400 kW
Auxiliary load power factor	0.8 lagging

Table 2.11 – Operating points specification.

	Machine A	Machine B
Machine type	PMSM	IM
Rated power (kW)	1,005	970
Rated speed (rpm)	800	744
Rated torque (Nm)	12,000	12,476
Mass (kg)	4,100	5,450
Torque p.u. mass (Nm/kg)	2.93	2.29
Efficiency at rated (%)	97.3	95.4

Table 2.12 – Parameters for PMSM/IM comparison.

reached, the current reduces to its steady state value.

Figure 2.10 shows the corresponding characteristic when in generating mode. The motor is accelerated to the desired speed (under no load), with the direct current observed to take on a negative (non-zero) value in order to permit over speeding of the machine. The quadrature current is decreased as a function of the maximum permissible current in the stator in order to prevent overloading. A negative torque (mechanical power fed from the shaft) is applied at 1s, with the quadrature current then settling to a negative steady state value, indicating real power being fed back to the electric supply. Characteristics for the induction machine drive are similar, except that the direct current takes on a non-zero value and is decreased accordingly during field-weakening.

The steady-state results of the two drives are compared in table 2.13 highlighting the current values together with overall drive efficiency. While the PMSM drive shows a higher efficiency during motoring condition, the efficiency during the generating period is marginally lower than the IM drive. This comes about since a larger current magnitude is now injected into the drive to force field-weakening, leading to

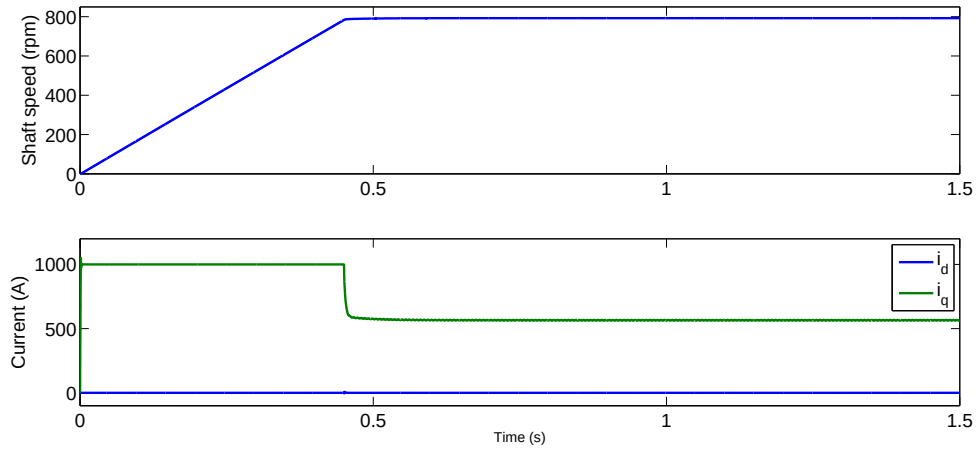

Figure 2.9 – Simulated PMSM step (motoring).

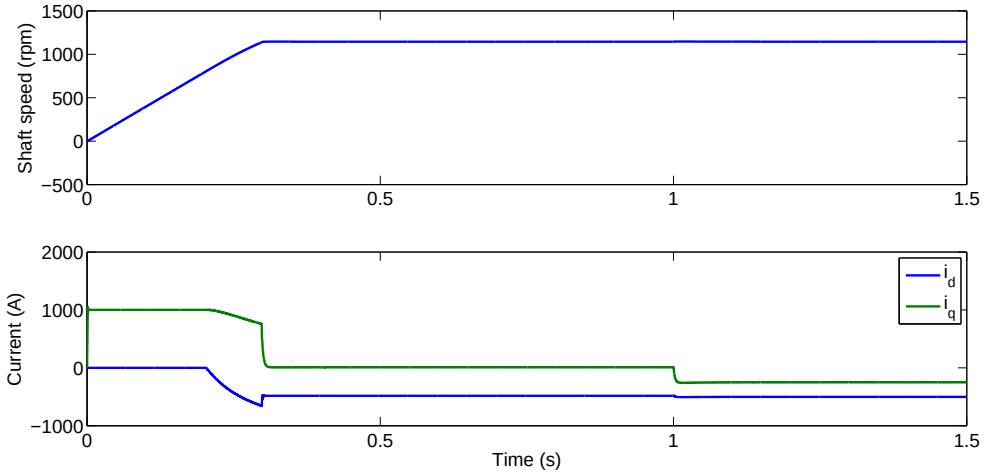

Figure 2.10 – Simulated PMSM step (generating).

	Motoring mode	Generating mode
i_d (A)	0	−500
i_q (A)	565	−250
Stator current (A)	565	559
Efficiency	97%	92%

(a) Steady-state characteristics of PMSM drive.

	Motoring mode	Generating mode
i_d (A)	247	170
i_q (A)	695	−450
Stator current (A)	737	481
Efficiency	95%	93%

(b) Steady-state characteristics of IM drive.

Table 2.13 – Steady-state characteristics of drives with different machines.

	Losses during manoeuvring period	Losses at sea
PMSM drive	39.26 kWh	851.35 kWh
IM drive	56.98 kWh	790.32 kWh
PMSM vs IM	−31%	7.7%

Table 2.14 – Comparison of losses between machine types.

higher (copper) losses. A typical journey of the RoRo in question (berth to berth) lasts around 28 hours, and combining the averaged powers of table 2.11 and the operational profile of table 2.10 with the results obtained, leads to the summarised losses of table 2.14. Clearly, though the PMSM drive shows a lower efficiency while generating at sea, when motoring an increased efficiency of around 31% can be realised. However, the greater proportion of time spent at sea implies that the energy lost will be greater [10].

Fundamentally, all energy on board a ship translates to an equivalent fuel cost. The losses at sea (when generating) are supplied by the main engine, while those during the manoeuvring period are supplied by the auxiliary generators. Based on the typical Specific Fuel Consumption (sfc) figures for these engine types [19], the equivalent fuel consumed to supply these losses, and the bunker cost [44] is shown in table 2.15. This illustrates how due to the lower cost of HFO used by the main engine, the economic savings due to the higher (generating) efficiency of the IM drive are much smaller since they are offset by the higher cost of the fuel used in the auxiliary generators, but when considering the total losses due to the operating profile, an overall improvement is seen with the IM drive. The resultant losses/savings will

therefore be determined based on the particular operating profile, highlighting the importance of considering the actual design conditions for which the system is to be designed [24, 45].

	Equivalent fuel loss during manoeuvring (MGO)	Equivalent fuel loss during at sea period (HFO)	Total equivalent cost of fuel to supply losses
PMSM drive	8.52kg	181.34kg	€79.75
IM drive	12.36kg	168.34kg	€76.76
PMSM vs IM	*−31%*	*+7.7%*	*+3.8%*

Table 2.15 – Economic comparison of losses due to different auxiliary drives.

Chapter 3

The cold ironing environment

Emissions from ships don't stop when vessels are berthed. Though the propulsion demand is zero, ships still need to run their onboard auxiliary plant, both for operational purposes (e.g. running of extractor fans, onboard cranes etc...) as well as for the onboard hotel load. This power is usually provided from the auxiliary generators, or alternatively (depending on the load levels involved) by a smaller onboard generator known as the emergency or harbour generator. These are typically diesel engines, producing emissions from the combustion of fossil fuels.

The operation of the onboard generators when in port can be minimised by connecting vessels to the shore electrical supply (a practice known as cold ironing) such that the power requirement is met by land-based generation, supplying the electrical energy from a centralised source. This gives a locally emission-free solution, though the resultant overall airborne emissions will be a function of the generation mix employed on land [14, 46–48]. Legislation, both current and upcoming, aims to incentivise and promote the uptake of cold ironing systems and reduce the emissions generated at berth. Within EU ports, the Sulphur Directive [49] limits the Sulphur content of fuels used by ships in EU ports to less than 0.1% by mass when the scheduled stay is longer than two hours. Ships which shut down all engines and use a shore electrical supply are considered compliant. A similar Sulphur limit is in place since 1 January 2015 in Emission Control Areas (ECAs), with a global Sulphur limit being reduced from 3.5% to 0.5% in 2020 (or 2025 pending a review in 2018) [50]. Shore supply is a solution to meeting these limits while berthed in harbour, providing an alternative to the use of expensive, low sulphur content fuel [48, 51, 52].

At the same time as increasingly stringent environmental requirements, newly developed technical standards aim at facilitating the expectations and requirements for both port operators as well as visiting vessels, by setting out the required components as well as quality of supply expected at the berths. Joint standard IEC/ISO/IEEE 80005-1 sets out the requirements for High Voltage Shore Connections (HVSC) [53], while IEC/IEEE 80005-3 (pre-standard) deals with Low Voltage Shore Connections (LVSC) [54] for vessels with a lower power demand based on similar concepts (such as the location of the frequency converter on shore and the need for galvanic isolation for each connection)[2]. The push for standardisation is aimed at easing ship to shore connections and hence help break down (one of the) barriers in the adoption of cold ironing.

From an electrical engineering point of view, the shore connection of vessels does not require new technologies or devices, but rather an application of existing systems to create feasible ship-to-shore connections [56]. Shore connection has been a common feature in shipyards, where long stays as well as onboard works would make the shutting down of shore generators a feasible consideration. Shipyards typically have shore connection facilities at quaysides, from which a cable is spooled to the berthed ship. Connection is made by means of bolted terminations onto a blacked out vessel – the provision here is for a one-off connection during the vessel's relatively prolonged stay. Ease of connection as well as seamless transfer of power are secondary considerations, and furthermore the vessel is generally not under normal operation during its stay. On the other hand, cold ironing during operational stays needs to be fast in connection, provide the demanded power and provide a safe and seamless transfer between ship and shore power.

The fundamental components required in a cold ironing system as per IEC/ISO/IEEE 80005-1 are shown in figure 3.1. This is a representative schematic showing the requirements for a single connection, and the salient components are discussed in the following sections. A number of electrical issues, especially in terms of protection and safety, are of concern to these shore connection installations. In [57], the authors discuss the dangerous touch voltages created in the case of a ship connected to the shore supply with a phase to ground fault in the system, arising because of a common earthing situation. Grounding is also discussed in [58], while [59] looks at

[2]Part 2 of the standard IEC/ISO/IEEE 80005-2 [55] (pre-standard) relates to the communication and control between ship and shore.

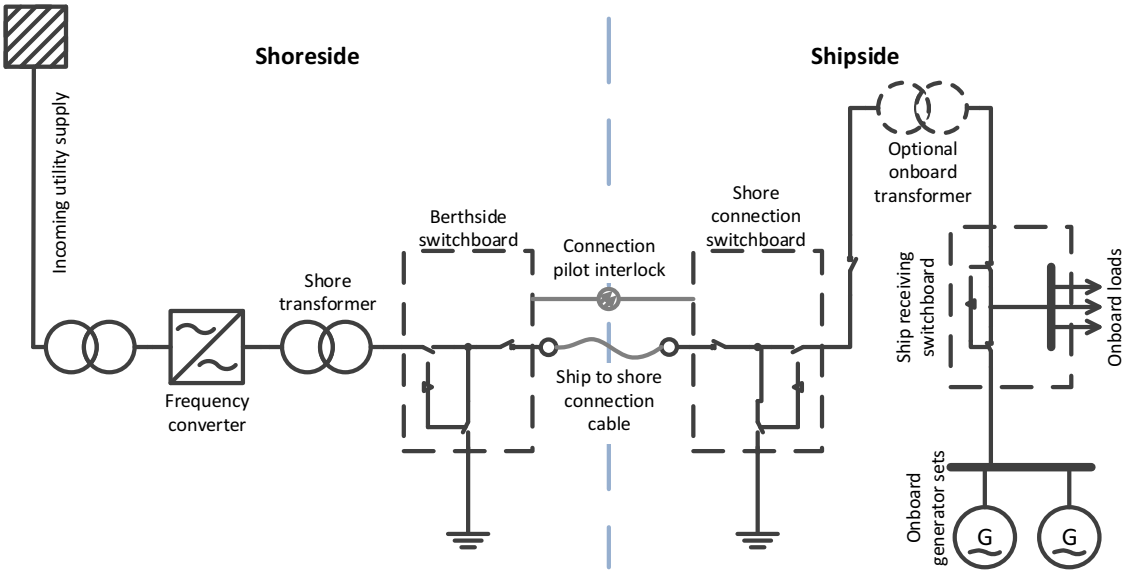

Figure 3.1 – Typical cold ironing system arrangement.

the more specific aspect of residual charge in the ship-to-shore cable and the need for a grounding switch. Surge protection is discussed in [60] outlining the need for surge arresters both on shoreside as well as onboard, with the grounding configuration determining type and rating of the protective devices. An additional protective concern is the short circuit current capability of the installation, which is addressed in [61]. Common to all these works is the appreciation of the fact that each project is unique, requiring an in depth study for each cold ironing installation [51]. In this work, the optimal shoreside configuration is investigated, together with the impact of the cold ironing system on the power quality.

3.1 Shoreside requirements

3.1.1 Transformers

At the utility point of connection, a step-down transformer is required to provide the Medium Voltage (MV) distribution for the cold ironing system from the High Voltage (HV) utility distribution voltage. This can be required in addition to the existing port substation or integrated into the current distribution system if there is sufficient margin for additional capacity.

This utility interface transformer can be placed at a distance from the berthside at any convenient location. Cabling must be provided from the transformer yard to the

required point of ship-to-shore connection.

At the connection points, a further transformer can be required for purposes of galvanic isolation of each ship to shore connection [53,54] . By providing a galvanically isolated supply for each connected vessel, any occurring fault should not affect adjacent consumers. The transformer can also provide a voltage level adjustment to match the voltage required by the vessel, if different from the shore voltage.

The shore arrangement is also necessary to provide a grounding system compatible with the vessel's original electrical grounding philosophy. ISO/IEC/IEEE 80005-1 calls for the connecting transformers to be of a DYn type, i.e. with a delta connected high voltage winding and a star connected low-voltage winding with access to the star point which is earthed through an earthing resistance. The fundamental idea is to maintain the ship's onboard grounding philosophy such that a similar ground fault protection and fault levels are unchanged.

Note on grounding arrangements

Vessels with a low voltage power system are generally isolated, i.e. ungrounded. This provision prevents total loss of supply in the case of a single ground fault [62]. This differs from shoreside installations where the priority is the immediate isolation of a faulted system. In the case of a high voltage system, the power system is grounded via High Resistance Grounding (HRG) at the generators' star point. This prevents floating high voltages and serves to limit any resultant fault currents to a value set by the Neutral Grounding Resistance (NGR)'s value. ISO/IEC/IEEE 80005-1 requires the ship's hull to be bonded to the shoreside ground in order to prevent hazardous touch potentials from developing (specified to be less than 30V). Thus the provision of a separate ground requires an isolating transformer – which is required by low voltage ships due to their 'non-standard' voltage level.

3.1.2 Automated earthing switch

An automated earthing switch with interlock is necessary to ensure safety of operating personnel when handling cables. This ensures that the cable is solidly earthed when the system is off, and should automatically be engaged on de-energisation of the cable. The earthing switch serves to ensure that the cable is fully discharged before

Rotary converter	Static converter
Fixed output frequency	Programmable output frequency
Permanent installation	Modular installation
Output paralleling is complex	Modular and expandable system
Downgraded operation is not possible after failure	Reduced power operation possible due to component failure

Table 3.1 – Comparison of rotary and static converters [65].

manual handling. Due to the cable's capacitive characteristics, significant energy can be stored in the cable length, which is quickly discharged by closure of the earthing switch [59].

3.1.3 Frequency converter

The conversion of frequencies is more costly than the conversion of voltage. Small systems can utilise rotating converters, which consist of a motor/generator pair coupled on a common shaft. The motor runs at the supply frequency, with the generator supplying power at the desired frequency. This is set by the choice of an appropriate pole number for the machines. Running at the same speed, the relation between the respective frequencies and poles is $f_m/P_m = f_g/P_g$ where the subscripts indicate the generating or motoring machines respectively. Thus for a conversion from 50Hz to 60Hz, the appropriate pole ratio will be $P_g : P_m = 6 : 5$. The disadvantages of rotating converters are that they required periodic maintenance on the rotating parts, as well as the need to have two fully rated machines of significant size. The efficiency of such a system is also likely to be lower than that for a stationary converter especially for part loadings [63]. With required multi-MW ratings, the cost and size of these rotary converters places them at a disadvantage compared to static converters.

Stationary converters utilise solid state power electronics to convert between frequencies via an intermediate DC link. Similarly to industrial drives, converters which utilise IGBTs and an active front end are available up to 2MVA, while for power ratings up to 14MVA, IGCT converters with 12-pulse diode front ends are possible [64]. The biggest disadvantage of these converters is the higher cost associated with them. Efficiencies are however higher than rotating converters, with an example of the efficiency plots across a range of loadings shown in figure 3.2 [63].

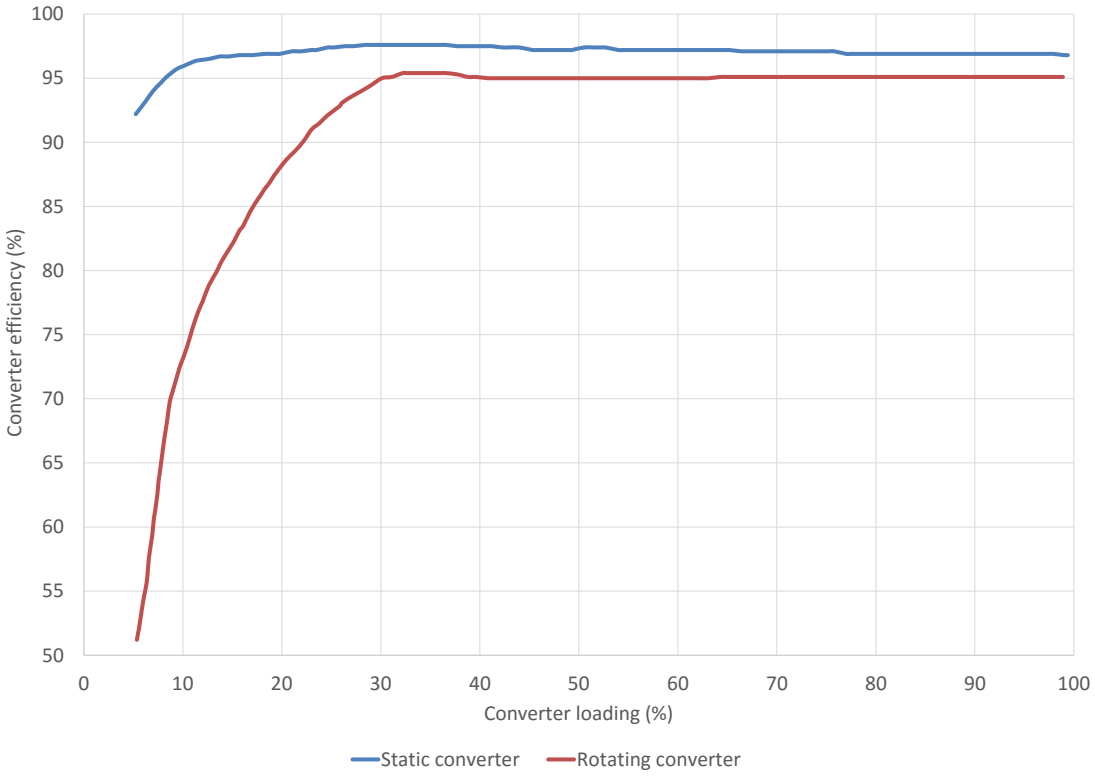

Figure 3.2 – Efficiency plots for static and rotary frequency converters [63].

High voltage converters are more expensive and specialised than their low voltage counterparts. Commercially available systems are offered with low voltage converters and step-down and step-up transformers at each end respectively [64, 66].

3.1.4 Communications interface

A communication interface is required to synchronise the shipboard supply with the shore grid when implementing a seamless transfer of power. This furthermore provdes added protection in that the connection can be shut down if a faulted condition is detected onboard. The communication cabling is integrated in the ship connection cable and is in the form of an optical fibre link. An international standard (part 2 of ISO/IEC/IEEE 80005) is currently being developed [55].

3.1.5 Shore connection switchboard

The shore connection switchboard includes the protection devices and earthing interlocks necessary for the safe connection and disconnection of the shore supply cable. This must be placed in a safe and secure location, in the form of cabinet

or cubicle. The location of this shore connection box must take into account the berthing location of vessels, as well as shoreside requirements such as the importance of not obstructing berthside crane operations. Each port setup will be an individual case, which must be tackled individually at project stage.

The location and frequency of these switchboards is an important consideration, whereby the possible number of connected ships according to their berthing position is hence determined. This choice is somewhat eased for berthing operations which permit only docking at predefined locations such as ferry terminals.

3.1.6 Shore cabling

An infrastructural backbone is required from the port substation to the shore connection boxes. This entails high voltage cables being laid across the port to connect the necessary points. Trenching would be required to route and protect the cables, and if not already present, this will represent a significant additional cost. This will be a chief limiting factor in terms of retrofitting ports with an HV infrastructure since major civil engineering works will be required, creating disruption to normal port operations.

3.2 Shipside requirements

3.2.1 Shore connection panel

Onboard the ship, the shore connection panel provides the physical connection receptacle for the connecting cables. It provides the protection relays and circuit breakers for onboard safety as well as interfacing to the onboard power management for synchronisation and protection. Physically it must be placed at a convenient yet secure location which allows for easy shoreside access.

This represents the biggest adaptation requirement since a physical space must be prepared at a suitable location. This location must be accessible from the shoreside as well as protectable from inclement weather. The location of the equipment will imply whether the vessel can berth alongside on any side. This is not a problem for vessels which consistently call at the same location, but can prove problematic if the

shore connection is aimed at multiple ports and berths. The same applies to the location of the connection along the ship. This links with the shoreside location of the connection panel, whose respective placement will determine the possibility of shore connections for individual ships. The frequency of placement will determine the possible number of vessels which can connect.

The actual connecting cable may either be held in an onboard spool with an associated derrick for handling, or be supplied by the port using some means of craning system. The advantage of having a ship supplied cable is that handling equipment such as cranes are minimised, since simply a spool coiling system is needed for cable retrieval and avoids having to lift heavy cables. The location (onboard or onshore) is ship-type specific, and is defined in [53].

3.2.2 Onboard transformer

An onboard transformer would be required if the vessel operates solely a low voltage system or a voltage level incompatible with that supplied from shore. This can be placed remote from the shore connection panel via a fixed installation. This transformer also provides the necessary galvanic isolation and serves to preserve the onboard grounding philosophy.

3.2.3 Ship receiving switchboard

This switchboard would generally be part of the main switchboard, and serves to distribute the shore power to the rest of the vessel's system. It would contain protection and metering facilities.

3.2.4 Power management modifications

Apart from the physical installation changes required on the system, a further requirement is the modification of the power/energy management system to handle the shore connection. This would imply the prioritisation of this source when available while maintaining a standby capacity from an onboard generator. The switchover between onboard and shore power must also be catered for, with the provision to provide synchronisation between the sources. In cases where a software

based management system is not used, this would imply changes in the protective and control relaying.

The changeover from onboard power to shore supply is permitted via two techniques, either load transfer via blackout or load transfer via automatic synchronisation. With the blackout option, the load transfer occurs onto a 'dead' ship once the onboard supply has been switched off. Clearly this has disadvantages in that power is lost for a brief interval while the changeover process is effected, but is an otherwise simple procedure. For ship loads which cannot sustain any power blackout, automatic synchronisation sees the temporary parallel operation of both shore and onboard supplies while the automatic synchroniser adjusts the supplies before switching over to the shore supply. A maximum transfer time limit is to be defined which if exceeded results in disconnection of the supply and sounding of an alarm. This seamless transfer is of course more desirable for cruise ships and ferries.

3.3 The environmental case

The shore connection of ships shifts the generation of emissions from the harbour area to the utility power generating stations located onshore. The harbour area is generally close to habitation but is also an area of heavy industrial activity. Ships running onboard auxiliary generators in order to provide their electricity needs contribute to this environment, hence cold ironing serves to limit the emissions produced in-harbour. Furthermore, the shoreside generating mix can also include renewable sources which are an emission-free solution during operation.

Emission factors consider a linear relationship between the energy converted by the prime mover and the emissions produced. Emission factors for the various pollutants (CO_2, SO_2, NO_x) for onboard auxiliary engines are found from literature, and in use within this work are those found in [19] used in previous sections, tabulated as table 2.6.

Similar figures the shoreside power option were calculated using data from various sources. Most relevant to this study are two documents published by the UK's Department of Energy and Climate Change (DECC) namely the UK Greenhouse Gas Inventory, 1990 to 2010 (UKGHGI) [67] and the Digest of United Kingdom Energy Statistics 2011 (DUKES) [68]. These both refer to 2010 as the latest year data is

Pollutant	Mean AE emissions (g/kWhe)	Power station emissions (g/kWhe)	Reduction (%)
NO_x	14.1	1.2	91.6
CO	0.9	0.2	75.3
SO_2	2.2	1.2	45.8
CO_2	718.6	542.6	24.5

Table 3.2 – Emission factors as used in [47].

Fuel	CO_2 emission factors (g/kWh) of electricity supplied		
	2008	2009	2010
Coal	910	908	909
Oil	651	653	653
Gas	401	402	398
All fossil fuels	607	593	590
All fuels (including nuclear and renewables)	495	448	458

Table 3.3 – Emission factors in DUKES report [68].

available when this work was carried out. The objective was to obtain emission figures for various sources, such that dependent on the generation mix selected, the appropriate emissions can be estimated. This approach can then be extended to various locations depending on the local generating mix, which if further detailed information is available can be improved with the local fuel emission factors.

3.3.1 Existing emission factors

In an assessment of cold ironing effectiveness, [47] reports use of the emission factors given in table 3.2 for the UK only, taking into account the generation mix in 2007.

The DUKES report itself gives some emission factors for CO_2 emissions (only) as table 3.3.

In the "2012 Guidelines to Defra / DECC's GHG Conversion Factors for Company Reporting" produced by AEA for the Department of Energy and Climate Change (DECC) and the Department for Environment, Food and Rural Affairs (Defra) [69] the emission factors in table 3.4 are given, again only considering CO_2.

These emission factors however are only valid for the UK and as can be seen there is an element of variation between the figures given in the studies. In order to

Year	CO_2 emission factors (g/kWh) of electricity supplied
2008	486.57
2009	447.18
2010	454.53

Table 3.4 – CO_2 emission factors from [69].

Fuel Source	Mass emission factors			Electricity statistics		Electrical energy emission factors		
	CO_2 (kt/Mt)	NO_x (kt/Mt)	SO_2 (kt/Mth)	Fuel Consumed	Electricity Supplied (GWh)	CO_2 (g/kWh)	NO_x (g/kWh)	SO_x (g/kWh)
Coal	610	4.31	4.07	40.23 MT	98,706	911.6	1.76	1.66
Fuel Oil	873	11.72	8.35	0.93 MT	4,357	683.2	2.5	1.78
Natural Gas	1.46	3.6×10^{-3}	5.32×10^{-5}	11,700 GTh	158,972	394	0.26	3.91×10^{-3}

Table 3.5 – Derived emission factors.

obtain generic factors, the emission factors were to be obtained for each fuel source, additionally including SO_2 and NO_x such that a complete shoreside emission picture could be produced.

3.3.2 New emission figures

The UKGHGI defines the mass emission factors utilised in the document to quantify emissions at source in kt/Mt of fuel consumed. These are given for CO_2, NO_x and SO_2 (among others). In order to convert these to g/kWh_e, the corresponding amount of fuel consumed was required, together with the electrical energy produced from each fuel type during the same time period. This data was correlated from the DUKES report, giving the derived emission factors of table 3.5 for CO_2, NO_x, and SO_2 (reported as SO_x).

In order to get the combined emission factor for the UK generation mix, use is made of the electricity share given in DUKES. From these a weighted average can be obtained giving table 3.6. It must be noted that these figures relate to electricity *supplied*, to which losses due to Transmission and Distribution (T&D) must be added. For the year 2010, the estimate for T&D losses (UK) are of 7% [68].

Fuel source	Share of electricity	CO_2 (g/kWh)	NO_x (g/kWh)	SO_x (g/kWh)
Coal	28%	911.6	1.8	1.7
Oil	1%	683.3	2.5	1.8
Gas	47%	394.0	0.3	0.0
Nuclear	16%	0.0	0.0	0.0
Renewables	7%	0.0	0.0	0.0
Weighted emission factors		*447.26*	*0.64*	*0.48*

Table 3.6 – Weighted emission factors for the UK.

Fuel	France	Germany	Spain	UK	Turkey	USA	China
Coal	5%	43%	13%	28%	35%	49%	79%
Oil	1%	2%	6%	1%	3%	1%	0%
Gas	4%	13%	37%	47%	60%	24%	1%
Nuclear	76%	23%	18%	16%	0%	21%	2%
Renewables	13%	12%	24%	7%	1%	2%	17%
Network losses	6.07%	4.22%	9.09%	7.00%	18.25%	6.70%	4.90%

Table 3.7 – Generation mix for various countries.

3.3.3 Worldwide electricity supply data

The emission factors presented so far relate to the UK case. The fuel-specific emission factors themselves will not vary excessively from country to country but the overall emission factor will be scaled according to the generation mix. The International Energy Agency (IEA) publishes yearly figures describing electricity generation mix, network losses as well as electricity cost [70] for its member countries, permitting the emission factors for generated electricity to be estimated.

Table 3.7 gives the percentage generation mix for various countries of interest. This is used in conjunction with the source based emission factors given in table 3.5 to provide the emission factors of table 3.8. The choice of country in these tables reflects interests of the TEFLES project consortium as well as the USA and China for a global perspective.

3.3.4 The case for– shoreside generation

One of the major constraints on cold ironing is the power demand placed on the utility supply by the berthed ships (e.g. the recommended rating for a cruise ship connection is for 16 MVA) [53]. If the existing port infrastructure does not have sufficient spare capacity, additional substations must be constructed and additional incoming

Country	CO_2 (g/kWh)	NO_x (g/kWh)	SO_2 (g/kWh)
United Kingdom	478.9	0.7	0.5
Spain	331.1	0.5	0.4
France	75.6	0.1	0.1
Germany	478.6	0.9	0.8
Turkey	684.1	1.0	0.8
United States	585.4	1.0	0.9
China	762.6	1.5	1.4

Table 3.8 – Weighted emission factors for generated electricity based on generating mix for various countries.

feeders might also be necessary, together with the associated protective switchgear, transformers and cabling. This all involves a significant potential additional cost which negatively affects the feasibility of new cold ironing systems.

Reduction of harbour demand by means of energy saving measures can be a way of providing sufficient spare capacity to accommodate extra loads, depending on the actual port power demands and loads, and the required extra power. For a large disparity between power availability and demand, the provision of extra supply would be necessary. In an effort to reduce the load on the utility, an alternative proposal is to provide power by generation within the harbour area using alternative sources [71].

Renewable sources within the harbour serve to improve the generation mix for the localised demand and can be considered within the developed model by adjustment of the generation mix (table 3.6). Ports can for example utilise unused roof area to install photovoltaic modules to sell power to the grid. In this case, maximising utilisation of renewable sources results in continuous income through feed-in tariffs and is independent on the profile of connected ships. Another alternative is the installation of a dedicated source which can be used on demand to supply in-harbour loads, cleaner than running the ships' onboard generators.

Generator sets are simple to install and operate and a number of fuel options are possible. With the aim of reducing emissions when compared to the current situation, a cleaner fuel than the diesel burnt onboard should be considered. Liquefied Natural Gas (LNG) is a fuel which is undergoing a surge in popularity in the marine sector. It is a clean-burning fuel with extremely low levels of particulate and Sulphur emissions [72–74]. This has resulted in an increase in the popularity of LNG as an onboard fuel, reflected in the growth in the number of LNG-fuelled ships, together

Emission	Emission factor (g/kWh)
CO_2	521.25
NO_x	2.085
SO_x	≈0
PM	≈0

Table 3.9 – Emission factors for LNG shore power [74].

with an increase in available bunkering facilities worldwide, and wider range of engine offerings by manufacturers. For this reason, LNG is considered as the alternative fuel used in this case in shoreside generating sets to supply portions of the shore supply network. This reflects interest by the harbour authorities in actually investing in an LNG infrastructure to provide vessel bunkering, and hence this permits examining the possibility of using this supply for shoreside use. The LNG supply is modelled in a similar manner to the shoreside supplies, i.e. by emission factors implemented as a Look Up Table. The emission factors used are given as table 3.9 [74].

3.4 The case port

As part of the TEFLES project, the Port of Vigo was a participant in the study, providing data as well as industrial insight and impetus on shore supply. The port is situated in North-West Spain, and consists of a five-berth RoRo terminal. Over the year in question (2012), the port has seen over four hundred RoRo visits from about fifty individual vessels ranging in size from 2,000 to 22,000 tonnes (deadweight) [75]. The terminal is illustrated in figure 3.3, indicating the locations of the five berths as well as the existing substation location. Trenches and provision for connection boxes (indicated in 3.3) are already available throughout the berthside area, though they are currently unused for shore connection.

The Port of Vigo also performed a survey with other port operators in their network, eliciting opinions on cold ironing. The results are summarised as figure 3.4 which rank perceived drivers and constraints according to impact on cold ironing uptake [76]. The biggest obstacles to cold ironing implementation are chiefly concerned with the expenses involved, together with the related issue of an insufficient (existing) utility supply capacity. This would involve additional cost if an upgrade of the existing installation would also be required. On the other hand, environmental benefits and the associated reputation and goodwill gains are seen as the most prominent drivers

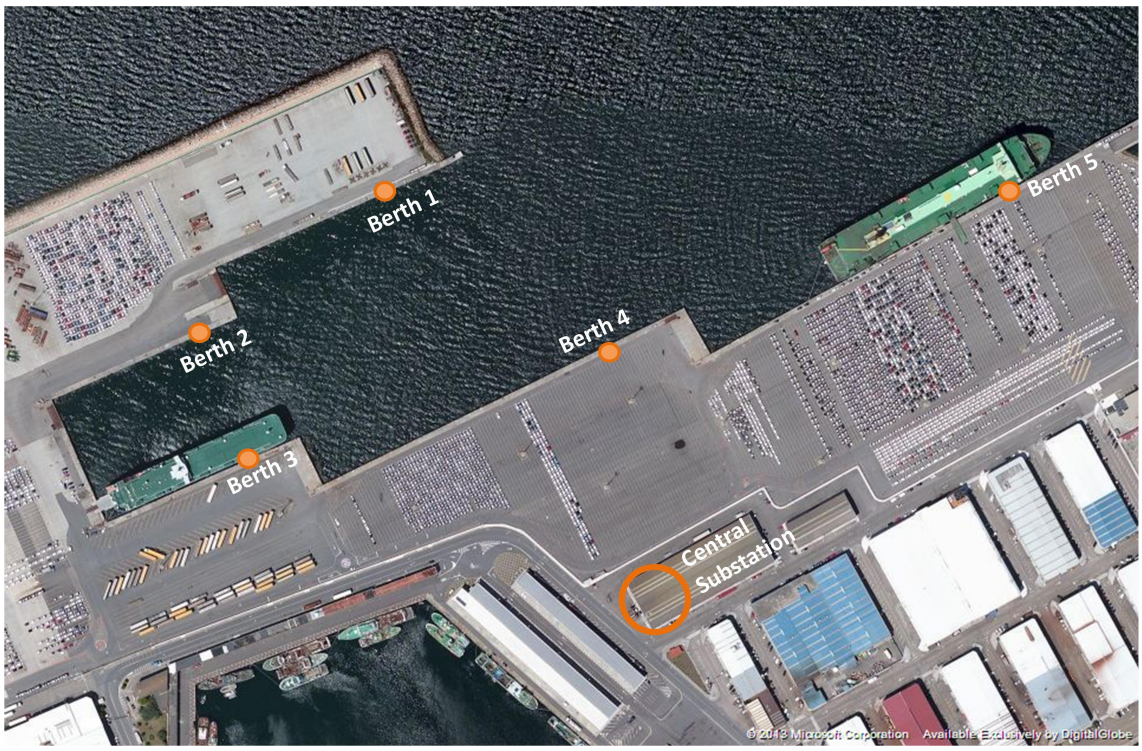

Figure 3.3 – Case port, berth locations overview.

for cold ironing adoption, together with the need to meet regulations.

Voltage and frequency limitations have also been noted to be perceived as an obstacle to cold ironing uptake. Once again this translates to increased cost as frequency and voltage must be matched from shore [53, 54]. The onboard supply frequency is highly dependent on the design of the vessel and its region of operation. Similarly, the shoreside frequency depends on the location, with Europe operating at 50Hz, while North America utilises 60Hz. Based on the information obtained by the port about visiting ships' onboard power systems [75], the charts in figure 3.5 were obtained, which illustrate the spread of onboard systems. The distribution of onboard frequency ratings is approximately 80% operating at 60Hz, with the rest rated at 50Hz. This is similar to the observations in [77], where a 70:30 spread was also observed. This highlights a disadvantage for European ports in that a frequency converter is essential, as otherwise the majority of visiting ships cannot be connected.

Most importantly, the information obtained from the visiting vessels also included the power demanded by the vessels while at berth. This was used to correlate berthed power demands with deadweight, from which a linear approximation (figure 3.6) was fitted, permitting power levels when berthed to be estimated for similar ships according to their size if more detailed information is not available. A power factor

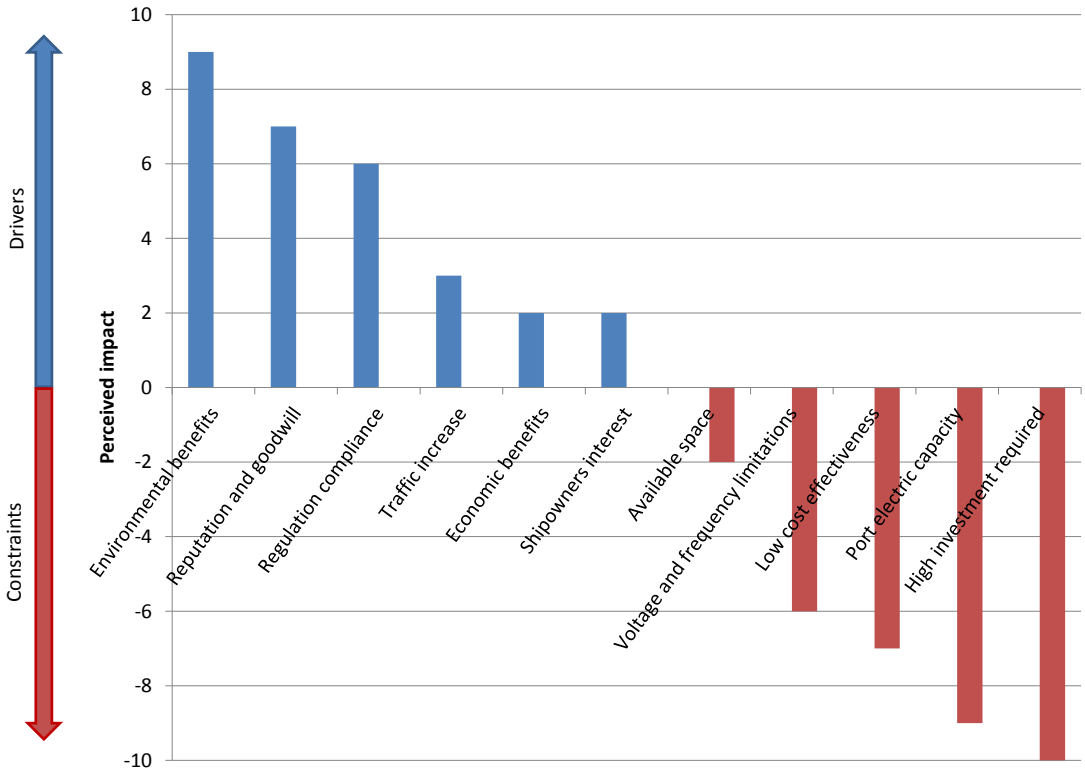

Figure 3.4 – Port operator feedback on cold ironing drivers and constraints [76].

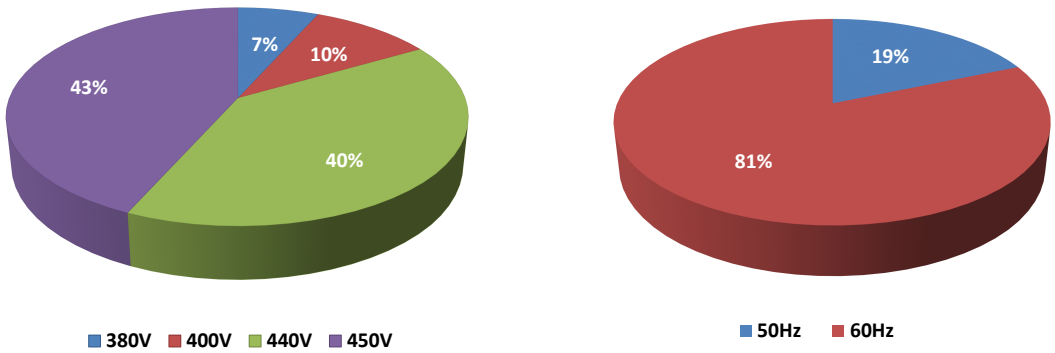

(a) Onboard voltage. **(b)** Onboard frequency.

Figure 3.5 – Shipboard power systems prevalence for visiting RoRo vessels.

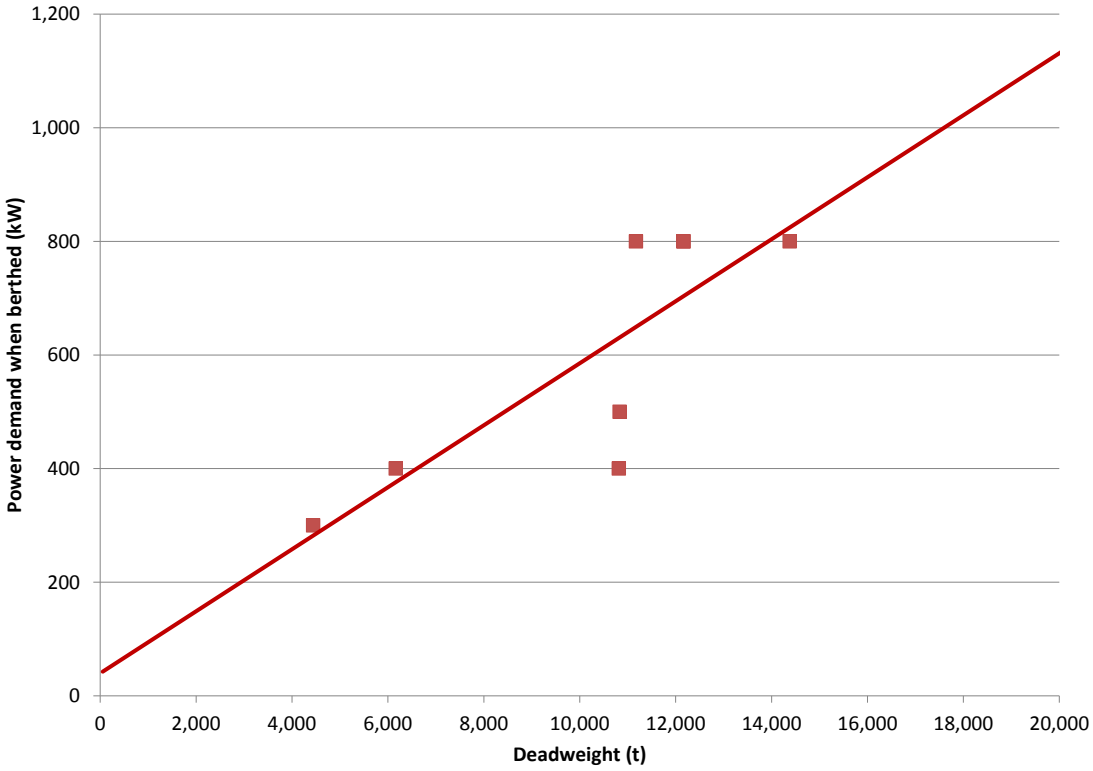

Figure 3.6 – Estimate of power demands when berthed as a function of deadweight.

of 0.8 is assumed, based on measurements on a case vessel from which more detailed information was available as well as additional operator feedback.

Chapter 4

Shore connection topologies and modelling

Extending the fundamental system of figure 3.1 to cater for multiple berths or connections provides for a number of different connection options and topologies. Each of these gives different operational characteristics with respect to efficiency, cost and operational flexibility [66]. These configurations differ mainly in the placement and ratings of the frequency converter/s and transformers leading to the three different topologies described in the next sections. In this study, the five berth existing RoRo terminal described previously (figure 3.3) is considered, following the existing trenching and hook-up points linking the berths and central substation.

4.1 Centralised topology

In the centralised distribution case, schematically shown in figure 4.1, frequency converter(s) are located centrally and remote from the berthside. The individual berths are then only provided with isolation/supply transformers. In order to permit flexibility and eliminate unnecessary losses, a double busbar system can be used, where each berth is connected either to the 50Hz or 60Hz bus according to its demand. This gives greater flexibility in sizing of the converter since the expected load diversity can therefore be taken into account [66].

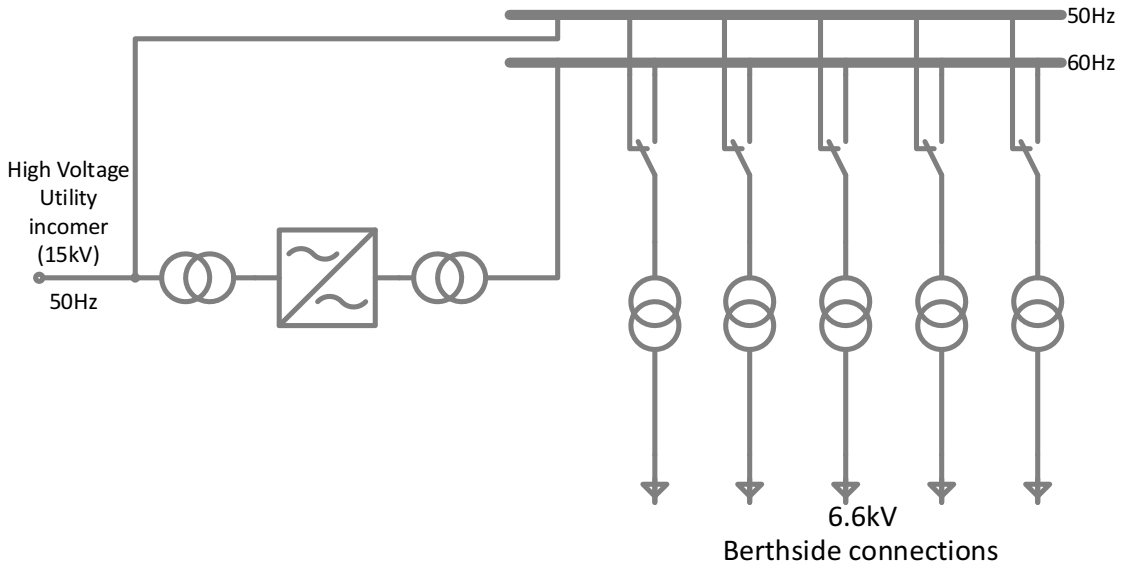

Figure 4.1 – Centralised cold ironing topology.

4.2 Distributed topology

In the distributed topology, the conversion and isolation is all performed at the berthside (or close by) for each individual connection as shown in figure 4.2. This gives greater operational flexibility in that each berth is wholly independent of the rest of the system. However each berthside converter will need to be rated to the maximum individual power demand, as load diversity cannot be taken advantage of. Furthermore such a topology involves a larger footprint at the berthside - a location where space is typically at a premium.

4.3 DC distribution topology

As a hybrid between the two previous topologies, a DC distribution topology (figure 4.3) mirrors industrial multi-drive systems (such as paper making or steel mills). This topology makes use of DC as the distribution medium, with a centrally located rectifier and distributed inverters at the berthside end. In effect this extends the DC link of the integrated frequency converter right up to the berthside. With a DC distribution, integration with any energy storage devices or alternative energy sources within the harbour is facilitated, as only a DC interface is required. However protection on DC systems is more complex when compared to AC systems (due to the lack of natural current zero) especially at higher voltages.

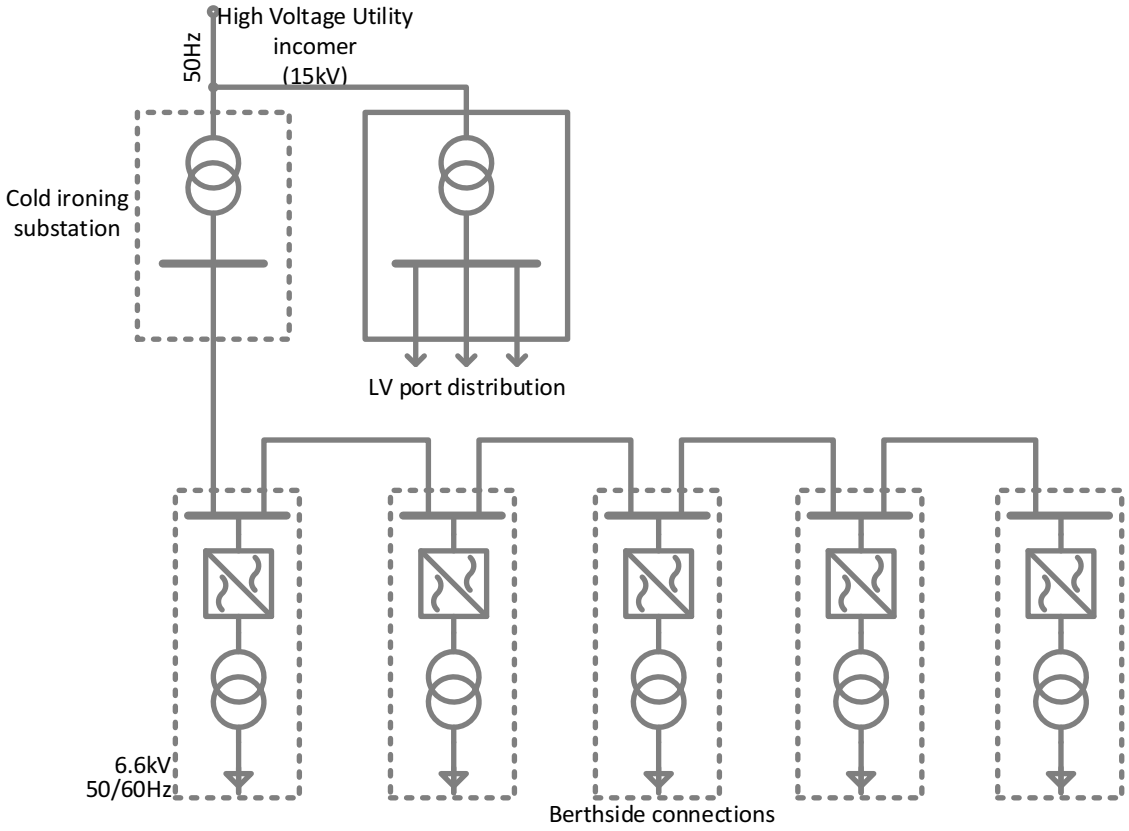

Figure 4.2 – Distributed cold ironing topology.

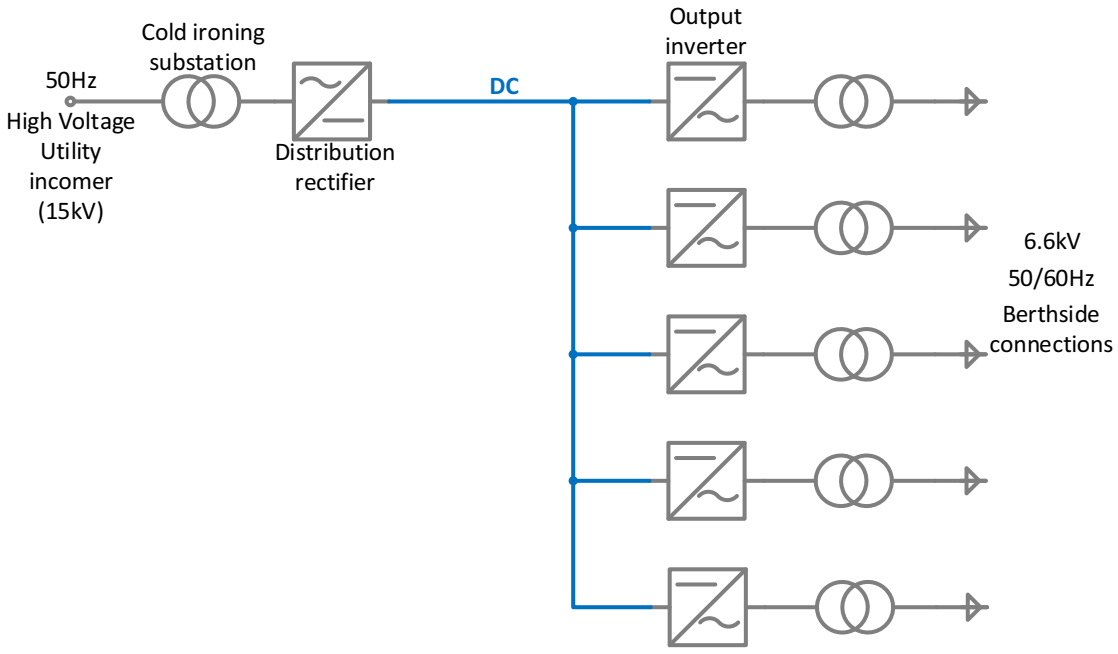

Figure 4.3 – DC distribution topology.

Attribute	Distributed topology	Centralised topology	DC distribution topology
Resilience	High	Less	Least
Component count	High	Least	Less
Berth footprint	High	Least	Less

Table 4.1 – Comparison of topology attributes.

Some of the attributes of the three topologies are comparatively ranked in table 4.1 chiefly in terms of installation space and reliability. Resilience refers to the ability of the cold ironing system to ride-through a single converter fault. In the distributed case, each connection is independent of the rest; hence a fault on any converter will not affect any other. In the centralised case, a fault on the centrally located converter will result in loss of power to all the 60Hz berths, but leaving the rest unaffected. Conversely, any fault in the rectifier stage in the DC distribution topology will shut down the whole system while a fault on one of the inverters will shut down its associated berth with no possibility of bypass operation.

4.4 Fitting in the LNG generation

In this study, the shoreside generation system was considered with an LNG-fuelled generator set replacing one or more of the individual berth connections of the cold ironing system as shown in figure 4.4. In this case berths 2 and 3 are supplied by LNG generators, while the remaining berths are connected to a distributed cold ironing network. This represents a situation where the benefits of a port with an LNG supply can be exploited by conventionally-fuelled vessels.

4.5 Modelling

In order to provide comparisons between the topologies described above, a parametric energy-centric model of the shoreside networks was developed. This permits various configurations and designs to be explored and examined within an automated script such that optimal designs can be identified. The comparison is to be performed on an efficiency basis; therefore circuit models which account for the various losses in the components are sufficient for modelling purposes. This also accounts for additional

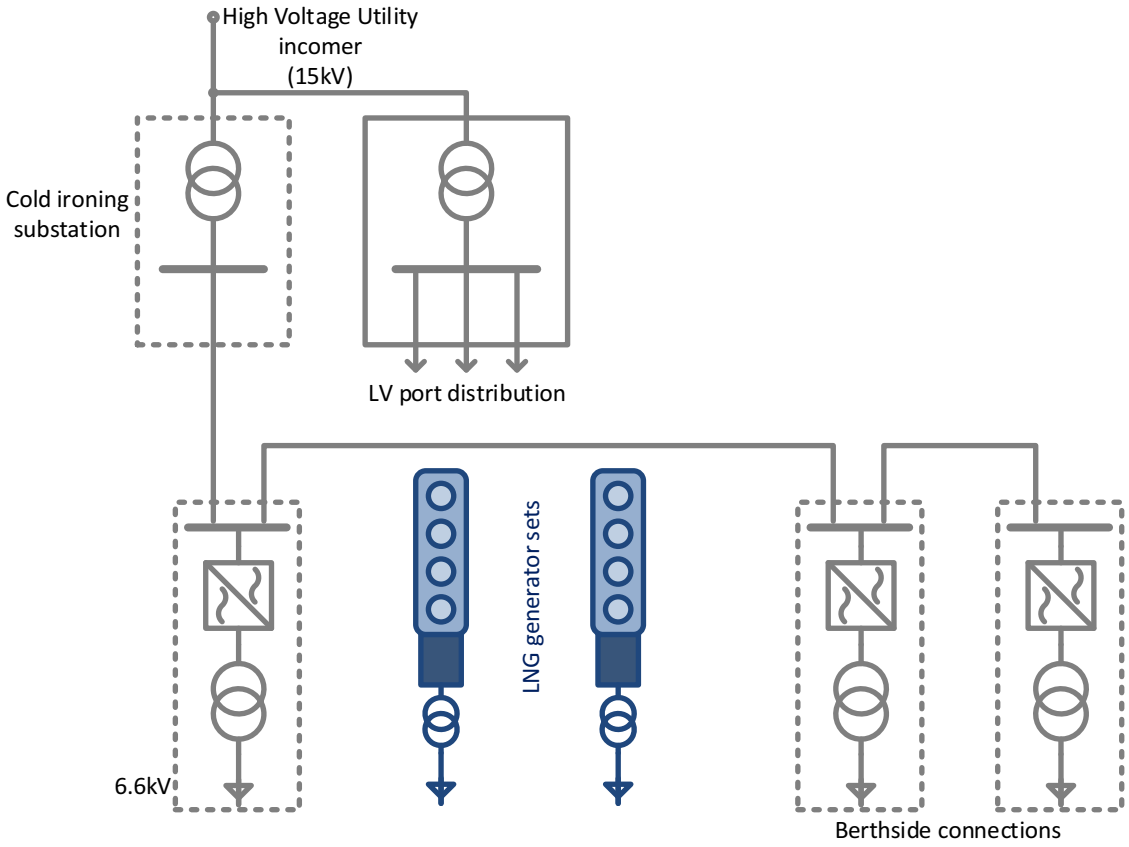

Figure 4.4 – Example of combined system with LNG generation for two berths within a distributed cold ironing system.

losses due to harmonics introduced by the switching converters, causing an increase in the RMS value of the current as well as additional magnetic losses in transformers. The transformer and frequency converter models are described in more detail in the next two sections, since these account for the majority of losses in the shore network.

The inputs to the models are the load profiles from the individual berths which determine the power flows through the shoreside network. The expectation is that the vessels' power is met without negatively affecting the power quality to the rest of the network. This constraint determines the electrical limits in accordance with [53] which must be met for satisfactory and interoperable operation according to the standardised requirements for cold ironing.

The fixed voltage input is that determined by the utility incomer at the port from the distribution network. This is considered fixed and serves as the reference bus from which the port distribution network's voltages are determined, providing the starting point for a power flow study. By having a fixed voltage input at the upstream node and a known power demand at the downstream ends of the network, the intermediate voltage and current quantities can be determined by successive iterations of the

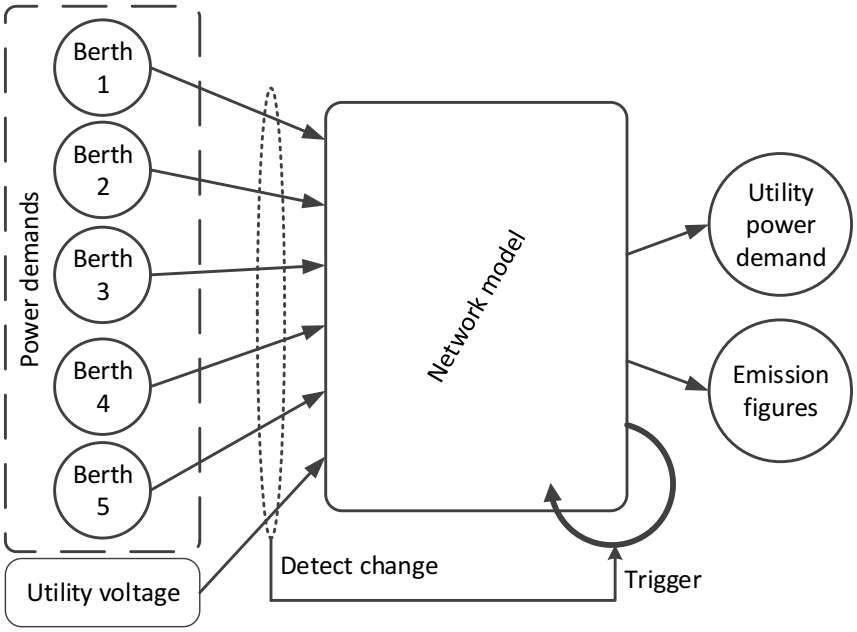

Figure 4.5 – Functional top-level diagram of cold ironing network model.

model until a steady-state solution is reached. This permits the simulation to be run only when changes in any of the inputs are detected, after which the values are held until the next detected change, speeding up simulation.

The functional top-level diagram of the simulation setup is illustrated in figure 4.5. It shows the inputs (left hand side) consisting of the berth power profiles and the utility voltage. The outputs (right hand side) of the simulation are the power demanded from the utility and the corresponding emission figures. The network model is housed within a do-while iteration loop. For the first iterate, the simulation is run until all the (internal) currents and voltages converge to a steady-state value, indicating that the simulation has reached a suitable solution. The output is then held until a change is detected, which avoids having to continuously run the simulation even when there are no changes to any of the variables involved.

4.5.1 Transformer model

The transformer depiction of figure 4.6a gives the equivalent circuit of a real transformer, which can be simplified by referring all elements to the primary side giving the referred equivalent circuit shown in figure 4.6b. In this equivalent circuit, the magnetisation branch (X_m in parallel with R_c) appears at the primary terminals. This branch accounts for the real power losses in the core (V_p^2/R_c) and the magnetising current ($-jV_p/X_m$). R_{eq} and X_{eq} represent the combined primary and

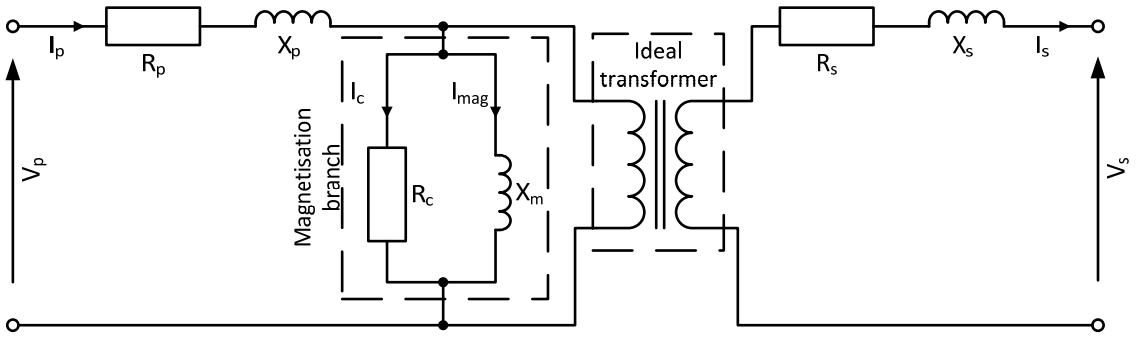

(a) Complete transformer circuit.

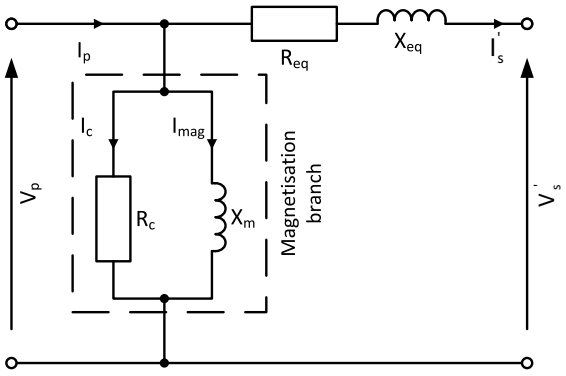

(b) Simplified transformer circuit.

Figure 4.6 – Transformer equivalent circuits.

secondary winding resistance and reactance respectively, referred to the primary. The actual transformer secondary output voltage (V_s) is given by $V_s = V_s^{'}/a$ where a is the transformer voltage ratio. Similarly the output current of the transformer on the secondary side is $I_s = aI_s^{'}$.

The input (primary) current I_p in figure 4.6b consists of three components: the current in the secondary $I_s^{'}$, the magnetising current I_{mag} and the current responsible for providing the no-load losses in the core, I_c. The no-load core loss (P_{noload}) is associated with eddy-current and hysteresis losses in the core and is represented by R_c. No-load losses are typically considered as fixed losses at 1% of the transformer's kVA rating and do not change with load. The magnetising current (I_{mag}) is typically constant at 4% of rated current, but lags the supply voltage by 90°. Load losses (P_{ll}) will vary according to the loading on the transformer, and can be classified as the losses due to resistance in the windings (P_{I^2R}) and losses due to stray flux linkage (P_{TSL}). These stray losses are caused by flux linkages with other transformer components. The transformer equivalent circuits of figure 4.6 are valid for the fundamental frequency. Additional losses are imposed on the transformer due to the non-sinusoidal nature of the actual current flowing through it. This is caused by

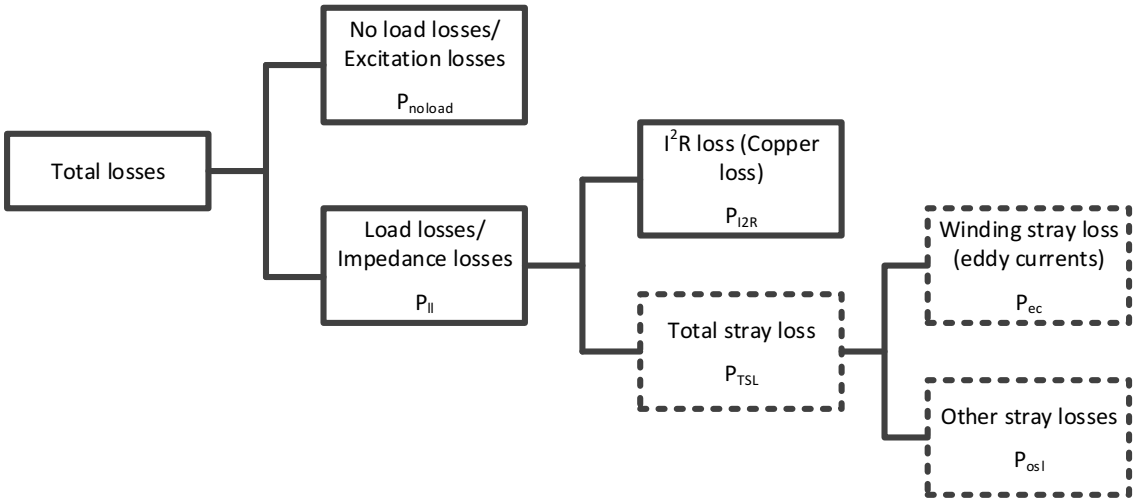

Figure 4.7 – Subdivision of transformer losses. [78]

non-linear loads connected downstream of the transformer drawing non-sinusoidal currents (such as frequency converter). These will result in the total RMS value of the current being greater than the fundamental, leading to additional Ohmic losses in the circuits. Within the magnetic circuit of a transformer, additional losses will occur due to the effect of harmonic currents on the magnetic core. These additional losses due to harmonic effects are quantified according to an estimation procedure defined by IEEE Std. C57.110-2008, [78] by applying the "transformer capability equivalent calculation using data available from certified test report", providing an estimate of the additional losses due to harmonics using limited available data on transformers. The classification of losses within a transformer can be summarised by figure 4.7 highlighting the loss classifications which are affected by the presence of harmonic currents.

The harmonic spectrum of the drawn current is used to calculate two harmonic loading factors for the additional eddy-current F_{HLec} and stray losses F_{HLstr}. These are described as equations 4.1 and 4.2, which define multipliers to the rated eddy current and stray losses based on the current's harmonic spectrum [78].

$$F_{HLec} = \frac{\sum_{h=1}^{h_{max}} \left(I_h/I_1\right)^2 h^2}{\sum_{h=1}^{h_{max}} \left(I_h/I_1\right)^2} \tag{4.1}$$

$$F_{HLstr} = \frac{\sum_{h=1}^{h_{max}} \left(I_h/I_1\right)^2 h^{0.8}}{\sum_{h=1}^{h_{max}} \left(I_h/I_1\right)^2} \tag{4.2}$$

where h is the particular harmonic number, with I_{h} being the corresponding harmonic

current magnitude. The losses have to be defined for rated conditions first using transformer nameplate data. From figure 4.7, the load losses (due to fundamental current flow) at rated voltage and current can be defined as $P_{LLR} = (P_{rat}/\eta_{rat} - P_{rat} - P_{noload)}$, where P_{noload} is the core loss, assumed a constant percentage of the transformer's rated kVA. In turn the total stray losses at rated are given as $P_{TSLR} = P_{LLR} - 3\left|I_{ph}^2\right| R_{ph}$ where I_{ph} is the rated phase current. The eddy current losses at rated are defined as being 33% of P_{TSLR} for oil-immersed transformers and 67% in dry-type transformers. The remainder is made up of other stray losses P_{OSLR} [78].

The rated losses are then scaled proportionally according to the RMS current through the transformer to represent the fundamental stray losses at that loading. The additional harmonic losses are then estimated by multiplying this figure by the harmonic loss factor calculated according to the current's harmonic spectrum. Together with the additional copper loss, $P_h = 3\left(|I_{rms}| - |I_1|\right)^2 R_{ph}$ gives the additional power losses due to harmonics in the transformer.

4.5.2 Frequency converter

The basic power electronic circuit of the frequency converter is shown in figure 4.8, with additional associated control algorithms and processing to maintain a 50Hz or 60Hz output, as desired. The losses associated with the converter are the switching and conduction losses in the switching devices themselves. Switching losses in the power electronic devices are due to the non-zero current and voltage waveforms during device turn-on and turn-off, while conduction losses are due to effective resistance of the devices while conducting current.

The voltage and current waveforms for a single device are illustrated as figure 4.9 together with the corresponding power losses, where V_s is the input voltage appearing across the switch when turned off, I_{on} is the steady state current through the switch and V_{on} is the (small) on-state voltage. The switching losses are given by equation 4.3. Similarly, equation 4.4 defines the conduction losses during the on state period (t_{on}), where $t_{c(on)}$ and $t_{c(off)}$ are the turn on and turn off times, respectively, and f_s is the switching frequency [79].

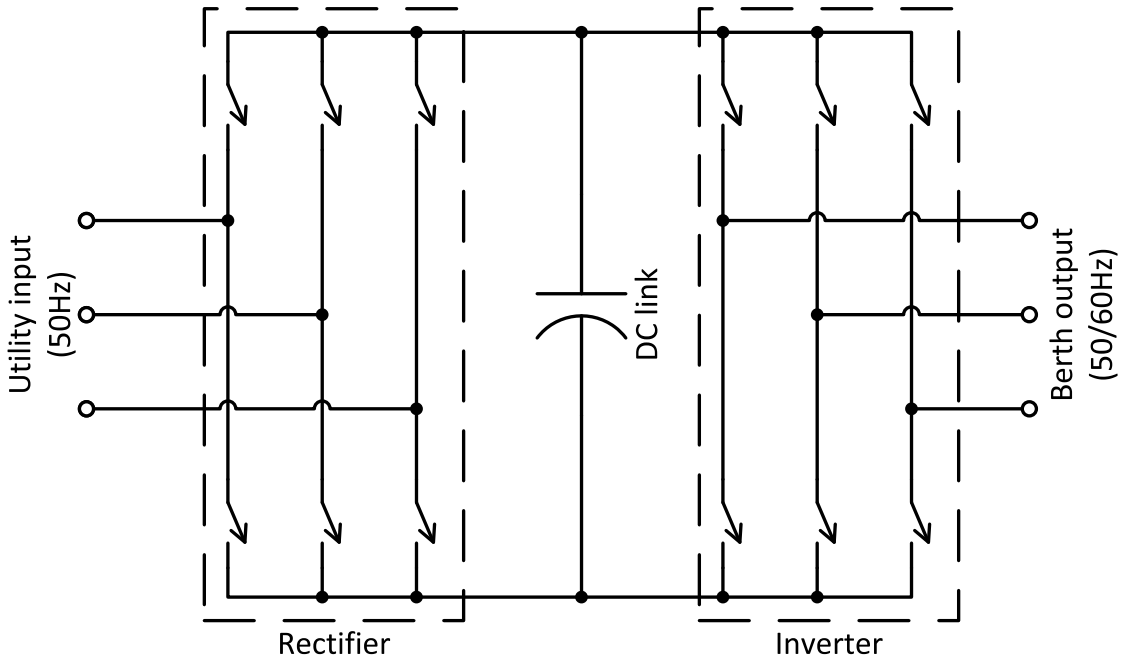

Figure 4.8 – Simple schematic diagram of frequency converter.

$$P_s = \frac{1}{2} V_s I_{on} f_s \left(t_{c(on)} + t_{c(off)} \right) \tag{4.3}$$

$$P_{on} = V_{on} I_{on} f_s t_{on} \tag{4.4}$$

With a fixed frequency output, power losses will vary according to the current through the device (i.e. the total load on the inverter). Additional losses are also produced in the passive components associated with the converter including the DC link capacitor and any filter inductances at the input. Losses in the DC link capacitor are associated with the RMS ripple current flowing through the capacitor, leading to a heating effect due to its Equivalent Series Resistance (ESR). Since the model is required to account for losses in the circuit, a Look Up Table (LUT) of converter efficiency with respect to percentage loading was obtained [63], with the detailed model implementing figure 4.9 developed in section 4.5.4.

4.5.3 Cost modelling

The installation of a cold ironing system is a significant undertaking and involves a considerable cost. Each case is an individual project which requires detailed costings and study, hence a specific and precise figure cannot be provided. Indicative costs

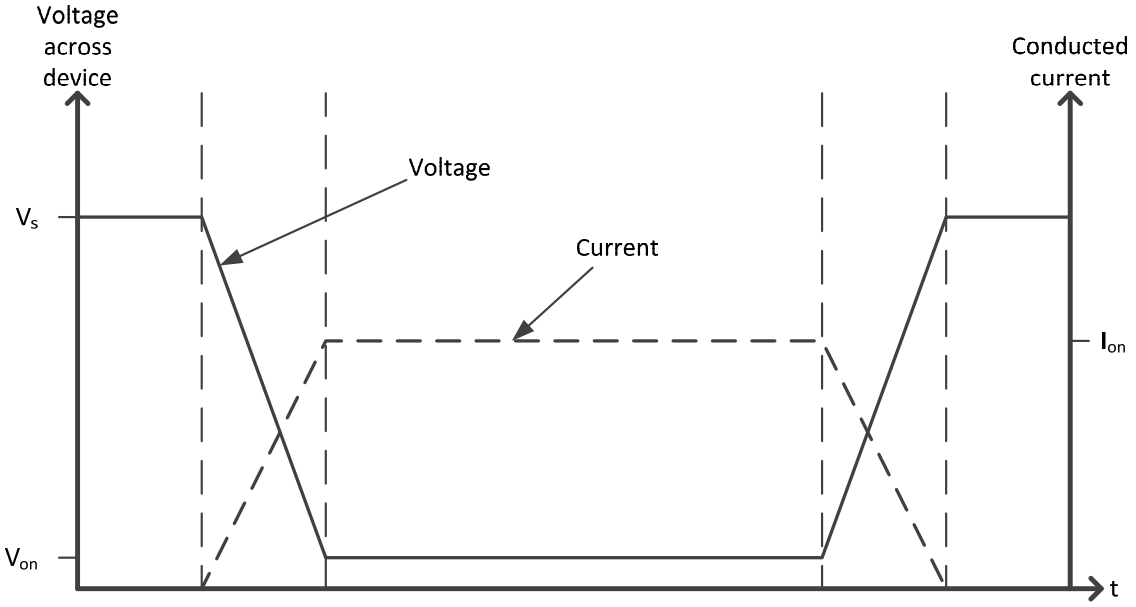

(a) Voltage and current waveforms.

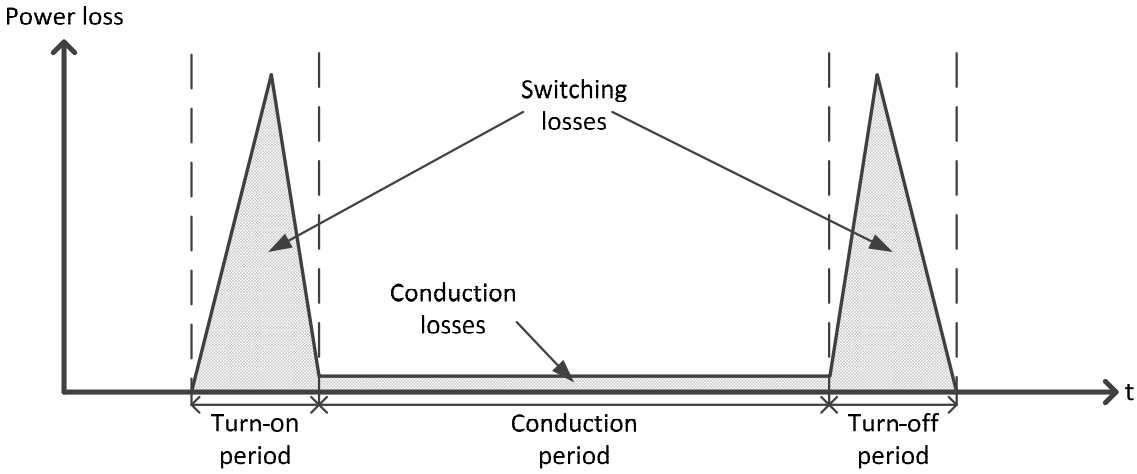

(b) Instantaneous power losses across power electronic device.

Figure 4.9 – Device switching waveforms and power loss characteristics.

can however be estimated, which can be used to quantitatively compare different topologies or systems.

These figures do not take into account the infrastructural works required for the installation as these are highly dependent on the actual location. Based on figures quoted in [77] and communication with a leading electrical equipment supplier, an indicative figure of €700/kW (including frequency converter) was estimated per berth. This does not take into account any infrastructural costs such as trenching or cabling which are highly installation specific.

For worthwhile investment, the cost of infrastructure should be recuperated within a reasonable amount of time. Hence the initial outlay should not be borne solely by the port authority but rather, other involved parties must contribute. If this cost is shared with visiting vessels, the actual cost of electricity supplied at the berthside can be higher than that generated onboard, negating any economic driver for cold ironing.

In order to provide meaningful comparisons between topologies, a cost metric must be accounted for. By normalising costs with respect to component ratings, an indicative figure can be obtained such that two topologies can be assessed based on relative costs.

The power electronic converters are much more expensive than transformers; hence a topology with more converters will be expected to be more expensive than one with a single central converter, although the cost of converter will increase with size. For modelling purposes, a transformer has been assigned a cost of 1pu/kVA, while a power electronic converter has been assigned a relative (conservative) cost of 3pu/kVA, in line with costs obtained from [77]. Similarly, costs for LNG systems will be assigned on a relative scale to the cold ironing system. In order to account for disparity in costs (especially due to the need for infrastructure), this will be a variable such that the crossover point (in terms of cost) between shoreside LNG and cold ironing can be estimated.

4.5.4 Detailed modelling

The first order models of the various components in the shore power network described in the previous sections were modelled in order to be able to give quantitative

estimates of the efficiencies of the different systems. These models were concerned with energy losses in the components of the systems involved, and hence focused on fast simulation times, in order to facilitate the consideration of a number of different configurations and setups. Fast events (such as semiconductor device switching) and controller dynamics were approximated by first order models and LUTs. These gave sufficient detail to quantify power losses for a given operating point. However these models do not give any indication of the actual electrical operation of the system and only account for the power flow study of the network.

A more detailed model of the shore supply network was additionally built using components from the SimPowerSystems toolbox. This would be used to investigate in further detail the results obtained by the first order models and the optimal search. Models are readily available for the transformers and other passive components, while a frequency converter subsystem model was assembled using the built-in semiconductor switches exhibiting the switching profiles of figure 4.9.. A detailed schematic diagram of the frequency converter implemented is shown in figure 4.10. This is of course very similar to the variable speed drive used for the auxiliary drives shown in figure 1.5, with the output frequency and voltage being the controlled quantities rather than motor speed.

Here a diode front end (uncontrolled bridge rectifier) is shown, which rectifies the supply to the intermediate DC link. An Insulated Gate Bipolar Transistor (IGBT) inverter is then used to modulate the voltage to provide a three-phase 60Hz output at the desired voltage [27]. This voltage must be filtered before being supplied to a consumer which expects a clean sinusoidal supply. The control algorithm in figure 4.10 implements a vector control strategy to generate the required output voltage waveforms, comprising a cascaded loop control with an outer voltage control loop, and a nested current controller. PI (Proportional and Integral) controllers are used, which are tuned to give the desired dynamic response of the controlled outputs. The Clarke and Park transformations are mathematical transformations which convert three-phase quantities to equivalent constant quantities in an synchronised orientation rotating at desired output frequency (f^* in figure 4.10). The corresponding inverse transformations feed the controlled output signals to the PWM generator, the output of which is used to switch on/off each individual IGBT in the inverter.

A Low Pass Filter (LPF) is shown at the output of the inverter, which diverts

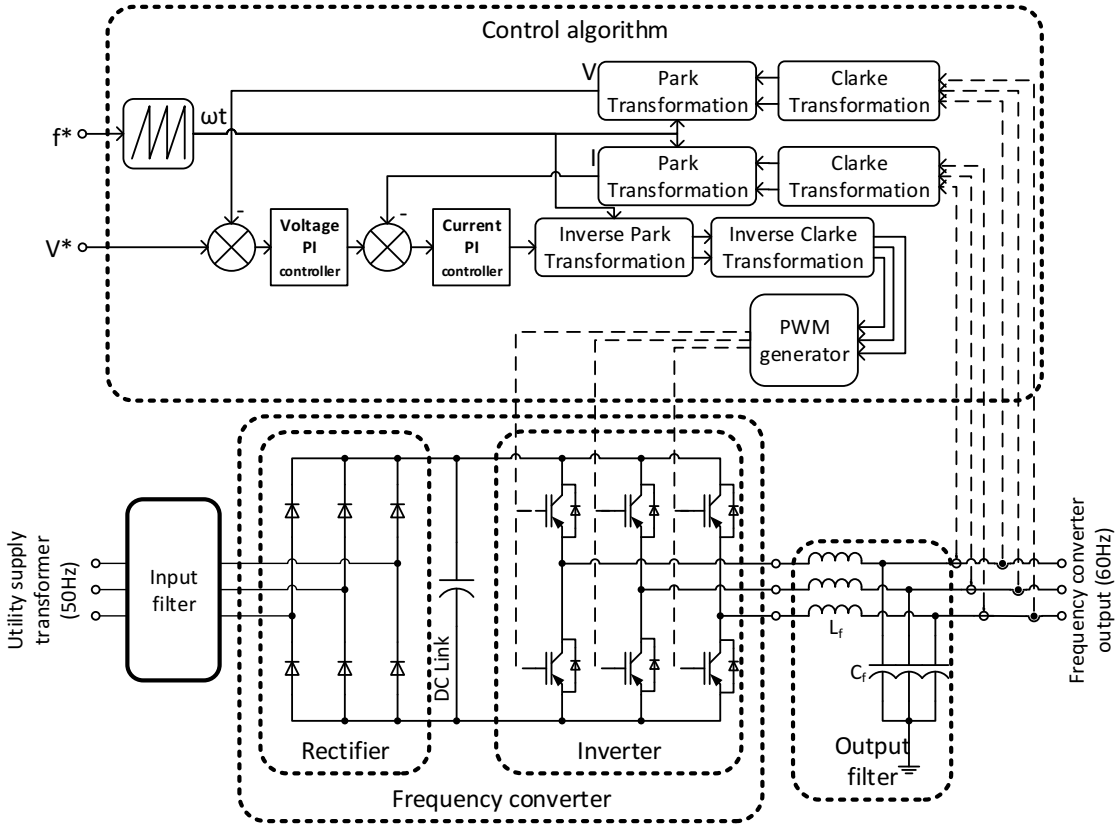

Figure 4.10 – Detailed frequency converter schematic.

the high frequency harmonic components of the PWM waveform to ground (via the capacitors) providing an output with a substantially reduced harmonic content. A simple inductive (L) filter can provide a limited amount of attenuation of high frequency harmonics, but this requires the use of a high switching frequency in the power electronic converter in order to produce an acceptable output. With the addition of a shunt capacitor, an LC filter can be obtained tuned for a given corner frequency (equation 4.5) [80]. The presence of a series filter component (the inductor L_f) results in a voltage drop when current flows through the filter. Hence the filter design must take into account an allowable voltage drop at the output which must be compensated for by the inverter raising its output voltage (within its limits) in order to regulate the output voltage.

$$f_c = \frac{1}{2\pi\sqrt{L_f C_f}} \tag{4.5}$$

For this study, the parameters of the output filter were chosen for a 5% voltage drop (at line frequency) and a corner frequency (f_c) of 400Hz, corresponding to a factor of one tenth of the inverter switching frequency of 4kHz, and are listed in table 4.2

Quantity	Symbol	Value
Supply side inductance	L_s	1.54mH
Supply voltage	V_s	15kV
Voltage PI controller proportional gain	K_{pv}	0.675
Voltage PI controller integral gain	K_{iv}	405
Current PI controller proportional gain	K_{pi}	6.75×10^{-5}
Current PI controller integral gain	K_{ii}	0.054
Switching frequency	f_s	4kHz
Filter inductance	L_f	5.3μH
Filter capacitance	C_f	30mF

Table 4.2 – Component values for frequency converter.

together with the value of supply side inductance. The transformer at the input of the converter is used to step down the input medium voltage supply (15kV in this instance) to a low voltage level of 480V, which permits the use of conventional low voltage power electronics. The voltage is then stepped up again at the output in order to provide the voltage level required by the berth connections (6.6kV) [63]. This transformer also provides the required galvanic isolation if supplying a single berth, otherwise additional isolation transformers are needed for each connection. With developments in transistor technology, high voltage devices would permit high voltage converters to be more commonplace, avoiding the need to step the voltages, reducing the current levels and hence the cabling requirements.

Chapter 5

Optimal search

The optimisation procedure aims to identify the best possible configuration of shoreside electrical network to provide shore power to berthed ships. The classical design methodology would be to design a network for a particular operating case, with components sized and chosen according to this particular scenario at one instant in time. By using an optimisation algorithm, a broader search space can be automatically considered, and by combining this with design-by-simulation, a network configuration can be chosen to best address a requirement based on a particular scenario.

The particular electrical configuration and component sizes can be described as a particular point in the search space, which consists of the set of all the possible network configurations. The complete search space clearly includes solutions which are infeasible. These particular configurations do not meet the requirements demanded of the network, such as the provision of sufficient power and the necessary power quality. Constraints are hence used to restrict the search space to its feasible region.

For a given load power profile, each particular electrical configuration will have a corresponding emission (and efficiency) level and cost. These quantities represent the *objectives* of the optimisation routine. Each point in the search space therefore maps to a corresponding point in the objective space, with the link being established by an objective function.

The objective function evaluates a configuration and returns a particular metric which is needed for quantitative comparisons with other solutions. In this case, the objective function returns the emissions produced by a particular (network)

configuration and power demand profile. This is obtained by running the developed Simulink model.

By providing this quantitative figure, different configurations can be meaningfully compared. Since the search space is defined by the large number of possible configurations, an optimisation procedure can also be termed to be a search operation, tasked with identifying an optimal configuration from the search space based on a quantifying metric in the objective space. A trivial method to identify the best configuration would be an enumerative method, whereby all the possible configurations are evaluated, and ranked according to their objective values. However this is clearly a very costly process as all the solutions would need to be evaluated, and additionally this process can only consider single objective problems [81].

Mathematically, linear systems can be optimised by techniques which are generally gradient-based searches through the search space. However these require a linear mathematical representation of the problem which can be difficult if not impossible to achieve in some cases. In non-linear problems such as the one at hand, these optimisation algorithms cannot be realised (easily), hence a more robust optimisation/search algorithm must be considered.

Evolutionary algorithms are a class of search routines which take inspiration from natural processes/phenomena to realise intelligent search processes able to handle non-linear and complex problems. Evolutionary algorithms offer advantages in that they work well with a wide range of problems, since they do not make underlying assumptions about the problem formulation. This makes them robust and able to work on non-linear and complex search spaces. Of course this comes at the expense of performance in that there is no algorithm which excels at every problem [81]. Evolutionary algorithms are particularly effective for finding the global optima of complex search spaces albeit perhaps at a computational expense when compared to optimisation algorithms specifically adapted for individual types of problems. In this application, robustness and general applicability to a wider range of problems were seen to be more important than algorithm speed.

In evolutionary algorithms, the problem to be optimised and the actual optimisation process are kept separate. The optimisation algorithm maintains a black-box approach to the problem at hand, requiring only the objective value to be returned for a particular combination of variables. This objective function is the link between the

search and objective spaces, and can be of any form as long as the input/output combination is as expected by the optimisation algorithm. This is ideal for the application at hand since the same Simulink models which are used for system design and study can now also be used for the optimisation process.

Genetic Algorithms and Particle Swarm Optimisation are two such algorithms which employ *directed* randomness to efficiently and effectively explore a search space [82]. Genetic Algorithms (GAs) employ a Darwinian process of survival of the fittest whereby solutions are identified in the search space by co-ordinate values termed chromosomes. By using reproduction and mutation operations on these chromosomes the search space can be intelligently explored by a process of accelerated evolution [45].

Particle Swarm Optimisation (PSO) on the other hand takes its cue from the social behaviour of swarming birds or fish. Each solution (configuration) is represented as a particle within the swarm, and the position of each particle is the configuration's description. Associated with each particle is its fitness value in the objective space. The PSO algorithm serves to steer the initially randomly located particles towards the global best value [83–85].

These two algorithms are similar in terms of robustness and ease of implementation, but in this work, PSO is considered due to generally superior speed of convergence towards optimal solutions [84, 86]. By virtue of the use of a swarm to perform the search, PSO implements a parallel search such that multiple areas of the search space are examined at the same time. This has the benefit of helping to ensure that global optima are identified rather than local extrema and makes PSO more efficient than GAs [87].

5.1 Particle Swarm Optimisation

Swarm intelligence considers the collective interactions and knowledge of a population of members which are individually 'dumb' but collectively smart. A swarm of birds (or shoal of fish) operate as a concerted entity, by sharing of each individual's knowledge such that overall, the whole swarm benefits. An example of swarm behaviour is illustrated when a flock of birds is searching for food. Once a member of the flock identifies a potential food source, the flock collectively drifts towards this new 'goal'.

This can be considered as an optimisation function, whereby the location of the food is the optimisation goal.

Particle Swarm Optimisation (PSO) traces its origins to the seminal work of Kennedy and Eberhart [85] by considering the social behaviour of a flock of birds and applying this biologically inspired computer algorithm to optimisation problems. In the application of PSO, the term *swarm* is used to describe the collection of individual agents, who are in turn termed the *particles* (analogy with flock and birds, or shoal and fish).

Associated with each particle is a fitness value, which serves as an indication of how well that particle meets the optimisation goal. Maintaining the bird/flock analogy, the fitness of a particle would be its proximity to food. Each particle is described by its Cartesian co-ordinates in the so-called search space. The search space has as many dimensions as there are variables, hence a particle is identified by a d-dimensional co-ordinate, where d is the number of parameters (variables) which can be controlled. In the bird flock case, this would be a three-dimensional space, representing physical space in xyz-coordinates.

The particles 'fly' around in the search space, exploring potential solution regions and successively converging towards particles which give better solutions due to the swarm's co-operative nature. Every particle therefore has an associated d-dimensional position as well as d-dimensional velocity vector.

The fitness value of each point represents each particle in an equivalent objective space such that each particle is mapped to a corresponding point from the search space by the fitness function(s). For O objectives, the objective space is of O-dimensions, with O corresponding fitness functions. Thus each particle can be described as a d-dimensioned Cartesian coordinate in the search space or an equivalent O-dimensioned Cartesian coordinate in objective space. This equivalent mapping is shown graphically as figure 5.1.

5.2 The algorithm

The underlying co-operative concept behind PSO mimics the social behaviour of an intelligent swarm in order to locate an optimal solution. Swarm intelligence therefore

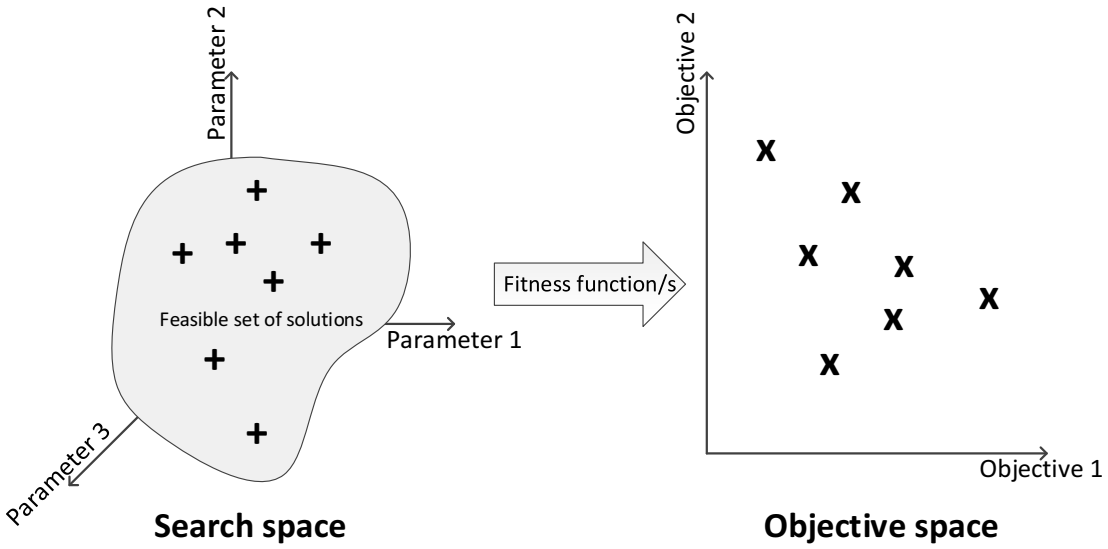

Figure 5.1 – Optimisation spaces showing mapped set of particles.

involves knowledge of other particles' fitness (objective values) as well as a particle's own fitness. The sharing of this information must therefore be implemented in an algorithm form. The PSO process is first introduced by considering a single objective optimisation case before additional objectives are introduced in subsequent sections.

By the nature of the concept of swarming, the search space is explored by a number of different particles in parallel, thus ensuring a speedy broad search of a large spread of locations. The search itself is the heart of the optimisation routine, and this is controlled within the velocity update procedure.

A particle in the search space has two quantities associated with it at each iteration – its location and velocity, described respectively as

$$\begin{aligned} \mathbf{x_i} &= [x_1, x_2, x_3, \ldots, x_n] \\ \mathbf{v_i} &= [v_1, v_2, v_3, \ldots, v_n] \end{aligned}$$

where n is the number of variables in the search space, and i is the particle number, up to the swarm size N.

The PSO procedure is initialised with an initial swarm of size N, consisting of randomly located particles with corresponding random velocities. Each particle's position at the next iteration is therefore calculated according to the simple equation of motion given by equation 5.1.

$$\mathbf{x_i}\,[\mathbf{ctr}+\mathbf{1}] = \mathbf{x_i}\,[\mathbf{ctr}] + \mathbf{v_i}\,[\mathbf{ctr}] \tag{5.1}$$

where [ctr] represents the current iteration. The calculation of each particle's velocity at successive iterations looks at the swarm's fitness and the particles' history in order to intelligently move towards the best solution. Two figures of merit can be defined which will determine this influence; the *particle_best* and the *global_best* values in objective space, together with the corresponding position coordinates *particle_best_loc* and *global_best_loc* respectively in the search space.

The particle best value is each individual particle's best location found so far, while the global best value is associated with the best location found by the whole swarm (with respect to the objective). The quantities are used to update each particle's velocity such that it will tend to migrate towards better locations while still exploring its vicinity. A particle's velocity at the next iteration is given by equation 5.2.

$$\begin{aligned}\mathbf{v_i}\,[\mathbf{ctr}+\mathbf{1}] \;=\; & W \times \mathbf{v_i}\,[\mathbf{ctr}] + \mathrm{C}_1 \times \mathrm{rand}\,(0,1) \times (\mathrm{pbest} - \mathbf{x_i}\,[\mathbf{ctr}]) \\ & + C_2 \times rand\,(0,1) \times (gbest - \mathbf{x_i}\,[\mathbf{ctr}])\end{aligned} \tag{5.2}$$

W is termed the inertia factor and determines the tendency of a particle to carry on in the same trajectory due to its own velocity. C_1 and C_2 are two constants which determine the weighted influence of the particle's historical best and the swarm's global best. Hence they describe the tendency of a particle to be attracted to its own or the swarm's historical best location and is illustrated graphically as figure 5.2. A particle will therefore have a velocity component proportional to its distance from the particle best and global best locations respectively as well as its own inertia to follow its original velocity. Empirically, the recommended value for W has been found to be 0.7, while C_1 and C_2 both equal to 1.47. This has been shown to give best balance between premature convergence and slow searches [88].

This simple formulation can be further tweaked into a more generic form which reformulates all the constants into a constriction factor [88]. This can directly control the constriction or explosion of the swarm, and improves the control of convergence by using only one control parameter. In this case, the velocity update equation is

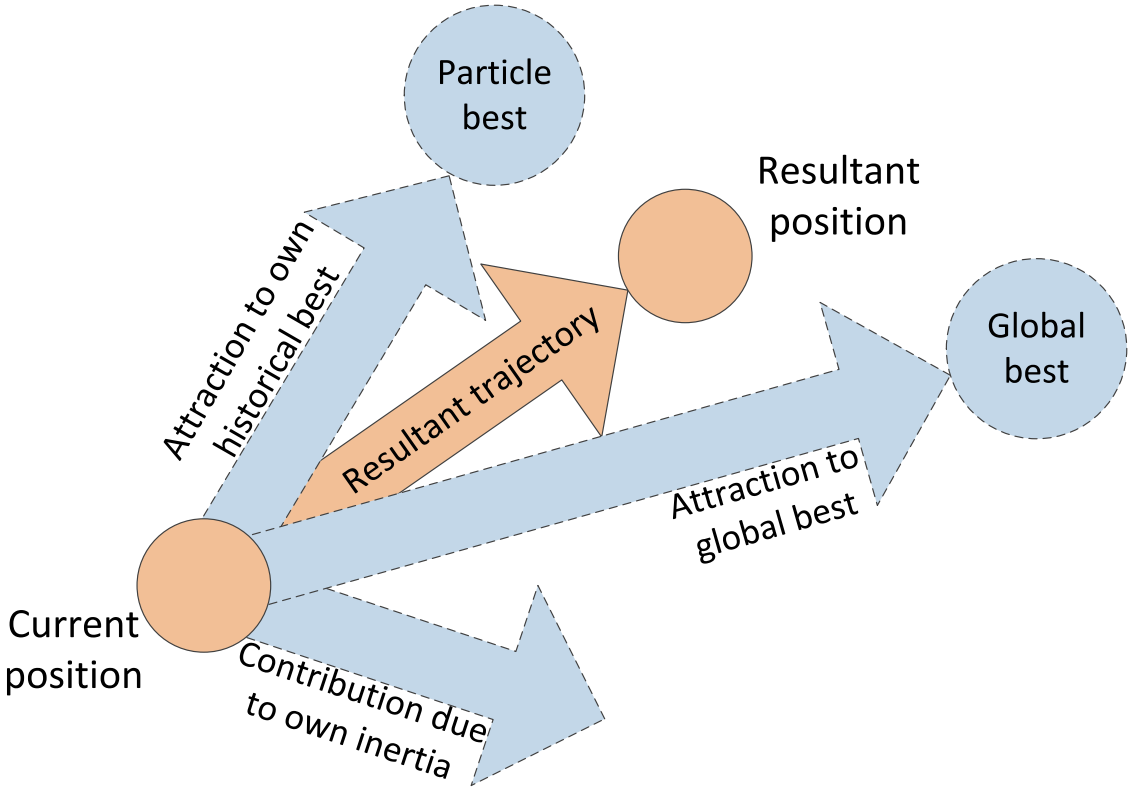

Figure 5.2 – Particle trajectory due to historical and swarm components (not to scale).

reformulated as

$$\begin{aligned} \mathbf{v_i}\left[\mathbf{t+1}\right] &= \chi \times \left[\mathbf{v_i}\left[\mathbf{t}\right] + \varphi_1 \times \text{rand}\left(0,1\right) \times \left(\text{pbest} - \mathbf{x_i}\left[\mathbf{t}\right]\right)\right. \\ &\quad \left. + \varphi_2 \times \text{rand}\left(0,1\right) \times \left(\text{gbest} - \mathbf{x_i}\left[\mathbf{t}\right]\right)\right] \end{aligned}$$

Where

$$\chi = \frac{2}{\left|2 - \varphi - \sqrt{\varphi^2 - 4\varphi}\right|}$$

and $\varphi_1 + \varphi_2 = \varphi > 4$.

χ is the constriction factor, and φ the control constant. Setting φ to 4.1 (> 4) leads to χ=0.729 which is in the same as the inertia factor in the previous case. With this formulation, the value of χ controls the particle's trajectory [84, 88].

This forms the underlying principle of the PSO algorithm, with the process repeated for a number of iterations N. The pseudocode for the basic PSO formulation is listed as algorithm 5.1.

The process is simple in that minimal information about the problem at hand is

Algorithm 5.1 Pseudocode for basic PSO algorithm.

1. Initialise population of size N with random position and velocity.
2. Evaluate each particle's fitness.
3. Update each particle's historical best position and swarm's global best position.
4. Calculate velocity at next iteration.
5. Update position at next iteration.
6. Repeat algorithm for set number of iterations.

required. This black box approach permits PSO to be applied to non-linear problems and requires only manual setting of the parameters in the velocity update equation. The objective function is the only link to the problem to be optimised, and the optimisation algorithm only requires the returned value. Hence the optimisation algorithm is independent (to a certain extent) of the actual problem to be optimised.

5.2.1 Neighbours

In the canonical velocity update equation (equation 5.2), the particles share information between the complete swarm in the form of the global best. This represents a fully connected swarm, where all information is shared between all the particles. This however has the danger of converging prematurely to local minimum. This risk can be reduced by using the concept of a local best, which has more chances to find a global optimum.

In this approach, the *gbest* location in the velocity update equation is replaced by a local best location *lbest*. This is the best location found so far from a smaller subset of the total swarm which each particle communicates with. Various topologies of swarm communication are possible, with the ring most typically used [89]. In this concept, the particles are numbered sequentially, and they then inform K (typically 3) neighbouring particles [83]. Thus information about local bests is gradually passed along the swarm, permitting the global swarm to explore further although at a slower overall rate.

For a minimisation problem, clearly a better solution would be one which returns a lower value from the objective function, with the best (optimal) solution being the one with the (globally) minimal objective value. However in real situations, the

addressing of a single objective could lead to impractical solutions being proposed. This comes about since concentrating solely on one objective necessarily neglects other considerations such that solutions can be unrealistic. Much more convincing solutions address compromises between concerns, such that best balance between conflicting objectives can be realised.

Hence, the consideration of multiple objectives for optimisation purposes is more realistic as it can consider conflicting objectives to identify best compromise solutions. This requires some modifications to the fundamental single objective algorithm in order to be able to handle multiple objectives.

5.3 Multi-Objective Particle Swarm Optimisation

Trivially, a multi-objective optimisation problem can be converted to a single objective one by means of a weighting vector. With this approach, the combined objective function is the weighted sum of the results of all objective functions, and a standard PSO algorithm can be used, working on the objective function:

$$O_{combined} = W_1O_1 + W_2O_2 + \ldots + W_oO_o$$

where W is the weighting factor for each objective for a total of O objective functions. However the selection of the weighting values is critical to the correct operation of the search algorithm in order to attach the required importance (weighting) to each objective function. Furthermore, any change in these values can give considerably different results. The root of this problem lies in a lack of *a priori* knowledge of the solutions' spread in objective space, and hence the distribution among the objectives [81].

A more natural approach towards multi-objective optimisation is the use of Pareto-ranking and the concept of non-domination. Briefly, a solution is said to dominate another if it is strictly better in at least one objective and no worse than the other in all objectives, and is hence assigned to a higher (better) rank. If solutions are in the same rank, i.e. non-dominated with respect to each other, then between these solutions, there is a certain amount of sacrifice in one objective for a gain in another. Figure 5.3 illustrates this graphically for a two objective minimisation problem with

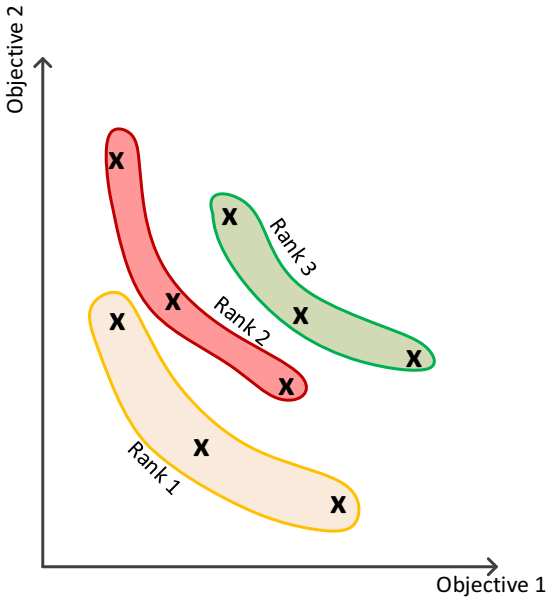

Figure 5.3 – Pareto-fronts on a two-objective, minimisation problem.

three Pareto-ranks identified. Here rank 1 represents the best set of equally optimal solutions, while ranks 2 and 3 are overall inferior solutions compared to the first rank.

With Multi-Objective Particle Swarm Optimisation (MOPSO), the aim is to search for solutions which make up the best possible rank of non-dominated solutions. The result of the optimisation is therefore not a single optimised solution, but rather a set of equally-best compromise solutions. In a two dimension problem, the Pareto-fronts form roughly parabolic curves, while in the case of a three-objective problem, the Pareto-fronts tend towards paraboloids, or bowl-shaped curves. It can be noted that a minimisation problem can be converted to a maximisation one by multiplication of the objective function with negative one (-1).

The final selection is then made from this optimal set of solutions based on higher-level decisions taken by the user considering also the search space results. This is generally intuitive, qualitative engineering judgement which cannot be easily integrated into automated code. In effect this represents the application of a weighting vector to the objectives. However this weighting is performed with hindsight on the obtained results, as opposed to a blind guess without knowledge of the distribution and location of solutions as in the case of an *a priori* weighting vector [81].

The core of MOPSO is therefore the ranking mechanism which identifies the dominated solutions and sorts them into the Pareto-ranks. The algorithm is changed to

Algorithm 5.2 MOPSO pseudocode.

1. Initialise population of size N with random position and velocity
2. Evaluate each particle's fitness in all objectives
3. Identify non-dominated set of particles and store in REP
4. Calculate velocity at next iteration by:
   - $Velocity\,[ctr+1] = W \times Velocity\,[ctr] + R_1 \times (Particle\_best\_loc - Position\,[ctr]) + C_1 \times (REP\,[h] - Position\,[ctr])$
5. Calculate position at next iteration by
   - $Position\,[ctr+1] = Position\,[ctr] + Velocity\,[ctr]$
6. Repeat algorithm

accommodate Pareto-ranking as the main measure of fitness between solutions but is fundamentally similar to the single-objective PSO described earlier. The pseudocode for the MOPSO algorithm is listed as algorithm 5.2 based on the MOPSO algorithm developed in [90].

In algorithm 5.2, the concept of a Repository (REP) is introduced, which is a store of the the solutions making up the first ranked Pareto-set. The size of REP is of course limited. In case the number of solutions in the first rank is greater than the size of REP, a selection must be made, based on some quantifiable measure.

Within the context of multi-objective optimisation, an additional crowding metric is defined. Its aim is to ensure sufficient exploration of the Pareto-front by emphasizing solutions which are in less crowded areas (in the objective space) and hence more unique. This reinforces a spread of solutions along the Pareto-front. A trivial technique would be the Euclidean distance between particles, however especially as the number of objectives increases, the complexity of this calculation increases sharply. Other approaches involve niching or other area-based counting techniques in order to give an indication of the relative crowding of different areas on the Pareto-front. These do however require additional parameters whose value significantly influences the outcome. A simpler approach as outlined in [91] simply considers the size of the largest hypercube which can be fitted around a solution without touching adjacent ones, giving an indication of how unique a solution is. This is used to quantify if a solution is 'better' than another if in the same rank in order to emphasize searches to

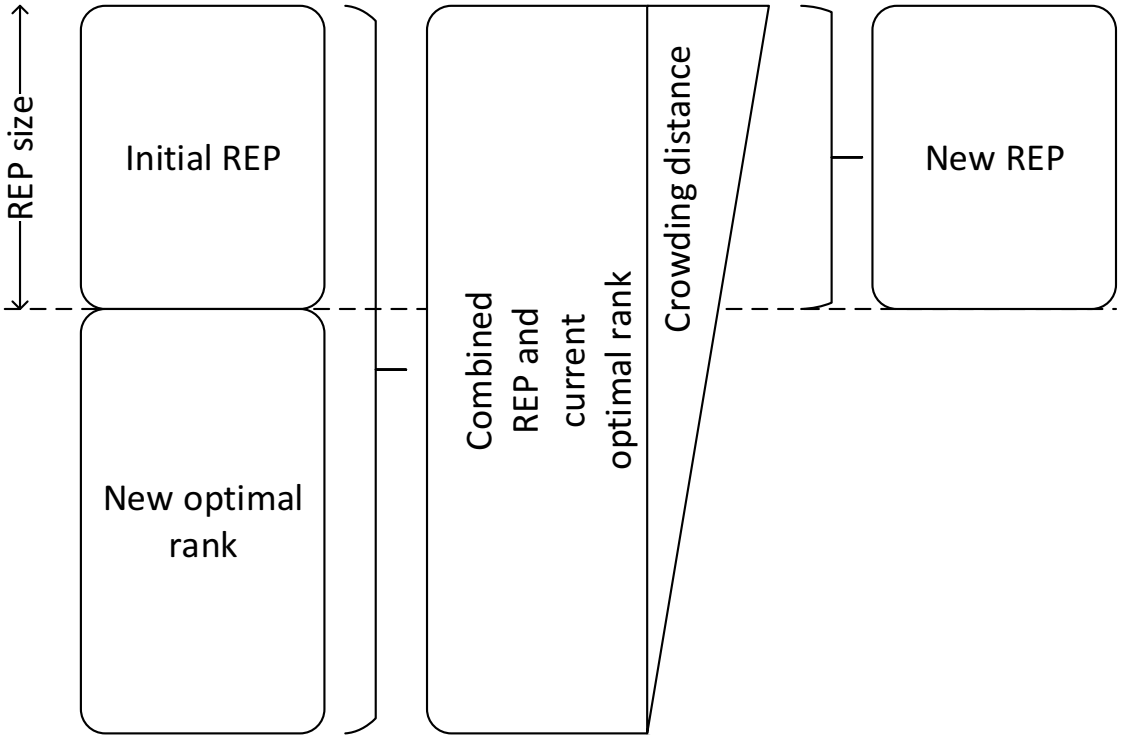

Figure 5.4 – Population and selection of REP.

less crowded areas of the solution space. Hence the REP memory is now a function of both rank, and crowding distance (the bigger the better). This is a modification from the original MOPSO developed in [90] and takes inspiration from aspects of multi-objective GA such as NSGA-II as developed in [91] and applied in [45] and [92].

REP is initially populated with solutions from the first rank. If this is greater than the size of REP, then the solutions are ranked according to crowding distance, and the REP filled up in descending order (illustrated in figure 5.4). Additionally, in the velocity update equation, the concept of global_best is also different in MOPSO in that there is no unique, globally best solution. Instead a Pareto-optimal solution is selected for each particle using binary tournament selection from the repository which contains the Pareto-front of rank 1. The crowding distance is again used as the discriminator between these equally optimal solutions.

5.4 Mutation operator

With any search algorithm, there is a risk of so-called premature convergence. This refers to the algorithm locating a local optimum rather than the global optimum. Thus though the algorithm would have converged, a true globally optimal solution would

not have been found. In multi-objective optimisation, this represents another Pareto-set which is dominated by the true Pareto-optimal one. Premature convergence is due to a number of factors, but is fundamentally a case of focus on exploitation of current solutions as opposed to exploration of new spaces. The balance of exploration vs exploitation therefore influences the security of finding global optima at the expense of algorithm performance.

Mutation represents a random perturbation through the search space which ensures that exploration will still occur even if the whole swarm has converged. This will obviously involve a penalty in terms of convergence speed, as the members of the swarm will perform random movements independent of the located solutions.

The principle behind mutation/perturbation is that a number of search space descriptor(s) are randomly modified according to a certain predefined probability. Uniform mutation randomly mutates particles with the same probability over all iterations. This ensures that exploration will take place until the final iteration. However this would involve the largest computational overhead. With variable probability mutation, the probability of mutation is progressively decreased with each iteration, such that initially a high percentage of the population is randomly perturbed (to have highest exploration) and towards the end of the algorithm, very few perturbations occur (exploiting the found solutions). This is much more computationally efficient, but requires tuning of additional parameters (mutation rate decrease). A widely accepted rule is that the mutation rate is inversely proportional to the number of dimensions in the search space [81]. For this work, uniform mutation was selected as it is the simplest to implement and will guarantee exploration until the very end.

In order to select particles for mutation, a random set of numbers (equal in size to the swarm) is generated. Any of these numbers which is less than the mutation probability constant is selected for mutation, and hence replaced by a random variable within the search space's limits. This occurs after the particles' new position has been calculated. Performance (final convergence speed) will correspondingly decrease, but robustness in locating optimal solution sets will increase.

5.5 Application to shore networks

The design and optimisation of an electrical network is a non-linear process which can be adapted to make use of an evolutionary algorithm as part of the design process in order to identify best configurations and component ratings [84, 86]. In the cold ironing implementation, the reduction of emissions is clearly a high priority of the system. This is directly related to the efficiency of the network and the associated losses along the distribution network, which depends on the operational flexibility and suitability of a particular network to the load profile. Hence the design process should aim to identify a network with the best overall energy efficiency. Furthermore, the emissions are also a function of the shoreside generation mix which varies according to the location of the port.

Three different fundamental electric network topologies have been identified which describe a centralised topology, a distributed topology and a DC distribution system (figures 4.1, 4.2 and 4.3 respectively) together with a hybrid cold ironing/LNG generation topology (figure 4.4). The optimisation process aims to identify the optimal configuration as well as optimal component values, and hence the component sizes are defined as the variable set, in addition to the actual network type.

The PSO algorithm can therefore be set up to vary the component sizes and network type to obtain minimised emissions as its objective. However this may not lead to practical solutions since by maximising component ratings, overall losses are reduced and hence emissions minimised. This would involve a considerable expense which makes such a system infeasible.

Therefore the consideration of a multi-objective search is more realistic as it permits a conflicting objective (such as the overall component cost) to be considered in addition to the drive for emission reduction. Each installation of cold ironing is unique, and presents its own individual challenges and requirements. Hence the costs associated with each case will be project specific and highly dependent on the actual situation (e.g. whether trenching is required, distance to berths etc. . .). Estimating the (absolute) cost of a cold ironing network is therefore highly unrealistic based solely on the system design.

For a meaningful comparison of costs between configurations, the component count and component ratings can be used to obtain the relative costs. By adopting a

per-unit system of cost, the total cost figure for each configuration can be calculated based on the number of devices and their rating. Each component is assigned a per-unit cost, taking the cost per kVA of a transformer as the base cost. Hence a multi-objective optimisation routine will strive to minimise cost as well as emissions.

5.6 Objective functions

Central to the functioning of the PSO algorithm, the objective functions establish the link between the search algorithm and the problem to be optimised (figure 5.1). This black box treatment of the problem to be optimised is the core of evolutionary algorithms' robustness and applicability to non-linear problems. The energy demanded from the utility is the first objective function, and is returned by the models developed in the previous sections.

The second objective function describes the cost associated with the network. This is clearly a highly subjective figure which depends on a large number of specific factors associated with each case. In order to make a meaningful comparison, the cost considered is a normalised cost which compares the expected costs of different topologies relative to each other. Transformer cost is considered at a base cost of 1pu/kVA, while power electronic converters are considered as 3pu/kVA based on typical costs as highlighted in [77]. Based on the number of each component in each configuration, the cost is calculated as the weighted sum of each component's rating. The cost of the LNG generator system is assumed as a variable, and will be tested at different values in order to examine the influence on results.

With a design-by-simulation approach, the objective function involves running a simulation of the network and evaluating the resultant emissions according to the local generation mix. The input to the simulation consists of the electrical power demand of the berthed vessels which is obtained from port authority data. This power profile should therefore reflect a typical period of time which is representative of the daily harbour usage. The actual network configuration is defined according to the particular solution as set by the PSO algorithm.

In order to limit the search to realistic solutions, the PSO algorithm makes use of constraints which limit the search to feasible solutions. This increases the efficiency of the algorithm, by discarding these unrealistic solutions. An example of a constraint

could be the definition of a maximum cost, which every feasible solution must meet. Any solution with a higher cost would be deemed infeasible and hence discarded.

The constraints in this case are handled by a hard limiting approach, i.e. in case a constraint is violated, the particular solution is rejected [93]. Two electrical constraints are accounted for in the model; within the objective function, checks are carried out to ensure that the electrical quality at the berthside connection is within limits (in terms of RMS values) as defined in ISO/IEEE/IEC 80005-1, and the second check ensures that none of the components are overloaded. In the case of constraint violation, a flag variable is set, and an infinite emission value is returned. This ensures that such solutions (configurations) which violate any of the constraints are heavily penalised and hence do not have any influence on successive iterations.

A real number representation in per-unit is used to define the variables. For the component ratings the per-unit values are scaled by the base value (selected as the largest available component size in kVA) in order to get absolute component sizes. For realistic solutions, component ratings are rounded to the nearest 50kVA. Similarly the choice of network topology is represented on a real scale between 0 and 1, with rounding intervals to the nearest third to identify which particular topology has been selected. This representation can be extended to any number of topologies/components by amending the base values and scaling factors. By having a normalised representation of variables, the search space is thus constrained along all its dimensions by interval confinement.

Particles can fly out of this search space, so a mechanism has to be included to restrict and return particles back within limits. In case a limit violation occurs, the offending particle is returned to the search space border, and its velocity is reversed. This will 'bounce' the particle back into the valid search space. In order to limit the exploration of the moving particles, a limit is also placed on the particle velocities. This is set at half the maximum distance of the search space [83], i.e. in case the size of a dimension being between 0 and 1, the velocity is limited to 0.5.

5.7 Port case study

The emission factors used in the optimisation routine are described in section 3.3, while the electrical constraints are as defined by ISO/IEEE/IEC 80005-1. These

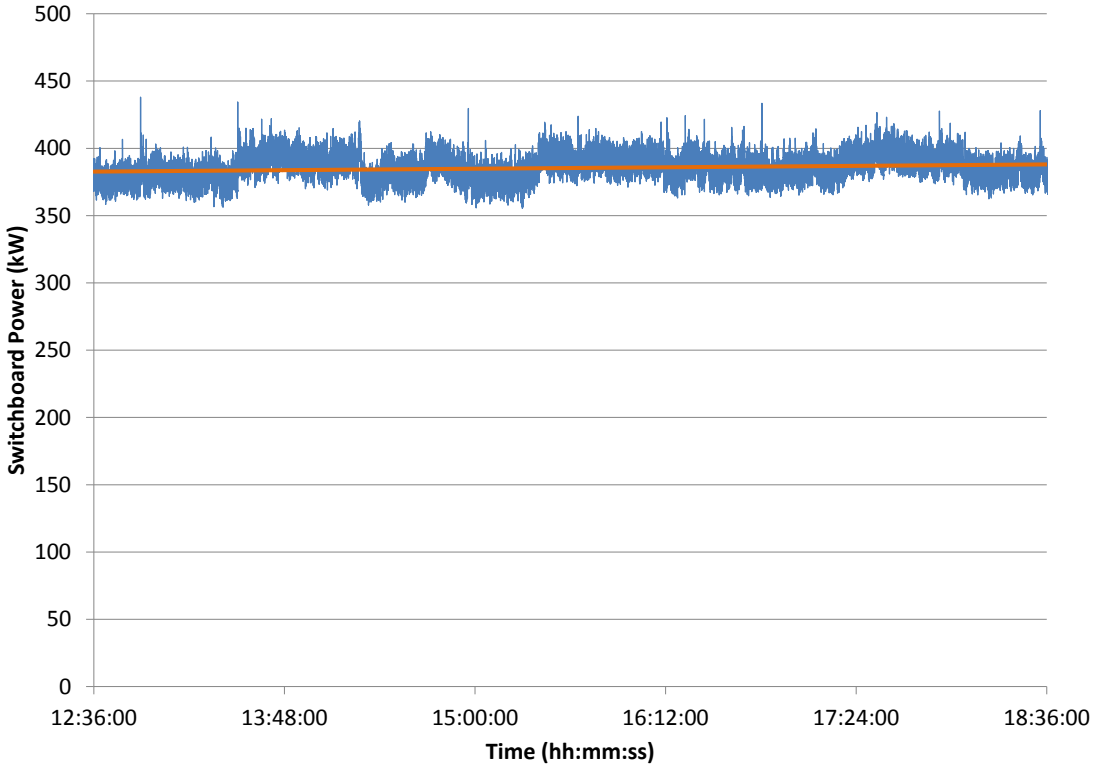

Figure 5.5 – Snapshot of measured and averaged load profile on MV Auto Baltic [42].

were used to perform the configuration search for an example case, where the port being considered consists of five berths, visited by RoRo vessels, shown as figure 3.3. The cable routes in this case exploit existing trenches running from the central substation to the individual berths.

Figure 5.5 shows an example of the actual measured power profile showing the variation in the RoRo vessel load. It can be seen to be quite stable and does not show significant variation. For the purpose of the identification of optimal networks, energy losses are the primary concern, with the analysis therefore considering the averaged value of the load.

Based on the historical visiting vessel itineraries as well as the demand correlation of figure 3.6 the power profile of berthed vessels can be estimated. For a typical day, the berth power demands (together with the total demand) are shown as figure 5.6. In addition to the power profile, associated with each berth is the frequency demanded by the berthed vessel. This defines whether a frequency converter is required or not, and therefore directly impacts the total efficiencies of the shore network.

Though representative, the profiles over a single day do not necessarily reflect the complete spectrum of visiting vessels. Hence, considering the profile over a whole

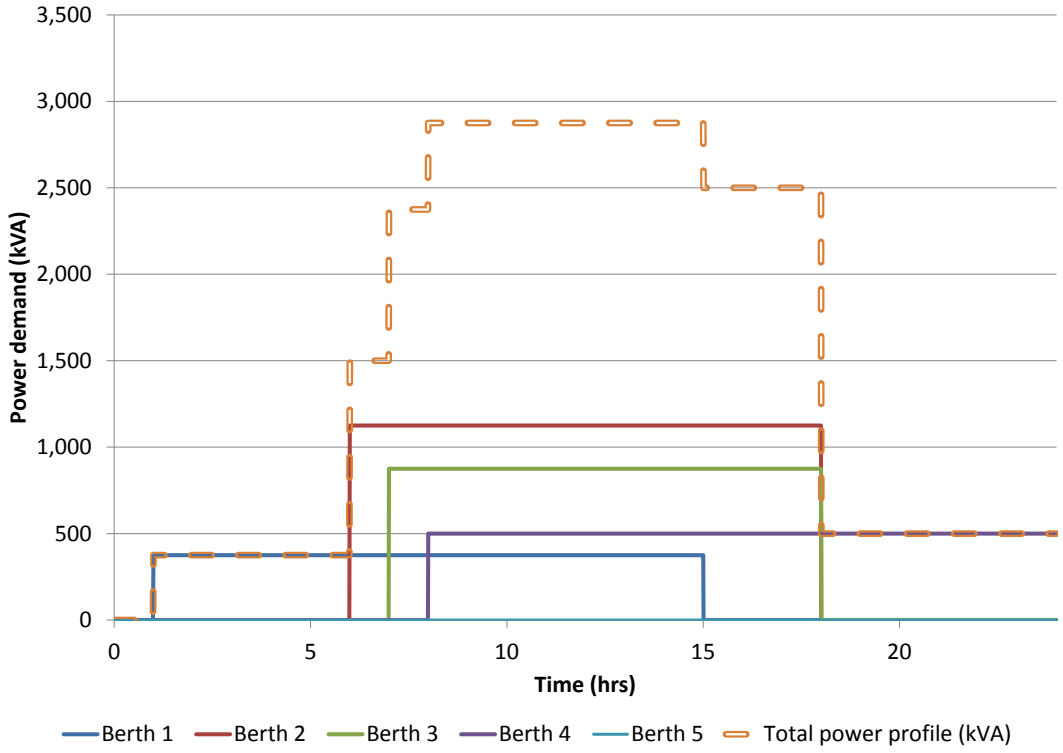

Figure 5.6 – Power profiles for typical day at port.

week gives a better indication of different power levels and frequency demands. A typical (working) week was chosen (14/03/2012 to 17/03/2012) and is shown as figure 5.7. The objective function calculation will be take correspondingly longer, due to simulation run times associated with this longer duration.

The optimisation procedure evaluates the energy demand for each network configuration as specified by the PSO, and verifies whether it meets the electrical constraints on voltage levels and overloading. Feasible solutions are then considered for the optimisation with respect to energy generated (at source) and normalised cost.

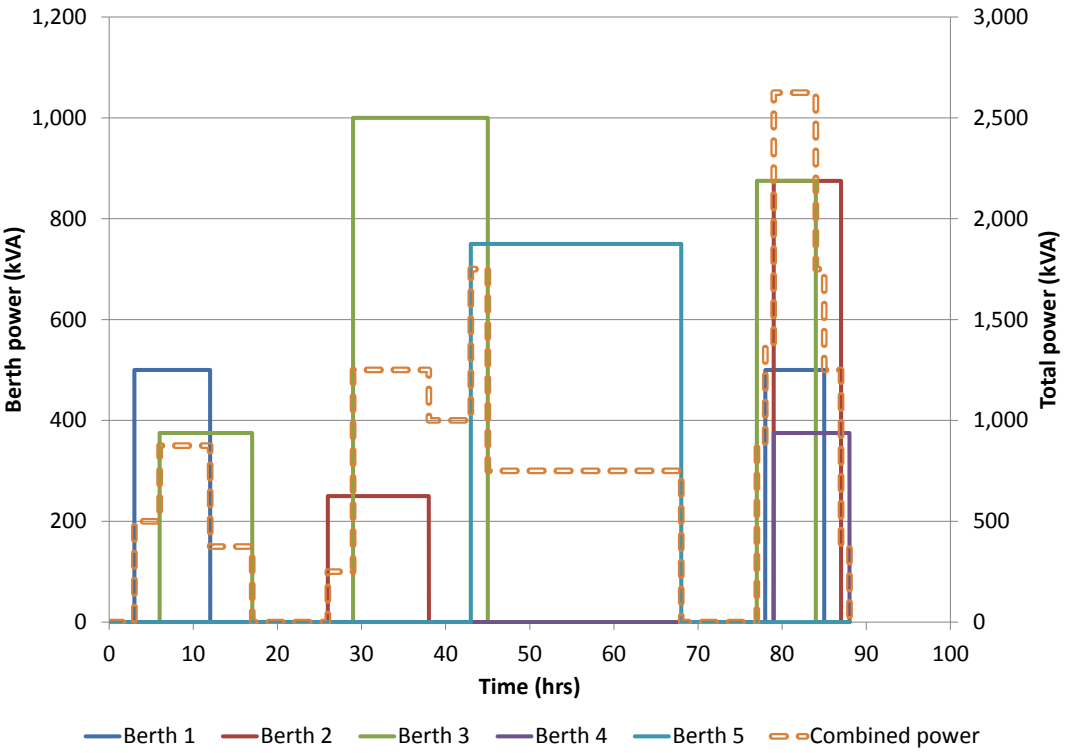

Figure 5.7 – Power profile over a week.

Chapter 6

Shore supply results

6.1 Cold ironing only

The optimisation was run over 500 iterations in order to identify the optimal set of solutions with respect to minimisation of energy demand (maximisation of total network efficiency) and minimisation of component ratings (and hence cost) considering solely a cold ironing solution. This is accomplished using the MOPSO algorithm and network models outlined in the preceding sections. The final configuration is manually chosen from this set of equally-optimal solutions based on actual preference for a configuration taking into account also search space information (not typically used by the PSO which only considers objective space information as a quantifying metric). The parameters used in the PSO are defined in table 6.1.

Figure 6.1 shows the progression of the Pareto-optimal sets (of rank 1) over all the iterations. This shows the progress of the optimal search, identifying solutions closer to the bottom left corner of the objective space, associated with minimising cost

Parameter	Value
Swarm size	20
Repository size	20
Number of iterations	500
Maximum particle velocity	0.5
Maximum berth rating	5MVA
Maximum central component rating	10MVA
Rating interval	50kVA
W (inertia constant)	0.4

Table 6.1 – Parameters used in MOPSO algorithm.

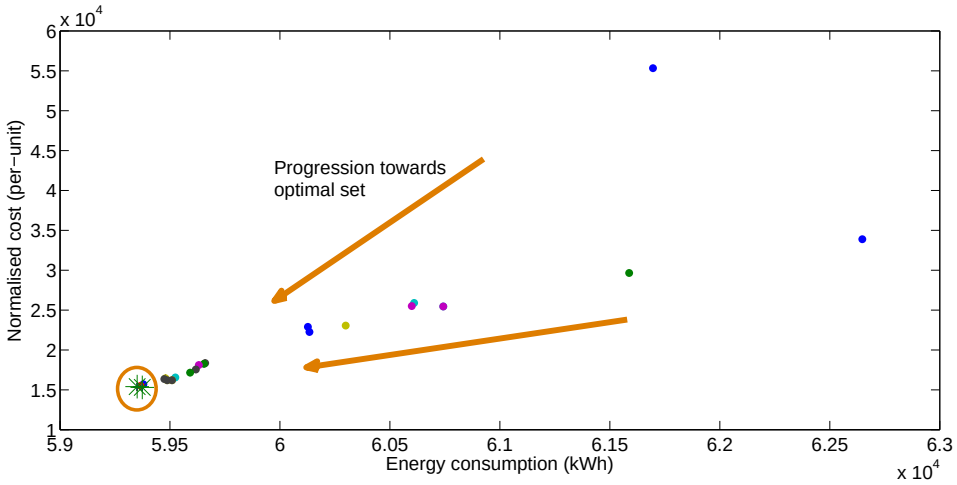

Figure 6.1 – Objective space progression illustrating the optimal Pareto-sets over 500 iterations. Only feasible solutions in the first rank are shown, and solutions found repeatedly in successive iterations are obscured by later solutions. Each colour indicates an individual iteration.

Component ratings (kVA)						Network type	Energy demand (kWh)	Total cost (pu)
Berth 1	Berth 2	Berth 3	Berth 4	Berth 5	Central			
700	1000	1050	550	900	2800	Centralised	59351	15400
550	1200	1050	400	900	2800	Centralised	59374	15300

Table 6.2 – Corresponding search space configurations of final Pareto-optimal set for optimised cold ironing network.

and energy consumption, with the final set of Pareto solutions (consisting of two solutions) highlighted. The corresponding search space description of the final Pareto-set is given in table 6.2. Clearly, a centralised network configuration (schematically described in figure 4.1) is most appropriate for this particular scenario, with two equally optimal solutions identified by the algorithm. One would give slightly higher efficiency, at the expense of slightly larger components (and hence more expensive). In the final selection, engineering judgement would be used, such as the need for extra rating margin to allow for future growth.

For meaningful results, the emissions and energy consumption from cold ironing must be compared with the current way of providing the onboard power, i.e. by running of the generator sets on each ship. Since generation is carried out in the vicinity of the consumers (onboard loads), transmission losses are kept to a minimum when compared to cold ironing, where power is generated remotely and has to be transmitted to the point of consumption. Furthermore it must be converted to the required voltage and frequency, each of which involves losses due to intrinsic inefficiencies in each conversion step. Additional losses are suffered because of

harmonics injected into the system by each power electronics stage.

The total (electrical) energy demand from the berthed vessels is of 53MWh. Clearly all the shore power solutions will have a higher energy demand due to the additional losses introduced by the shore supply systems, giving an overall energy efficiency of around 90%. The comparison should therefore be made with respect to the emissions generated in each case, which are obtained from the emission factors for auxiliary engines (table 2.6) and each locale's generation mix, additionally accounting for the averaged transmission losses.

Selecting the first solution from table 6.2, and comparing the environmental performance of the cold ironing system with the onboard generation for a number of different locations[3] gives the emission figures of table 6.3. This includes the additional transmission losses associated with each location and the specific generation mix. The energy generated is greater since the transmission and cold ironing network losses must also be supplied when compared to the onboard generation. The resultant emissions are then seen to be highly dependent on the generation mix of the location where the ship is berthed. The actual source of electricity cannot be defined, but the choice of determining emission by country was made as it represents a specific energy mix policy. Clearly, countries with a high renewable (e.g. Spain) or nuclear mix (e.g. France) will have much lower resultant emissions compared to the onboard generation or other coal-fired locations.

For the selection of countries considered in table 6.3, NO_x emissions are reduced across the board. CO_2 is reduced in all cases other than those with a very high percentage mix of coal (such as China). The situation with SO_x emissions is slightly less clear, especially with the use of low sulphur fuel used onboard. Irrespective of the actual generation mix however, localised emissions in harbour are reduced, as the auxiliary generators can now be turned off. This is one of the major drivers of cold ironing, since in-harbour emissions are eliminated - a location which is typically highly industrialised yet close to human habitation. Hence cold ironing is always beneficial to the harbour area, with the actual balance of emissions needing to be analysed with respect to the generation mix employed. In the case of Spain, CO_2 emissions are practically halved when compared to the current situation with onboard generation.

[3]The selection of countries reflects the interest in the TEFLES project consortium.

Solution	Energy generated (kWh)	CO_2 (kg)	NO_x (kg)	SO_x (kg)	
				0.1% S content	0.25% S content
Onboard generation	53144	36669	739	23	58
Spain					
Cold ironing	64748	19651	30	20	
Difference	+22%	-46%	-96%	-13%	-65%
UK					
Cold ironing	63547	28422	41	31	
Difference	+20%	-22%	-94%	+34%	-46%
China					
Cold ironing	62259	45262	87	82	
Difference	+17%	+23%	-88%	+256%	+41%

Table 6.3 – Comparison of environmental performance for optimised cold ironing network. The Sulphur emissions are given for two different Sulphur content fuels (used onboard).

6.2 Cold ironing with shoreside generation

One of the major concerns highlighted by operators is a constraint in terms of the allowable power to be drawn from the existing utility supply (figure 3.4). Based on the existing loads and the actual infrastructure from the utility, the margin for additional loads can be slim. In such a case, new substations or distribution lines/cables could be required to supply the additional expected load, greatly increasing the capital expenditure required for the cold ironing installation (and hence making it even more unattractive).

Shoreside generation involves the installation of generation sources within the harbour area to provide a contribution towards the harbour power demands. This can help to reduce the power required from the utility, making the installation more cost-effective. Once again, this is highly dependent on the actual location.

As discussed previously, LNG is an alternative supply to cold ironing being considered in this study. Shoreside LNG generation involves the use of modified diesel engines to run on LNG, either as dual-fuel or spark-ignition types. LNG is widely touted as a clean fuel alternative to diesel, with lower emissions, proven reserves and a lower fuel cost. Considering a complete Life Cycle Analysis (LCA) however, the CO_2 emission

advantage is less clear cut, and the issue of methane slip (unburned methane) can even negate greenhouse warming benefits [72]. However, particulate emissions and SO_2 emissions are practically zero when burning LNG.

Table 3.9 lists the emission factors for an LNG-fuelled generator set [74] in terms of the electrical energy produced. It is appreciated that though LNG use will significantly reduce the impact on acidification and eutrophication, the greenhouse gas emissions when looking at the complete LCA are not significantly reduced when compared to diesel fuel [72].

In this scenario, the LNG system is considered as being an alternative to the cold ironing system, in providing electrical power to the berthed ships. An example of the hybrid topology being proposed is given in figure 4.4, which shows two berths being supplied by shoreside LNG, while the other three berths are supplied by a distributed cold ironing topology. By using the search algorithm described earlier, the search space is now expanded to include various configurations with multiple combinations of shoreside LNG generation or cold ironing at the different berths.

The objective functions must be modified in this case since different sources are being compared. The consideration of demanded energy is not a valid comparison, since cold ironing involves additional transmission losses. Rather, emissions must be compared on a direct basis between the different sources, thus the search algorithm must take into account the actual generation mix.

The cost function must also be modified to take into account the different systems being used. Similarly to the previous search considering only the cold ironing network, a relative cost on a per-unit basis is used. Once again, the costs associated with the LNG-fuelled generation system are highly variable and installation specific (e.g. whether onsite LNG infrastructure already exists or needs to be installed). Thus the cost figure is given on a per-unit basis, and the optimisation is repeated for various cost values of the LNG system, permitting the various emergent sets of solutions to be considered dependent on the cost per kVA of the shoreside LNG system (accounting for all the necessary components) compared to the cost per kVA of the cold ironing system.

Figure 6.2 shows four Pareto-optimal sets of combined shoreside LNG generation and cold ironing configurations in the objective space (in this case showing only CO_2 emissions for clarity). Four distinct sets can be discerned, roughly parabolic in

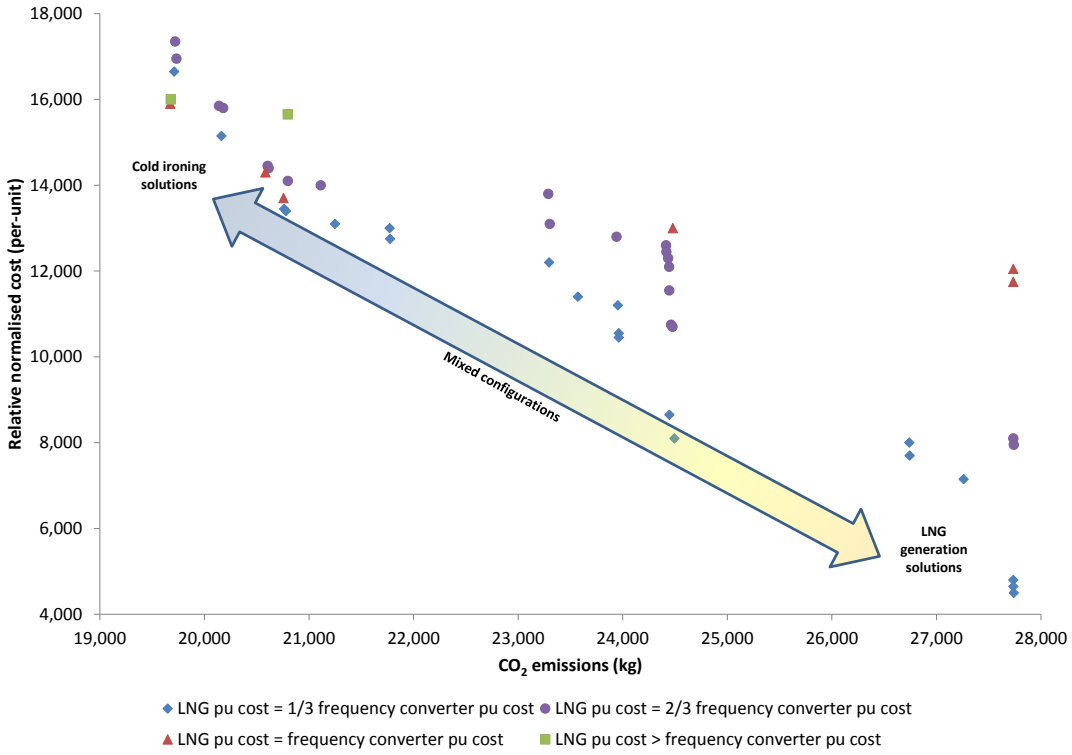

Figure 6.2 – Various optimal solution sets for mixed shoreside LNG generation and cold ironing systems for different per-unit costs.

nature, and stacked according to the progressive cost of the LNG systems.

Each configuration presents a different combination of LNG-fuelled generator and cold ironing connections (one such case exemplified as figure 4.4). Clearly with higher per-unit cost of the LNG generation system, the search algorithm favours predominantly cold ironing configurations (confirmed from examination of the search space description), while when the specific cost of the LNG system is lower, cold ironing loses out on cost, although the configuration with lowest emissions (CO_2) is still a cold ironing one.

In terms of SO_2 however, shoreside LNG generation would be much cleaner since the emission factor for this is practically zero. Cold ironing solutions clearly are superior in terms of emissions (CO_2), but with a lower cost per kVA of the LNG solutions, lower-cost (but higher emitting) configurations with mixed LNG generation are also possible. This demonstrates the compromise nature of multi-objective optimisation, which balances trade-offs for equally optimal solution sets.

Taking an example configuration from the set where the shore-side LNG generation has a per-unit cost of one third of the frequency converter's per-unit cost, a selected configuration is described as table 6.4. In this configuration, two of the berths are

Configuration	Component ratings (kVA)						Topology	Emissions (kg)			Total cost (pu)
	Berth 1	Berth 2	Berth 3	Berth 4	Berth 5	Central		CO_2	SO_x	NO_x	
Cold ironing	750			900	1050	1350	Centralised	23964	10	75	10450
Shoreside LNG		1000	1350				Distributed				

Table 6.4 – Example configuration for mixed LNG/Cold Ironing system with shoreside LNG generation system per-unit cost being $^1/_3$ of the cost per kVA of frequency converter.

supplied with an LNG generation system, while the rest are supplied by a smaller cold ironing network using a centralised topology. This gives a lower cost solution than that highlighted in the (solely) cold ironing configuration, but at slightly higher resultant emissions.

Another possible configuration, valid for a higher LNG system cost of 2/3 the frequency converter's per-unit cost gives the results of table 6.5, where the LNG system is restricted to the lower demand berths.

These results are valid for the generation mix considered (Spain in this case) for this particular scenario. For other generation mixes with a dominance of coal generation, cold ironing could prove less attractive in terms of emissions than shoreside LNG generation, dependant on the actual relative cost as highlighted by figure 6.2.

This technique permits the identification of cost-effectiveness of alternative technologies to be examined based on their relative cost, permitting the search algorithm to be applied to various scenarios by the adjustment of the cost's base value. Optimal solutions are a case of selecting the best compromise between conflicting objectives to make for real practicable configurations. Cold ironing is a highly effective solution in reducing emissions in-harbour, but is not a necessarily a universal solution when considering net emissions. Shoreside generation (such as using LNG) can help to make cold ironing more effective and realisable, and when evaluated using a multi-objective

Configuration	Component ratings (kVA)						Topology	Emissions (kg)			Total cost (pu)
	Berth 1	Berth 2	Berth 3	Berth 4	Berth 5	Central		CO_2	SO_x	NO_x	
Cold ironing		1100	1350		1550	1900	Centralised	21113	18	46	14000
Shoreside LNG	650			550			Distributed				

Table 6.5 – Example configuration for mixed LNG/Cold Ironing system with shoreside LNG generation system per-unit cost being $^2/_3$ of the cost per kVA of frequency converter.

optimisation algorithm, can be used to identify suitable mixed configurations for a given scenario [14].

6.3 The electrical aspect

Among the most important electrical characteristics of any power distribution network is the quality of the power delivered to the load. Power quality can be measured by the level of deviation of the voltage supply from the ideal sinusoidal waveform with the desired amplitude and frequency. The connection of a load should not have adverse effects on the supply network. Equally, the supply to any downstream loads should not be negatively affected by any interactions between the load and supply network. In a cold ironing scheme, the quality of supply needs to be examined at the berthside, as berthed ships expect a guaranteed minimum level of power quality, while also ensuring that the operation of the shore connection system does not adversely affect other consumers connected to the same utility supply [53].

An ideal electrical system supplies and draws sinusoidal voltage and current waveforms. However, the presence of power electronic devices creates a non-linear system due to the turn-on and turn-off operations of these controlled switches. Hence the real waveforms observed consist of a large number of higher order harmonics superimposed

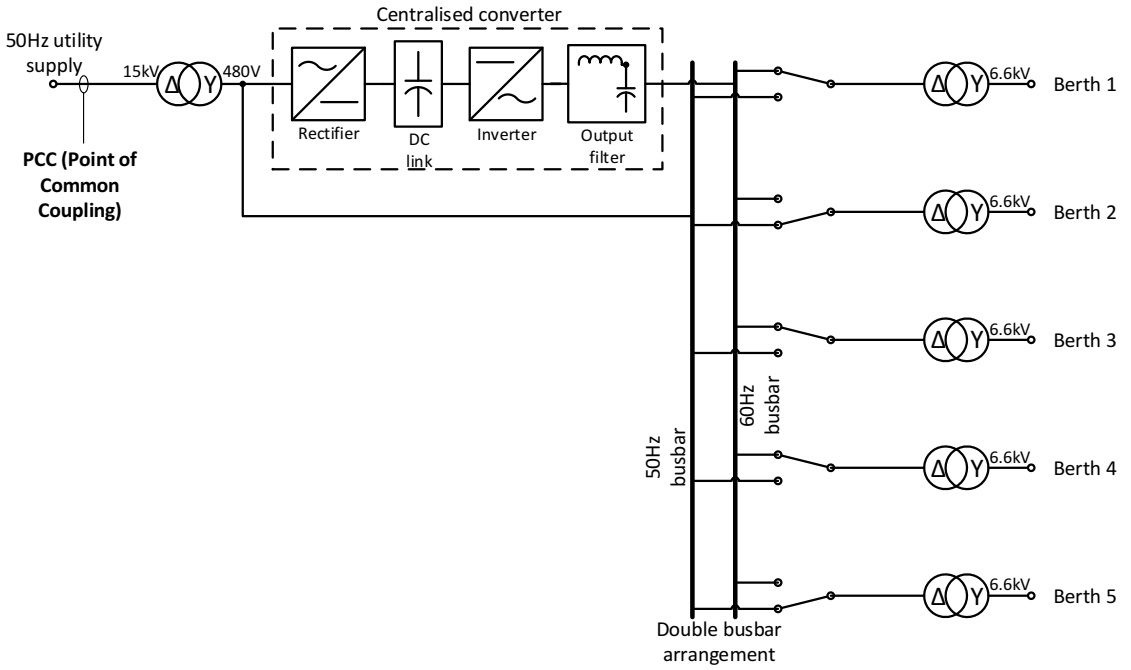

Figure 6.3 – Detailed centralised distribution topology schematic.

on the fundamental 50 Hz or 60 Hz frequency.

The presence of harmonic currents means that the total Root Mean Squared (RMS) current flowing in the system is higher (for any given load), increasing the Ohmic losses. Furthermore, transformers and other magnetic components suffer from increased losses at higher frequencies, leading to additional power losses as highlighted in figure 4.7. In addition, the presence of harmonic currents will cause a corresponding potential drop across the supply impedance, leading to a distorted voltage at the supply. This results in other consumers being affected by this non-sinusoidal supply. Hence, various standards and requirements are in place to ensure that equipment/systems meet a minimum level of harmonic content. The harmonic content is quantified by the Total Harmonic Distortion (THD), which for a distorted current waveform is defined by equation 6.1, where I_h are the individual harmonic components making up the waveform and I_1 is the fundamental waveform. This is measured at the Point of Common Coupling (PCC), which is the point in the power system closest to the user where the system operator could offer service to another customer as marked in figure 6.3 [94].

$$THD = \sqrt{\frac{\sum_{h=2}^{\infty} I_h^2}{I_1^2}} \tag{6.1}$$

Figure 6.3 shows in more detail the setup of the centralised topology, identified as the most appropriate configuration for the scenario being considered (results of table

Berth number	Load (kVA)	Line Voltage (V)	Deviation from nominal	Voltage THD at berth
1	500	6,459	2.1%	0.66%
2	800	6,441	2.4%	0.66%
3	1,000	6,414	2.8%	0.65%
4	350	6,473	1.9%	0.67%
5	700	6,447	2.3%	0.66%
			Input current THD	55.46%
			Voltage THD at PCC	5.33%
			Overall efficiency	90.4%

Table 6.6 – Steady-state quantities for system of figure 6.3.

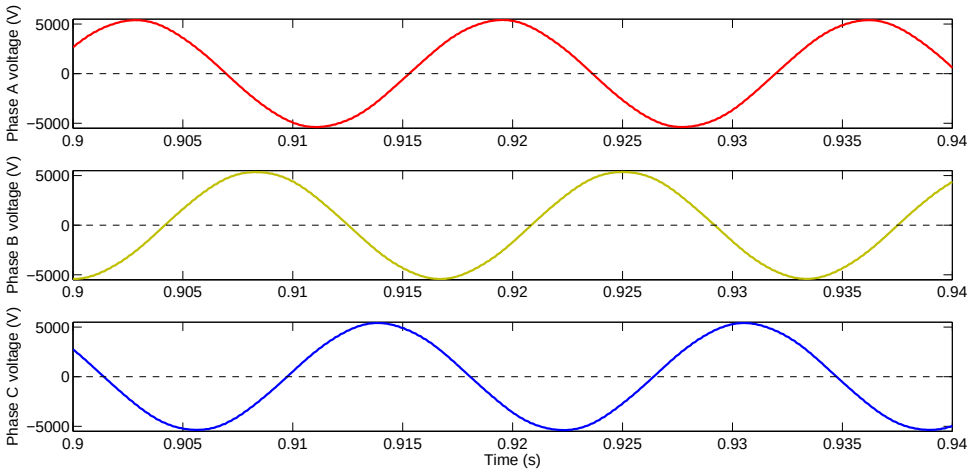

Figure 6.4 – Voltage waveforms at berth 1.

6.2 and figure 6.1). Table 6.6 shows a snapshot of the steady state operation of the system. The steady state RMS values of the output voltages for all the berths are within the 3% permitted deviation from the nominal (6.6kV) [53]. Figure 6.4 shows the voltage waveform as supplied to a vessel connected to berth 1 (figure 6.3) with a 500kVA load. The frequency spectrum of the Phase A voltage waveform is shown in figure 6.5. This shows how some harmonic distortion is still present at the output which would not be discernible from a simple visual inspection of the time domain waveforms. Of interest here are the harmonics (attenuated) around the 4kHz band, which correspond to the sidebands around the switching frequency of the converter. The THD value for this output is 0.66%, and none of the individual harmonics exceeds 3%. The supply to berth 1 is therefore well within the acceptable THD limits. Similar plots are seen for the other berths and other phases, and these results are tabulated in Table 6.6 showing how all outputs to all berths are within the acceptable THD limits.

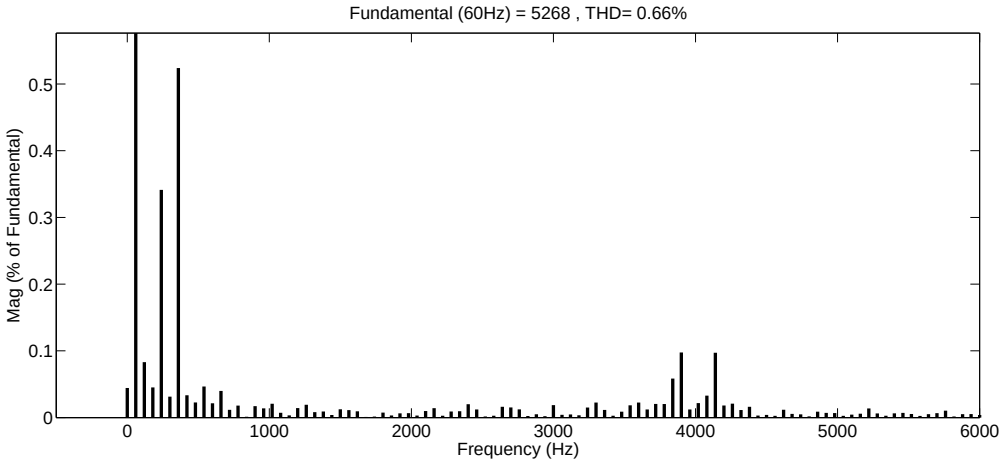

Figure 6.5 – FFT of output voltage at berth 1.

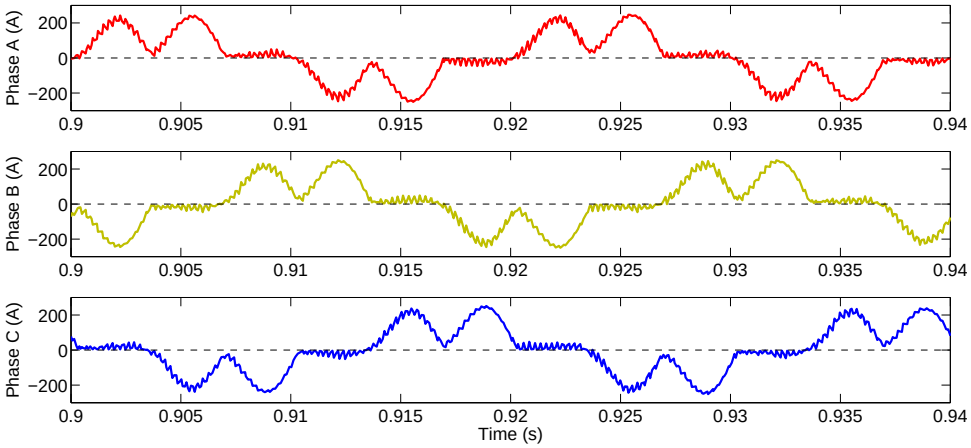

Figure 6.6 – Input current from utility supply.

At the supply side, figure 6.6 shows the input currents drawn from the utility at the 15kV Point of Common Coupling (PCC) which is the point on a power supply system where other loads would be connected (figure 6.3). This clearly shows the six pulse operation associated with the use of a diode bridge rectifier with a capacitive DC link (six pulses of the dc waveforms for every ac supply cycle). This waveform is far from sinusoidal, with a significant 5th harmonic component at 250Hz (for a 50Hz supply), together with additional higher frequency harmonics. Seen in the frequency domain, this is confirmed by figure 6.7 which shows the FFT of the input current as measured at the PCC. In this case, the THD is above 50%, with very large low frequency harmonics which exceed the minimum levels as set by standardisation bodies. Table 6.7 and Table 6.8 list the acceptable voltage and current THD limits at the PCC as specified by IEEE 519 standard [94].

The effect of this distorted supply current on the supply voltage waveform (due to

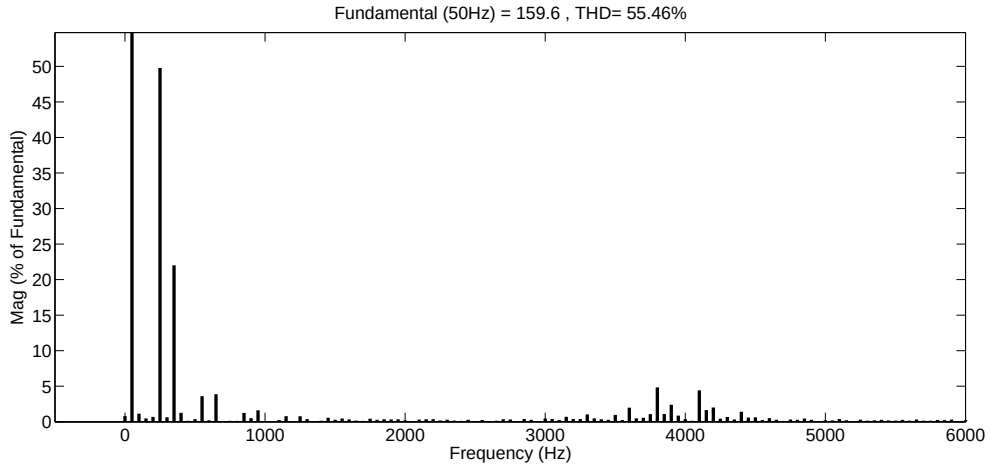

Figure 6.7 – FFT of input current.

Bus voltage (V)	Individual harmonic (%)	Total harmonic distortion THD (%)
V≤1.0kV	5.0	8.0
1kV<V≤69kV	3.0	5.0
69kV<V≤161kV	1.5	2.5
161kV<V	1.0	1.5

Table 6.7 – Voltage distortion limits at PCC [94].

I_{sc}/I_1	Odd harmonic order h (%)					Total Harmonic Distortion (%)
	3≤h<11	11≤h<17	17≤h<23	23≤h<35	35≤h≤50	
<20	4.0	2.0	1.5	0.6	0.3	5.0
20<50	7.0	3.5	2.5	1.0	0.5	8.0
50<100	10.0	4.5	4.0	1.5	0.7	12.0
100<1000	12.0	5.5	5.0	2.0	1.0	15.0
>1000	15.0	7.0	6.0	2.5	1.4	20.0

Table 6.8 – Current distortion limits for general distribution systems [94]. I_{sc} is the maximum short-circuit current at the PCC while I_L is the maximum fundamental demand load current.

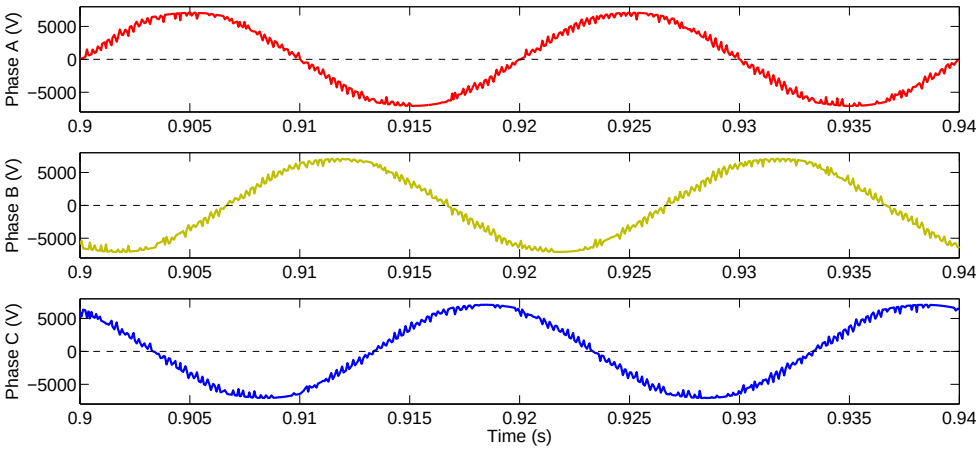

Figure 6.8 – Voltage at Point of Common Coupling (PCC).

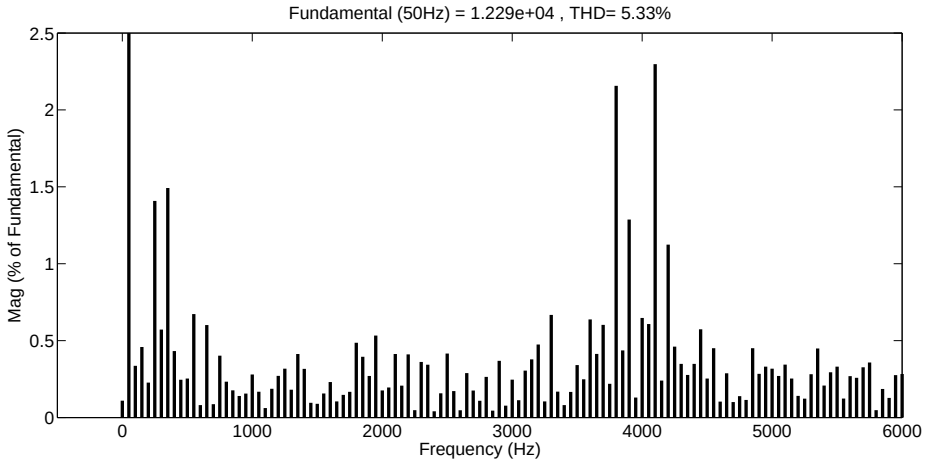

Figure 6.9 – FFT of voltage at point of common coupling.

the presence of the supply side impedance) is seen in figure 6.8. Figure 6.9 shows the harmonic spectrum of this voltage waveform at the Point of Common Coupling (PCC), showing a THD of 5.33%. This level of harmonic content at the input is unacceptable (from table 6.7), as this imposes voltage distortion to other consumers connected at the same point. A distorted voltage will in turn cause distorted currents to flow, which can cause improper operation for connected equipment. The high frequency currents also impose additional losses on the utility transformers, as well as increasing the overall loading due to higher RMS currents.

6.3.1 Transient conditions

Steady-state stability and RMS voltage and current values within acceptable limits are extremely important considerations for stable and secure cold ironing operation

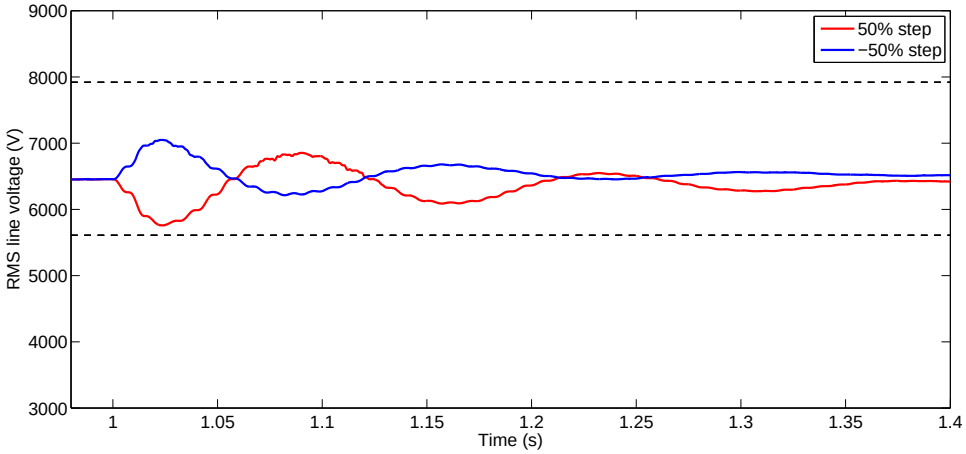

Figure 6.10 – Transient response of terminal voltage at berth 1 in response to a ±50% load step change at time 1s. The dotted lines indicate the +20%/-15% permitted limits for transient conditions.

that meets the requirements of both parties involved. The power profiles of figure 5.7 are averaged quantities which are indicative of the average power demands of the berthed vessels. The actual load profile (figure 5.5) will show more fluctuations and variations due to the intermittent nature of the onboard loads. The switching on/off of loads will induce oscillations which must not adversely affect the rest of the system. Limits on transient conditions are set out in [53] as being +20% and -15% for voltage excursions from nominal for the largest expected load step. This expected load step when berthed is to be documented for each ship which must then be matched to the expected response from the shore supply to ensure that limits are respected.

Figure 6.10 shows the responses of the RMS value of the output voltage to a ±50% step change in load on berth 1. In all cases, the output voltage is maintained within the transient limits indicated by the dotted lines on the plot. The perturbation was observed at the berth connections, in order to examine the effect a load transient onboard the ship would have on the actual terminal voltage. The transient response will of course be different for different installations, depending on the dynamic characteristics of the frequency converter implemented, influenced by controller time constants and the values of passive circuit components.

6.3.2 Harmonic mitigation

Various measures can be taken to improve the utility connection so that it meets the required standards. The connection of a passive filter at the input (similar to the way the output of the converter is filtered) is a possible solution (LCL filter shown as figure 6.11a), but large values of passive components are required. An active front end (figure 6.11b) can be used instead of the uncontrolled diode bridge rectifier. This takes the form of the controlled inverter stage replicated at the input stage. Having controlled switches at the input gives numerous benefits, including a much smaller DC link ripple (or a corresponding DC capacitor size reduction) giving also a cleaner input (and hence smaller input filter). The input currents can be controlled, such that the power factor is controlled to be unity. This does come at the significant expense of an additional controlled power electronic stage. Another power electronic option would be to install an active filter, which utilises a current-mode controlled power electronic converter to counter the input distortion current by injecting inverse harmonics, minimising the use/size of passive components (figure 6.11c). This, however, is a more expensive and less efficient option, when compared to passive filters [95].

Another solution which offers reduced current distortion at the input is the use of a higher pulse-number rectifier. A 12-pulse rectifier (figure 6.11d) makes use of a transformer with both a star and a delta connected output winding to utilise the 30° phase difference between the voltage waveforms of the two sets of windings. This produces twelve DC pulses per supply cycle (compared to the six pulses produced by a standard three-phase rectifier circuit) and a stepped AC current waveform eliminating all harmonics below 550 Hz (the 11th harmonic) for a lower input current THD. A 24-pulse arrangement can be produced by combining two 12-pulse systems with a 15° phase shift between the primary windings. This will produce 24 DC pulses per supply cycle, and a much smoother AC current waveform, eliminating all current harmonics below the 23rd.

The results show that the selected centralised system is able to meet the output requirements both in terms of steady state voltage values as well as meeting harmonic distortion limits for the berth connections. However, the study has highlighted the significant harmonic content at the input of the shore connection system, with THD values in excess of acceptable limits. Clearly, the use of power electronics generates

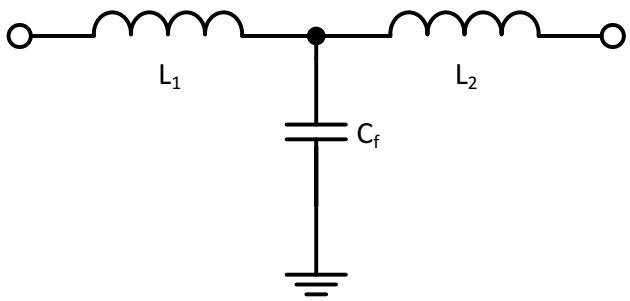

(a) LCL filter.

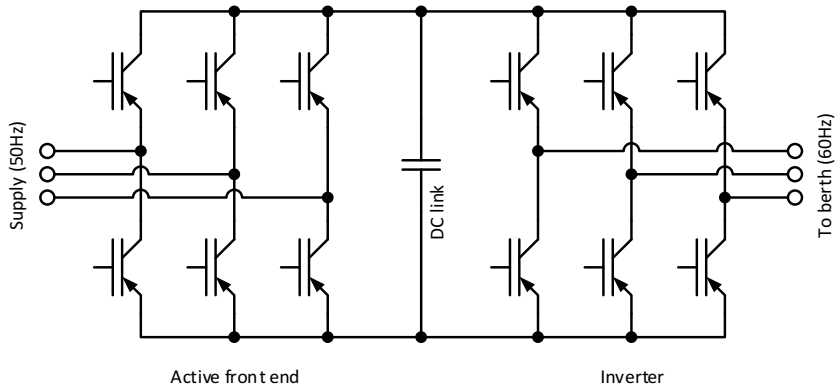

(b) Active Front End.

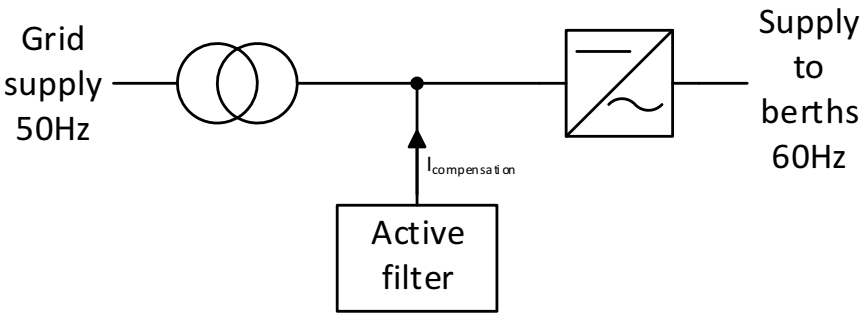

(c) Active filter.

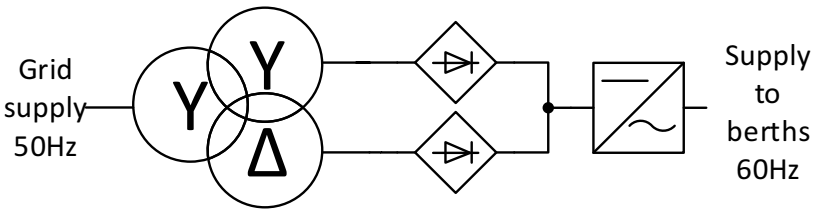

(d) 12-pulse rectifier.

Figure 6.11 – Harmonic mitigation measures.

significant harmonic content which must be managed in order not to adversely affect other consumers connected to the same supply network. Operating within the required harmonic limits is a necessary precondition to connection and represents a shared responsibility between system operators and users.

The use of an onshore power supply is beneficial to the immediate harbour area, as the use of onboard generators is reduced. Yet it must be ensured that the onshore power supply system does not have an adverse impact on the electrical utility, a process for which detailed simulations are well suited. After all, reducing airborne pollution must not come at the expense of increased electrical pollution [15].

Chapter 7

Onboard energy management

7.1 The motivation for energy management

One of the major benefits of onboard electrification is the ease of integration of multiple sources and energy storage. Of course, with increased integration also comes increased complexity. The management of energy is now more complicated since power can be provided from a number of different sources.

A vessel must perform a mission - carriage of cargo, passengers, towing etc... and this is possible within an operating envelope defined by environmental conditions taken into account during vessel design. The machinery systems on board are designed to cope with the expected environmental operating states, with sufficient margins for degradation as well as abnormal or extreme conditions. The onboard Power Management System's (PMS) role is to ensure that sufficient power is available at any instance in time to the onboard machinery as required for the vessel to fulfil its mission requirements.

An Energy Management System (EMS) takes this a step further and provides a higher level of control whose main purpose is minimisation of overall consumption, a concept which is not taken into account by the PMS. The EMS functions as a top-level controller, giving setpoints to the PMS. The PMS is in turn responsible for ensuring that sufficient power is available to the machinery systems, with the possibility of overriding the EMS' setpoints if necessary. The EMS can be seen therefore as an optional system which however is required in order to fully exploit the benefits of multiple sources and storage systems. Power after all, is nothing without

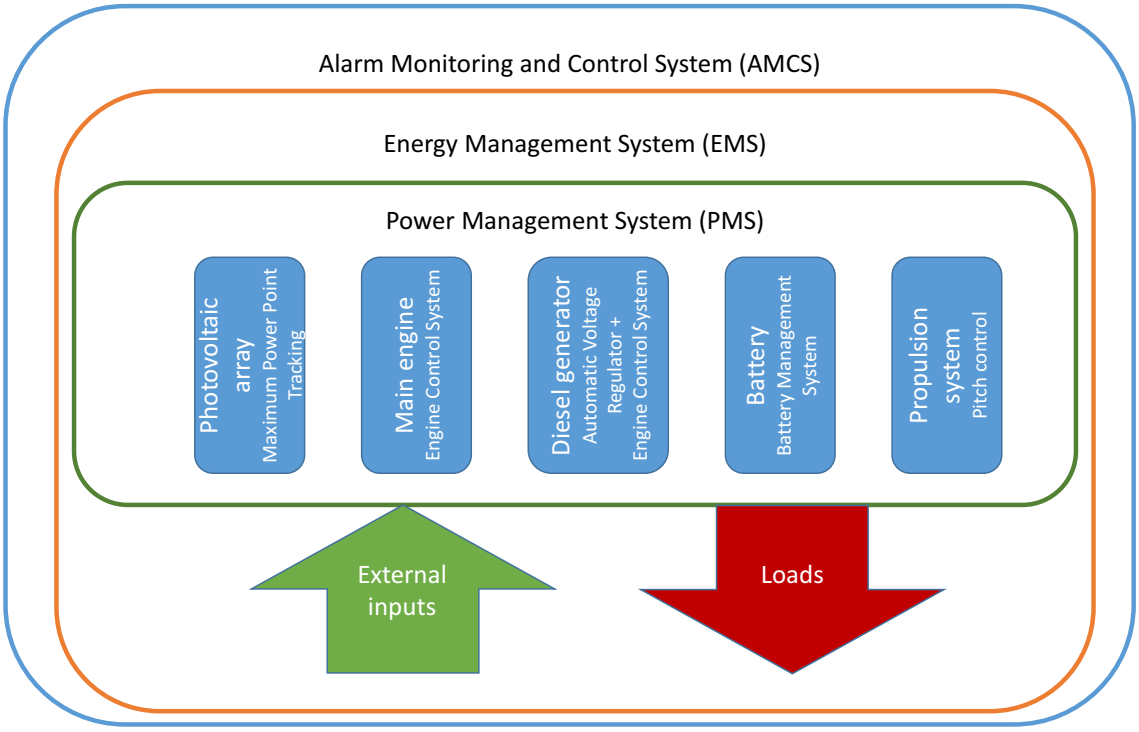

Figure 7.1 – Overview of hierarchy of the various onboard controllers.

control.

The hierarchy of onboard controllers is shown in figure 7.1. The highest level of control is the Alarm Monitoring and Control System (AMCS), which implements a supervisory role on the vessel, but does not inherently provide any machinery setpoints. The AMCS brings together all the alarms and supervisory controls for cohesive presentation and management by the bridge personnel. The EMS is the next level down, and encompasses the whole onboard system, with a view to realise optimised operation. In turn, the PMS ensures that the setpoints defined by the EMS are followed as closely as possible, but has the ability to override these in order to ensure that safety and mission are not compromised. Finally, each component has its own controller, shown in figure 7.1 for a variety of sources which attempts to implement the setpoint passed down from the PMS as closely as possible. This can be overridden by these lower level controllers in order to ensure safe operation of the component [96].

The machinery controllers, AMCS and PMS are conventional controllers, which are already found installed onboard vessels and come in classification society approved setups. The EMS is the focus of this work, where the management of energy from a multitude of sources on a shipboard environment provides scope for operational savings as well as automating decision processes. In the INOMANS^{2}HIP project, a

Parameter	Quantity	Unit
Length overall	182.77	m
DWT	12,359	tonnes
Speed	21	kt
Freight capacity	2715	lane meters
Main Engines	4 x 5760	kW
Main engines speed	510	rpm
Auxiliary generators	2 x 1500	kW
Propulsion type	2 x CPP	
Propeller speed	130	rpm

Table 7.1 – Case vessel main parameters [97].

case vessel was used as the focus of the work, with all data and studies based on this ship. The vessel in question is a RoRo ship, with main particulars as listed in table 7.1 and the machinery configuration shown in figure 7.2.

As part of the INOMANS2HIP project, a new hybridized machinery system, shown as figure 7.3, was designed for retrofit to the case vessel to examine the possibilities of reducing fuel consumption. Four main engines are installed (as in the current existing setup), powering two CPPs via a step-down gearbox. The shaft generators are replaced by two bidirectional auxiliary drives, with a battery storage system installed on each DC link. This DC link is the scope for future expansion into a DC distribution system. The batteries are specified as two units of 2MWh each, connected at a nominal voltage of 674V DC of a LiFePo type [98]. The auxiliary drives permit bidirectional power flow between the onboard electrical grid and the gearbox, linking the electrical and mechanical systems. The drives are rated at 2MVA at a grid voltage level of 450V, and consist of two back-to-back converters and a 1,200kW induction machine connected to the gearbox. A photovoltaic (PV) system was also added, which based on maximum available area of 1,994m^2 permits the installation of PV modules with a total rating of 300kWp [97]. A cold ironing supply is also provided, able to charge the batteries as well as providing the onboard auxiliary load. Additionally, two electrical generators connected to a Waste Heat Recovery System (WHRS) are installed on main engines 2 and 3. These contribute to the onboard electric grid when the main engines are running by recovering energy from the exhaust gases.

The vessel sails a fixed route between the UK and the Netherlands, at constant speed while at sea, with a constant electrical load of 850kW. The (averaged) operational

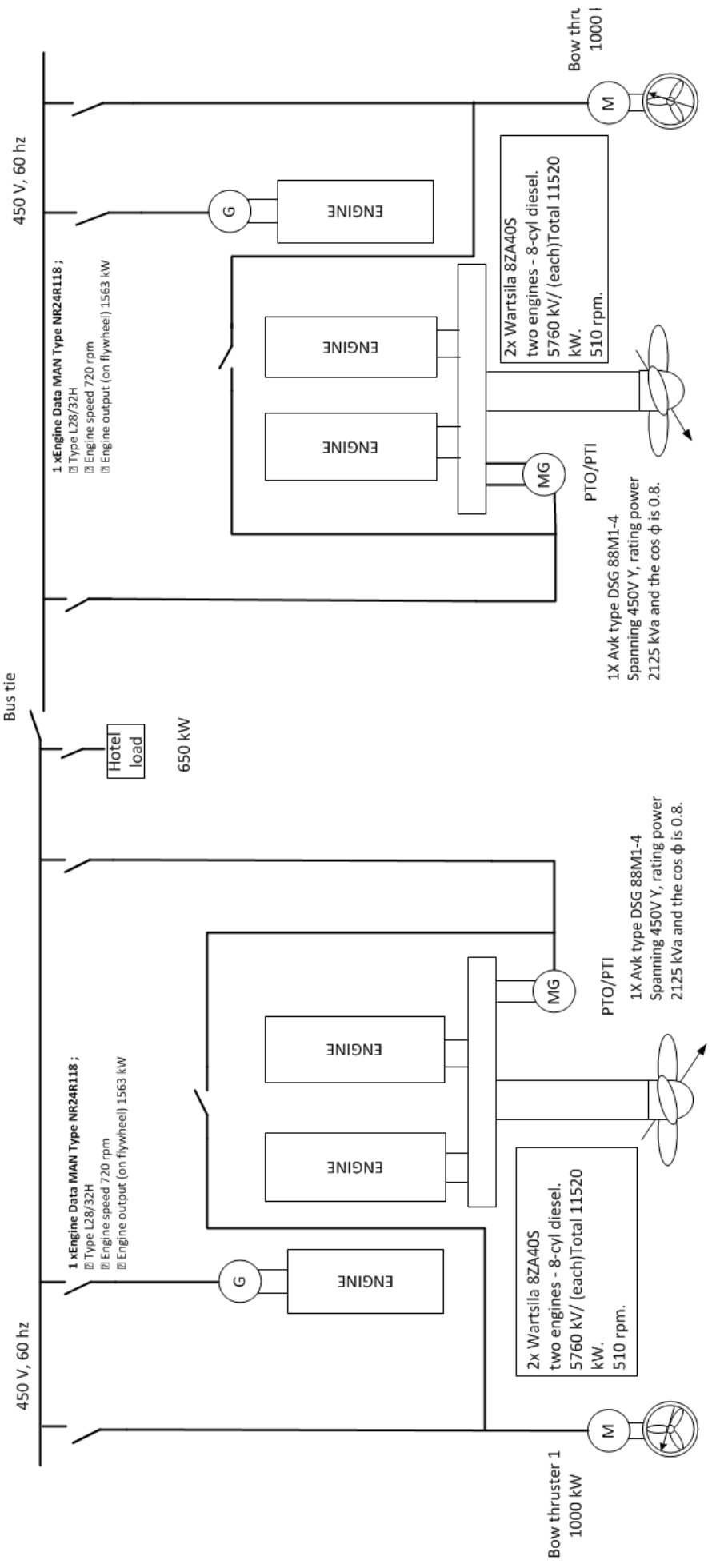

Figure 7.2 – Existing vessel machinery configuration [97].

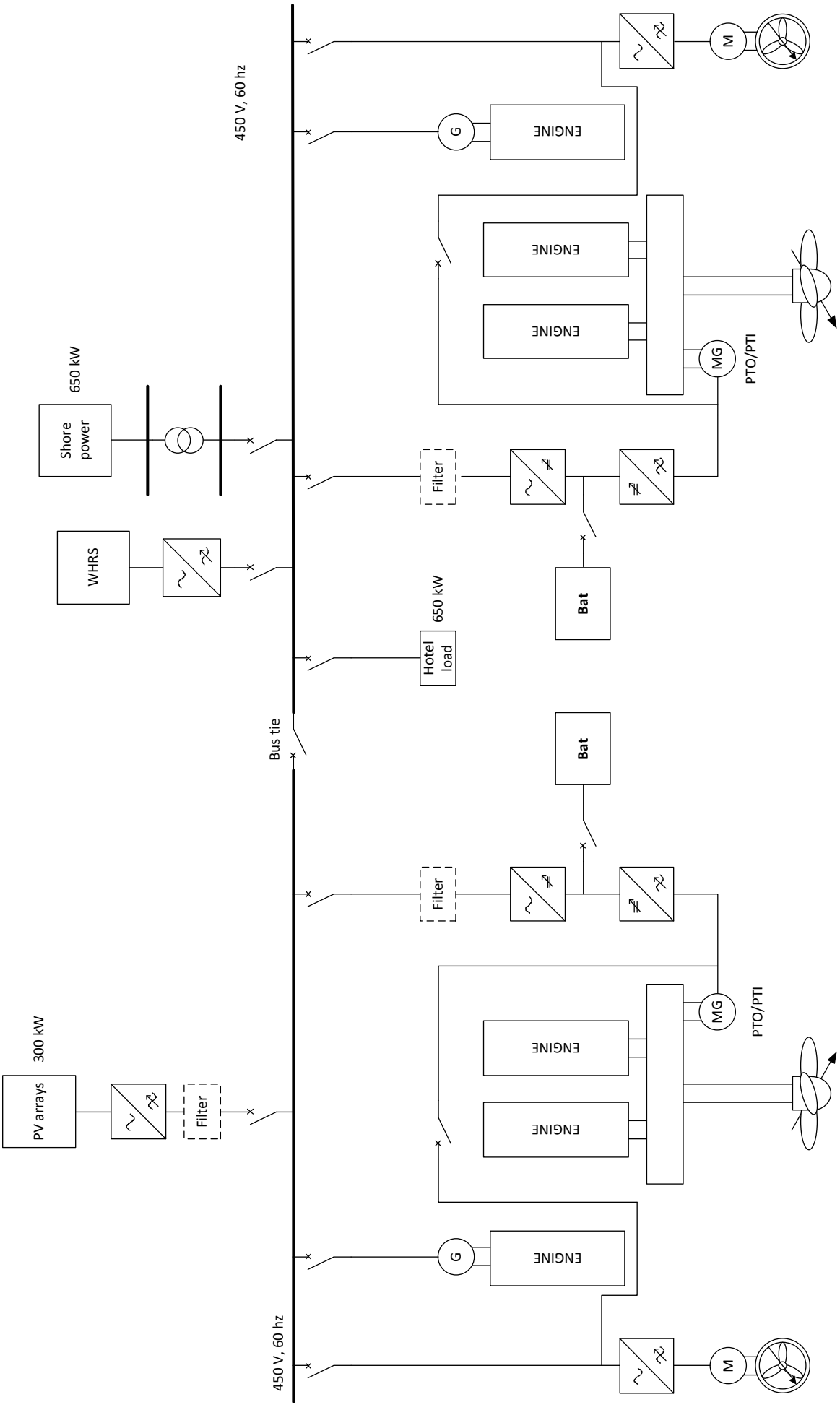

Figure 7.3 – Refit configuration for lowest emissions [97].

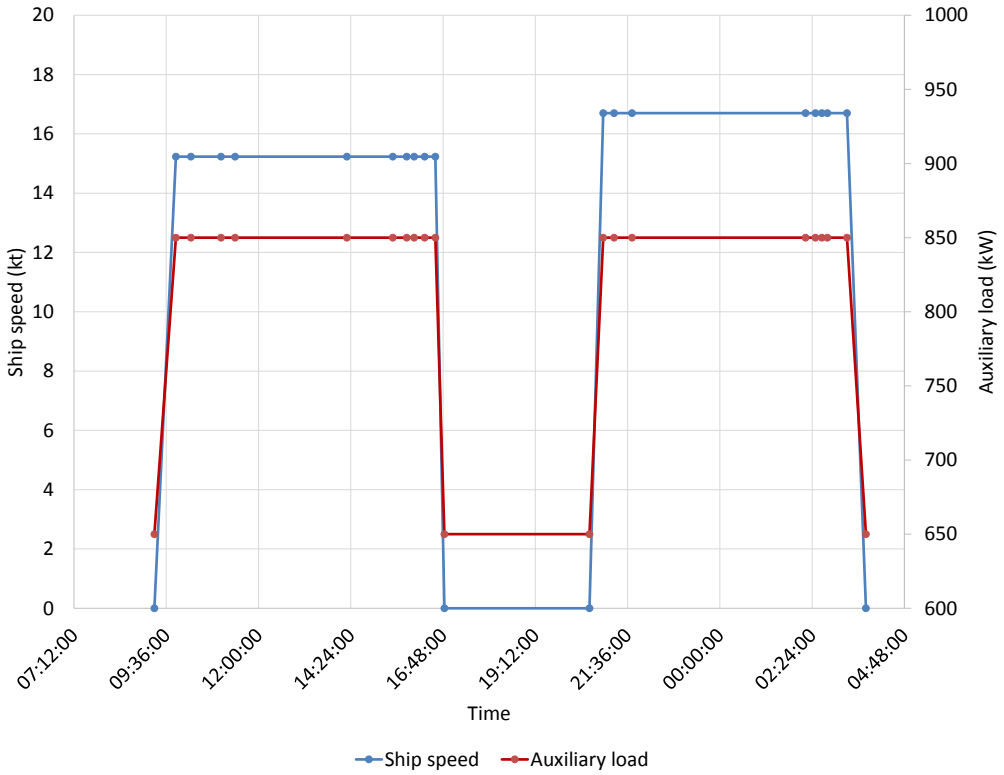

Figure 7.4 – Vessel operating profile.

profile of the vessel is shown in figure 7.4 for a return journey. With this data available, and the proposed new configuration, an EMS was proposed to be developed to control the new system to minimise fuel consumption over the voyage.

Within the project, the case vessel was modelled using the proprietary modelling software GES (Generic Energy Systems), developed by project partners TNO (Netherlands Organisation for Applied Scientific Research) [99]. GES was created by TNO as a software tool to model ship energy systems by means of energy flow analysis, using the bond graph method [100]. The software is able to model mechanical, thermal as well as electrical components with custom component models available for all onboard machinery. The GES model considers steady-state energy flows, and hence does not simulate transient conditions. The motivation behind the software is to evaluate different machinery configurations and examine steady state performance characteristics of machinery. Of interest to the EMS application is the capability of quickly returning the fuel consumption value for a particular configuration. A screenshot of the model developed in GES for the configuration of 7.3 is shown in figure 7.5.

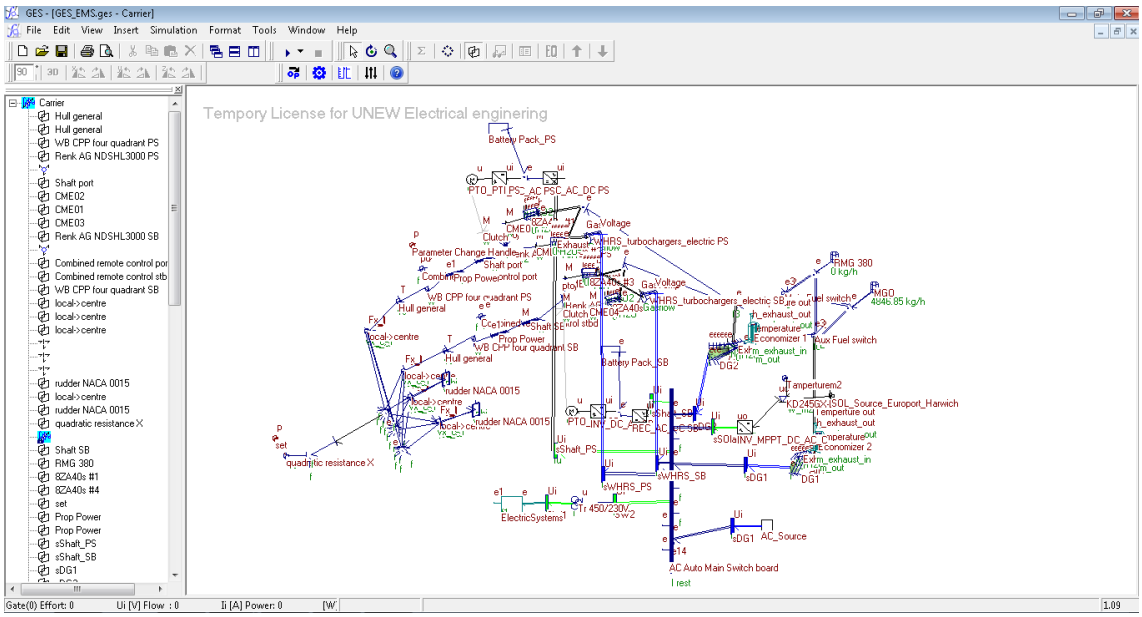

Figure 7.5 – GES model screenshot.

7.2 Energy management

The complexity in onboard energy management arises chiefly out of the handling of multiple different sources, and the variation in time of stored energy. In automotive hybrids, the number of sources and consumers is much lower, leading to a simpler problem formulation. Rule-based EMS can provide adequate results, but the complexity of formulating rules to encompass all possible scenarios will imply that their performance is inferior in all but the simplest cases [101].

Energy management looking at global optimisation using heuristic or mathematical algorithms can deliver superior results, but enter into the issue of no (or limited) *a priori* knowledge of the future energy demands. For real time application of optimal energy management, a suitable cost function must be formulated in order to be able to perform optimisation at each instant of interest [101].

Gradient based searches and numerical optimisation approaches require the cost function to be expressible as a linear function. This is the approach adopted in most optimal energy controllers found in literature which use variants of linear programming applied to linearised models [101–105]. These consider linear models of propulsion systems (both marine and vehicular) together with consideration of the load profile (based on historical data) to control setpoints across a voyage. With the models being intrinsically linked to the optimisation algorithm, modifications and reapplication to different systems are somewhat laborious and require reworking

of the EMS. As part of the project's motivation, a more generic scheme was desired which would give more flexibility and expansion potential for application to different vessels.

Beyond vehicular energy management, further inspiration can be found in power systems in what is fundamentally an economic dispatch problem. In this case, generator configurations are identified to provide the required power at the lowest possible cost, taking into account constraints in terms of unit commitment and ramping constraints. Again these typically use numerical algorithms with linear models to implement a load flow analysis. An interesting approach is to use Particle Swarm Optimisation to identify these optimal configurations [106–108]. The major benefits of using PSO (or other evolutionary-inspired algorithms) is when the system in question is relatively complex compared to a traditional transmission system. With storage and other nonlinear components, or when adaptation to other systems is desirable, the use of a black box optimisation algorithm can lead to a more flexible implementation.

The idea adopted in INOMANS^{2}HIP was to develop an EMS using PSO to optimise the configuration of the vessel's machinery systems during the voyage, without prior knowledge of the vessel's profile. Since shore supply is (considered to be) available, constraints such as the need to ensure that energy storage devices are full at the end of the voyage are not required [102], giving further freedom to the EMS routine. The theory and working behind PSO have been explained in chapter 5, and in the following sections, the implementation of the PSO algorithm to the EMS case is discussed.

7.3 Development of the EMS

The application of the PSO algorithm to the onboard energy optimisation scheme is summarised as figure 7.6. The PSO is the optimisation algorithm at the centre, coded in Matlab. The GES model outlined in figure 7.5 serves as the objective function, which returns the fuel consumption as the fitness value. Constraints are also handled within the GES models, with violations of any constraints passed to the EMS as warning flags. These constraints are operational ones, particularly on the machinery systems. The algorithm then returns the optimal system configuration in

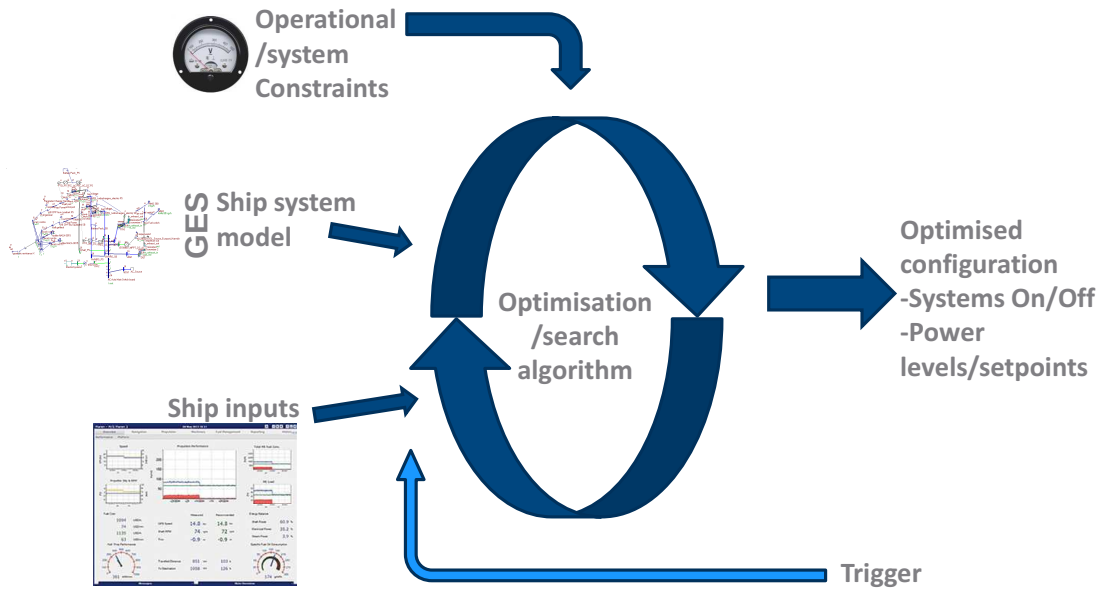

Figure 7.6 – Overview of operational EMS.

Variable	Type
ME1	On/Off
ME2	On/Off
ME3	On/Off
ME4	On/Off
DG1	On/Off
DG2	On/Off
PTO/PTI 1	Setpoint
PTO/PTI 2	Setpoint
Propeller operating mode	Mode selection
PS Battery current	Setpoint
SB Battery current	Setpoint

Table 7.2 – Variables in optimisation scheme.

terms of power setpoints as well as on/off selection of machinery. The variables are summarised as table 7.2, together with their type.

Table 7.2 shows the different types of variables involved, with the On/Off variables being binary while the others are of a continuous nature. This discrete nature of the On/Off variables can be treated by rounding continuous position vectors to the nearest integer, with 0.5 being the threshold [84].

The algorithm is to be triggered at predetermined times through the voyage taking as inputs the ship's particular condition at that time, namely speed, auxiliary load, solar irradiance (needed to calculate the PV array contribution) and wind direction and speed. Once the algorithm is completed, the vessel's configuration is updated accordingly. Of course, it is not expected that the actual profile will be fixed in

between update periods, but the PMS will control the power share in between these periods, prior to the EMS updating the configuration for optimal generation.

The basic premise of the optimisation at each step is to minimise the total fuel consumption. This however does not take into any account the wider operational constraints of the vessel's operation. As an example, each engine will return the same fuel consumption value, hence there is no discriminant and due to the stochastic nature of the optimisation, at each optimisation step, the optimal configuration could be one with a different engine selected each time, yet still returning the same (or very similar) fuel consumption. Hence the basic algorithm was modified to include a penalty function which looks at the previous configuration, and calculates the Hamming distance (number of discrete bit changes) to the new particle location. A proportional penalty is then applied to the returned fuel consumption figure, ranging from 0% if the configuration is the same, to a 20% penalty if the configuration is completely different. This reinforces the algorithm to preferentially select a configuration which is similar to the previously operating setup as much as possible, avoiding frequent turning on and off of diesel engines, yet prioritising fuel consumption minimisation.

7.4 A note on constraints

The search space is multi-dimensional, with the number of dimensions equal to the number of parameters in the search. The search space is theoretically infinite – but this does not represent a real implementation. In any practical application the search space is limited since parameters have limits on the actual values they can take. Hence the search space is said to be constrained to a feasible set of possible solutions, which is a subset of the total possible search space.

The objective space is correspondingly constrained, as a consequence of the constraints imposed on the search space. This constraining on the search space parameters is termed interval confinement and is therefore the realistic values which the search parameters can take [93].

For the problem at hand, the parameters are the setpoints of the machinery components, which map to the fuel consumption of the resultant configuration by use of the GES ship model. Clearly the setpoints of the machinery are constrained by the actual

limits which the setpoints can take – e.g. diesel engine setpoints cannot be negative, while limits in terms of the maximum loading must be respected. Hence for simplicity, setpoints are constrained between 0 and 1 (inclusive) which is the normalised per-unit power loading on each component. For components which permit bidirectional power flow, values less than 0.5 represent power flowing into the component, while greater than 0.5 implies power flowing out. This normalisation facilitates the setup of the algorithm, with the values then un-normalised in the fitness function. The interval confinement therefore ensures that only valid setpoints are selected, however this still does not guarantee that the solution selected is feasible.

Other constraints come in to play which are not immediately apparent from the search space but must be evaluated from the fitness function. These include additional machinery constraints which are obtained from the GES simulation (e.g. overspeeding of rotating machinery) or actual operational setpoints not being met (e.g. vessel speed not reached).

The straightforward treatment of constraints is by a hard limiting approach, which was adopted and described in the previous PSO implementation in chapter 5. Here a solution which violates a constraint is penalised by assigning infinity to the objective value (fuel consumption in this case). This means that that solution is discarded when it comes to selection of successive population updates, and was seen to give satisfactory results.

However in this application, at steady state too many variations in the setpoints were observed. These could be explained as solutions being found close to the global optimum (in objective space) but not the actual optimum itself. Clearly a better solution had been found in previous waypoints but not found again. With a hard limit approach, when a solution is discarded, all information related to that particular configuration is lost. This implies that a solution which has good 'concepts' but violates a constraint will not be able to propagate these concepts to the next iterations, effectively artificially limiting the search space.

A solution to this is to treat constraints with a soft penalty approach, where a solution is not discarded for violating a constraint, but rather penalised in proportion to the level of constraint violation. This therefore supports solutions which do not violate any constraints, but at the same time small levels of constraint violation do not imply a total rejection of a solution [93]. This is explained graphically by figure

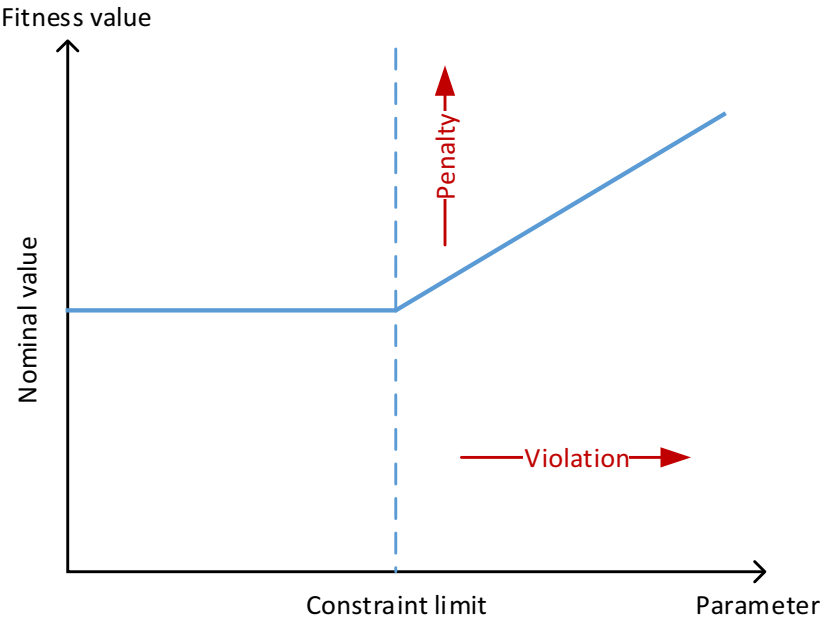

Figure 7.7 – Soft constraint handling for a single constraint.

7.7 which illustrates the linear penalty approach to a constraint violation.

The approach taken is to return the degree of violation in per-unit (e.g. level of overspeed, overload etc...) which is then summed and added to the fuel consumption value. By using a per-unit system for the constraints, these can be directly compared. Additionally, weighting can be applied to the different constraints in order to prioritise satisfaction of particular constraints over others. The disadvantage is that the choice of this weighting vector is very sensitive to variations. Hence for a more balanced approach, a non-weighted sum was used in this case.

A further consideration is the relative values of the constraints and objective. If the objective value returned by the fitness function is several orders of magnitude different than the per-unit constraint violations, then the soft approach to constraints requires adjustment such that the values are comparable, as otherwise the constraints are insignificant.

The constraints considered are listed below, divided according to soft or hard approach.

Hard constraints:

- Reverse power to shore supply
- Speed setpoint not met

Parameter	Symbol	Value
Swarm size	N	20
Total iterations	-	300
Informed neighbourhood size	K	3
Memory control parameter	φ_1	2.05
Co-operation control parameter	φ_2	2.05

Table 7.3 – Parameters implemented in PSO.

- Auxiliary power not supplied
- Main engine reverse power flow
- Main engine over/under speed
- Diesel generator reverse power flow
- GES convergence problem

Soft constraints:

- Battery state of charge over limit
- Battery state of charge under limit
- Main engine power overload
- Diesel generator power overload
- Auxiliary drive power overload
- Hamming distance from previous configuration

The PSO algorithm was implemented with the parameters as summarised in table 7.3.

The pseudocode of the algorithm is summarised as algorithm 7.1.

7.5 Handling of batteries

With the objective being the reduction of fuel consumption, the provision of power from clean sources other than the diesel engines will be preferred since this will result in reduced fuel usage. By assuming that the batteries are of zero cost, the discharge

Algorithm 7.1 Pseudocode for single objective PSO developed for EMS.

1. Initialise random particle locations of swarm size N
2. Initialise random particle velocities
3. Round binary particle locations to [0/1]
4. Evaluate fitness function
5. Populate pbest and gbest with best solutions
6. Evaluate velocity update equation
7. Calculate new particle positions and round where necessary
8. Evaluate fitness function
9. Update particle best if new fitness is better
10. Update global/local best if new fitness is better
11. Repeat from step 6 until maximum iterations is reached

will be maximised in order to reduce the fuel cost as much as possible. While correct from an optimisation point of view, this does not present a true picture of the cost of battery power. By maximising discharge simply because the state of charge permits it, the potential for prospective (better) savings at a later point of the voyage is lost.

The model was therefore modified to assign a cost to the energy stored as a function of the source used to charge the battery. This takes the form of an accumulator whose value is given by the amount of charge put into the battery together with the amount of fuel used to supply this energy, leading to an equivalent specific fuel consumption (eSFC) figure in g/kWh. The battery is assumed to maintain the constant charge rate for the duration of the waypoint, such that the state of charge at the end of the waypoint can be estimated by linear interpolation. Equation 7.1 defines the eSFC at the end of the waypoint ($eSFC_2$) as the weighted sum of the previous energy stored in the battery (E_1) and the current eSFC ($eSFC_1$) together with the charged energy and the average SFC used to charge the battery.

$$eSFC_2 = \frac{E_1 \times eSFC_1 + \Delta E \times SFC_{avg}}{E_2} \tag{7.1}$$

SFC_{avg}refers to the average specific fuel consumption (in g/kWh) of the energy

sources when charging the battery. It is given as the sum of fuel consumption (in g/s) of each diesel engine supplying the electric system divided by the total sum of power (in kW) being supplied by these engines as $SFC_{avg} = {}^{\Sigma FC}/_{\Sigma P}$. Equation 7.1 can be expressed more conveniently as equation 7.2 since the stored energy can be expressed as a fraction of the nominal capacity of the battery in terms of the state of charge (SOC) which results in equation 7.2

$$eSFC_2 = \frac{SOC_1 \times eSFC_1 + \Delta SOC \times SFC_{avg}}{SOC_1 + \Delta SOC} \tag{7.2}$$

When discharging, the eSFC is maintained constant at its previous value. The concept can be visualised as being analogous to a bucket of paint - the actual colour in the bucket (eSFC) is dependent on the quantity of paint added from different buckets, which mix to form a homogeneous colour. When discharging, the colour of the paint remains unchanged.

7.6 Testing of the EMS

In order to test the algorithm and validate results, the scheme was tested on a simplified configuration without any energy storage capacity. This "low-cost" configuration is shown as figure 7.8 and refers to the simplest incremental addition of machinery to the existing setup (of figure 7.2) [97]. The chief difference is a bidirectional capacity of the auxiliary drive giving PTO/PTI capability as described in chapter 1 of this thesis.

The algorithm was tested repeatedly at a number of speed setpoints independently of each other to observe convergence. The optimisation was run five times at speed setpoints of 5, 10, 15 and 20 knots. The results are summarised in table 7.4 and figure 7.9. Figure 7.9 shows the optimal fuel consumption progression in objective space across the PSO's iterations, together with metrics such as the average swarm fitness and average *pbest* values which give an indication of the general swarm fitness progression. This shows four distinct convergences for the four speed setpoints (with the same auxiliary power demand of 850kW) indicating how the same point has been found every time. The corresponding results in the search space are summarised in table 7.4 together with the objective space values (fuel consumption figures). These

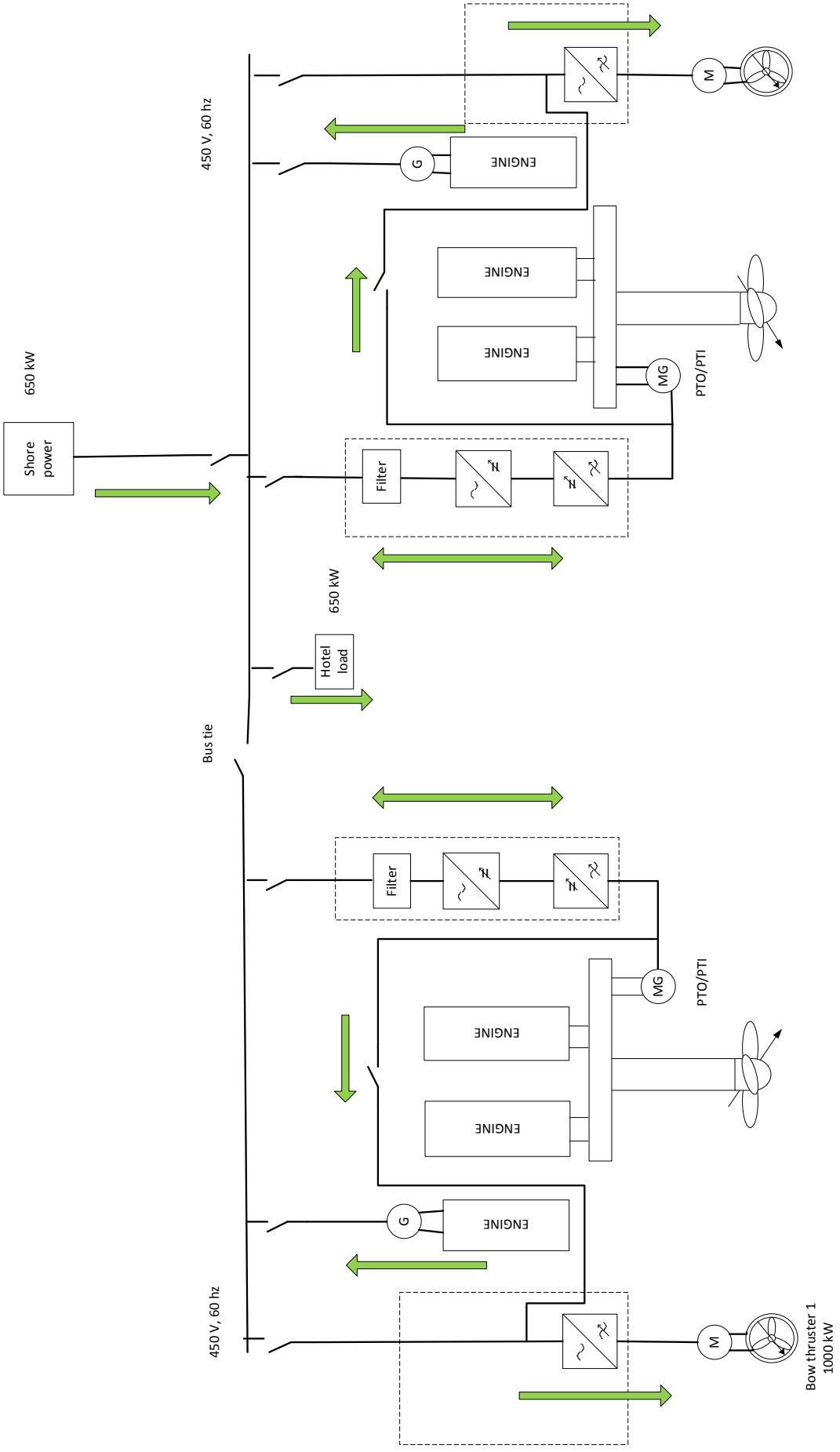

Figure 7.8 – Simplified low-cost configuration for testing. Arrows indicate direction of power flows. [97]

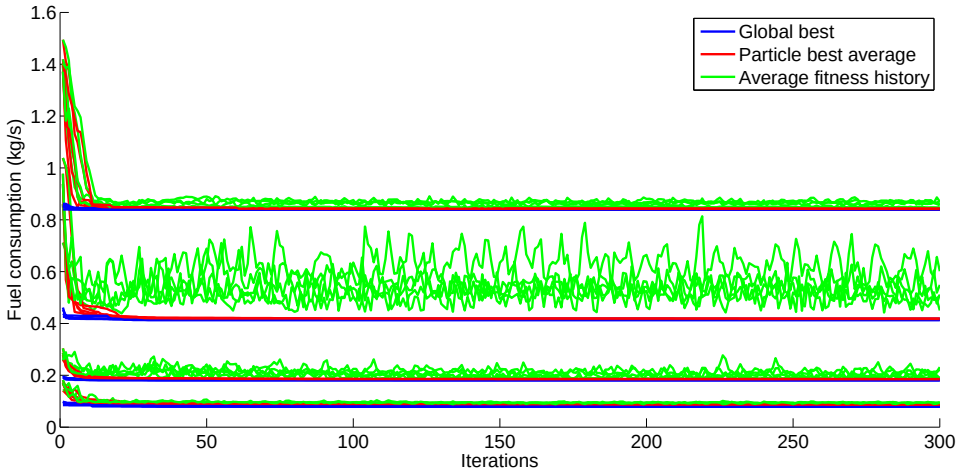

Figure 7.9 – Fitness progression for four speed setpoints for five repetitions each.

represent the optimal configurations found, i.e. the final points on the blue trace in figure 7.9.

From observation of the fuel consumption figures, it can be seen how the objective values are all close to each other, indicating that the global optimum (or very close to it) is being found every time. In all cases, the propeller operating mode is mode 1, which is variable revolutions mode. A positive power through the auxiliary drive implies that the drive is operating in motoring mode (PTI). It can be seen especially by looking at the PTO/PTI levels how different setpoints will still give the same (or very similar) objective values. Similarly, the combination of main and auxiliary engines, is very broad, since all main engines return the same fuel consumption.

7.6.1 Voyage testing

Following testing of the convergence of the PSO EMS on the low cost configuration, the EMS was applied to the voyage profile with the low cost configuration and validated against an EMS using the simplex method (a linear programming optimisation algorithm) as implemented [103]. This algorithm is built in to GES and was formulated by project partners to validate the PSO EMS approach. The simplex method calculates objective values at simplex vertices, which are the boundaries established by constraints in the search space. By examining the impact on the objective value by movement along the constraint limits, the vertices are successively explored by geometric processes of reflection, expansion and contraction of the simplices. When movement along any of the simplex boundaries does not realise any

ME1	ME2	ME3	ME4	DG1	DG2	PTOPTI1 V/f setpoint	PTOPTI 2 V/f setpoint	Propeller select mode	Fuel consumption (kg/s)	Speed setpoint (kt)	Auxiliary power demand (kW)
0	1	0	0	1	0	-0.11	-0.09	1	0.0794	5	850
0	0	1	0	1	0	-0.06	-0.11	1	0.0794	5	850
1	0	0	0	1	0	-0.11	-0.16	1	0.0794	5	850
0	0	1	0	1	0	0.15	-0.11	1	0.0794	5	850
0	0	1	0	1	0	-0.02	-0.11	1	0.0794	5	850
1	0	0	1	1	0	0.11	0.16	1	0.1815	10	850
0	1	1	0	0	1	-0.67	0.15	1	0.1815	10	850
1	0	0	1	0	1	-0.63	-0.67	1	0.1815	10	850
1	0	1	0	1	0	0.10	0.18	1	0.1815	10	850
1	0	1	0	1	0	0.14	0.13	1	0.1818	10	850
1	0	1	0	1	0	0.51	-0.33	1	0.4130	15	850
0	1	1	0	0	1	0.51	0.51	1	0.4168	15	850
0	1	1	0	1	0	0.51	-0.34	1	0.4130	15	850
0	1	0	1	1	0	0.54	-0.37	1	0.4130	15	850
0	1	1	0	1	1	0.50	-0.32	1	0.4169	15	850
1	1	1	1	1	0	-0.45	-0.36	1	0.8390	20	850
1	1	1	1	1	0	0.56	0.55	1	0.8389	20	850
1	1	1	1	1	0	-0.42	-0.39	1	0.8390	20	850
1	1	1	1	1	0	0.48	0.62	1	0.8391	20	850
1	1	1	1	1	0	0.25	0.28	1	0.8398	20	850

Table 7.4 – Configuration results for low cost configuration for independent setpoints.

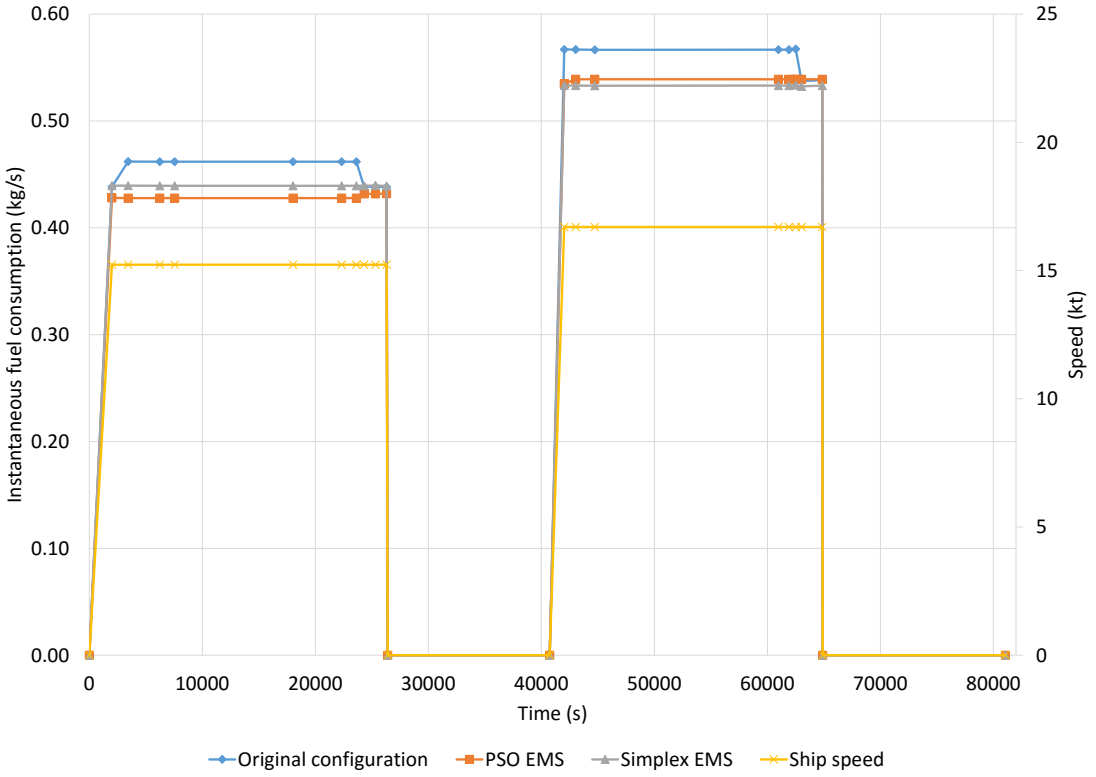

Figure 7.10 – Fuel consumption profiles comparison for configuration with no battery storage.

objective improvement then the extreme value has been identified [109]. In this case, associated with each vertex is the fuel consumption (returned by GES) depending on the particular control parameters.

Both EMS algorithms were applied to the same voyage profile (of figure 7.4) and the results are summarised as the plot in figure 7.10. This shows the fuel consumption profiles across the waypoints as optimised by the PSO and the Simplex EMS respectively, together with the original case consumption in kg/s.

The fuel consumption points with both EMS algorithms are all lower than the original figures for the conventional configuration. Figure 7.11 expands the profile returned by the PSO EMS to illustrate the power supplied by the main engines and diesel generators (combined) and the power to and from the auxiliary drive. The fuel consumption values for the PSO EMS are lower than those obtained by the Simplex EMS in the first voyage. In the return leg, the PSO EMS fuel consumption values are 1.7% higher than those returned by the Simplex algorithm, which is explained by different limits on power setpoints on the auxiliary drive between the two EMSs[4].

[4]The simplex algorithm is part of the GES software. It therefore has much tighter control of internal variables and limits. It is also much faster since it does not need to pass variables through an external interface.

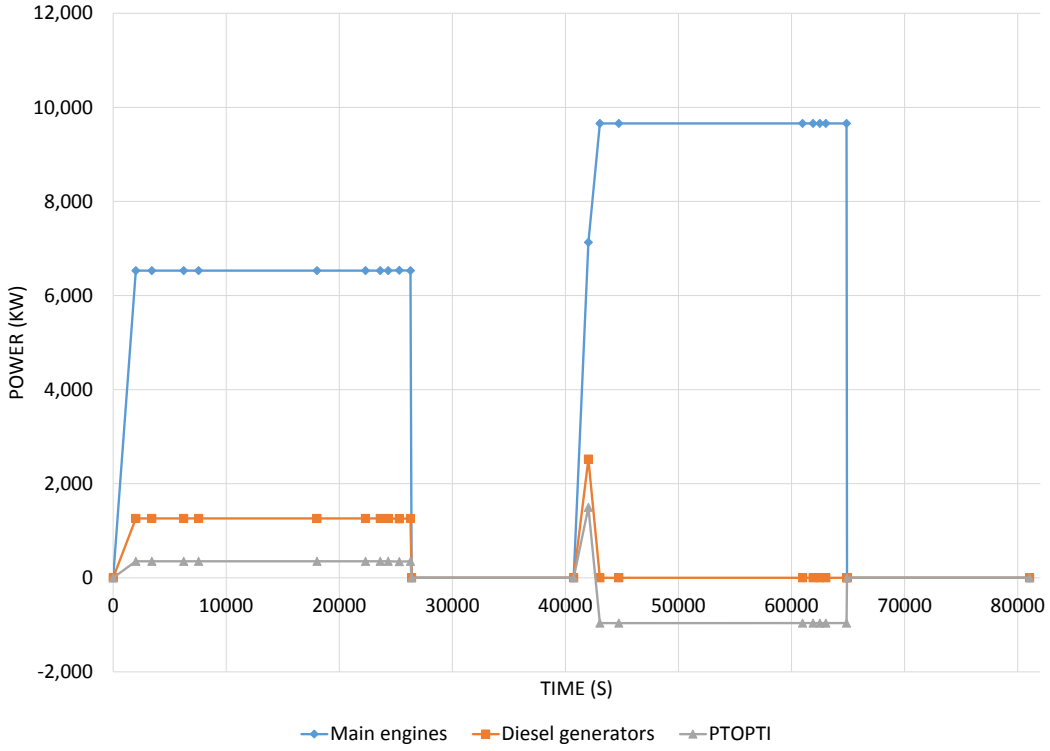

Figure 7.11 – Power setpoints profiles using PSO EMS for configuration with no onboard storage.

From figure 7.11, the fuel savings compared to the original configuration can be explained by the use of the auxiliary drive as a PTO/PTI. In the first leg of the voyage (at the lower ship speed), the diesel generators are used to supplement the main engines in PTI mode, while for the return leg, the diesel generators are unloaded and the auxiliary load is provided from the main engines via the auxiliary drive in PTO mode.

The actual configuration setpoints are described in table 7.5 which lists the search space results of the EMS over the voyage. Table 7.6 gives additional information with the power setpoints of the machinery components as defined by the configurations of table 7.5. Across the whole voyage, the vessel with the original configuration returned a fuel consumption of 25.64 tons. With the new low-cost configuration and the EMS using the simplex method, the fuel consumption is reduced to 24.42tons, while with the PSO EMS the fuel used is 24.26tons. This gives savings of 4.8% and 5.4% respectively.

The difference in fuel savings between the two EMS algorithms is very small and is due to the PSO EMS being able to find a better setpoint for the auxiliary drive (within the setpoint limits). However the biggest motivation for adopting the PSO

Setpoint				Configuration									Result
Time (s)	Ship speed (kt)	Aux power (kW)	Shore power avail.	ME1	ME2	ME3	ME4	DG1	DG2	PTOPTI1	PTOPTI2	Propeller operating mode	Fuel cons. (kg/s)
0	0	650	1	0	0	0	0	0	0	-0.30	0.89	1	0.0000
2009	15.23	850	0	0	1	1	0	1	0	-0.25	-0.43	1	0.4279
3427	15.23	850	0	1	0	1	0	1	0	0.48	-0.31	1	0.4278
6240	15.23	850	0	1	0	1	0	1	0	-0.34	0.51	1	0.4278
7552	15.23	850	0	1	0	1	0	1	0	-0.28	0.45	1	0.4279
18024	15.23	850	0	1	0	1	0	1	0	0.49	-0.32	1	0.4278
22326	15.23	850	0	1	0	1	0	1	0	-0.36	-0.32	1	0.4278
23626	15.23	850	0	1	0	1	0	1	0	0.52	0.50	1	0.4278
24321	15.23	850	0	1	0	1	0	1	1	-0.40	-0.28	1	0.4318
25311	15.23	850	0	1	0	1	0	1	1	0.46	-0.29	1	0.4318
26302	15.23	850	0	1	0	1	0	1	1	-0.25	0.43	1	0.4318
26400	0	650	1	0	0	0	0	0	0	0.51	0.53	1	0.0000
40736	0	650	1	0	0	0	0	0	0	0.57	0.54	2	0.0000
42029	16.70	850	0	0	1	0	1	1	1	0.79	0.80	1	0.5350
43042	16.70	850	0	1	1	1	1	1	1	0.21	0.21	1	0.5390
44724	16.70	850	0	1	1	1	1	1	1	0.30	0.12	1	0.5391
60978	16.70	850	0	1	1	1	1	1	1	0.23	-0.68	1	0.5390
61905	16.70	850	0	1	1	1	1	1	1	0.25	0.17	1	0.5390
62508	16.70	850	0	1	1	1	1	1	1	0.10	0.32	1	0.5391
63026	16.70	850	0	1	1	1	1	1	1	-0.64	0.18	1	0.5390
64858	16.70	850	0	1	1	1	1	1	1	0.14	0.28	1	0.5391
64900	0	650	1	0	0	0	0	0	0	0.57	0.54	2	0.0000
81058	0	650	1	0	0	0	0	0	0	0.55	0.56	1	0.0000

Table 7.5 – Setpoints for low cost configuration.

Time (s)	Component power setpoints (kW)										
	ME1	ME2	ME3	ME4	DG1	DG2	PTOPTI PS	PTOPTI SB	Shaft PS	Shaft SB	Cold ironing
0	0	0	0	0	0	0	0	0	0	0	668
2009	0	3,085	3,445	0	1,262	0	350	0	3,312	3,312	0
3427	3,328	0	3,202	0	1,262	0	114	236	3,312	3,312	0
6240	3,263	0	3,267	0	1,262	0	177	173	3,312	3,312	0
7552	3,136	0	3,393	0	1,263	0	301	51	3,312	3,312	0
18024	3,312	0	3,217	0	1,262	0	129	221	3,312	3,312	0
22326	3,315	0	3,215	0	1,262	0	126	224	3,312	3,312	0
23626	3,246	0	3,283	0	1,262	0	193	157	3,312	3,312	0
24321	3,398	0	3,131	0	0	1,262	45	305	3,312	3,312	0
25311	3,370	0	3,166	0	0	1,256	73	272	3,312	3,312	0
26302	3,085	0	3,444	0	0	1,263	350	1	3,312	3,312	0
26400	0	0	0	0	0	0	0	0	0	0	668
40736	0	0	0	0	0	0	0	0	0	0	668
42029	0	3,586	0	3,546	1,261	1,261	729	768	4,176	4,176	0
43042	2,414	2,414	2,415	2,415	0	0	-482	-482	4,176	4,176	0
44724	2,320	2,320	2,509	2,509	0	0	-298	-666	4,176	4,176	0
60978	2,396	2,396	2,433	2,433	0	0	-446	-518	4,176	4,176	0
61905	2,375	2,375	2,454	2,454	0	0	-405	-559	4,176	4,176	0
62508	2,538	2,538	2,292	2,292	0	0	-722	-242	4,176	4,176	0
63026	2,385	2,385	2,445	2,445	0	0	-424	-540	4,176	4,176	0
64858	2,495	2,495	2,335	2,335	0	0	-638	-326	4,176	4,176	0
64900	0	0	0	0	0	0	0	0	0	0	668
81058	0	0	0	0	0	0	0	0	0	0	668

Table 7.6 – Power setpoints for low cost configuration using PSO EMS.

EMS is the greater ease in adapting the EMS to the configuration at hand. Since the PSO uses a black box approach, the EMS and cost function (GES function) are much less interlinked, with only the passing to and fro of variables and setpoints (as per figure 7.6). This ease of adaptation is the chief proposition for adoption and further development of the PSO EMS in the rest of the project.

7.7 Implementation

The EMS was now applied to the new configuration (figure 7.3), running every waypoint in order to optimise the configuration at each step. The waypoints are based on the navigational waypoints obtained from the vessel's crew. Since these are position dependent, the duration of these is variable and in some cases stretches to the order of hours. Though power levels are unchanged, with energy storage, the batteries' state of charge will vary significantly over the course of the setpoint duration, hence an update was scheduled every half an hour (unless the waypoint has been reached).

Figure 7.12 summarises the results of the simulated voyage using the PSO EMS. This clearly shows the batteries' state of charge profiles, being discharged initially (starting from a full state of charge) till empty (lower limit assumed at 20%). The state of charge is then maintained at this level till the ship is berthed, at which point the vessel is considered to connect to an onshore power supply, whereby the batteries are charged from the shore. This is then repeated for the second leg of the voyage. The batteries are used to provide power to the propulsion system via the auxiliary drive (PTI mode). The fitness function (slightly higher than the actual fuel consumption in figure 7.12) reflects the use of the equivalent fuel consumption associated with the batteries. It can be seen how compared to the original case with the conventional configuration, the fuel consumption is lower throughout the complete voyage.

Power is shown in figures 7.13 and 7.14 for the same profile using the PSO EMS. The shaft power is the (combined) power provided to the propulsion shafts while the auxiliary demand is the power demanded by the onboard auxiliary plant. The shore supply reflects the power supplied from a cold ironing supply when berthed. This meets the demands of the onboard auxiliary load as well as charging of the onboard

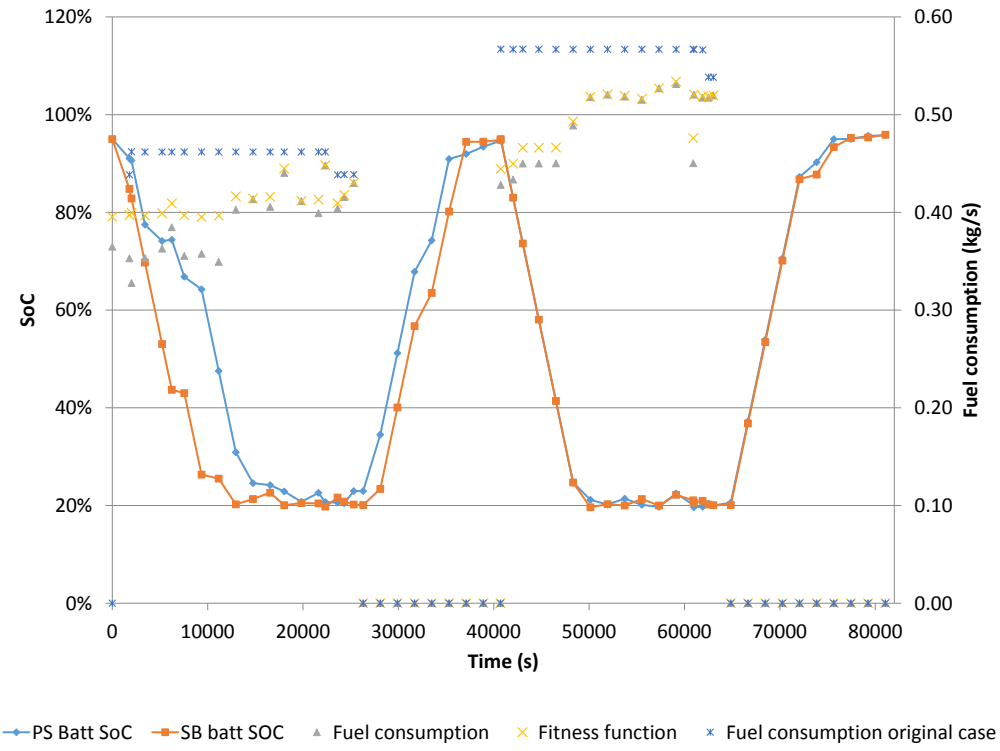

Figure 7.12 – Resultant profiles for voyage of figure 7.4 with configuration including onboard energy storage. Fuel consumption (new configuration) is compared to the original case fuel consumption, with the fitness function also shown.

battery storage as seen in figure 7.12.

The battery's initial eSFC was set to be equal to the (nominal) SFC of the diesel generators. The batteries are gradually discharged over the initial stages of the first leg of the voyage, contributing to propulsion power via the auxiliary drive in PTI mode and the auxiliary load. Once the lower discharge limit is reached, power is switched to the main engines, with minor fluctuations via the auxiliary drive in order to provide the auxiliary supply and keep the batteries within limits. Power is then supplied to the onboard grid via the PTO such that the diesel generators are unloaded.

When berthed, a cold ironing supply is available, which is able to provide the onboard auxiliary load as well as charge the batteries. This is considered as zero cost (in terms of fuel consumption) since no fuel is being consumed onboard and serves to preferentially select the shore supply over any other onboard source. The EMS in fact converges (correctly) to solutions with power being supplied solely from the shore supply. With charging from a 'zero' cost supply, the batteries' eSFC is diluted down to a lower cost than in the initial leg, leading to a stronger emphasis on battery

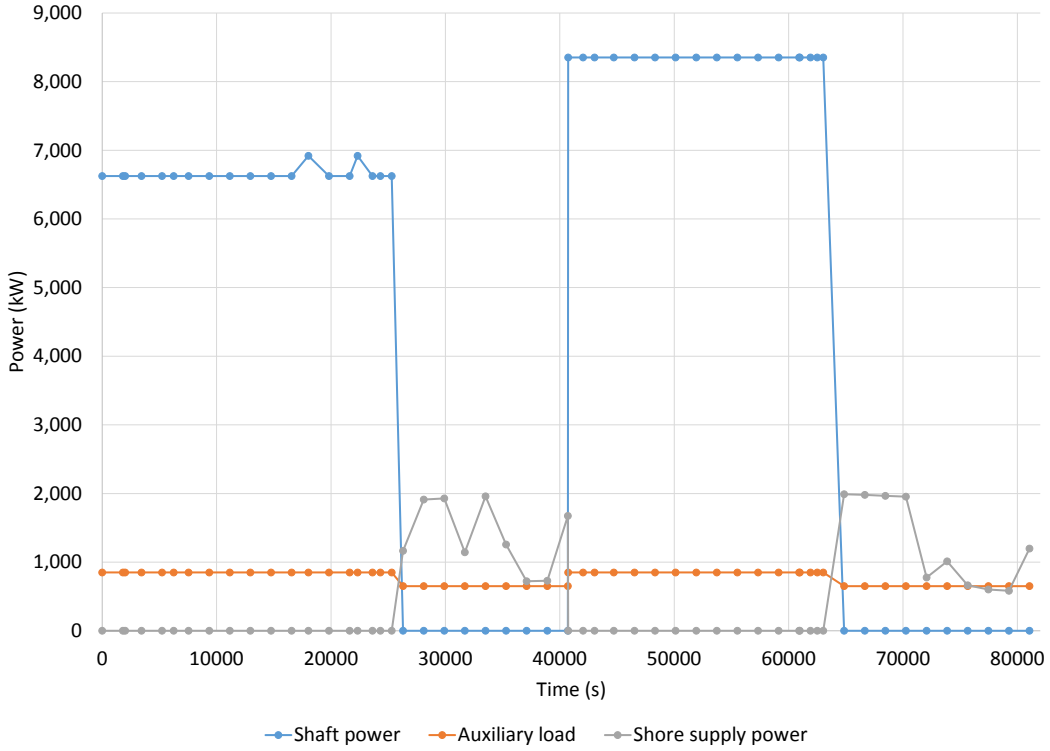

Figure 7.13 – Shaft powers, auxiliary load and shore supply power for ship voyage with EMS and configuration with onboard storage.

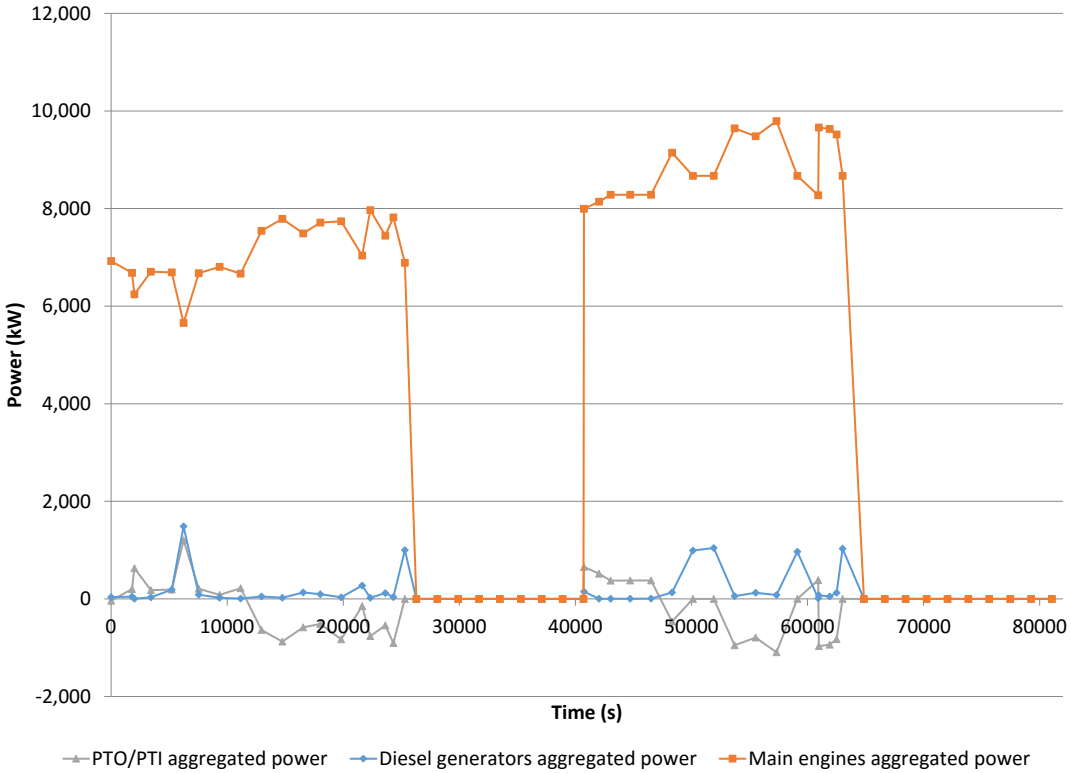

Figure 7.14 – Resultant profile showing power profiles over voyage for PTO/PTI, main engines and diesel generators for configuration with onboard storage. Power is summed across all units in configuration.

use in the second leg. Because of the higher vessel speed on the second leg, there is clearly (from figure 7.14) a continuous contribution via the auxiliary drive in PTI mode, initially supplied from the batteries, and once these have been discharged, a continuous feed-in in PTO mode.

The results in the search space are summarised in table D.1, corresponding to the objective space results of figure 7.12. This gives an illustration of the output from the EMS algorithm which would be used as setpoints for the real-world application of the EMS as per figure 7.6. Further insight to complement the plots of figures 7.13 and 7.14 can be seen in table D.2 which lists the power flows through the components result from the setpoints of table D.1.

The actual power flow is determined by the PMS built in as part of the model in GES. This determines the power demanded from each source and ensures that power is balanced between all components. An essential part of the EMS algorithm is to ensure that the desired setpoint is met by a particular configuration, which of course depends on the PMS action as well as the availability of sufficient power by a particular configuration.

From table D.2 and figure 7.14, it is apparent that there are variations in the power levels between waypoints through the components in spite of the propulsion and auxiliary powers being constant (averaged). The power available from the PV array varies with the solar irradiation (which varies throughout the day, conditions etc...). Furthermore, the state of charge in the batteries varies with use, hence changing the power available from the batteries when approaching limits. This variation is mitigated somewhat by the penalty function adopted with respect to the changes in variables 1-6 (on/off of diesel engines). A similar approach was tested which considered the geometric distance between solutions across all the variables. It was observed however that this significantly restricted the freedom of the search such that there was a very high dependence on the initial solution found and due to this restricted freedom suboptimal fuel consumption over the voyage was being realised.

From figure 7.12, comparison of the instantaneous fuel consumption values shows how the overall figures are less than the original case. Summed up across the intervals, the original setup returned a fuel consumption of 25.64 tons while with the new configuration and EMS the return journey was completed using 22.12tons of fuel, a saving of 13.7% [17].

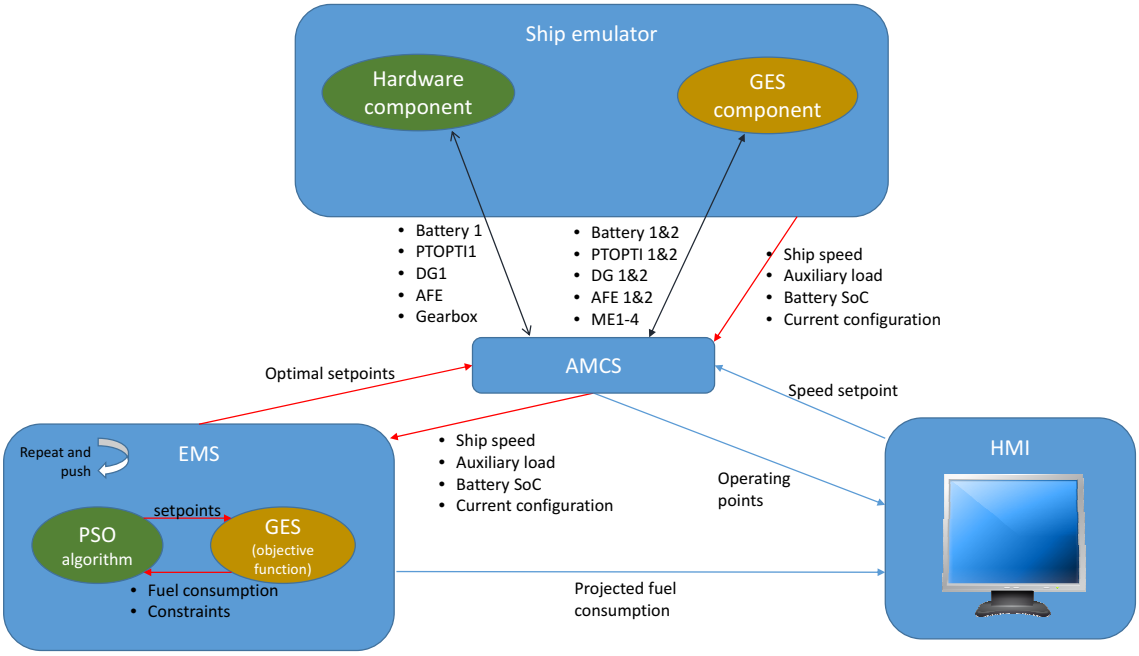

Figure 7.15 – Demonstrator setup overview.

7.8 Installation

As part of the INOMANS^{2}HIP project, a working hardware demonstrator has been set up to showcase the results of the project. This work is being carried out by project partners and involves the setting up of a number of hardware cabinets housing drives, power converters and batteries to emulate part of the system of figure 7.3. The demonstrator is aimed at being a tangible illustration of the project's work. An overview of the demonstrator is shown in figure 7.15, illustrating the various entities which make up the system. Three separate components make up the demonstrator, bringing together the three major aspects of the INOMANS^{2}HIP project.

The HMI (Human Machine Interface) is being designed by project partners, taking into account bridge ergonomics together with aspects of how to best illustrate energy/fuel savings and motivate improved performance [110]. On the demonstrator, this is hosted on a PC, and uses four screens (see figure 7.18) to graphically showcase results and user-friendly information. This uses proprietary software and builds on existing HMIs as used by project partners.

The ship emulator is a composite system consisting of a Hardware In the Loop (HIL) component as well as a master software model of the ship system, built in GES [109]. The ship emulator includes the PMS and component level controllers for the vessel. The GES model is the main emulator, which passes

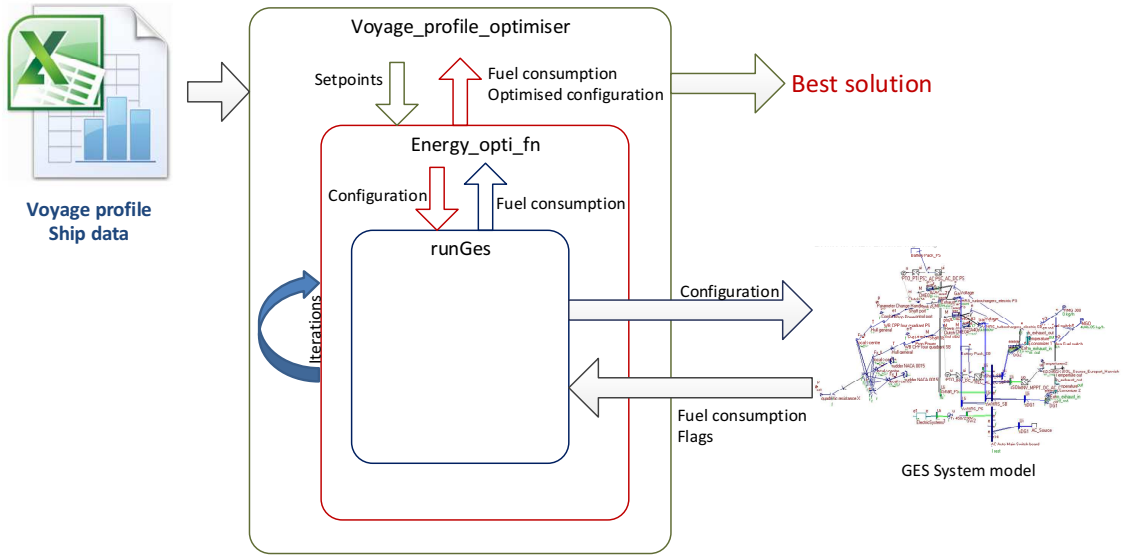

Figure 7.16 – Overview of optimisation scripts for modular implementation of EMS.

the relevant setpoints required by the HIL component (via the AMCS) to follow and track the matching model blocks.

The EMS is hosted on a separate PC, consisting of another instance of GES, being called by the PSO algorithm described in the previous section [109]. The scripts were set up in a generic and modular way, so that interfacing, optimisation and overall functions are kept separate, permitting changes and adaptations according to the application. The links between the various scripts together with the variables passed between them is summarised as figure 7.16, illustrating the modular approach to the EMS.

The highest level control module of the demonstrator is the AMCS which handles communications between the various entities of the demonstrator. The EMS receives the setpoints from the AMCS, performs the optimisation routine, and returns the optimal setpoints to the AMCS. These optimal setpoints are in turn sent to the ship emulator and the HMI for display purposes.

The single line diagram of the demonstrator hardware setup is shown as figure 7.17. The components are described as follows:

Component 1 is a motor/generator pair rated at 5kVA which emulates a diesel generator

Component 2 is a 100Wp photovoltaic module and MPPT inverter which emulates the PV array. Due to the low rating of the available unit and the lack of control

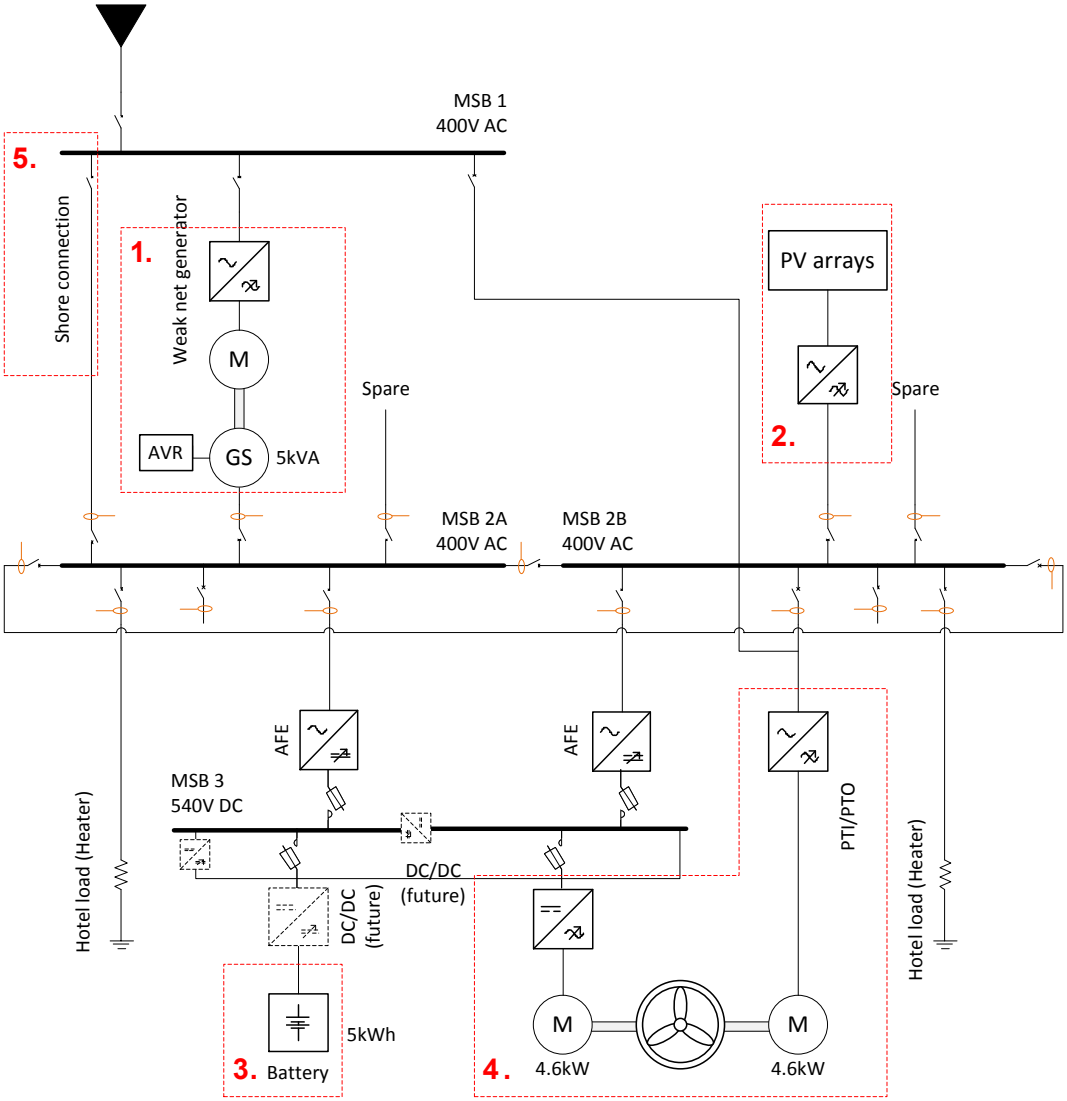

Figure 7.17 – Single line diagram of demonstrator setup. Numbered components are the power sources on the vessel [96].

of the solar irradiation in the demonstrator, this component is not considered significant in the setup.

Component 3 is a 5kWh unit of four Lithium-ion batteries

Component 4 is a 5kVA motor/generator pair which emulates the auxiliary drive and the gearbox node where this is connected

Component 5 is a separate feeder which represents the shore connection, effectively bypassing the generator set.

MSB1 is an incoming busbar, external to the shipboard power system and is only relevant on the demonstrator.

MSB2 represents the main AC bus on the vessel (figure 7.3) where all the sources and loads are connected.

MSB3 is a DC bus which at the current stage represents the DC link of the bidirectional converters of the auxiliary drives at the point where the batteries are interfaced. This is scope for future expansion into a DC grid for future work (beyond the current scope of INOMANS^{2}HIP).

Figures 7.18 and 7.19 show various views of the demonstrator as set up at the partner premises. As of writing (September 2015), the hardware units are still being commissioned. The EMS has been tested with the GES emulator, and seen to match the results obtained with the standalone instance as described in the previous chapters.

Figure 7.18 – Complete demonstrator view. HMI is displayed on the four central screens. EMS runs on the lower computer, while upper computer runs HMI system.

(a) Left hand side cabinet showing emulated diesel generator motor/generator pair.

(b) Right hand side cabinet, showing PTO/PTI motor generator pair and battery location (not installed yet).

Figure 7.19 – Hardware cabinets of the demonstrator setup.

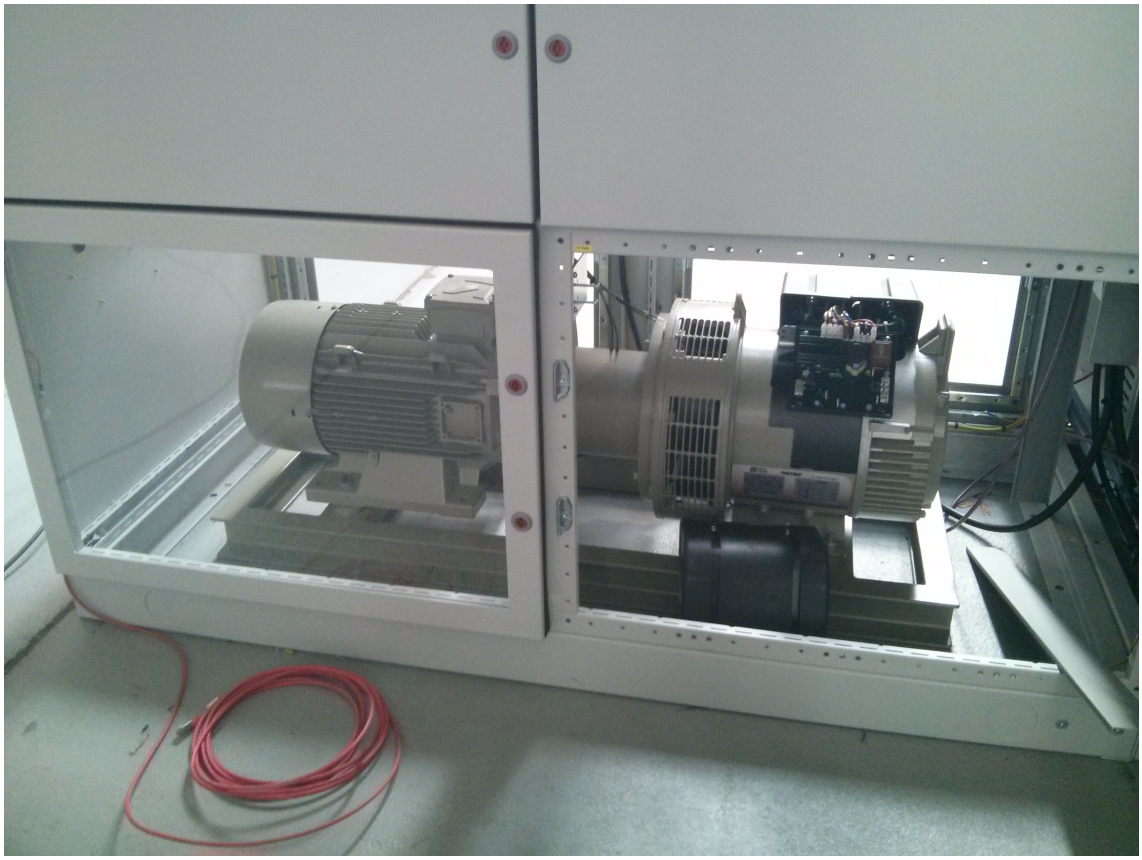

Figure 7.20 – Motor-generator pair emulating diesel generator.

Chapter 8

Discussion

Shipboard electrification is a topic of growing importance in modern marine vessels, evidenced by the number of research publications in the area. Electrification brings about the potential for economy and savings due to *flexibility* - in operation, installation and design.

Savings have been the main motivator behind the work in this thesis, focussing on emission and fuel savings. Environmental legislation and drivers are motivating more environmentally-friendly ships. That, as well as actual monetary savings returned to ship operators by investing in environmental technologies on board their ships. Being green is therefore economically sound.

A wide range of energy saving devices and technologies exist, both in concept and commercial stages. The cost-benefit ratio of each will be the major determinant in uptake - a factor which is different according to the ship type, and most importantly, each ship's operation. Consideration of the operational profile is fundamental to understanding the impact of any energy saving technology and verifying results.

Hybridisation combines two or more systems in order to exploit the benefits of each. The choice of hybrid components, as well as the operation of the complete system needs to be correctly designed in order to elucidate the desired results. A mermaid is a perfect example of a (mythological!) marine hybrid - by adapting the lower half from fish and a human top half, the hybrid system is perfectly able to exploit the best of both worlds i.e. dexterity and manoeuvrability at sea from each half. If the chosen halves were reversed, then the result will be far from ideal...at least for operation at sea.

The same understanding can be extended to a hybridised vessel using auxiliary drives. The conventional main propulsion system permits the easiest and most economical means of propulsion at sustained speed. At low speeds however, suboptimal operation occurs. The auxiliary system on the other hand can realise better loadings, and supply power from other sources (e.g. batteries) more easily. The link between the auxiliary and main propulsion systems is established by the bidirectional capability of the auxiliary drive. The cost/benefit of such a hybrid system needs to be examined in conjunction with the usage of the vessel by considering its operating profile.

A RoRo was taken as a case study for examining auxiliary drives. Various electrical machines were considered for their suitability, focusing on permanent magnet synchronous machines and induction machines. Low speed machines are able to be mounted directly on the propeller shaft, but are large and expensive. Higher-speed machines need reduction gearing, reducing efficiency compared to direct-drive installations. However, they are less bulky and cheaper than similarly rated low speed equivalents. The differences in savings was seen to be quite small between the topologies, with the low-speed, permanent magnet machine showing the lowest losses. With medium-speed and high-speed engines, a reduction gearbox is an integral part of the installation, hence taking advantage of this required component and utilising a higher-speed machine installed on the high-speed side of the gearbox is more attractive due to the lower capital outlay of the machines.

By switching over to the auxiliary system during the manoeuvring period, fuel savings of around 46% were observed with similar reductions in CO_2. Furthermore, by drawing power from the auxiliary generators running on MGO, Sulphur reductions in the order of 96% were seen. This brings forward the flexibility introduced by the auxiliary drive, in that operation in sensitive areas can be facilitated by changing over the power source without requiring fuel changeovers.

The bidirectional auxiliary drive also permits generation and feeding back power to the auxiliary system. This is the typical usage of a shaft generator when the vessel is underway, with the use of the power electronic converter permitting generation at variable speeds. The operating profile of the vessel and the times spent in each mode determine the overall savings based on the auxiliary drive's operating envelope. For the system under consideration, the electric machines would be operated under field-weakening while generating, potentially disadvantaging permanent magnet machines

when compared to induction machines. This was observed to be the case for the vessel's operating profile, such that when taking into account the different costs of fuel used by each system, the auxiliary drive using a permanent magnet machine returned an overall fuel cost of around 4% higher than one using an induction machine. This comes about due to the small relative amount of time spent in manoeuvring mode, where the permanent magnet machine's operation was more efficient. By spending more time in generating mode under field-weakening operation, the induction machine was seen to give greater overall savings. However, because of the higher cost of the MGO used during manoeuvring, savings due to motoring via the auxiliary drive are proportionally weighted higher than those due to savings due to generating via the auxiliary drive.

This analysis was carried out by building detailed models of the hybridised propulsion system, and generating efficiency LUTs according to the determined operating points. This permits quick, energy-focused simulations to be run, considering efficiency losses in the chain, and with the use of emission factors, convert this resultant energy demand into equivalent airborne emissions.

Apart from reducing the actual emissions, the location where they are generated is also of importance. The harbour area is of particular sensitivity due to proximity to human habitation and the resultant direct impact on human health. Emissions from ships do not cease once the vessel is stationary, but ships typically continue to burn fuel while berthed in order to provide the onboard auxiliary load. A solution to eliminate these in-harbour emissions is the use of an onshore power supply to provide the required power from the shoreside grid, permitting the onboard generators to be turned off.

Standardisation efforts have resulted in the publication of international standards to attempt at homogenising expectations and requirements for both vessel and harbour operators. This should theoretically permit compliant vessels to plug in to any compliant port for a truly plug-and-play solution. Of course, uptake is still limited but prospects are bright for popularisation of standardised shore supplies. The infrastructural requirements are not insignificant, especially on the shoreside which entails the highest costs. One of the major equipment requirements is a frequency converter, required to provide 60Hz supplies (as found on most vessels) from 50Hz shoreside grids.

In line with requirements, a number of shore network topologies can emerge to provide the required power to a number of berths in harbour. The choice of a single, centralised frequency converter to supply the whole system, or a number of smaller, distributed converters each supplying a single berth are two of the main questions to be answered at the system design stage. Once again, consideration of the operating profile provides the information required to answer this question.

Matching of system to usage is a complex multi-variable task, and the use of computer algorithms can be used to aid in identifying superior configurations or otherwise. Network type and component sizing all add up to a highly-nonlinear search space, making linear programming approaches complex to formulate. Particle Swarm Optimisation is a heuristic search algorithm inspired by the swarming behaviour of a group of organisms, which are individually dumb, but collectively intelligent. By sharing information throughout this swarm while flying around and exploring the search space, solutions can be identified to which the swarm gradually converges. Of course a goal must be set for this swarm, and in this case the goal is to minimise emissions, by maximising efficiency of the shore network.

This efficiency is quantified by modelling, where a parametrised power-flow model of the various shore networks was built, able to give the efficiency of a particular shore network configuration. By varying component ratings, as well as network topology, a large search space needed to be explored to identify configurations giving lowest emissions. A PSO algorithm was created to identify the best configuration considering the expected loading profile for a case harbour over a typical week.

Minimising a single goal (emissions) gives correct solutions. But not necessarily realistic solutions. Considering solely one objective results in the search steering in a headlong charge towards that solution which minimises that goal. From a real-world perspective, neglecting practical aspects such as cost, weight, size etc... can result in the solution being infeasible.

Considering multiple objectives at the same time gives rise to the idea of a set of compromise solutions rather than a single focused solution. The word compromise in this case should not have negative connotations associated with it. Rather it is the addressing of conflicting objectives, and satisfying each to give balanced, realistic solutions. With multi-objective PSO, the result is a Pareto-optimal set of solutions, where each solution gives a benefit in one objective for a corresponding sacrifice in

another. In this application, cost is a major concern to shore supply installations, so identifying solutions giving a balance between capital cost and resultant efficiency was seen to be a suitable measure.

Cost is however highly subjective, so using absolute figures was felt to be too sensitive to any variations. Instead components were assigned a per-unit relative cost based on their kVA rating. The resultant multi-objective PSO therefore focuses its search on identifying solutions which maximise efficiency, while minimising system cost. For the scenario being considered, a centralised topology was seen as being the most appropriate, giving the best tradeoff between costs and emissions.

The actual resultant emissions are dependent on the berth location and the country's generation mix. For the case of Spain, where the case harbour was located, CO_2 emissions are reduced by about 46%, together with a 13% Sulphur reduction when compared to low Sulphur content fuel. However, in countries where the shoreside generation mix is highly reliant on fossil fuels (particularly coal-fired stations), the outlook is less positive. Sulphur emissions are among the ones which are most at risk especially when compared to low-Sulphur fuel mandated for use in European harbours. Irrespective of the actual generation mix however, the in-harbour emissions will be reduced by the use of shore supply, shifting emission generation further inland and supplying power through the distribution network.

This distribution network can create a constraint in the setup of a new shore supply network due to any limitations with spare capacity on the existing supply to the port. Upgrading of the connection to the network can be costly, further increasing capital expense. A possible workaround is considering onsite power generation from green sources, reducing the demand from the distribution network. Furthermore, the (localised) generation mix can be improved, reducing the net airborne emissions depending on the source of power. At periods of low berthed demand, the generating plant could potentially be used as a distributed generator, feeding back to the grid.

Liquefied Natural Gas as a marine fuel is a concept which has been given increasing attention in recent years, touted as a cleaner alternative to diesel fuel used onboard. Using LNG as a fuel for onshore generating sets can be an attractive and feasible solution, especially if a port is investing in LNG infrastructure for supplying vessels. Compared to diesel fuel, combustion of LNG practically eliminates Sulphur emissions and particulate matter, while also reducing CO_2. In order to include the consideration

of LNG-fuelled generators in the shoreside network, the network models were modified to permit replacement of nodes with onshore generator sets, together with the relevant emission factors. Accounting for the per-unit cost of the LNG-fuelled generators was however less straightforward due to even greater subjectivity than the shore network components (e.g. ready availability of LNG, maximum footprint available etc...).

The cost of the onshore generators was therefore considered as a further variable in the optimisation setup, where the multi-objective PSO was repeatedly run with different per-unit costs of the onshore generator system in order to examine the influence on the resultant configurations. It was observed that when the LNG system's per-unit cost was greater than the frequency converter's per-unit cost, there was no advantage either in emissions (considering CO_2) or cost in selecting any LNG-fuelled generators for any of the berths. With decreased costs of the LNG-fuelled generators, cheaper overall solutions could be realised at the cost of slightly higher emissions in hybrid configurations of various degrees. This once again highlights the nature of multi-objective optimisation, in that benefits in one objective are at the expense of another. The final solution selection from this equally-optimal set is done using higher-level information and engineering judgement.

The engineering aspects of shore supply networks do not stop at minimising the losses in the system. With the use of (possibly multiple) power electronic converters of a significant power rating, harmonics become an important consideration of the system design. Compatibility must be ensured both at the berthside, where vessels expect a supply of a satisfactory quality, as well as at the incoming supply side, where harmonics can adversely impact other users on the network. This was studied by building detailed models of a centralised shore supply network, such that the magnitude of harmonics could be observed at the point of common coupling with typical supply inductances. It was seen how berth supplies were of a satisfactory quality even with a simple filter, however significant distortion was observed propagated to the supply side, requiring mitigating measures to manage harmonic content. Installation of filters or other compensation components will invariably increase losses to an extent, however a non-compliant network will not be permitted to operate on the distribution network.

Minimising losses is not only a design issue, but is also affected by operational choices and decisions. The shore supply network is passive in nature in that a demand must

be met, and supplied from the grid with a certain amount of inevitable losses. With an onboard electrified power system, a multitude of supplies are available, together with a number of loads of different type and magnitude. When coupled with onboard storage, the energy picture becomes even more complex and convoluted.

Lowering emissions becomes a dynamic and ever-changing challenge, which must balance the needs of supplying power of sufficient quantity and of the necessary quality, to the machinery components as required to perform the vessel's mission. An Energy Management System is designed to do exactly that - provide power from a suitable combination of sources in order to meet a particular goal. In this work, that goal is the minimisation of fuel consumption and emissions.

Minimisation implies an optimisation of some sort, or a search for a particular combination of setpoints of the onboard machinery to maximise/minimise a particular objective. Two aspects can again be identified - quantifying the objective value in objective space, and developing an algorithm to identify the variables which realise this in the search space. Using an algorithm such as PSO gives a black box approach to this problem, where the objective function (calculation of fuel consumption) and the actual search algorithm are separate and communicate with each other by simply exchanging variables, requiring little information about the problem at hand. This gives the advantage of being easily adaptable to different setups by modifying the number and type of variables together with the addition of relevant constraints.

Though developed for a particular case study, an EMS using a PSO algorithm was developed with the aim of presenting a generic EMS. The case vessel is a RoRo ship which was modelled parametrically to enable different configurations to be examined in terms of their resultant fuel consumption. The RoRo was modelled with a proposed green refit configuration, which included bidirectional auxiliary drives, battery storage, photovoltaic arrays and a shore supply connection. The fuel consumption is therefore the result of the machinery configuration (diesel engines on/off) and the setpoints of the various components.

With voyage data available for the vessel, the PSO EMS aims to minimise the fuel consumption for the duration of a particular waypoint. This has to take into account the equivalent cost of the energy stored in the batteries, whose energy is not free, but assigned an equivalent specific fuel consumption, based on the source of power used to charge them. This approach was validated with an EMS developed using

linear programming on a simplified configuration without energy storage. Results from both algorithms were seen to give similar results, with fuel savings of around 5% based on a typical return voyage. The advantages of the PSO algorithm are more apparent in the ease with which the consideration of storage was implemented to the algorithm, which proved cumbersome with the linear programming approach.

With the addition of batteries, the fuel savings rise to above 13%, based on usage of batteries during initial stages of each leg, and operation of the auxiliary drives in PTO and PTI modes when underway. Most importantly however is the modularity of the EMS, with separate objective function and optimisation routines and only the transferring of setpoints in one direction, and returning of objective values in the other direction.

8.1 Scope for future work

The work on the EMS is planned to be implemented on a working demonstrator with a working Hardware In the Loop model. This work is being carried out by project partners, with the EMS to be running on a realtime setup mimicking a real vessel voyage. Beyond the application on the demonstrator, various other aspects which are worthy of further examination and development have been identified.

- Introducing consideration of future consumption if a setpoint is maintained. By linear interpolation, a setpoint is projected at a future point in time and examined by running the objective function again, returning a further estimated future fuel consumption value. Due to uncertainty, this fuel consumption figure can be added to the current value with appropriate scaling to give a combined weighted objective value. The disadvantage of this is the doubling of computational time required due to running of the objective function twice. This can of course be extended to return fuel consumption values at an arbitrary number of future waypoints.

- Treatment as a multiple objective optimisation was implemented and tested, minimising for fuel consumption and difference from previous configuration. However for application as an EMS, a single solution is required to be applied by the PMS. Automating selection of a single compromise solution proved to

be problematic, especially due to solutions being close together in the objective space, but being significantly different in search space. Furthermore it was seen that the results over the voyage were extremely sensitive to the selection of the initial configuration at the first waypoint.

The study on auxiliary drives considered an auxiliary system powered by diesel generators. The addition of energy storage and the effect this has on the shore supply network when charged by the cold ironing supply is an interesting examination, since this would raise the power demands of berthed ships, and additionally inject harmonics due to the non-linear nature of the battery chargers. At the point of discharge, additionally considering the equivalent cost of emissions of the stored energy could give interesting results, especially if the vessel sails between two countries with very different generation mixes.

8.2 Conclusions

In an environmentally-conscious world, minimisation of energy is of significant interest to all parties involved in the marine sector. Not only does minimisation of energy reduce emissions, but it can also give lower operating costs. Onboard energy can be considered a naval architecture concern, where the amount of energy stored onboard a vessel is a finite quantity, constrained by the size of fuel tanks. To a certain extent, the rate at which this stored chemical energy is converted to a more useful form is a marine engineering issue, relating to the machinery systems installed onboard.

Engineering is therefore responsible for ensuring that most useful energy is obtained from the onboard fuel. With electrification, the chemical energy is converted to an intermediate stage in the form of electrical energy - a form which is very convenient to control. This flexibility and convenience gives the potential to elucidate better operational efficiencies from the onboard machinery system. This realisation of efficiency improvement however is not obvious, but must be matched to the energy usage profile. Apart from improvement at the conversion stages, electrification also facilitates the input of energy from outside the hull boundaries by plugging in an electric cable to a shore supply, once again giving the potential to reduce emissions and green vessel operations within the harbour area.

This work has used computer simulations coupled with real-world operational data to demonstrate emission and fuel consumption reductions facilitated by electrification, focusing on auxiliary drives, shore supply and real-time energy management. The importance of consideration of the operating profile has been highlighted from this work, together with the use of a black-box search algorithm to assist in decision-making, based on increasingly complex machinery systems.

- Auxiliary drives are able to significantly reduce the emissions produced during slow sailing by sourcing power from onboard auxiliary generators.
  - CO_2 emissions during the manoeuvring period were demonstrated to be reduced by around 45% for a case study.
- Onshore power supply can eliminate emissions produced in-harbour with the net emissions produced being a function of the generation mix employed on shore.
  - For a case study port in Spain, CO_2 emissions were demonstrated to be reduced by around 46% while corresponding UK case would see reductions of around 22%.
  - Countries with a high dependence on coal generation would see an increase in emissions.
- Mixed generation systems can be employed to minimise supply demand on the local grid.
  - Sets of equally optimal solutions identified giving tradeoffs between cost and emissions reduction based on shoreside LNG generation systems.
- Energy management systems can reduce fuel consumption by optimal utilisation of onboard energy sources.

Fossil-fuels are not likely to be eliminated as the main source of energy onboard vessels in the foreseeable future, yet electric systems can help in making the most out of this finite resource. Increased electrification of onboard systems is a trend expected to be continued in the coming years with a number of enablers and facilitators on the cards. DC distribution is one such facilitator, providing easier and convenient

interfacing of more-electric loads and storage systems. Going hand-in-hand, power electronics are a related enabler, both on the conversion side at each end of the distribution system as well as for protection purposes on the DC network.

This thesis has given an appreciation of some of the benefits possible with the use electrification on marine vessels as well as the importance of consideration of the operating profile. Economics and environmentalism are clearly a driver for adoption, but without an insight into the realisable improvements (if any), enthusiasm for takeup is likely to be muted. Electrification is a facilitator, but unlocking the improvements depends on fitting the right key. And that key is unique to each scenario.

References

[1] C.-C. Chang, "Marine energy consumption, national economic activity, and greenhouse gas emissions from international shipping," *Energy Policy*, vol. 41, pp. 843–848, 2012.

[2] D. P. McArthur and L. Osland, "Ships in a city harbour: An economic valuation of atmospheric emissions," *Transportation Research Part D: Transport and Environment*, vol. 21, pp. 47–52, 2013.

[3] RINA, *Significant ships of 2008*, T. Knaggs, Ed. London: The Royal Institution of Naval Architects, 2008.

[4] ——, *Significant ships of 2009*, N. Savvides, Ed. London: The Royal Institution of Naval Architects, 2009.

[5] ——, *Significant ships of 2010*, N. Savvides, Ed. London: The Royal Institution of Naval Architects, 2010.

[6] ——, *Significant ships of 2011*, N. Savvides, Ed. London: The Royal Institution of Naval Architects, 2011.

[7] ——, *Significant Ships of 2012*, N. Savvides, Ed. London: The Royal Institution of Naval Architects, 2012.

[8] D. Chang, T. Rhee, K. Nam, K. Chang, D. Lee, and S. Jeong, "A study on availability and safety of new propulsion systems for LNG carriers," *Reliability Engineering & System Safety*, vol. 93, no. 12, pp. 1877–1885, 2008.

[9] E. Sciberras, B. Zahawi, D. J. Atkinson, A. Juandó, M. Solla, and A. Sarasquete, "Auxiliary drives for emissions reduction," in *Low Carbon Shipping Conference, Newcastle upon Tyne 2012*. Newcastle University, 2012.

[10] E. A. Sciberras, B. Zahawi, and D. J. Atkinson, "Simulation-based efficiency evaluation of auxiliary drives for marine vessels," in *13th International Conference on Computer and IT Applications in the Maritime Industries*, V. Bertram, Ed. Hamburg: Technische Universität Hamburg Harburg, 2014, pp. 427–436.

[11] E. A. Sciberras, B. Zahawi, D. J. Atkinson, and A. Juandó, "Electric auxiliary propulsion for improved fuel efficiency and reduced emissions," *Proceedings of the Institution of Mechanical Engineers, Part M: Journal of Engineering for the Maritime Environment*, vol. 229, no. 1, pp. 36–44, 2015.

[12] E. A. Sciberras, B. Zahawi, D. J. Atkinson, and A. Juandó, "Cold ironing for greener port stays," in *Low Carbon Shipping Conference, London 2013.* UCL, 2013.

[13] E. A. Sciberras and B. Zahawi, "Emissions reduction while at port," in *Green Ports Energy Conference*, Vigo, June 2013.

[14] E. A. Sciberras, B. Zahawi, D. J. Atkinson, A. Juandó, and A. Sarasquete, "Cold ironing and onshore generation for airborne emission reductions in ports," *Proceedings of the Institution of Mechanical Engineers, Part M: Journal of Engineering for the Maritime Environment*, vol. 230, no. I, pp. 67–82, 2016.

[15] E. A. Sciberras, B. Zahawi, and D. J. Atkinson, "Electrical characteristics of cold ironing energy supply for berthed ships," *Transportation Research Part D: Transport and Environment*, vol. 39, pp. 31–43, 2015.

[16] E. Sciberras, B. Zahawi, and D. J. Atkinson, "Reducing shipboard emissions – assessment of the role of electrical technologies," *Transportation Research Part D: Transport and Environment*, 2016, submitted for peer review.

[17] E. A. Sciberras, B. Zahawi, and D. J. Atkinson, "Managing shipboard energy – a stochastic approach," *IEEE Transactions on Transportation Electrification*, 2016, submitted for peer review.

[18] Royal Academy of Engineering, *Future ship powering options; exploring alternative methods of ship propulsion*, London, Jul. 2013, no. 978-1-909327-01-6.

[19] D. Cooper, "Representative emission factors for use in quantification of emissions from ships associated with ship movements between ports in the european

community," IVL Swedish Environmental Research Institute Ltd., Göteborg, Tech. Rep., May 2002.

[20] H. K. Woud and D. Stapersma, *Design of propulsion and electric power generation systems*. London: IMarEST, The Institute of Marine Engineering, Science and Technology, 2008, ch. Propulsion and electric power, pp. 41–88.

[21] N. Schofield, H. Yap, and C. Bingham, "Hybrid energy sources for electric and fuel cell vehicle propulsion," in *Vehicle Power and Propulsion, 2005 IEEE Conference*, Sept 2005, pp. 522–529.

[22] H. K. Woud and D. Stapersma, *Design of propulsion and electric power generation systems*. London: IMarEST, The Institute of Marine Engineering, Science and Technology, 2008, ch. Power plant concepts, pp. 103–130.

[23] J. Prousalidis, I. Hatzilau, P. Michalopoulos, I. Pavlou, and D. Muthumuni, "Studying ship electric energy systems with shaft generator," in *Electric Ship Technologies Symposium, 2005 IEEE*, July 2005, pp. 156–162.

[24] J. Buckingham, "Naval economy and flexibility," in *Low Carbon Shipping Conference, Newcastle upon Tyne 2012*. Newcastle University, 2012.

[25] ——, "Hybrid drives for efficiency," in *Low Carbon Shipping Conference, London 2013*. UCL, 2013.

[26] G. Castles, G. Reed, A. Bendre, and R. Pitsch, "Economic benefits of hybrid drive propulsion for naval ships," in *Electric Ship Technologies Symposium, 2009. ESTS 2009. IEEE*, April 2009, pp. 515–520.

[27] N. Mohan, T. M. Undeland, and W. P. Robbins, *Power electronics: converters, applications, and design*. John Wiley & Sons, 2003.

[28] Z. Zhu and D. Howe, "Electrical machines and drives for electric, hybrid, and fuel cell vehicles," *Proceedings of the IEEE*, vol. 95, no. 4, pp. 746–765, April 2007.

[29] D. Alexander, D. Rummler, A. Mohtashamian, G. Robinson, M. Zahzah, C. T. Farr, and G. E. Poole, "Hybrid electric drive evaluation for CG 47 class guided missile cruisers," *Naval Engineers Journal*, vol. 122, no. 2, pp. 67–77, 2010.

[30] D. Alexander, T. Lo, J. Bravo, and Y. Fleytman, "Integrated main reduction gears for hybrid drive surface ship applications," in *Electric Ship Technologies Symposium (ESTS), 2011 IEEE*, April 2011, pp. 345–352.

[31] J. F. Gieras, *Advancements in electric machines*. Springer, 2009, ch. High power density machines, pp. 70–80.

[32] F. Caricchi, F. Crescimbini, and O. Honrati, "Modular axial-flux permanent-magnet motor for ship propulsion drives," *Energy Conversion, IEEE Transactions on*, vol. 14, no. 3, pp. 673–679, Sep 1999.

[33] J. F. Gieras, *Advancements in electric machines*. Springer, 2009, ch. Other types of novel motors, pp. 115–133.

[34] R. de Doncker, D. W. J. Pulle, and A. Veltman, *Advanced Electrical Drives Analysis, Modeling, Control*. Springer, 2011, ch. Control of Synchronous machine drives, pp. 193–221.

[35] S. Morimoto, Y. Takeda, T. Hirasa, and K. Taniguchi, "Expansion of operating limits for permanent magnet motor by current vector control considering inverter capacity," *IEEE Transactions on Industry Applications*, vol. 26, no. 5, pp. 866–871, 1990.

[36] R. de Doncker, D. W. J. Pulle, and A. Veltman, *Advanced Electrical Drives Analysis, Modeling, Control*. Springer, 2011, ch. Control of Induction machine drives, pp. 303–336.

[37] M. Godjevac, J. Drijver, L. de Vries, and D. Stapersma, "Evaluation of losses in maritime gearboxes," *Proceedings of the Institution of Mechanical Engineers, Part M: Journal of Engineering for the Maritime Environment*, 2015.

[38] MAN, "Shaft generators for the MC and ME engines," MAN Diesel & Turbo, Copenhagen, Tech. Rep., January 2011.

[39] J. Carlton, *Marine propellers and propulsion*. Butterworth-Heinemann, 2012, ch. 2, pp. 11–28.

[40] H. K. Woud and D. Stapersma, *Design of propulsion and electric power generation systems*. London: IMarEST, The Institute of Marine Engineering, Science and Technology, 2008, ch. Diesel engines, pp. 191–262.

[41] A. J. Murphy, S. J. Weston, and R. J. Young, "Reducing fuel usage and CO_2 emissions from tug boat fleets: Sea trials and theoretical modelling," *International Journal of Maritime Engineering*, vol. 154, pp. A31–A41, 2012.

[42] A. Juandó, "Report on recorded data analysis and conclusions from sea measurements," *TEFLES project deliverable 3.2*, 2012.

[43] C. Vossen, "Diesel electric propulsion on sigma class corvettes," in *Electric Ship Technologies Symposium (ESTS), 2011 IEEE*, pp. 288–291.

[44] Bunkerworld. (2014, 19/03/2014) Bunkerworld prices - latest prices. http://www.bunkerworld.com/prices/.

[45] E. Sciberras and R. Norman, "Multi-objective design of a hybrid propulsion system for marine vessels," *Electrical Systems in Transportation, IET*, vol. 2, no. 3, pp. 148–157, September 2012.

[46] C.-C. Chang and C.-M. Wang, "Evaluating the effects of green port policy: Case study of Kaohsiung harbor in Taiwan," *Transportation Research Part D: Transport and Environment*, vol. 17, no. 3, pp. 185–189, 2012.

[47] W. J. Hall, "Assessment of CO_2 and priority pollutant reduction by installation of shoreside power," *Resources Conservation and Recycling*, vol. 54, no. 7, pp. 462–467, 2010.

[48] T. Zis, R. J. North, P. Angeloudis, W. Y. Ochieng, and M. G. Harrison Bell, "Evaluation of cold ironing and speed reduction policies to reduce ship emissions near and at ports," *Maritime Economics & Logistics*, vol. 16, no. 4, pp. 371–398, 2014.

[49] The European Parliament and the Council of the European Union, "Directive 2012/33/EC," *Official Journal of the European Union*, November 2012.

[50] IMO, "Annex VI, Prevention of Air Pollution from Ships," *MARPOL 73/78, International Convention for the Prevention of Pollution from Ships*, 2005.

[51] R. Winkel, U. Weddige, D. Johnsen, V. Hoen, and S. Papaefthimiou, "Shore side electricity in Europe: Potential and environmental benefits," *Energy Policy*, 2015, eprint ahead of print.

[52] J. Prousalidis, G. Antonopoulos, C. Patsios, A. Greig, and R. Bucknall, "Green shipping in emission controlled areas: Combining smart grids and cold ironing," in *Electrical Machines (ICEM), 2014 International Conference on*, Sept 2014, pp. 2299–2305.

[53] "IEC/ISO/IEEE Utility Connections in port–Part 1: High Voltage Shore Connection (HVSC) Systems–General requirements," *IEC/ISO/IEEE 80005-1:2012*, July 2012.

[54] "Utility connections in port - Part 3: Low Voltage Shore Connection (LVSC) Systems - General requirements, IEC PAS 80005-3," vol. IEC PAS 80005-3, 2014.

[55] "IEC/IEEE 80005-2 - Utility connections in port–Part 2: High and Low voltage shore connection systems - Communication for monitoring and control," 2015.

[56] M. Martelin, I. Fazlagic, and R. Skinner, "ABB shore connection: effectively reducing emissions from ports," ABB AB, Tech. Rep., 2010.

[57] G. Sulligoi, D. Bosich, A. da Rin, and F. Tosato, "An examination of mutual influences between high-voltage shore-connected ships and port earthing systems during phase-to-ground faults," *Industry Applications, IEEE Transactions on*, vol. 48, no. 5, pp. 1731–1738, Sept 2012.

[58] D. Paul and B. Chavdarian, "A closer look at the grounding of shore-to-ship power supply system," in *Industrial Commercial Power Systems Technical Conference - Conference Record 2009 IEEE*, May 2009, pp. 1–7.

[59] D. Paul, P. Chavdarian, and V. Haddadian, "Cable-capacitance discharge time with and without the application of grounding device," *Industry Applications, IEEE Transactions on*, vol. 47, no. 1, pp. 286–291, Jan 2011.

[60] D. Paul and V. Haddadian, "Transient overvoltage protection of shore-to-ship power supply system," in *Petroleum and Chemical Industry Conference (PCIC), 2010 Record of Conference Papers Industry Applications Society 57th Annual*, Sept 2010, pp. 1–8.

[61] M. Ion, M. Megdiche, D. Radu, S. Bacha, and D. Hadbi, "Increasing the short-circuit current in a shore connection system," in *PowerTech (POWERTECH), 2013 IEEE Grenoble*, June 2013, pp. 1–6.

[62] S. Panetta, "Shipboard electrical system grounding," in *Electric Ship Technologies Symposium (ESTS), 2015 IEEE*, 2015, pp. 358–363.

[63] X. Yang, G. Bai, and R. Schmidhalter, "Shore to ship converter system for energy saving and emission reduction," in *Power Electronics and ECCE Asia (ICPE & ECCE), 2011 IEEE 8th International Conference on.* IEEE, 2011, pp. 2081–2086.

[64] ABB, "Enabling the shore-to-ship connection - static frequency converters," Tech. Rep., 2011.

[65] S. Cissoko and D. Radu, "Selecting the frequency conversion system for shore connection," Schneider Electric Industries SAS, Tech. Rep., 2015.

[66] P. Ericsson and I. Fazlagic, "Shore-side power supply," Master of Science Thesis, Department of Energy and Environment, Chalmers University of Technology, Göteborg, Sweden, 2008.

[67] K. Brown, L. Cardenas, J. MacCarthy, T. Murrells, Y. Pang, N. Passant, G. Thistlethwaite, A. Thomson, and N. Webb, *UK Greenhouse Gas Inventory, 1990 to 2010.* Didcot, Oxfordshire: AEA Technology plc, April 2012.

[68] I. MacLeay, K. Harris, and A. Annut, "Digest of United Kingdom energy statistics 2011," Department of Energy and Climate Change, Tech. Rep., 2011.

[69] AEA, "2012 Guidelines to Defra/DECC's GHG Conversion Factors for Company Reporting," AEA for the Department of Energy and Climate Change (DECC) and the Department for Environment, Food and Rural Affairs (Defra), Tech. Rep., May 2012.

[70] IEA, "Key world energy statistics," International Energy Agency, Tech. Rep., 2012.

[71] I. S. Seddiek, M. A. Mosleh, and A. A. Banawan, "Fuel saving and emissions cut through shore-side power concept for high-speed crafts at the Red Sea in

Egypt," *Journal of Marine Science and Application*, vol. 12, no. 4, pp. 463–472, 2013.

[72] S. Bengtsson, K. Andersson, and E. Fridell, "A comparative life cycle assessment of marine fuels: liquefied natural gas and three other fossil fuels," *Proceedings of the Institution of Mechanical Engineers, Part M: Journal of Engineering for the Maritime Environment*, vol. 225, no. 2, pp. 97–110, 2011.

[73] S. K. Bengtsson, E. Fridell, and K. E. Andersson, "Fuels for short sea shipping: A comparative assessment with focus on environmental impact," *Proceedings of the Institution of Mechanical Engineers, Part M: Journal of Engineering for the Maritime Environment*, vol. 228, no. 1, pp. 44–54, 2013.

[74] M. Bagniewski, "LNG fuel for ships. a chance or a must?" Det Norske Veritas Poland Sp. z o.o, Gdynia, Poland, Tech. Rep., 2012.

[75] J. Pérez Prat and A. Juandó, "Report on the state of the art," *TEFLES project deliverable 7.1*, 2012.

[76] A. Juandó, E. Sciberras, and A. Casal, "Report on drivers and operational constraints for effective low-emissions shore power strategy," *TEFLES project deliverable 7.2*, 2013.

[77] J. Smits, "Shore Connected Power for the ferry/Ro Ro vessels in the port of Rotterdam," Holland Marine Equipment BV, Tech. Rep., 2008.

[78] "IEEE Recommended Practice for Establishing Liquid-Filled and Dry-Type Power and Distribution Transformer Capability When Supplying Nonsinusoidal Load Currents," *IEEE Std C57.110-2008 (Revision of IEEE Std C57.110-1998)*, pp. 1–52, Aug 2008.

[79] N. Mohan, T. M. Undeland, and W. P. Robbins, *Power electronics: converters, applications, and design.* John Wiley & Sons, Inc, 2003, ch. Desired characteristics in controllable switches, pp. 20–24.

[80] K. Ahmed, S. Finney, and B. Williams, "Passive filter design for three-phase inverter interfacing in distributed generation," in *Compatibility in Power Electronics, 2007. CPE '07*, 2007, pp. 1–9.

[81] K. Deb, *Multi-Objective Optimization using Evolutionary Algorithms*. Chichester, UK: Wiley, 2001.

[82] R. C. Eberhart and Y. Shi, "Comparison between genetic algorithms and particle swarm optimization," in *Evolutionary Programming VII*. Springer, 1998, pp. 611–616.

[83] M. Clerc, *Particle Swarm Optimization*. ISTE Ltd, 2006.

[84] Y. del Valle, G. Venayagamoorthy, S. Mohagheghi, J.-C. Hernandez, and R. Harley, "Particle swarm optimization: Basic concepts, variants and applications in power systems," *Evolutionary Computation, IEEE Transactions on*, vol. 12, no. 2, pp. 171–195, April 2008.

[85] J. Kennedy and R. Eberhart, "Particle swarm optimization," in *Neural Networks, 1995. Proceedings., IEEE International Conference on*, vol. 4, Nov 1995, pp. 1942–1948 vol.4.

[86] I. Musa, S. Gadoue, and B. Zahawi, "Integration of distributed generation in power networks considering constraints on discrete size of distributed generation units," *Electric Power Components and Systems*, vol. 42, no. 9, pp. 984–994, 2014.

[87] R. Hassan, B. Cohanim, O. De Weck, and G. Venter, "A comparison of particle swarm optimization and the genetic algorithm," in *Proceedings of the 1st AIAA multidisciplinary design optimization specialist conference*, 2005, pp. 18–21.

[88] M. Clerc and J. Kennedy, "The particle swarm - explosion, stability, and convergence in a multidimensional complex space," *Evolutionary Computation, IEEE Transactions on*, vol. 6, no. 1, pp. 58–73, Feb 2002.

[89] J. Kennedy and R. Mendes, "Neighborhood topologies in fully informed and best-of-neighborhood particle swarms," *Systems, Man, and Cybernetics, Part C: Applications and Reviews, IEEE Transactions on*, vol. 36, no. 4, pp. 515–519, July 2006.

[90] C. Coello, G. Pulido, and M. Lechuga, "Handling multiple objectives with particle swarm optimization," *Evolutionary Computation, IEEE Transactions on*, vol. 8, no. 3, pp. 256–279, June 2004.

[91] K. Deb, A. Pratap, S. Agarwal, and T. Meyarivan, "A fast and elitist multiobjective genetic algorithm: NSGA-II," *IEEE Transactions on Evolutionary Computation*, vol. 6, no. 2, pp. 182–197, 2002.

[92] B. Ji, X. Song, E. Sciberras, W. Cao, Y. Hu, and V. Pickert, "Multiobjective design optimization of IGBT power modules considering power cycling and thermal cycling," *Power Electronics, IEEE Transactions on*, vol. 30, no. 5, pp. 2493–2504, May 2015.

[93] Z. Michalewicz and M. Schmidt, *Evolutionary optimization*. Springer Science & Business Media, 2002, vol. 48, ch. Evolutionary algorithms and constrained optimization, pp. 57–86.

[94] "IEEE recommended practice and requirements for harmonic control in electric power systems," *IEEE Std 519-2014 (Revision of IEEE Std 519-1992)*, pp. 1–29, June 2014.

[95] H. Akagi, "Active harmonic filters," *Proceedings of the IEEE*, vol. 93, no. 12, pp. 2128–2141, Dec 2005.

[96] S. Gunput, P. Rampen, F. Xinqian, E. Sciberras, and H. van Vugt, "Energy management implementation report," *INOMANS2HIP project deliverable 5.1*, 2015.

[97] D. Mitropoulou, S. Gunput, P. Rampen, C. Meijer, P. Sebrechts, and W. van der Pennen, "Cargo global electrical diagram," *INOMANS2HIP project deliverable 3.3*, 2014.

[98] T. Horiba, "Lithium-ion battery systems," *Proceedings of the IEEE*, vol. 102, no. 6, pp. 939–950, Jun. 2014.

[99] H. van Vugt, "Available internal energy profiles of various components," *INOMANS2HIP project deliverable 4.1*, 2014.

[100] L. de Vries, "Ship energy design and service simulations combined with real-time propulsion performance management approach," in *13th International Conference on Computer and IT Applications in the Maritime Industries*, 2014.

[101] A. Sciarretta, M. Back, and L. Guzzella, "Optimal control of parallel hybrid electric vehicles," *Control Systems Technology, IEEE Transactions on*, vol. 12, no. 3, pp. 352–363, 2004.

[102] T. Vu, A. Ayu, J. Dhupia, L. Kennedy, and A. Adnanes, "Power management for electric tugboats through operating load estimation," *IEEE Transactions on Control Systems Technology*, 2015, eprint ahead of print.

[103] H. Grimmelius, P. de Vos, M. Krijgsman, and E. van Deursen, "Control of hybrid ship drive systems," in *10th international conference on computer and IT applications in the maritime industries.*, V. Bertram, Ed. Hamburg: Technische Universität Hamburg Harburg, 2011.

[104] F. D. Kanellos, J. M. Prousalidis, and G. J. Tsekouras, "Control system for fuel consumption minimization–gas emission limitation of full electric propulsion ship power systems," *Proceedings of the Institution of Mechanical Engineers, Part M: Journal of Engineering for the Maritime Environment*, vol. 228, no. 1, pp. 17–28, 2014.

[105] B. Zahedi, L. E. Norum, and K. B. Ludvigsen, "Optimized efficiency of all-electric ships by dc hybrid power systems," *Journal of Power Sources*, vol. 255, pp. 341–354, 2014.

[106] M. Abido, "Optimal power flow using particle swarm optimization," *International Journal of Electrical Power & Energy Systems*, vol. 24, no. 7, pp. 563–571, 2002.

[107] M. A. Abido, "Environmental/economic power dispatch using multiobjective evolutionary algorithms," *Power Systems, IEEE Transactions on*, vol. 18, no. 4, pp. 1529–1537, 2003.

[108] S. A. Pourmousavi, M. H. Nehrir, C. M. Colson, and C. Wang, "Real-time energy management of a stand-alone hybrid wind-microturbine energy system using particle swarm optimization," *Sustainable Energy, IEEE Transactions on*, vol. 1, no. 3, pp. 193–201, 2010.

[109] H. van Vugt, E. Sciberras, and A. Breijs, "Optimised energy exchange management algorithms between all the equipment," *INOMANS2HIP project deliverable 4.2*, 2014.

[110] H. van den Broek, T. Hof, H. van Vugt, T. Bradley, L. Brown, and J. Heslop, "HMI criteria and mimics," *INOMANS2HIP project deliverable 4.3*, 2014.

Appendix A

Shore supply network models

The following figures illustrate the Simulink models developed to represent the various shoreside network topologies for onshore power supply. Figure A.1 shows the top level diagram which contains the berth power information together with the simulation execution control. Figures A.2 to A.4 show the actual network model for the various topologies which are contained in the top level diagram in the conditionally executed subsystem. Figure A.5 shows the transformer model, with the additional harmonic loss factors.

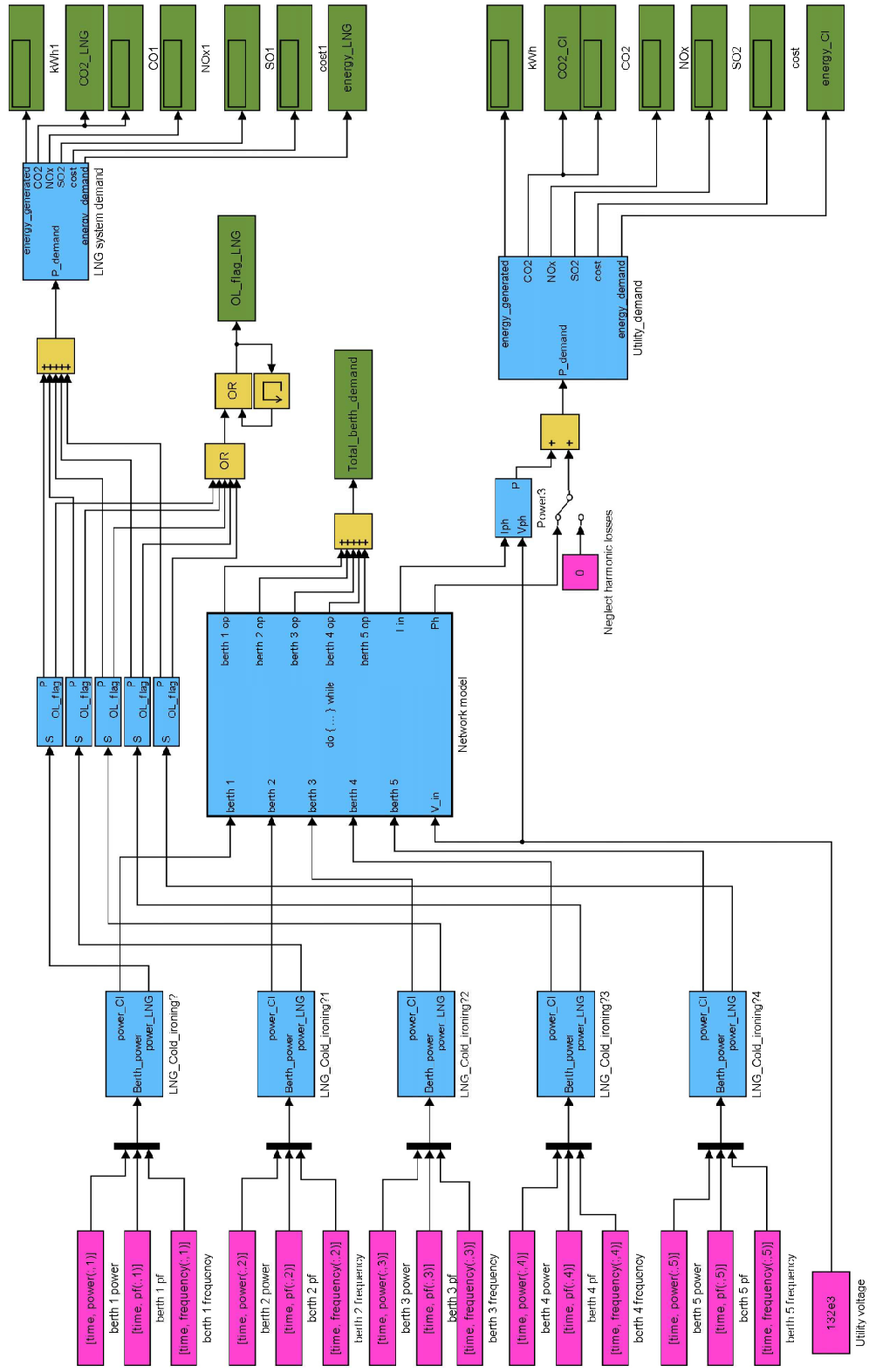

Figure A.1 – Top level simulation model of shore network.

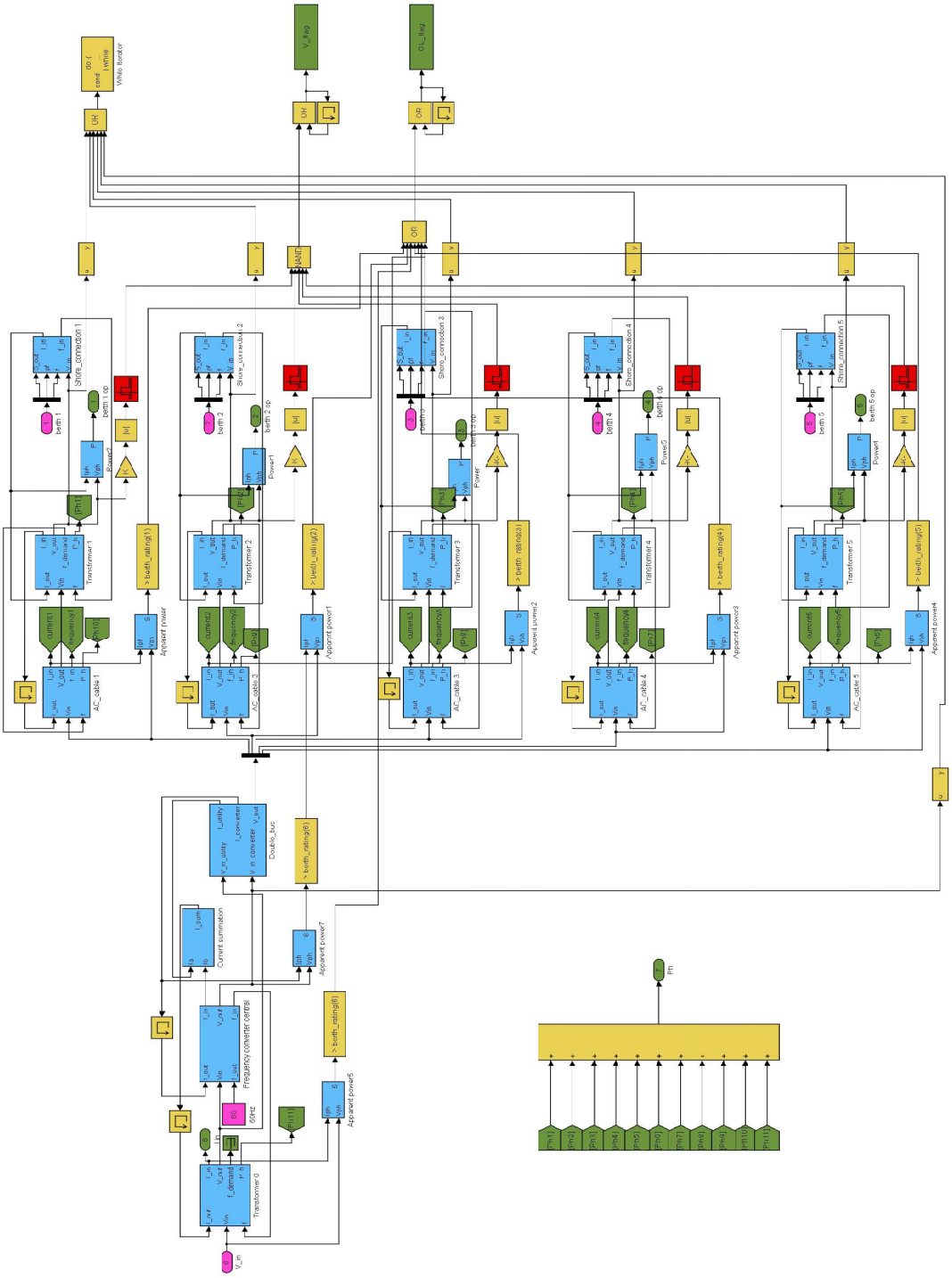

Figure A.2 – Centralised topology network model.

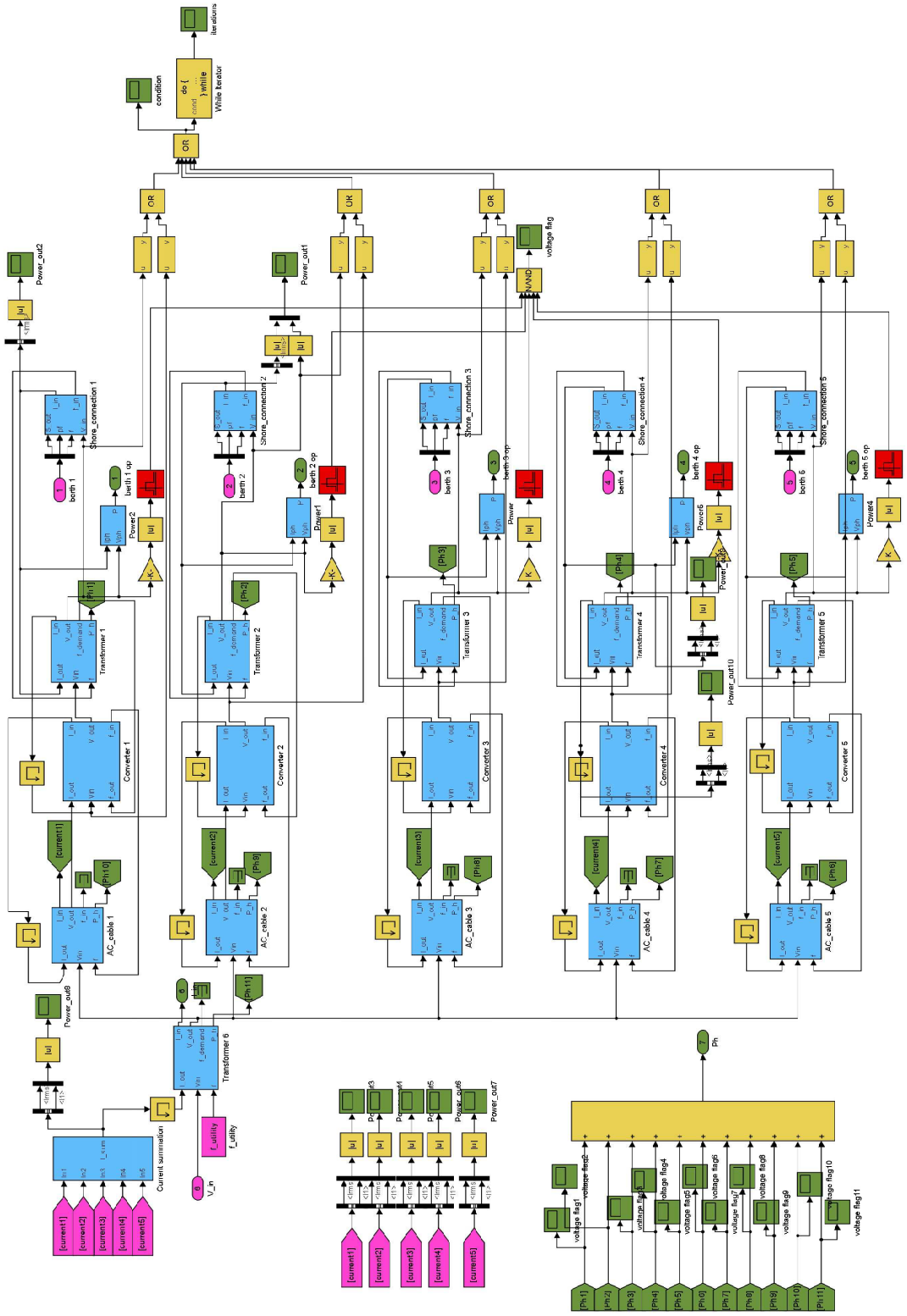

Figure A.3 – Distributed topology network model.

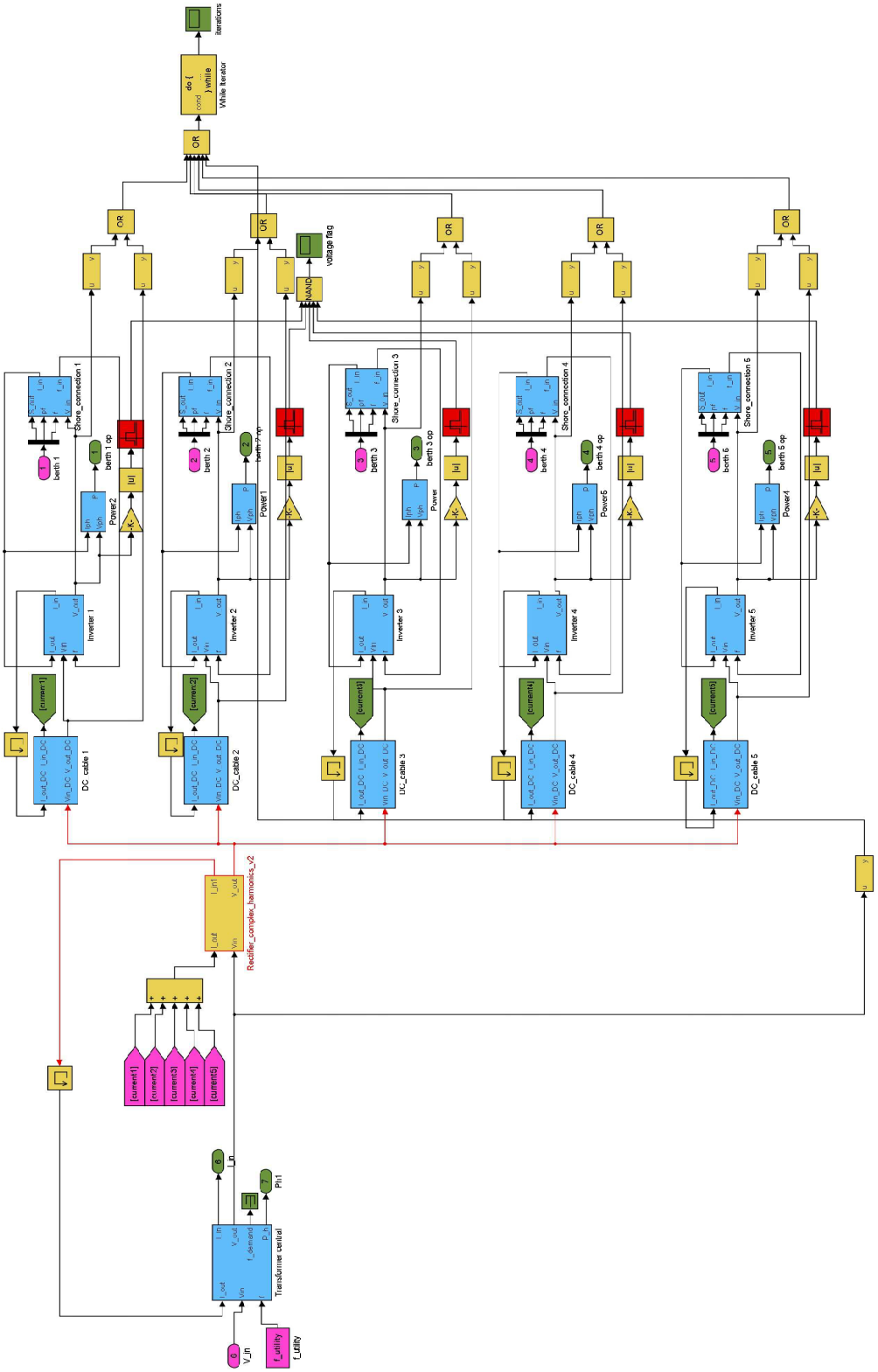

Figure A.4 – DC topology network model.

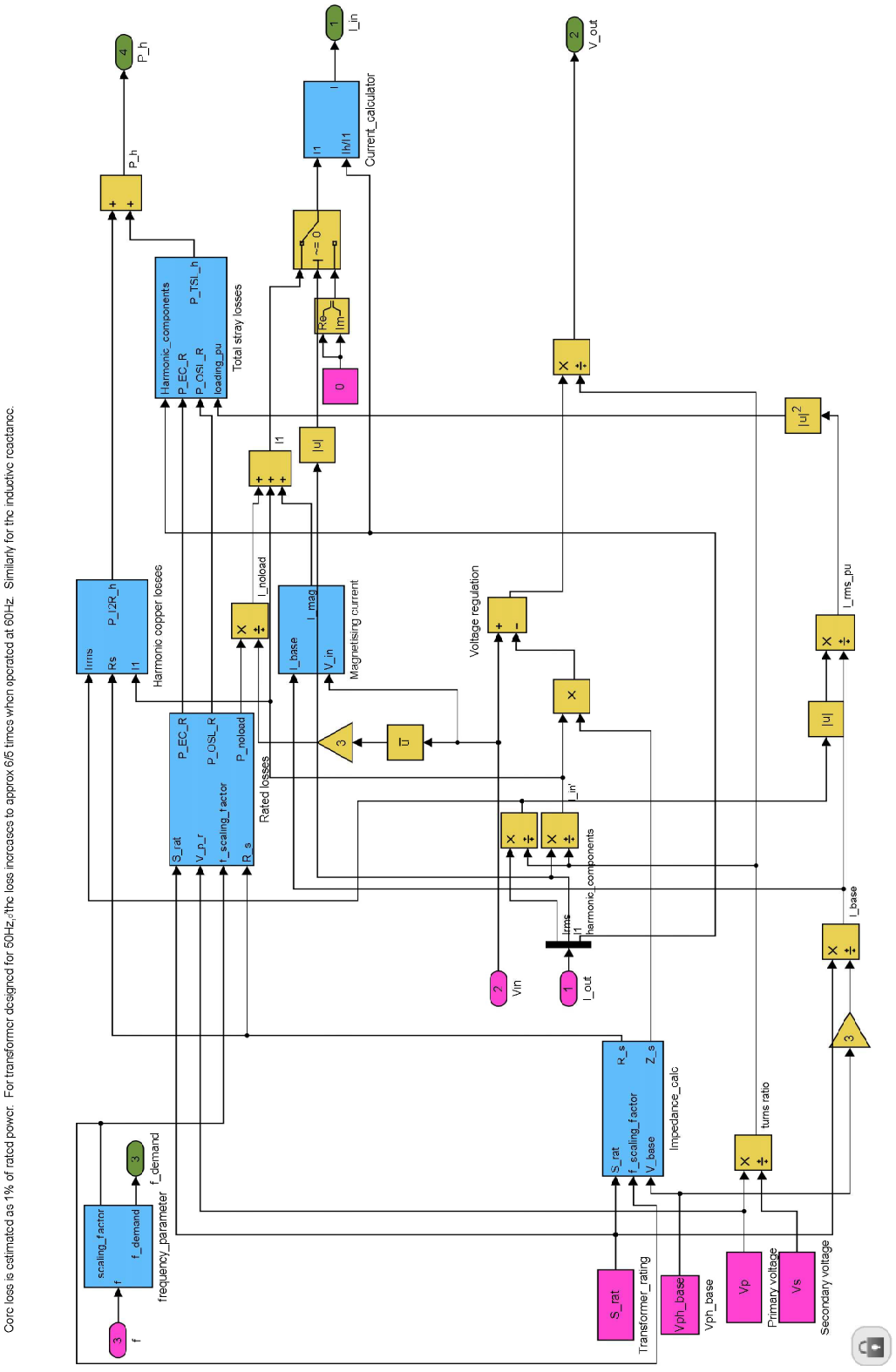

Figure A.5 – Transformer model.

Appendix B

Multi-Objective PSO code

The code in this section relates to the optimisation script developed for the identification of optimal network topology for onshore power supply. The main script is the top level script that contains the PSO algorithm with all associated parameters, and calls the objective function (Simulink models) as well as the other internal functions.

B.1 Main algorithm script

```
%% Main algorithm script for multi-objective PSO
clear

% Initialisation

%PSO parameters
% Inertia weighting
W = 0.4; %Constant inertia

N = 20; %Population size
d = 12; %Number of variables
%1:5 are berth ratings, 6 is central rating, 7 is shoreside
  topology choice
O = 2; %Number of objectives
REP_size = 20; %Size of external repository to store Pareto
  fronts
iterations = 1000; %Number of iterations to perform

%Mutation rate as 1/number of dimensions (search space)
```

```
18 mut_rate = 1/d;
19
20 %Limits on velocity and location (normalised)
21 v_max = 0.5;
22 x_max = 1;
23 x_min = 1e-3; %Prevents division by zero erros in device LUTs
24
25 %Scaling
26 %Population location is normalised (0,1]
27 max_rat_berth = 5e6; %Maximum berth rating to scale particle
     positions
28 max_rat_central = 10e6; %Maximum central device rating for
     scaling
29 num_topos = 3; %number of possible topologies
30 %Vector for berth rating scaling
31 %Berth ratings rounded to nearest 100kW
32 max_rat(1:5) = max_rat_berth;
33 max_rat(6) = max_rat_central;
34 rat_interval = 50e3; %Rating intervals for rounding
35
36 %Binary cutoff for LNG or cold ironing
37 threshold = 0.5; %threshold function for binary variable
38 LNG_CI_select_list = false(N,5); %selection mask
39
40 %Cost function parameters
41 %a) Uniform cost allocation
42 unit_cost = 1; %Cost per Watt (pu)
43 max_cost = sum(unit_cost.*max_rat);
44 %b) Corrected cost estimate allocation
45 cost_trafo = 1; %1pu (per kVA)
46 cost_converter = 3; %3pu (per kVA)
47 cost_LNG = 2; %3pu (per kVA)
48
49 %Load parameters and profiles for simulink models
50 cold_ironing_parameters_opt_02;
51
52 %Define models to be used as cell of strings
53 models = cellstr(char('centralised_system_iterations_updated_03'
     ,...  %1
54     'distributed_system_iterations_updated_03',...  %2
```

```
55      'DC_system_iterations_updated_04')); %3
56  %Strings refer to .mdl files in current directory
57
58  %Empty arrays to store results/historical progressions
59  results = zeros(N,d); %final population
60  gbest_hist = zeros(iterations,1); %history of global best
61  gbest_loc_hist = zeros(iterations,d); %history of global best
      locations
62  pbest_hist = zeros(N,O,iterations); %history of average particle
      best
63  POP_loc_hist = zeros(N,d,iterations); %history of all particle
      locations
64
65  %% Initialise population with random velocities and locations (
      normalised)
66  %Column 1 = x1, column 2 = x2, ... column d = xd
67  %Row 1 = particle 1, row 2 = particle 2, ... row N = xN
68  POP_loc = x_min + (x_max-x_min).*rand(N,d); %Random array for
      population particle locations
69  POP_vel = -v_max + (v_max-(-v_max)).*rand(N,d); %Random array for
       population particle velocities
70
71  % Initialise individual particles' memory spaces
72  fitness = zeros(N,O); %Empty array for fitness values
73  pbest = zeros(N,O); %Empty array for particle best fitness value
74  pbest_loc = zeros(N,d); %Empty array for corresponding best
      fitness value location
75
76  % External repository
77  REP_loc = zeros(REP_size,d); %Repository for particle location
78  REP_fitness = inf.*ones(REP_size,O); %Repository for particle
      fitness
79
80  % Initial configurations
81  berth_rating_list =  bsxfun(@times, max_rat,POP_loc(:,1:6));
82  POP_loc(:,1:6) = bsxfun(@rdivide,berth_rating_list,max_rat);
83  POP_loc(:,7) = round((num_topos-1)*POP_loc(:,7))/(num_topos-1);
84  mdl_list = models(1+(num_topos-1)*POP_loc(:,7));
85  LNG_CI_select_list(POP_loc(:,8:12)>=threshold) = true; %1 => Cold
       ironing O=>LNG
```

```
86
87 load_system(models)
88
89 %% Main algorithm loop
90 for ctr = 1:iterations
91     %Evaluate fitness of each particle based on location
92
93     %for each particle...
94     for ctr2 = 1:N
95         berth_rating = berth_rating_list(ctr2,:); %Load berth
             rating values
96         LNG_CI_select = LNG_CI_select_list(ctr2,:); %Load LNG/CI
             options
97         mdl = mdl_list{ctr2}; %Load model topology
98         simOut = sim(mdl,'ReturnWorkspaceOutputs','on'); %Run
             simulation
99         V_flag = simOut.get('V_flag'); %Flag for berth voltage
             violation
100        OL_flag = simOut.get('OL_flag')|simOut.get('OL_flag_LNG')
             ; %Flag for berth overload violation
101        if (V_flag == 1 || OL_flag == 1)
102            fitness(ctr2,:) = inf; %Penalise fitness if any flag
                 violation occurs...
103        else
104            fitness(ctr2,1) = simOut.get('CO2_LNG')+simOut.get('
                 CO2_CI'); %...otherwise store CO2 figure
105
106            % Corrected cost estimate allocations
107            if (1+(num_topos-1)*POP_loc(ctr2,7)) == 1
108                %Centralised topology
109                fitness(ctr2,2) = sum(cost_trafo.*LNG_CI_select
                     .*(berth_rating(1:5)/1e3)) + (cost_trafo+
                     cost_converter)*berth_rating(6)/1e3 + sum(
                     cost_LNG.*not(LNG_CI_select).*(berth_rating(1:5)
                     /1e3));
110            elseif (1+(num_topos-1)*POP_loc(ctr2,7)) == 2
111                %Distributed topology
112                fitness(ctr2,2) = sum((cost_trafo+cost_converter)
                     .*LNG_CI_select.*(berth_rating(1:5)/1e3)) +
                     cost_trafo*berth_rating(6)/1e3 + sum(cost_LNG.*
```

```
                not(LNG_CI_select).*(berth_rating(1:5)/1e3));
113         elseif (1+(num_topos-1)*POP_loc(ctr2,7)) == 3
114             %DC topology
115             fitness(ctr2,2) = sum((cost_trafo+0.8*
                  cost_converter).*LNG_CI_select.*(berth_rating
                  (1:5)/1e3)) + (cost_trafo)*berth_rating(6)/1e3 +
                   sum(cost_LNG.*not(LNG_CI_select).*(berth_rating
                  (1:5)/1e3));
116         else
117             %Catch errors
118             fitness(ctr2,2) = inf;
119         end
120     end
121 end
122
123 %For first iterate, initialise records of best locations
124 if ctr == 1
125     pareto_front = identify_pareto(fitness); %identify pareto
        set of solutions
126     pbest = fitness; %particle best is assigned to current
        fitness
127     pbest_loc = POP_loc; %particle best location is assigned
        to current location
128     REP_loc(1:length(find(pareto_front)),:) = POP_loc(
        pareto_front,:); %repository for coordinates of pareto
        front
129     REP_fitness(1:length(find(pareto_front)),:) = fitness(
        pareto_front,:); %repository for fitnesses of pareto
        front
130     REP_distance = eval_crowding(REP_fitness); %evaluate
        crowding distance between particles in objective space
131 else
132     %Update pbest if new fitnesses are better
133     for ctr3 = 1:N
134         %compare between new fitness and pbest to see if
            dominated
135         pair_test = [fitness(ctr3,:); pbest(ctr3,:)];
136         pair_test_loc = [POP_loc(ctr3,:); pbest_loc(ctr3,:)];
137         mask = identify_pareto(pair_test); %perform pareto
            test on particle best and corresponding new fitness
```

```
138             %if non-dominated, randomly choose one
139             if all(mask)
140                 select = randi(2,1);
141                 pbest(ctr3,:) = pair_test(select,:);
142                 pbest_loc(ctr3,:) = pair_test_loc(select,:);
143             else
144                 select = find(mask,1);
145                 pbest(ctr3,:) = pair_test(select,:);
146                 pbest_loc(ctr3,:) = pair_test_loc(select,:);
147             end
148         end
149
150         %update repository with new particles
151         [REP_fitness,REP_loc,REP_distance] = build_REP(REP_size,
              REP_fitness,REP_loc,fitness,POP_loc);
152     end
153
154     %calculate new particle velocities
155     h = select_from_REP(N,REP_fitness,REP_distance); %generate
      list of particles from repository to be used for velocity
      update
156     POP_vel = W.*POP_vel + rand(N,d).*(pbest_loc-POP_loc) + rand(
      N,d).*(REP_loc(h,:)-POP_loc); %calculate new velocities
157
158     %store current population location
159     %(necessary for end condition evaluation)
160     POP_loc_CURR = POP_loc;
161
162     %calculate new particle positions
163     POP_loc = POP_loc + POP_vel;
164
165     % MUTATION
166     %assume uniform mutation - each particle, and each dimension
      has same
167     %probability of being mutated on all iterations.
168     mutation_select = logical(rand(size(POP_loc)) < mut_rate); %
      identify what is to be mutated
169     POP_loc(mutation_select) = rand(size(find(mutation_select)));
        %replace masked coordinates
170
```

```
171     %correct position to limits
172     POP_loc(POP_loc > x_max) = x_max;
173     POP_loc(POP_loc(:,1:6) < x_min) = x_min;
174     POP_loc((POP_loc(:,7) < 0),7:12) = 0;
175     POP_vel(POP_loc > x_max | POP_loc < 0) = (-1).*POP_vel(
          POP_loc > x_max | POP_loc < 0); %Reflect particles beyond
          boundary back into
176
177     % round population locations to rating interval values up to
          x_max
178     POP_loc(:,1:6) = bsxfun(@times,(rat_interval./max_rat),ceil(
          bsxfun(@times,POP_loc(:,1:6),(max_rat/rat_interval))));
179     POP_loc(:,7) = round((num_topos-1)*POP_loc(:,7))/(num_topos
          -1);
180     POP_loc(:,8:12) = round(POP_loc(:,8:12));
181
182     berth_rating_list = bsxfun(@times, max_rat,POP_loc(:,1:6)); %
          get berth ratings
183     mdl_list = models(1+(num_topos-1)*POP_loc(:,7)); %Get list of
           model names
184     LNG_CI_select_list = logical(POP_loc(:,8:12));
185     pbest_hist(:,:,ctr) = pbest; %store particle best values
186     POP_loc_hist(:,:,ctr) = POP_loc_CURR;
187
188     disp(ctr)
189
190     %store current pareto front data
191     valid_REP = all(REP_loc~=inf,2);
192     berth_rating_REP = bsxfun(@times,max_rat,REP_loc(valid_REP
          ,1:6));
193     mdl_list_REP = models(1+(num_topos-1)*REP_loc(valid_REP,7));
194     config_REP = REP_loc(valid_REP,8:12);
195     total_cost = REP_fitness(valid_REP,2);
196     CO2 = REP_fitness(valid_REP,1);
197
198     %generate plot of pareto front
199     plot(CO2,total_cost,'+')
200     xlabel('CO2 emissions (kg)')
201     ylabel('Cost (normalised)')
202     hold all
```

```
203 end
204
205 %Emphasise final Pareto front and redraw to emphasize
206 plot(CO2,total_cost,'*','MarkerSize',10)
207 elapsed_time = toc; %...stop timer to calculate elapsed time
```

B.2 Build repository function

```
1  function [new_REP_obj,new_REP_loc, new_REP_distance] = build_REP(
     REP_size, REP_obj, REP_loc, current_fitness, current_loc)
2  %ES 25/03/2013
3
4  %builds repository containing first non-dominated front (rank 1)
5
6  new_REP_obj = inf*ones(size(REP_obj)); %instantiate empty
     repository for fitnesses (infinity for minimisation problem)
7  new_REP_distance = zeros(length(REP_obj),1); %instantiate empty
     repository for crowding distance
8  new_REP_loc = inf*ones(size(REP_loc)); %instantiate empty
     repository for particle locations
9
10 %builds the new generation's external repository with new pareto
     front
11 combined_pop_obj = vertcat(REP_obj,current_fitness); %concatenate
      fitnesses
12 combined_pop_loc = vertcat(REP_loc,current_loc); %concatenate
     locations
13 new_pareto_mask = logical(identify_pareto(combined_pop_obj)); %
     identify pareto front of combined swarm
14 %size of combined_pop = size_REP + N
15 new_pareto = combined_pop_obj(new_pareto_mask,:); %new pareto
     front
16 new_distance = eval_crowding(new_pareto); %crowding distance of
     new front
17 new_loc = combined_pop_loc(new_pareto_mask,:); %new locations
18 %if there are more elements than REP size, choose the less
     crowded
19 %solutions
20 if length(new_pareto) > REP_size
```

```
21      [~,index] = sort(new_distance,'descend');
22      new_elements = index(1:REP_size);
23      new_REP_obj = new_pareto(new_elements,:);
24      new_REP_distance = new_distance(new_elements);
25      new_REP_loc = new_loc(new_elements,:);
26      %if REP size is bigger fit all into REP
27  else
28      new_REP_obj(1:size(new_pareto,1),:)=new_pareto;
29      new_REP_distance(1:size(new_pareto,1))=new_distance;
30      new_REP_loc(1:size(new_pareto,1),:) = new_loc;
31  end
```

B.3 Crowding distance evaluation function

```
1  function [demi_perimeter] = eval_crowding(fitness)
2  %ES 25/03/2013
3
4  %calculates dimensions of largest hybercube which can be fitted
     around a
5  %solution without touching adjacent ones, giving indication of
     crowding in
6  %vicinity of particle
7
8  [num_elements,~] = size(fitness);
9
10 max_fitness = max(fitness,[],1); %determine maximum fitness for
     scaling purposes
11 fitness_scaled = bsxfun(@ldivide,max_fitness,fitness); %normalise
     fitnesses - this creates hybercubes as otherwise
     hyperparallelipids are formed
12 [fitness_sorted, index] = sortrows(fitness_scaled); %sort in
     ascending order according to first objective function.
13 demi_perimeter_sorted = zeros(num_elements,1); %create empty
     vector for demiperimeters
14 %end points have infinite demi-perimeter - emphasizes search
     towards ends
15 demi_perimeter_sorted(1)=inf;
16 demi_perimeter_sorted(num_elements)=inf;
17 for ctr = 2:(num_elements-1)
```

```
    %if particles are identical assign zero distance to de-
      emphasize
    if (all(fitness_sorted(ctr+1,:) == fitness_sorted(ctr,:)) &&
      all(( fitness_sorted(ctr-1,:) == fitness_sorted(ctr,:))))
        demi_perimeter_sorted(ctr) = 0;
    else
        %demi-perimeter calculated as difference of adjacent
          fitness values
        demi_perimeter_sorted(ctr) = sum(abs(fitness_sorted(ctr
          +1,:)-fitness_sorted(ctr-1,:)));
    end
end
demi_perimeter(index) = demi_perimeter_sorted;
```

B.4 Pareto identification function

```
function [non_dom_mask] = identify_pareto(fitness)
%ES 25/03/2013
%Identifies Pareto-optimal set of solutions based on their
  fitness values.
%Considers a biobjective minimisation problem

pop_size =size(fitness,1); %number of particles in population
  being considered

%Initialise storage arrays
n = zeros(pop_size,1); %number of other solutions which dominate
  each solution
non_dom_mask = zeros(pop_size,1); %logical mask for non-dominated
   set

% function assumes minimisation problem
for a = 1:pop_size
    %only need whether element is dominated by other elements in
      swarm
    %condition 1: solution is no worse than other in all
      objectives
    mask_1 = fitness(:,1) <= fitness(a,1) & fitness(:,2) <=
      fitness(a,2);
```

```
    %condition 2: solution is strictly better than others in at
      least one
    %objective
    mask_2 = fitness(:,1) < fitness(a,1) | fitness(:,2) < fitness
      (a,2);
    n(a) = sum(mask_1 & mask_2); %determine number of dominating
      solutions
    if n(a) == 0 %if non-dominated...
        non_dom_mask(a) = 1; %assign to Pareto front
    end
end
non_dom_mask = logical(non_dom_mask);
```

B.5 Select from REP function

```
function [h] = select_from_REP(N,REP,distance)
%ES 25/03/2013
%selects particles from external repository to perform
  claculation of
%particles' new velocities

feasible_solns_indices = find(all(REP~=inf,2));
feasible_solns_distances = distance(feasible_solns_indices);

random_int = randi(length(feasible_solns_indices),N,2); %random
  integers for binary tournament selection
mask = feasible_solns_distances(random_int(:,1)) >=
  feasible_solns_distances(random_int(:,2)); %perform binary
  tournament selection based on distance metric
h(mask) = random_int(mask,1); %for mask=TRUE assign elements from
   first column of h
h(~mask) = random_int(~mask,2); %for mask=FALSE assign elements
  from second column of h
h = feasible_solns_indices(h);
```

Appendix C

EMS optimisation code

The EMS optimisation code is a single objective optimisation algorithm which is based on the PSO algorithm as described in the previous section. The main control script controls the execution of the EMS, which is contained in the optimisation script. In turn an additional internal function is used to interface with GES (objective function).

C.1 Main control script

```
% Voyage optimisation loop for low emissions model

% Script reads waypoint information from excel and triggers
  optimisation algorithm at
% each waypointpoint.

%Clear workspace and initialise
clear
clc
ctr = 1;
iterations = 200; %number of iterations to be performed for each
  optmisation

%Read profile from xls data
data = xlsread('profile_load.xlsx','Lowemissprofile','E5:K60');

%Separate data to individual profiles
speed_profile = data(:,1); %ship speed (kt)
```

```
aux_profile = data(:,2)*1e3; %auxiliary power demand (kW)
CI_avail = data(:,3); %Cold ironing availability (0/1)
delta_t = data(:,5); %time intervals (s)
DayTime = data(:,6); %Day/time for solar irradiance
ShipDirection = data(:,7); %Read info about ship heading

[numel,~] = size(speed_profile); %Number of points in time

%Empty arrays for storing results
configuration_results = zeros(numel,11);
FC = zeros(numel,1);
info = zeros(numel,22);

%Battery SoC data
Q_init = zeros(numel,2); %initial SoC for each point 2x batteries
Q_init(1,:) = [0.95 0.95]; %start fully charged
Q_nom = 3000*3600; %nominal capacity in As
eSFC = zeros(numel+1,2);
eSFC(1,:) = [200 200]./(3600*1000); %initial equivalent sfc

h = actxserver('GES.Application');
parent = 0;

%% Loop through waypoints
for ctr = 1:numel
    disp(ctr)
    %For first point, initialise batteries' SOC
    if ctr == 1
        SOC_PS = Q_init(1,1);
        SOC_SB = Q_init(1,2);
        config_old = zeros(1,11); %Uncomment to disable history
    else
        %Linear model for Battery SoC
        Q_init(ctr,1) = (Q_init(ctr-1,1)*Q_nom-
          configuration_results(ctr-1,10)*delta_t(ctr-1))/Q_nom;
        Q_init(ctr,2) = (Q_init(ctr-1,2)*Q_nom-
          configuration_results(ctr-1,11)*delta_t(ctr-1))/Q_nom;
        SOC_PS = Q_init(ctr,1);
        SOC_SB = Q_init(ctr,2);
        config_old = configuration_results(ctr-1,:);
```

```
55          config_old(9) = config_old(9)-1;
56
57      end
58      SOC = [SOC_PS, SOC_SB]*100;
59      [configuration_results(ctr,:),FC(ctr),info(ctr,:),eSFC(ctr
          +1,:)]=energy_opti_fn_emiss(h,parray,speed_profile(ctr),
          aux_profile(ctr),CI_avail(ctr),iterations,SOC,eSFC(ctr,:),
          delta_t(ctr),config_old,DayTime(ctr));
60  end
61
62  P_oppoints = info(:,1:16);
63  FC_components = info(:,17:22);
```

C.2 Optimisation script

```
1   function [solution, FC_optimal,P_components,eSFC_next] =
      energy_opti_fn_emiss(h,parray,vs,Aux_power,CI_ENABLE,iterations,
      SOC,eSFC_batt,duration,config_old,DayTime)
2   % Single objective PSO with lbest
3   % to identify optimal configuration wrt FC
4   % Variables are:
5   % Main Engine(s) On/Off
6   % combinator mode selection
7   % PTO/PTI setpoint
8   % Battery current setpoint
9
10  % ES 11/11/2014
11
12  % Inputs:
13  % 1) vs = ship speed in knots
14  % 2) Aux_power = auxiliary power demand in Watts
15  % 3) CI_Enable = option whether cold ironing is available [0/1]
16  % 4) Iterations = number of iterations PSO algorithm is to
      perform
17  % 5) SOC = current state of charge (%) of the batteries
18  % 6) duration = length of time (s) the current setpoint is to be
      maintained
19
20  % Outputs:
```

```
21 % 1) solution = optimal configuration (variables explained in
     section PSO
22 % initialisation)
23 % 2) FC_optimal = fuel consumption (in one GES timestep) of
     optimal
24 % configuration
25 % 3) P_PTOPTI = power setpoints (W) of the PTOPTI drives
26
27 % Determine propeller operating mode
28 %  0 - AHEAD/ASTERN automatic constant speed
29 %  1 - AHEAD variable RPM
30 %  2 - AHEAD constant RPM
31 %  3 - ASTERN variable RPM
32 %  4 - ASTERN constant RPM
33
34 % ************************************
35 % Run rng('shuffle') once at start
36 % ************************************
37
38 % close all
39 % clear
40 % clc
41
42 % Timer to give indication of time for solution
43 % Only for development purposes
44 timerVal = tic;
45
46 %% Set parameters and build link to GES
47 % % These can be set as function parameters. Enable here to run
     as script
48 % % and comment function line.
49 % vs = 15; %Ship speed in knots
50 % Aux_power = 350e3; %Aux power in kW
51 % CI_ENABLE = 0; %Availability of shore power [0/1]
52 % iterations = 100; %number of iterations to perform
53 % SOC = [100 100]; %State of charge of batteries (%)
54 % duration = 1800; %duration of setpoint (s)
55
56 BATT_RAT_CURR = 1000; %Battery rated current (for normalising
     results)
```

```
57
58 %% PSO Initialisation
59
60 %PSO parameters
61 C1 = 2.05; %Acceleration constant for memory
62 C2 = 2.05; %Acceleration constant for cooperation
63 C = C1 + C2; %Sum of constants
64 Chi = 2/abs(2-C-sqrt(C^2-4*C)); %Constriction factor as per
     delvalle08
65 PENALTY = 1.2; %penalty for most different solution (Hamming
     distance)
66
67 N = 20; %Population size
68 d = 11; %Number of variables
69 %Variables are:
70 % 1 = ME1
71 % 2 = ME2
72 % 3 = ME3
73 % 4 = ME4
74 % 5 = DG1
75 % 6 = DG2
76 % 7 = PTOPTI1 V/f setpoint (cts)
77 % 8 = PTOPTI2 V/f setpoint (cts)
78 % 9 = Combinator mode
79 % 10 = PS battery current setpoint (cts)
80 % 11 = SB battery current setpoint (cts)
81 BINARY_PARTICLES = [1 2 3 4 5 6 9];
82 ONOFF_PARTICLES = [1 2 3 4 5 6];
83 CTS_PARTICLES = [7 8 10 11];
84
85 %Limits on velocity and location (normalised)
86 x_max = 1;
87 x_min = 0;
88 v_max = (x_max-x_min)/2; %Limit vel to... (for continuous
     variables)
89
90 K = 3; %size of information neighbourhood (when using lbest)
91
92 %Empty arrays to store results/historical progressions (use for
93 %development)
```

```
94
95  % results = zeros(N,d); %final population
96  gbest_hist = zeros(iterations,1); %history of global best
97  gbest_loc_hist = zeros(iterations,d); %history of global best
      locations
98  pbest_avg_hist = zeros(iterations,1); %history of average
      particle best
99  avg_fitness_hist = zeros(iterations,1); %history of average
      fitness per iteration
100 POP_loc_hist = zeros(N,d,iterations); %history of all particle
      locations
101 POP_vel_hist = zeros(N,d,iterations); %history of all particle
      locations
102 fitness_hist = zeros(N,iterations); %history of all particle
      fitnesses
103
104 %% Initialise population with random velocities and locations (
      normalised)
105 %Column 1 = x1, column 2 = x2, ... column d = xd
106 %Row 1 = particle 1, row 2 = particle 2, ... row N = xN
107 POP_loc = x_min + (x_max-x_min).*rand(N,d); %Random array for
      population particle locations
108 POP_vel = -v_max + (v_max-(-v_max)).*rand(N,d); %Random array for
       population particle velocities
109
110 %If previous configuration is valid then initialise particle at
      random to
111 %be equal to the previous configuration.
112 if (sum(config_old) ~= 0)
113     POP_loc(randi(N,1),:) = config_old;
114 end
115
116 % Initialise individual particles' memory spaces
117 pbest = inf.*zeros(N,1); %Empty array for particle best fitness
      value
118 pbest_loc = zeros(N,d); %Empty array for corresponding best
      fitness value location
119
120 % Global best results
121 gbest = inf; %Global best fitness value (0 for minimisation)
```

```
122 gbest_loc = zeros(1,d); %Global best fitness value location
123 lbest_loc = zeros(N,d); %location of local best particle
124
125 %Preparing of parameters
126 POP_loc(:,BINARY_PARTICLES) = round(POP_loc(:,BINARY_PARTICLES));
      %round particles to binary [0/1]
127
128 %Create fixed neighbourhood
129 lbest_fixed = (1:N)';
130 lbest_fixed = repmat(lbest_fixed,1,3);
131 lbest_fixed(:,1) = lbest_fixed(:,1)-1;
132 lbest_fixed(:,3) = lbest_fixed(:,3)+1;
133 % %for not-include self...
134 lbest_fixed(1:2:N,2) = lbest_fixed(1:2:N,2)+(K-1);
135 lbest_fixed(2:2:N,2) = lbest_fixed(2:2:N,2)-(K-1);
136 % correct circular ring
137 mask_fixed_GT = ((lbest_fixed) > N);
138 lbest_fixed(mask_fixed_GT) = lbest_fixed(mask_fixed_GT)- N;
139 mask_fixed_LT = ((lbest_fixed) < 1);
140 lbest_fixed(mask_fixed_LT) = lbest_fixed(mask_fixed_LT) + N;
141
142 % Start GES
143 invoke(h,'GesStartRun');
144 ctr_cumul = 0; %cumulative counter to be used with GesRun
145
146 %% Main algorithm loop
147 %Runs for predetermined number of iterations
148 for iteration_counter = 1:iterations
149     %Evaluate fitness of each particle based on location
150     fitness = inf*ones(N,1); %Initialise empty array for fitness
        values to inf
151     fitness_clean = inf*ones(N,1);
152     P_components_temp = zeros(N,22);
153     eSFC_temp = zeros(N,2);
154
155     % Iterate for each particle
156     for particle_iteration_ctr = 1:N %For each particle
157         % Call function runGes to evaluate fitness
158         [fitness(particle_iteration_ctr),P_components_temp(
              particle_iteration_ctr,:),Constraints,eSFC_temp(
```

```
        particle_iteration_ctr,:)] = runGesEmiss(POP_loc(
        particle_iteration_ctr,:),vs,Aux_power,h,CI_ENABLE,
        ctr_cumul,SOC,eSFC_batt,duration,DayTime,parray);
159     if sum(config_old) == 0 %If initial configuration or if
        history is to be disabled...
160         weight_hist = 1;
161     else %otherwise consider the previous configuration
162         weight_hist = (1-PENALTY)*(sum(POP_loc(
            particle_iteration_ctr,ONOFF_PARTICLES) ==
            config_old(ONOFF_PARTICLES)))/length(ONOFF_PARTICLES
            )+1; %calculate linear penalty wieght for different
            configuration
163     end
164     %penalise solution if cold ironing is available and
165     %batteries are being discharged
166     if (CI_ENABLE == 1) && (P_components_temp(
        particle_iteration_ctr,15)>0 || P_components_temp(
        particle_iteration_ctr,16)>0)
167         weight_batt = 1;
168     else
169         weight_batt = 0;
170     end
171
172     weight_constraints = sum(Constraints);
173     fitness_clean(particle_iteration_ctr) = fitness(
        particle_iteration_ctr);
174     fitness(particle_iteration_ctr) = weight_hist*fitness(
        particle_iteration_ctr)+ weight_constraints +
        weight_batt;
175     ctr_cumul = ctr_cumul+1; %increment cumulative counter
        for GesRun index
176 end
177
178 fitness_hist(:,iteration_counter) = fitness;
179
180 %Identify global best (for minimisation)
181 [gbest_curr,gbest_curr_ind] = min(fitness);
182
183 %For first iterate initialise records of best locations
184 if (iteration_counter == 1)
```

```
185         pbest = fitness;
186         pbest_loc = POP_loc;
187         gbest = gbest_curr;
188         gbest_loc = POP_loc(gbest_curr_ind,:);
189         P_components = P_components_temp(gbest_curr_ind,:);
190         fitness_actual = fitness_clean(gbest_curr_ind);
191         eSFC_next = eSFC_temp(gbest_curr_ind,:);
192     else
193         %Update pbest if new fitnesses are better
194         mask = fitness < pbest; %(< for minimisation)
195         pbest(mask) = fitness(mask);
196         pbest_loc(mask,:) = POP_loc(mask,:);
197         %update gbest if better
198         if gbest_curr < gbest
199             gbest = gbest_curr;
200             gbest_loc = POP_loc(gbest_curr_ind,:);
201             P_components = P_components_temp(gbest_curr_ind,:);
202             fitness_actual = fitness_clean(gbest_curr_ind);
203             eSFC_next = eSFC_temp(gbest_curr_ind,:);
204         end
205     end
206
207     %obtain lbest
208     %Selection of informants...
209
210     %     %Random neighbourhood
211     %     for particle_counter = 1:N
212     %         informed = randperm(N,K); %random selection of K
      particles (including self)
213     %         [lbest_val,lbest_ind] = min(fitness(informed)); %
      find fittest
214     %         if lbest_val == inf %if all solutions are
      infeasible randomly select particle
215     %             lbest_ind = randi(K,1);
216     %         end
217     %         lbest = informed(lbest_ind);
218     %         lbest_loc(particle_counter,:) = POP_loc(lbest,:);
219     %     end
220
221     %     Ring neighbourhood
```

```
222     for particle_counter = 1:N
223         informed = lbest_fixed(particle_counter,:);
224         %          [lbest_val,lbest_ind] = min(fitness(informed));
              %find fittest
225         [lbest_val, lbest_ind] = min(pbest(informed)); %find
              fittest from pbest
226         if lbest_val == inf %if all solutions are infeasible
              randomly select particle
227             lbest_ind = randi(K,1);
228         end
229         lbest = informed(lbest_ind);
230         %          lbest_loc(particle_counter,:) = POP_loc(lbest
              ,:);
231         lbest_loc(particle_counter,:) = pbest_loc(lbest,:); %look
              only in pbests
232     end
233
234
235     %calculate new particle velocities
236     %Un/Comment method to be used...
237
238     %...with inertia factor
239     %for gbest...
240     %      POP_vel = W.*POP_vel + C1.*rand(N,d).*(pbest_loc-
          POP_loc) + C2.*rand(N,d).*(bsxfun(@minus,gbest_loc,POP_loc))
          ;
241     %for lbest...
242     %          POP_vel = W.*POP_vel + C1.*rand(N,d).*(pbest_loc-
          POP_loc) + C2.*rand(N,d).*(lbest_loc-POP_loc);
243
244     %...with constriction factor
245     %for gbest...
246     %      POP_vel = Chi.*(POP_vel + C1.*rand(N,d).*(pbest_loc-
          POP_loc) + C2.*rand(N,d).*(bsxfun(@minus,gbest_loc,POP_loc))
          );
247     %for lbest...
248     POP_vel = Chi.*(POP_vel + C1.*rand(N,d).*(pbest_loc-POP_loc)
          + C2.*rand(N,d).*(lbest_loc-POP_loc));
249
250     %      %...FIPS with constriction factor
```

```
251     %     Pfi = (C/K).*rand(N,K);
252     %     for particle_counter = 1:N
253     % %         Pm(particle_counter,:) = sum(Pfi(particle_counter
          ,:)'.*pbest_loc(lbest_fixed(particle_counter,:)',:),1)./sum(
          Pfi(particle_counter,:));
254     % %           [~,IX] = sort(pbest(lbest_fixed(
          particle_counter,:)),'ascend');
255     % %           WK(IX) = [1, 0.75 0.5];
256     %           WK = 1;
257     %           WKPfi  = Pfi(particle_counter,:)'.*WK';
258     % %           Pm(particle_counter,:) = sum(bsxfun(@times,Pfi(
          particle_counter,:)',pbest_loc(lbest_fixed(particle_counter
          ,:)',:)),1)./sum(Pfi(particle_counter,:));
259     %           Pm(particle_counter,:) = sum(bsxfun(@times,WKPfi,
          pbest_loc(lbest_fixed(particle_counter,:)',:)),1)./sum(WKPfi
          );
260     %     end
261     %     pbest_loc(lbest_fixed,:);
262     %     Pm = sum(Pfi.*fitness(lbest_fixed),2)./sum(Pfi,2);
263     %     Pm = (C1.*pbest_loc + C2.*lbest_loc)./C;
264     %     POP_vel = Chi.*(POP_vel + C.*(Pm-POP_loc));
265
266     POP_vel_hist(:,:,iteration_counter) = POP_vel; %Store
          velocities history
267
268     %store current population location
269     %(necessary for end condition evaluation)
270     POP_loc_CURR = POP_loc;
271
272     %% Binary probabilistic correction
273
274     S = 1./(1+exp(-POP_vel(:,BINARY_PARTICLES)));
275
276     %% calculate new particle positions
277     %     POP_loc = POP_loc + POP_vel;
278     POP_loc(:,CTS_PARTICLES) = POP_loc(:,CTS_PARTICLES) + POP_vel
          (:,CTS_PARTICLES);
279     POP_loc(:,BINARY_PARTICLES) = round(S);
280
281     %calculate new particle positions
```

```
282     POP_loc = POP_loc + POP_vel;
283
284     %correct position to limits
285     POP_loc(POP_loc > x_max) = x_max;
286     POP_loc(POP_loc < x_min) = x_min;
287
288     POP_vel(POP_vel>v_max)=v_max;
289     POP_vel(-POP_vel>v_max)=-v_max;
290
291     gbest_hist(iteration_counter)=gbest;
292     gbest_loc_hist(iteration_counter,:) = gbest_loc;
293     mask_avg = (pbest~=inf & pbest~=0);
294     pbest_avg_hist(iteration_counter) = sum(pbest(mask_avg))/sum(
          mask_avg);
295
296     avg_fitness_hist(iteration_counter) = sum(fitness(fitness~=
          inf))/sum(fitness~=inf);
297
298     POP_loc_hist(:,:,iteration_counter) = POP_loc_CURR;
299
300     %check for termination
301     %       if gbest<=tolerance
302     %           break
303     %       end
304     %       disp(iteration_counter) %show iteration number (
          development purposes)
305 end
306
307 %Stop GES
308 invoke(h,'GesStopRun')
309
310 %% Plot history
311 % newplot
312
313 plot(gbest_hist)
314 hold on
315 plot(pbest_avg_hist,'r')
316 % plot(avg_fitness_hist,'g')
317 legend('Global best','Particle best average');%,'Average fitness
      history')
```

```
318 xlabel('Iterations')
319 ylabel('Fuel consumption')
320
321 %% Load optimal config...
322 % Pass as function output the optimal configuration (global best)
323 solution = gbest_loc;
324 % FC_optimal = gbest;
325 FC_optimal = fitness_actual;
326 solution(9) = solution(9)+1; %un-normalise combinator mode
327 solution([7 8]) = solution([7 8]).*2-1; %un-normalise PTO/PTI
      setpoints
328 solution([10 11]) = (solution ([10 11]).*2-1).*BATT_RAT_CURR; %
      unnormalise battery discharge currents
329
330 toc(timerVal)
```

C.3 GES interfacing

```
1  function [fitness,P_components,Constraints,eSFC_batt_next] =
     runGesEmiss(params,vs,Aux_power,h,CI,index,SOC,eSFC_batt,
     duration,DayTime,parray)
2  %Calls open GES model and uses GESRUN method
3  %requires external GESstartRun and GesStopRun calls
4
5  % ES 11/11/2014
6
7  % Inputs:
8  % 1) params = configuration to be evaluated
9  % 2) vs = ship speed in knots
10 % 3) Aux_power = auxiliary power demand in Watts
11 % 4) h = handle to active GES model
12 % 5) CI = Availability of cold ironing on/off
13 % 6) index = cumulative index for use with runGES
14 % 7) SOC = State of charge of batteries (%)
15 % 8) duration = duration of current setpoint (s)
16
17 % Outputs:
18 % 1) fitness = fuel consumption over one GES timestep as sum of
     MGO and HFO
```

```
% 2) P_PTOPTI = PTOPTI drives mechanical pwoer flow (W)

% global sfc_batt_PS sfc_batt_SB

%Parameters
PTO_rating = 1200e3; %rating of PTO/PTI to un-normalise variables
BATT_CURR = 1000; %maximum battery current
SOC_MIN = 0.2;
SOC_MAX = 0.95;
BATT_RAT = 3000*3600; %Battery nominal capacity (As)
eSFC_batt_next = eSFC_batt;
% CI = 0; %on/off of cold ironing...for future use to be in
  function call

%Initialise GES model

set(h,'GesSet','vs',0.5144*vs); %Ship speed in m/s
set(h,'GesSet','FuelMain',2); %Set Main Fuel switch to HFO (3)
set(h,'GesSet','FuelAux',1); %Set Aux Fuel switch to MGO
set(h,'GesSet','AUX_POWER',Aux_power); %Set constant auxiliary
  power demand
set(h,'GesSet','CI_ENABLE',CI); %Set availability of cold ironing
   on/off
set(h,'GesSet','SOC_INIT_PS',SOC(1)); %Set initial state of
  charge or PS battery
set(h,'GesSet','SOC_INIT_SB',SOC(2)); %Set initial state of
  charge of SB battery
set(h,'GesSet','DayTime',DayTime); %Set time of day for solar
  irradiance LUT

%Load configuration to GES

set(h,'GesSet','ME1',params(1));
set(h,'GesSet','ME2',params(2));
set(h,'GesSet','ME3',params(3));
set(h,'GesSet','ME4',params(4));
set(h,'GesSet','DG1',params(5));
set(h,'GesSet','DG2',params(6));
set(h,'GesSet','PTO_VF_SET_PS',params(7)*2-1);
set(h,'GesSet','PTO_VF_SET_SB',params(8)*2-1);
```

```
53 set(h,'GesSet','Combinator',params(9)+1);
54 set(h,'GesSet','BATT_CURR_PS',(params(10)*2-1)*BATT_CURR);
55 set(h,'GesSet','BATT_CURR_SB',(params(11)*2-1)*BATT_CURR);
56
57 % Turn on/off PTO/PTI clutch and breaker in GES if PTO/PTI is off
58 if (params(7)*2-1) == 0
59     set(h,'GesSet','PTO_PS_SWITCH',0);
60 else
61     set(h,'GesSet','PTO_PS_SWITCH',1);
62 end
63
64 if (params(8)*2-1) == 0
65     set(h,'GesSet','PTO_SB_SWITCH',0);
66 else
67     set(h,'GesSet','PTO_SB_SWITCH',1);
68 end
69
70 %Clear flags
71 set(h,'GesSet','FLAG_engine',0);
72 set(h,'GesSet','FLAG_shaft',0);
73 set(h,'GesSet','FLAG_BATT',0);
74 set(h,'GesSet','FLAG_generator',0);
75 set(h,'GesSet','FLAG_SB',0);
76 set(h,'GesSet','FLAG_PTOPTI',0);
77
78 set(h,'GesSet','cumul_FC',0);
79 set(h,'GesSet','cumul_FC_MGO',0);
80 set(h,'GesSet','P_PTO_PTI_SB',0);
81 set(h,'GesSet','P_PTO_PTI_PS',0);
82 % set(h,'GesSet','warning_out',0);
83 % set(h,'GesSet','error_out',0);
84 set(h,'GesSet','AUX_SUPPLY',0);
85 set(h,'GesSet','speed_readout',0);
86
87 %Run GES!
88 set(h,'GesRun',index);
89 invoke(h,'GesWaitRun');
90
91 %Read flags from GES model
92 FLAG_engine = get(h,'GesGet','FLAG_engine'); %get engine flag
```

```
93  FLAG_shaft = get(h,'GesGet','FLAG_shaft'); %get shaft flag
94  FLAG_generator = get(h,'GesGet','FLAG_generator'); %get generator
      flag
95  FLAG_batt = get(h,'GesGet','FLAG_BATT'); %get battery flag
96  FLAG_SB = get(h,'GesGet','FLAG_SB'); %get switchboard flag
97  FLAG_PTOPTI = get(h,'GesGet','FLAG_PTOPTI'); %get PTOPTI flag
98  FLAG_hist = FLAG_engine + FLAG_shaft + FLAG_generator + FLAG_batt
      + FLAG_SB + FLAG_PTOPTI;
99
100 SPEED_READOUT = get(h,'GesGet','speed_readout'); %get speed
      readout
101 FC_HFO = get(h,'GesGet','cumul_FC'); %read HFO consumption
102 FC_MGO = get(h,'GesGet','cumul_FC_MGO'); %read MGO consumption
103 FC = FC_HFO + FC_MGO;
104 AUX_SUPPLY = get(h,'GesGet','AUX_SUPPLY');
105 warning_out = get(h,'GesGet','warning_out');
106 error_out = get(h,'GesGet','error_out');
107
108 %Read setpoints and component fuel consumption
109 P_PTO_PTI_SB = get(h,'GesGet','P_PTO_PTI_SB');
110 P_PTO_PTI_PS = get(h,'GesGet','P_PTO_PTI_PS');
111 P_DG1 = get(h,'GesGet','P_DG1');
112 P_DG2 = get(h,'GesGet','P_DG2');
113 P_ME1 = get(h,'GesGet','P_ME1');
114 P_ME2 = get(h,'GesGet','P_ME2');
115 P_ME3 = get(h,'GesGet','P_ME3');
116 P_ME4 = get(h,'GesGet','P_ME4');
117 P_SSB = get(h,'GesGet','P_SSB');
118 P_SPS = get(h,'GesGet','P_SPS');
119 P_CI = get(h,'GesGet','P_CI');
120 P_WHRSPS = get(h,'GesGet','P_WHRSPS');
121 P_WHRSSB = get(h,'GesGet','P_WHRSSB');
122 P_SOLAR = get(h,'GesGet','P_SOLAR');
123 P_BATTPS = get(h,'GesGet','P_BATTPS');
124 P_BATTSB = get(h,'GesGet','P_BATTSB');
125 OBJ = get(h,'GesGet','OBJ');
126 Pout_tot = get(h,'GesGet','Pout_tot');
127
128 P_COLLATE = [P_ME1, P_ME2, P_ME3, P_ME4, P_DG1,P_DG2,P_PTO_PTI_PS
      , P_PTO_PTI_SB,P_SPS,P_SSB,P_CI,P_WHRSPS,P_WHRSSB,P_SOLAR,
```

```
  P_BATTPS,P_BATTSB];

FC_ME1 = get(h,'GesGet','FC_ME1');
FC_ME2 = get(h,'GesGet','FC_ME2');
FC_ME3 = get(h,'GesGet','FC_ME3');
FC_ME4 = get(h,'GesGet','FC_ME4');
FC_DG1 = get(h,'GesGet','FC_DG1');
FC_DG2 = get(h,'GesGet','FC_DG2');

FC_COLLATE = [FC_ME1,FC_ME2,FC_ME3,FC_ME4,FC_DG1,FC_DG2];

%% Constraints

%Read overload values...
P_ol_ME1 = get(h,'GesGet','P_ol_ME1');
P_ol_ME2 = get(h,'GesGet','P_ol_ME2');
P_ol_ME3 = get(h,'GesGet','P_ol_ME3');
P_ol_ME4 = get(h,'GesGet','P_ol_ME4');
P_ol_DG1 = get(h,'GesGet','P_ol_DG1');
P_ol_DG2 = get(h,'GesGet','P_ol_DG2');
P_ol_PTO_PTI_PS = get(h,'GesGet','P_ol_PTO_PTI_PS');
P_ol_PTO_PTI_SB = get(h,'GesGet','P_ol_PTO_PTI_SB');

P_ol = [P_ol_ME1, P_ol_ME2, P_ol_ME3, P_ol_ME4, P_ol_DG1,
  P_ol_DG2, P_ol_PTO_PTI_PS, P_ol_PTO_PTI_SB];

% ...guess SoC at end of duration...
SOC_1_end = (SOC(1)*BATT_RAT/100-(params(10)*2-1)*BATT_CURR*
  duration)/BATT_RAT;
SOC_2_end = (SOC(2)*BATT_RAT/100-(params(11)*2-1)*BATT_CURR*
  duration)/BATT_RAT;
if SOC_1_end >= SOC_MAX
    SOC_ol_Batt1 = SOC_1_end-SOC_MAX;
elseif SOC_1_end < SOC_MIN
    SOC_ol_Batt1 = abs(SOC_1_end-SOC_MIN);
else
    SOC_ol_Batt1 = 0;
end
if SOC_2_end >= SOC_MAX
    SOC_ol_Batt2 = SOC_2_end-SOC_MAX;
```

```
165 elseif SOC_2_end < SOC_MIN
166     SOC_ol_Batt2 = abs(SOC_2_end-SOC_MIN);
167 else
168     SOC_ol_Batt2 = 0;
169 end
170
171 SOC_ol = [SOC_ol_Batt1, SOC_ol_Batt2];
172
173 %% Detect flags and penalise solutions
174 if (FLAG_hist>0 ) %If any of the machinery flags is set
175     fitness_temp = inf;
176 elseif AUX_SUPPLY == 0 %If no power is delivered to aux system
177     fitness_temp = inf;
178 elseif abs(SPEED_READOUT-0.5144*vs) > 0.01 %if speed setpoint is
      not met
179     fitness_temp = inf;
180 elseif P_CI < 0
181     fitness_temp = inf;
182 elseif (warning_out >0 || error_out>0)
183     fitness_temp = inf;
184 else
185
186     %% Assign equivalent fuel consumption batteries
187     % %     Change of SOC
188     delta_SOC_PS = SOC(1)/100 - SOC_1_end;
189     delta_SOC_SB = SOC(2)/100 - SOC_2_end;
190
191     numon = sum(P_COLLATE(1:6)>0);
192     if numon == 0
193         avg_sfc = 0;
194     else
195         avg_sfc = sum(FC_COLLATE)./sum(P_COLLATE(1:6)); %g/Ws
196     end
197     %
198     if P_BATTPS < 0 %if charging
199         eSFC_batt_next(1) = ((SOC(1)/100)*eSFC_batt(1) + abs(
              delta_SOC_PS)*avg_sfc)/(SOC(1)/100+abs(delta_SOC_PS));
200         FC_BATTPS = 0;
201     elseif P_BATTPS >= 0 %if discharging
202         FC_BATTPS = P_BATTPS*eSFC_batt(1);
```

```
203         eSFC_batt_next(1) = eSFC_batt(1);
204     else
205         FC_BATTPS = 0;
206         eSFC_batt_next(1) = eSFC_batt(1);
207     end
208
209     if P_BATTSB < 0 %if charging
210         eSFC_batt_next(2) = ((SOC(2)/100)*eSFC_batt(2) + abs(
              delta_SOC_SB)*avg_sfc)/(SOC(2)/100+abs(delta_SOC_SB));
211         FC_BATTSB = 0;
212     elseif P_BATTSB >= 0  %if discharging
213         FC_BATTSB = P_BATTSB*eSFC_batt(2);
214         eSFC_batt_next(2) = eSFC_batt(2);
215     else
216         FC_BATTSB = 0;
217         eSFC_batt_next(2) = eSFC_batt(2);
218     end
219
220     fitness_temp = FC + FC_BATTPS/1000 + FC_BATTSB/1000; %
          otherwise save fuel consumption figure!
221     fitness_temp = fitness_temp/(Pout_tot/(1000*3600)); %
          calculate esfc (total) kg/kWh
222 end
223
224 fitness = fitness_temp; %return fuel consumption figure
225 P_components = [P_COLLATE,FC_COLLATE]; %return PTOPTI power
      levels
226 Constraints = [P_ol SOC_ol]; %return constraints
```

Appendix D

Voyage setpoint results

These two tables list the search space results which are described in section 7.7.

Setpoint					Configuration results										
Time (s)	Duration (s)	Speed (kt)	CI [0/1]	Aux. load (kW)	ME1	ME2	ME3	ME4	DG1	DG2	PTOPTI1	PTOPTI2	Prop mode	BATT_PS	BATT_SB
0	1800	15.23	0	850	0	1	0	1	1	1	-0.43	-0.44	1	236.62	612.63
1800	209	15.23	0	850	0	1	0	1	1	1	-0.49	0.58	1	229.75	1000.00
2009	1418	15.23	0	850	0	1	0	1	1	1	0.39	0.15	1	1000.00	1000.00
3427	1800	15.23	0	850	0	1	0	1	1	1	-0.48	0.57	1	201.43	1000.00
5227	1013	15.23	0	850	0	1	0	1	1	1	0.41	0.35	1	-27.52	1000.00
6240	1312	15.23	0	850	0	1	0	1	1	1	0.44	1.00	1	622.99	55.60
7552	1800	15.23	0	850	0	1	0	1	1	1	0.45	0.51	1	155.74	1000.00
9352	1800	15.23	0	850	0	1	0	1	1	1	0.45	0.44	1	1000.00	49.65
11152	1800	15.23	0	850	0	1	0	1	1	1	0.35	0.46	1	1000.00	316.59
12952	1800	15.23	0	850	1	1	0	1	1	1	-1.00	0.69	1	378.70	-66.47
14752	1800	15.23	0	850	1	1	0	1	1	1	-1.00	0.57	1	23.30	-76.95
16552	1472	15.23	0	850	1	1	1	0	1	1	-1.00	0.71	1	96.04	186.68
18024	1800	15.23	0	850	1	1	1	0	1	1	-0.75	0.53	2	125.57	-25.14
19824	1800	15.23	0	850	1	1	1	0	1	1	-1.00	0.59	1	-108.29	4.20
21624	702	15.23	0	850	1	1	1	0	1	1	-0.53	0.45	1	290.25	98.71
22326	1300	15.23	0	850	1	1	1	0	1	1	-0.25	-0.44	2	7.94	-153.87
23626	695	15.23	0	850	1	1	1	0	1	1	-0.80	0.32	1	21.31	128.92
24321	990	15.23	0	850	1	1	1	0	1	1	-1.00	0.56	1	-269.45	64.67
25311	991	15.23	0	850	1	1	1	0	1	1	-1.00	1.00	1	-0.03	10.29
26302	1800	0	1	650	0	0	0	0	0	0	-0.27	-0.10	1	-694.43	-196.51
28102	1800	0	1	650	0	0	0	0	0	0	-0.42	0.05	1	-1000.00	-1000.00
29902	1800	0	1	650	0	0	0	0	0	0	-1.00	-1.00	1	-1000.00	-1000.00
31702	1800	0	1	650	0	0	0	0	0	0	-0.05	-0.50	2	-384.33	-406.28
33502	1800	0	1	650	0	0	0	0	0	0	-1.00	0.50	1	-1000.00	-1000.00
35302	1800	0	1	650	0	0	0	0	0	0	1.00	0.81	2	-61.58	-855.27
37102	1800	0	1	650	0	0	0	0	0	0	-1.00	-1.00	1	-88.65	-3.19
38902	1800	0	1	650	0	0	0	0	0	0	-1.00	-1.00	2	-74.35	-20.30
40702	34	0	1	650	0	0	0	0	0	0	-1.00	0.71	2	-1000.00	-522.71
40736	1293	16.70	0	850	0	1	0	1	0	1	0.28	0.59	1	1000.00	1000.00
42029	1013	16.70	0	850	0	1	1	1	0	1	0.62	0.50	1	1000.00	1000.00
43042	1682	16.70	0	850	1	1	1	1	0	1	0.47	0.30	1	1000.00	1000.00
44724	1800	16.70	0	850	1	1	1	1	0	1	0.38	0.56	1	1000.00	1000.00
46524	1800	16.70	0	850	1	1	1	1	1	1	0.56	0.39	1	1000.00	1000.00
48324	1800	16.70	0	850	0	1	1	1	1	1	0.78	-1.00	1	213.27	304.75
50124	1800	16.70	0	850	0	1	1	1	1	1	1.00	-1.00	1	58.43	-37.72
51924	1800	16.70	0	850	0	1	1	1	1	1	1.00	-1.00	1	-71.85	14.72
53724	1800	16.70	0	850	1	1	1	1	1	1	0.33	-1.00	1	75.50	-78.48
55524	1800	16.70	0	850	1	1	1	1	1	1	-0.91	0.53	1	24.87	78.97
57324	1800	16.70	0	850	1	1	1	1	1	1	0.42	-0.98	1	-165.71	-130.17
59124	1800	16.70	0	850	1	1	1	1	1	1	1.00	-1.00	1	139.58	66.10
60924	54	16.70	0	850	1	1	1	1	1	1	0.62	0.44	1	1000.00	1000.00
60978	927	16.70	0	850	1	1	1	1	1	1	-1.00	0.34	1	-10.22	-43.94
61905	603	16.70	0	850	1	1	1	1	1	1	-0.99	0.54	1	-117.78	137.00
62508	518	16.70	0	850	1	1	1	1	1	1	-1.00	0.61	1	81.70	24.21
63026	1832	16.70	0	850	1	1	1	0	1	1	-1.00	1.00	1	-32.90	-2.28
64858	1800	0	1	650	0	0	0	0	0	0	0.91	0.17	1	-1000.00	-1000.00
66658	1800	0	1	650	0	0	0	0	0	0	1.00	-0.55	1	-1000.00	-1000.00
68458	1800	0	1	650	0	0	0	0	0	0	-1.00	1.00	2	-1000.00	-1000.00
70258	1800	0	1	650	0	0	0	0	0	0	-1.00	1.00	2	-1000.00	-1000.00
72058	1800	0	1	650	0	0	0	0	0	0	0.88	0.36	1	-181.60	-58.18
73858	1800	0	1	650	0	0	0	0	0	0	-0.89	-1.00	2	-283.26	-336.41
75658	1800	0	1	650	0	0	0	0	0	0	1.00	-1.00	2	-3.03	-112.35
77458	1800	0	1	650	0	0	0	0	0	0	-1.00	1.00	2	-38.11	-5.22
79258	1800	0	1	650	0	0	0	0	0	0	0.63	1.00	2	-6.30	-33.54
81058	1800	0	1	650	0	0	0	0	0	0	1.00	-0.70	1	-1.65	-993.36

Table D.1 – Table of resultant configurations (search space) for figure 7.12.

Time (s)	ME1	ME2	ME3	ME4	DG1	DG2	PTOPTI 1	PTOPTI 2	Shaft PS	Shaft SB	Cold ironing	Solar	Batt PS	Batt SB
0	0	3,452	0	3,474	0	36	-7	-28	3,312	3,312	0	153	153	397
1800	0	3,571	0	3,111	0	46	-123	325	3,312	3,312	0	158	149	648
2009	0	3,379	0	2,863	0	3	64	566	3,312	3,312	0	158	648	648
3427	0	3,552	0	3,152	0	34	-105	285	3,312	3,312	0	162	131	648
5227	0	3,413	0	3,278	0	188	30	162	3,312	3,312	0	163	-18	648
6240	0	3,415	0	2,240	1,276	213	29	1,174	3,312	3,312	0	163	404	36
7552	0	3,398	0	3,278	0	87	46	163	3,312	3,312	0	163	101	648
9352	0	3,392	0	3,414	0	22	52	30	3,312	3,312	0	162	648	32
11152	0	3,287	0	3,378	0	7	154	65	3,312	3,312	0	159	648	205
12952	2,325	2,325	0	2,894	0	48	-1,174	537	3,312	3,312	0	154	245	-43
14752	2,325	2,325	0	3,139	0	24	-1,174	298	3,312	3,312	0	148	15	-50
16552	2,325	2,325	2,840	0	0	131	-1,174	589	3,312	3,312	0	141	62	121
18024	2,101	2,101	3,512	0	0	96	-594	80	3,459	3,459	0	138	81	-16
19824	2,325	2,325	3,090	0	0	34	-1,174	346	3,312	3,312	0	129	-70	3
21624	1,827	1,827	3,385	0	76	200	-203	58	3,312	3,312	0	118	188	64
22326	2,108	2,108	3,752	0	0	23	-608	-154	3,459	3,459	0	110	5	-100
23626	2,112	2,112	3,222	0	0	120	-759	217	3,312	3,312	0	105	14	84
24321	2,325	2,325	3,169	0	0	37	-1,174	268	3,312	3,312	0	98	-175	42
25311	2,325	2,325	2,240	0	801	200	-1,174	1,174	3,312	3,312	0	92	0	7
26302	0	0	0	0	0	0	0	0	0	0	1,166	91	-450	-127
28102	0	0	0	0	0	0	0	0	0	0	1,912	78	-648	-648
29902	0	0	0	0	0	0	0	0	0	0	1,927	63	-648	-648
31702	0	0	0	0	0	0	0	0	0	0	1,144	46	-249	-263
33502	0	0	0	0	0	0	0	0	0	0	1,960	30	-648	-648
35302	0	0	0	0	0	0	0	0	0	0	1,256	18	-40	-554
37102	0	0	0	0	0	0	0	0	0	0	722	6	-57	-2
38902	0	0	0	0	0	0	0	0	0	0	729	1	-48	-13
40702	0	0	0	0	0	0	0	0	0	0	1,675	0	-648	-339
40736	0	3,985	0	4,009	0	149	340	317	4,176	4,176	0	0	648	648
42029	0	3,945	2,097	2,097	0	2	379	136	4,176	4,176	0	0	648	648
43042	2,130	2,130	2,012	2,012	0	3	73	302	4,176	4,176	0	0	648	648
44724	2,103	2,103	2,038	2,038	0	4	124	252	4,176	4,176	0	0	648	648
46524	2,032	2,032	2,109	2,109	0	5	263	114	4,176	4,176	0	0	648	648
48324	0	3,597	2,774	2,774	0	131	718	-1,182	4,176	4,176	0	0	138	197
50124	0	3,121	2,774	2,774	792	200	1,182	-1,182	4,176	4,176	0	0	38	-24
51924	0	3,121	2,774	2,774	845	200	1,182	-1,182	4,176	4,176	0	0	-47	10
53724	2,048	2,048	2,774	2,774	0	56	232	-1,182	4,176	4,176	0	0	49	-51
55524	2,675	2,675	2,066	2,066	0	125	-990	197	4,176	4,176	0	0	16	51
57324	2,147	2,147	2,749	2,749	0	81	39	-1,133	4,176	4,176	0	0	-107	-84
59124	1,561	1,561	2,774	2,774	767	200	1,182	-1,182	4,176	4,176	0	0	90	43
60924	1,973	1,973	2,164	2,164	0	13	379	6	4,176	4,176	0	0	648	648
60978	2,774	2,774	2,057	2,057	0	74	-1,182	216	4,176	4,176	0	0	-7	-28
61905	2,759	2,759	2,058	2,058	0	48	-1,152	214	4,176	4,176	0	0	-76	89
62508	2,774	2,774	1,985	1,985	0	124	-1,182	356	4,176	4,176	0	0	53	16
63026	2,774	2,774	3,121	0	829	200	-1,182	1,182	4,176	4,176	0	0	-21	-1
64858	0	0	0	0	0	0	0	0	0	0	1,989	1	-648	-648
66658	0	0	0	0	0	0	0	0	0	0	1,979	11	-648	-648
68458	0	0	0	0	0	0	0	0	0	0	1,966	24	-648	-648
70258	0	0	0	0	0	0	0	0	0	0	1,953	37	-648	-648
72058	0	0	0	0	0	0	0	0	0	0	775	52	-118	-38
73858	0	0	0	0	0	0	0	0	0	0	1,011	66	-184	-218
75658	0	0	0	0	0	0	0	0	0	0	664	80	-2	-73
77458	0	0	0	0	0	0	0	0	0	0	601	95	-25	-3
79258	0	0	0	0	0	0	0	0	0	0	582	112	-4	-22
81058	0	0	0	0	0	0	0	0	0	0	1,198	128	-1	-644

Table D.2 – Table of power flows for each setpoint (kW).

Appendix E

Drive controller code

This chapter lists the drive control algorithm developed to implement the auxiliary drive models including field weakening. The algorithm is implemented in C-code and embedded in the Simulink drive model as an S-function.

```
// File : controller.c
// Author: EAS
// Abstract: complete drive controller implementing
  field weakening for PM machine

#define S_FUNCTION_NAME  controller_complete_v4
#define S_FUNCTION_LEVEL 2

#include "simstruc.h"
#include <math.h>

#define PI 3.141592653589793
#define SAMPLE_TIME 100e-6
#define V_MAX 1/sqrt(2)
#define I_MAX 1000
#define K_inv 800



// int I_MAX = 800;
// int K_inv = 800; //inverter gain (DC link)
```

```
20
21 // double I_mag = 0; //current magnitude
22
23 int mode = 4;
24 int flag = 0;
25
26 //machine parameters
27 int P = 4;
28 double psi_rd = 2.15;
29 double L = 0.001;
30
31 //PI controller constants
32 double K_curr = 3.825e-3;
33 double Ki_curr = 7.65;
34
35 double K_speed = 1000;
36 double Ki_speed = 20000;
37
38 /*=================*
39  * Build checking *
40  *=================*/
41
42 /* Function: mdlInitializeSizes
    ================================================
43  * Abstract:
44  *   Setup sizes of the various vectors.
45  */
46 static void mdlInitializeSizes(SimStruct *S)
47 {
48     ssSetNumSFcnParams(S, 0);
49     if (ssGetNumSFcnParams(S) != ssGetSFcnParamsCount(S
       )) {
50         return; /* Parameter mismatch will be reported
```

```
        by Simulink */
51  }
52
53  ssSetNumDiscStates(S, 5);
54  //1 speed error accumulator
55  //2 id error accumulator
56  //3 iq error accumulator
57  //4 V_mag error accumulator
58  //5 theta_e
59
60  if (!ssSetNumInputPorts(S, 6)) return;
61  ssSetInputPortWidth(S, 0, DYNAMICALLY_SIZED); //w*
62  ssSetInputPortWidth(S, 1, DYNAMICALLY_SIZED); //w
63  ssSetInputPortWidth(S, 2, DYNAMICALLY_SIZED); //ia
64  ssSetInputPortWidth(S, 3, DYNAMICALLY_SIZED); //ib
65  ssSetInputPortWidth(S, 4, DYNAMICALLY_SIZED); //ic
66  ssSetInputPortWidth(S, 5, DYNAMICALLY_SIZED); //
      theta
67
68  ssSetInputPortDirectFeedThrough(S, 0, 1);
69  ssSetInputPortDirectFeedThrough(S, 1, 1);
70  ssSetInputPortDirectFeedThrough(S, 2, 1);
71  ssSetInputPortDirectFeedThrough(S, 3, 1);
72  ssSetInputPortDirectFeedThrough(S, 4, 1);
73  ssSetInputPortDirectFeedThrough(S, 5, 1);
74
75  if (!ssSetNumOutputPorts(S,8)) return;
76  ssSetOutputPortWidth(S, 0, DYNAMICALLY_SIZED); //vd
77  ssSetOutputPortWidth(S, 1, DYNAMICALLY_SIZED); //vq
78  ssSetOutputPortWidth(S, 2, DYNAMICALLY_SIZED); //va
79  ssSetOutputPortWidth(S, 3, DYNAMICALLY_SIZED); //vb
80  ssSetOutputPortWidth(S, 4, DYNAMICALLY_SIZED); //vc
81  ssSetOutputPortWidth(S, 5, DYNAMICALLY_SIZED); //
```

```
     theta_e
82     ssSetOutputPortWidth(S, 6, DYNAMICALLY_SIZED); //
     theta_e
83     ssSetOutputPortWidth(S, 7, DYNAMICALLY_SIZED);
84
85     ssSetNumSampleTimes(S, 1);
86
87     /* specify the sim state compliance to be same as a
       built-in block */
88     ssSetSimStateCompliance(S, USE_DEFAULT_SIM_STATE);
89
90     /* Take care when specifying exception free code -
      see sfuntmpl_doc.c */
91     ssSetOptions(S,
92             SS_OPTION_WORKS_WITH_CODE_REUSE |
93             SS_OPTION_EXCEPTION_FREE_CODE |
94             SS_OPTION_USE_TLC_WITH_ACCELERATOR);
95 }
96
97
98 /* Function: mdlInitializeSampleTimes
     =========================================
99  * Abstract:
100 *    Specifiy that we inherit our sample time from the
     driving block.
101 */
102 static void mdlInitializeSampleTimes(SimStruct *S)
103 {
104
105     ssSetSampleTime(S,0,SAMPLE_TIME);
106     ssSetOffsetTime(S,0,0);
107
108 }
```

```
109
110 #define MDL_INITIALIZE_CONDITIONS
111 /* Function: mdlInitializeConditions
    ========================================
112  * Abstract:
113  *    Initialize continuous states to zero
114  */
115 static void mdlInitializeConditions(SimStruct *S)
116 {
117     real_T *x0 = ssGetDiscStates(S);
118     int_T  i;
119
120     *x0++ = 0.0;
121
122     for (i=0; i<=4; i++) {
123         *x0++ = 0.0;
124     }
125 }
126
127 /* Function: mdlOutputs
    ============================================================
128  * Abstract:
129  */
130 static void mdlOutputs(SimStruct *S, int_T tid)
131 {
132     int_T             i;
133     InputRealPtrsType AN0 =
      ssGetInputPortRealSignalPtrs(S,0); //wd
134     InputRealPtrsType AN1 =
      ssGetInputPortRealSignalPtrs(S,1); //w
135     InputRealPtrsType AN2 =
      ssGetInputPortRealSignalPtrs(S,2); //ia
```

```
136     InputRealPtrsType AN3 =
         ssGetInputPortRealSignalPtrs(S,3); //ib
137     InputRealPtrsType AN4 =
         ssGetInputPortRealSignalPtrs(S,4); //ic
138     InputRealPtrsType AN5 =
         ssGetInputPortRealSignalPtrs(S,5); //theta_e
139
140     double            *y0    =
         ssGetOutputPortRealSignal(S,0);
141     double            *y1    =
         ssGetOutputPortRealSignal(S,1);
142     double            *y2    =
         ssGetOutputPortRealSignal(S,2);
143     double            *y3    =
         ssGetOutputPortRealSignal(S,3);
144     double            *y4    =
         ssGetOutputPortRealSignal(S,4);
145     double            *y5    =
         ssGetOutputPortRealSignal(S,5);
146     double            *y6    =
         ssGetOutputPortRealSignal(S,6);
147     double            *y7    =
         ssGetOutputPortRealSignal(S,7);
148
149     int_T             width0 = ssGetOutputPortWidth(S
         ,0);
150     int_T             width1 = ssGetOutputPortWidth(S
         ,1);
151     int_T             width2 = ssGetOutputPortWidth(S
         ,2);
152     int_T             width3 = ssGetOutputPortWidth(S
         ,3);
153     int_T             width4 = ssGetOutputPortWidth(S
```

```
    ,4);
154 int_T             width5 = ssGetOutputPortWidth(S
    ,5);
155 int_T             width6 = ssGetOutputPortWidth(S
    ,6);
156 int_T             width7 = ssGetOutputPortWidth(S
    ,7);
157
158 double            *x     = ssGetDiscStates(S);
159
160 double wd, w, w_e;
161 double id, idd;
162 double iq, iqd;
163 double error_speed, error_iq, error_id;
164 double sin_theta, cos_theta, wrap_angle;
165 double v_alpha, v_beta, v_a, v_b, v_c;
166 double ia, ib, ic;
167 double i_alpha, i_beta;
168 double d_corr, q_corr; //correction terms
169 double vd, vq ,vdc, vqc;
170 double theta_e;
171 double V_mag;
172 double x0_temp, x1_temp, x2_temp;
173 double w_lim = K_inv/sqrt(pow(psi_rd,2)+pow((L*
    I_MAX),2)); //calculate speed limit for Maximum
    flux linkage locus
174
175 // Read analogue inputs
176 wd = *AN0[0];
177 w = *AN1[0];
178 ia = *AN2[0];
179 ib = *AN3[0];
180 ic = *AN4[0];
```

```
181     x[4] = *AN5[0]*P;
182
183     w_e = w*(double)P; //electrical speed
184     sin_theta = sin(x[4]);
185     cos_theta = cos(x[4]);
186
187 //      Clarke transformation
188     i_alpha = 0.666666*ia - 0.333333*ib - 0.333333*ic;
189     i_beta = 0.577350*(ib - ic);
190
191     //Park transformation
192     id = cos_theta*i_alpha + sin_theta*i_beta;
193     iq = -sin_theta*i_alpha + cos_theta*i_beta;
194     I_mag = sqrt(pow(id,2)+pow(iq,2)); //magnitude of
          current
195     V_mag = sqrt(pow(vd,2)+pow(vq,2)); //magnitude of
          voltage
196     //Correction terms
197     //d channel
198     d_corr = -w_e*L*iq/K_inv;
199     //q channel
200     q_corr = w_e*(L*id + psi_rd)/K_inv;
201
202     //
          ////////////////////////////////////////////////////////
203     //Speed loop
204     error_speed = wd - w; //speed error
205     x0_temp = x[0];
206     x[0] = x[0] + error_speed;
207     iqd = K_speed*error_speed + Ki_speed*SAMPLE_TIME*x
          [0];
208
```

```
209     //Integrator anti-windup
210     if (iqd > I_MAX){
211         iqd = (double)I_MAX;
212         x[0] = x0_temp;
213     }
214     else if (iqd < -I_MAX){
215         iqd = -(double)I_MAX;
216         x[0] = x0_temp;
217     }
218 
219     //Detect overspeed
220     if (w_e > w_lim)
221     {
222         if (sqrt(pow(-w_e*L*iq,2)+pow(w_e*psi_rd+w_e*L*
              id,2)) <= V_MAX*K_inv){
223             idd = 0;
224         }
225         else
226         {
227             idd = (-psi_rd+sqrt(pow((K_inv/w_e),2)-pow
                  ((L*iq),2)))/L;
228             if (sqrt(pow(idd,2)+pow(iqd,2))> I_MAX)
229                 iqd = sqrt(pow(I_MAX,2)-pow(idd,2));
230         }
231     }
232 
233     else{
234         idd = 0;
235     }
236 
237     ////////////////////////////////////
238     //Current loops
239     //direct current
```

```
240     error_id = idd - id;
241     x1_temp = x[1];
242     x[1] = x[1] + error_id;
243 
244     vd = K_curr*error_id + Ki_curr*SAMPLE_TIME*x[1];
245     vd = vd + d_corr; //add correction
246     if (vd > V_MAX){
247         vd = (double)V_MAX;
248         x[1] = x1_temp;
249     }
250     else if (vd < -V_MAX){
251         vd = -(double)V_MAX;
252         x[1] = x1_temp;
253     }
254 
255     //quadrature current
256     error_iq = iqd - iq;
257     x2_temp = x[2];
258     x[2] = x[2] + error_iq;
259     vq = K_curr*error_iq + Ki_curr*SAMPLE_TIME*x[2];
260     vq = vq + q_corr; //add correction
261     if (vq > V_MAX){
262         vq = (double)V_MAX;
263         x[2] = x2_temp;
264     }
265     else if (vq < -V_MAX){
266         vq = -(double)V_MAX;
267         x[2] = x2_temp;
268     }
269 
270     vdc = vd;
271     vqc = vq;
272     V_mag = sqrt(pow(vd,2) + pow(vq,2));
```

```
273
274     if (V_mag <= V_MAX) {
275         vdc = vd;
276         vqc = vq;
277     }
278     else if (sqrt(pow(vd,2) + pow(q_corr,2)) <= V_MAX )
         {
279         vdc = vd;
280         vqc = sqrt(pow(V_MAX,2)- pow(vq,2));
281         x[1] = x1_temp;
282         x[2] = x2_temp;
283     }
284     else{
285         vdc = sqrt(pow(V_MAX,2)-pow(q_corr,2));
286         x[1] = x1_temp;
287         x[2] = x2_temp;
288         vqc = q_corr;
289     }
290     ////////////////////////////////////
291
292     //Inverse Park transformation
293     v_alpha = vdc*cos_theta - vqc*sin_theta;
294     v_beta = vdc*sin_theta + vqc*cos_theta;
295
296     //Inverse Clarke transformation
297     v_a = v_alpha;
298     v_b = -0.5*v_alpha + 0.866025*v_beta;
299     v_c = -0.5*v_alpha - 0.866025*v_beta;
300
301     //outputs
302     *y0++ = vd;
303     *y1++ = vq;
304     *y2++ = 1.5*v_a;
```

```
305     *y3++ = 1.5*v_b;
306     *y4++ = 1.5*v_c;
307     *y5++ = id;
308     *y6++ = iq;
309     *y7++ = flag;
310 }
311 
312 /* Function: mdlTerminate
    =============================================================
313  * Abstract:
314  *    No termination needed, but we are required to
       have this routine.
315  */
316 static void mdlTerminate(SimStruct *S)
317 {
318 }
319 
320 #ifdef  MATLAB_MEX_FILE    /* Is this file being
       compiled as a MEX-file? */
321 #include "simulink.c"      /* MEX-file interface
       mechanism */
322 #else
323 #include "cg_sfun.h"       /* Code generation
       registration function */
324 #endif
```